

NASA CONTRACTOR  
REPORT



N71-17581

NASA CR-1677

NASA CR-1677

CASE FILE  
COPY

BRAYTON CYCLE VAPOR CHAMBER  
(HEAT PIPE) RADIATOR STUDY

by E. E. Gerrels and J. W. Larson

Prepared by

GENERAL ELECTRIC COMPANY

Philadelphia, Pa. 19101

for Lewis Research Center



1. Report No. NASA CR-1677	2. Government Accession No.	3. Recipient's Catalog No.	
4. Title and Subtitle BRAYTON CYCLE VAPOR CHAMBER (HEAT PIPE) RADIATOR STUDY		5. Report Date February 1971	6. Performing Organization Code
		8. Performing Organization Report No. GESP-7030	
7. Author(s) E. E. Gerrels and J. W. Larson		10. Work Unit No.	11. Contract or Grant No. NAS 3-10615
9. Performing Organization Name and Address General Electric Company King of Prussia Park Philadelphia, Pennsylvania 19101		13. Type of Report and Period Covered Contractor Report	
		14. Sponsoring Agency Code	
12. Sponsoring Agency Name and Address National Aeronautics and Space Administration Washington, D.C. 20546			
15. Supplementary Notes			
16. Abstract The vapor chamber (heat pipe) radiator is defined and evaluated as a potential candidate for rejecting waste heat from a Radioisotope Brayton Cycle space power system. A comparison is made with an operationally equivalent conduction fin radiator. Both radiators employed DC-200 heat transfer fluid within the primary ducts and aluminum as the basic structural material. Vapor chamber fluids are evaluated and selected for thermal performance and containment within the radiator. Vapor chamber compatibility and performance tests are made for a number of candidate fluids. Preliminary designs are developed for both conduction fin and vapor chamber radiator concepts. A comparison shows no significant advantages attributable to the Brayton cycle vapor chamber radiator where reliability and meteoroid criteria specify 0.99 to 0.999 probability of survival over a five-year lifetime.			
17. Key Words (Suggested by Author(s)) Brayton cycle Nuclear space power systems Radiators Heat pipe		18. Distribution Statement Unclassified - unlimited	
19. Security Classif. (of this report) Unclassified	20. Security Classif. (of this page) Unclassified	21. No. of Pages 279	22. Price * \$3.00



## FOREWORD

The work described in this report was conducted by the General Electric Missile and Space Division under NASA contract NAS 3-10615. Mr. James P. Couch, Space Power Systems Division, NASA Lewis Research Center, was the Project Manager. The report was originally issued as General Electric report GESP-7030.





## TABLE OF CONTENTS

<u>Section</u>		<u>Page</u>
1	INTRODUCTION . . . . .	1
1.1	General Discussion . . . . .	1
1.2	Study Objectives, Goals and Tasks . . . . .	3
1.3	Report Contents . . . . .	3
2	SUMMARY . . . . .	4
2.1	Introduction . . . . .	4
2.2	Vapor Chamber Evaluation and Selection . . . . .	5
2.3	Vapor Chamber Fin Radiator Design . . . . .	8
2.4	Conduction Fin Radiator Design . . . . .	10
2.5	Vapor Chamber (Heat Pipe) Tests . . . . .	10
2.6	Radiator Evaluation and Comparison . . . . .	12
2.7	Conclusion . . . . .	14
3	RADIATOR REQUIREMENTS . . . . .	15
3.1	General Discussion. . . . .	15
3.2	Powerplant and Configuration Specifications. . . . .	16
3.3	Performance Criteria . . . . .	16
3.4	Vapor Chamber Working Fluid Criteria . . . . .	19
3.5	Life Expectancy Considerations . . . . .	19
3.6	Meteoroid Criteria . . . . .	21
3.7	Structural Criteria . . . . .	24
3.8	Structural Environmental Criteria . . . . .	25
3.8.1	Ground Handling Criteria . . . . .	25
3.8.2	Launch, Lift-Off, Boost Criteria. . . . .	26
3.8.3	Orbital Operation Criteria. . . . .	28
3.9	Atmospheric Environmental Criteria. . . . .	29
4	WORKING FLUID SELECTION . . . . .	30
4.1	General Discussion . . . . .	30
4.1.1	Specific Work Requirements . . . . .	30
4.1.2	Vapor Chamber Fin Principles. . . . .	31
4.2	Physical Properties of Working Fluids . . . . .	36
4.2.1	Fluid Requirements . . . . .	36
4.2.2	Identification of Candidate Fluids. . . . .	37

# TABLE OF CONTENTS (Cont'd)

<u>Section</u>		<u>Page</u>
	4.2.3 Preliminary Fluid Performance Analysis . . . . .	40
	4.2.4 Compatibility of Candidate Working Fluids with Aluminum . . . . .	50
4.3	Analytical Comparative Evaluation . . . . .	55
	4.3.1 Analytical Model of Vapor Chamber Fin . . . . .	55
	4.3.2 Comparison of Vapor Chamber Performance Using Candidate Working Fluids . . . . .	73
4.4	Tests for Compatibility of Materials . . . . .	92
	4.4.1 Technical Approach . . . . .	92
	4.4.2 Capsule Design and Fabrication . . . . .	93
	4.4.3 Capsule Filling and Sealing . . . . .	95
	4.4.4 Capsule Test Apparatus . . . . .	99
	4.4.5 Capsule Test Results . . . . .	104
	4.4.6 Evaluation and Conclusions for the Selection of Vapor Chamber Working Fluids . . . . .	129
5	RADIATOR DESIGN . . . . .	134
	5.1 Design Concepts . . . . .	134
	5.1.1 General Discussion . . . . .	134
	5.1.2 Vapor Chamber Fin Radiator Design . . . . .	135
	5.1.3 Conduction Fin Radiator Design . . . . .	141
	5.2 Performance Analysis . . . . .	146
	5.2.1 Methodology . . . . .	146
	5.2.2. Results . . . . .	154
	5.3 Structural Analysis . . . . .	171
	5.3.1 General Discussion . . . . .	171
	5.3.2 Conduction Fin Radiator . . . . .	182
	5.3.3 Vapor Chamber Fin Radiator. . . . .	184
	5.4 Fabrication and Assembly . . . . .	190
	5.4.1 Vapor Chamber Fin Radiator. . . . .	190
	5.4.2 Conduction Fin Radiator . . . . .	197
	5.5 Weight Comparison . . . . .	204
6	VAPOR CHAMBER TEST PROGRAM	210
	6.1 General Discussion . . . . .	210
	6.2 Test Program Objectives . . . . .	211

## TABLE OF CONTENTS (Cont'd)

<u>Section</u>		<u>Page</u>
6.3	Vapor Chamber Test Configurations . . . . .	212
6.3.1	Design Considerations . . . . .	212
6.3.2	Vapor Chamber Design . . . . .	214
6.4	Test Program . . . . .	215
6.4.1	Test Setup . . . . .	215
6.4.2	Instrumentation. . . . .	220
6.4.3	Test Procedure. . . . .	223
6.5	Test Results. . . . .	226
6.5.1	Test Data . . . . .	226
6.5.2	Test Accuracy . . . . .	233
6.6	Test Conclusions . . . . .	235
7	VAPOR CHAMBER RADIATOR EVALUATION AND CONCLUSIONS . . . . .	236
7.1	General. . . . .	236
7.2	Evaluation Criteria Summary . . . . .	236
7.3	Evaluation Summary . . . . .	237
7.4	Conclusions . . . . .	242
8	REFERENCES . . . . .	244
APPENDIX A:	TABULATED VALUES OF FLUID PROPERTIES . . .	247
APPENDIX B:	SPECIFICATION NO. P1224-2-BRAYTON CYCLE SPACE POWER SYSTEM ATMOSPHERIC ENVIRONMENTAL SPECIFICATION . . . . .	264

## LIST OF ILLUSTRATIONS

<u>Figure</u>		<u>Page</u>
1-1	Power Module Configuration . . . . .	2
1-2	Eight MW Vehicle Concept Interplanetary Configuration. . . . .	2
2-1	Vapor Chamber Radiator Design Characteristics Summary . . . . .	9
2-2	Conduction Fin Radiator Design Characteristics Summary. . . . .	11
2-3	Comparison of Vapor Chamber Fin to Conduction Fin Primary Radiators . . . . .	13
3-1	Trend in Launch Vehicle Dynamic Loads . . . . .	25
3-2	Acoustic Noise Frequency Spectrum . . . . .	27
4-1	Vapor Chamber Flow Dynamics . . . . .	33
4-2	Capillary Flow Parameters vs Temperature for Vapor Chamber Working Fluids . . . . .	42
4-3	Dimensionless Capillary Flow Parameter vs Temperature for Various Fluids . . . . .	43
4-4	Vapor Flow Parameter vs Temperature for Various Fluids . . . . .	45
4-5	Cicchelli and Bonilla Correlation . . . . .	46
4-6	Critical Heat Flux vs Temperature for Various Fluids . . . . .	47
4-7	Vapor Pressure vs Temperature for Various Fluids . . . . .	48
4-8	Total Yearly Ionization Dose (1 gm/cm <sup>2</sup> Aluminum Shielding, Polar Orbits). . . . .	49
4-9	Vapor Chamber Radiator Panel . . . . .	55
4-10	Individual Vapor Chamber Element . . . . .	56
4-11	Vapor Chamber Thermal Schematic . . . . .	57
4-12	Variation of Fin Effectiveness with Radiation Modulus for Fin Radiating from Two Sides . . . . .	61
4-13	Heat Transfer Rate vs Temperature of A Single Vapor Chamber . . . . .	63
4-14	Vapor Chamber Heat Radiated Per Unit Radiator Mass . . . . .	63
4-15	Conduction Fin Thickness vs Vapor Chamber Tube Diameter and Temperature . . . . .	64
4-16	Conduction Fin Length vs Vapor Chamber Tube Diameter and Temperature . . . . .	64
4-17	Individual Vapor Fin Evaporation Surface Thermal Flux vs Temperature . . . . .	73
4-18	Evaporative Vapor $\Delta T$ Comparison . . . . .	79

# LIST OF ILLUSTRATIONS (Cont'd)

<u>Figure</u>		<u>Page</u>
4-19	Condensing Temperature Loss . . . . .	80
4-20	Condenser Length Limit . . . . .	80
4-21	Effect of Tube Wall Thickness and Temperature on Vapor Chamber Fin Heat Radiated Per Unit Radiator Mass . . . . .	81
4-22	Probability That 70 Percent or More Units Survive as a Function of Unit Reliability . . . . .	86
4-23	Correlation of Individual Vapor Chamber Survival Probability Required to Achieve Fixed Overall Radiator Success Probability Against Vapor Chamber Survival Fraction . . . . .	87
4-24	Fin Effectiveness vs $\lambda$ Radiation Modulus( $\frac{2\sigma\epsilon L^2 T^3}{K_t}$ ) for Fin Radiating from Two Sides . . . . .	88
4-25	Aluminum Capsule . . . . .	94
4-26	Capsule Filling System . . . . .	96
4-27	Cross Section of Fill Tube Pinch-off Potted in Epoxy Cement (C67112007) . . . . .	99
4-28	Capsule Test Apparatus (C67101205) . . . . .	100
4-29	Schematic of Thermocouple Circuit . . . . .	101
4-30	Sectioned Aluminum Capsule Following Heating to 170°F with Methyl Alcohol (C67100450) . . . . .	106
4-31	Capsule Test Data for n-Pentane . . . . .	108
4-32	Capsule Test Data for Benzene . . . . .	109
4-33	Capsule Test Data for Water in 321 Stainless Steel . . . . .	111
4-34	Capsule Test Data for Ammonia . . . . .	113
4-35	Capsule Test Data for Freon 11, Capsule No. 1 (T=156°F) . . . . .	115
4-36	Capsule Test Data for Freon 11, Capsule No. 2 (T=222°F) . . . . .	116
4-37	Capsule Test Data for Freon 114, Capsule No. 1 (T=155°F) . . . . .	117
4-38	Capsule Test Data for Freon 113, Capsule No. 2 (T=225°F) . . . . .	118
4-39	Capsule Test Data for Toluene . . . . .	120
4-40	Capsule Test Data for n-Heptane . . . . .	121
4-41	Capsule Test Data for CP-32 . . . . .	123
4-42	Capsule Test Data for CP-34 . . . . .	125
4-43	Capsule Test Data for n-Butane, Capsule No. 1 . . . . .	126
4-44	Capsule Test Data for n-Butane, Capsule No. 2 . . . . .	128
5-1	Configuration Possibilities. . . . .	135
5-2	Vapor Chamber Radiator Conceptual View. . . . .	136
5-3	Final Primary Duct-Evaporator Configuration . . . . .	138

# LIST OF ILLUSTRATIONS (Cont'd)

<u>Figure</u>		<u>Page</u>
5-4	Alternative Design . . . . .	139
5-5	Staggered Vapor Chambers . . . . .	139
5-6	Condensing Wick . . . . .	140
5-7	Central Fin Design . . . . .	141
5-8	Offset Chamber Configuration . . . . .	142
5-9	Reynolds Number Versus Hydraulic Diameter . . . . .	144
5-10	Model for Finned Duct Conduction Fin Radiator . . . . .	146
5-11	Heat Transfer Coefficients for Laminar and Turbulent Flow Versus Hydraulic Diameter . . . . .	147
5-12	Comparison of Convective Conductance for Laminar and Turbulent Flows . . . . .	147
5-13	Effect of Survival Probability Distribution Between Ducts and Chambers on Vapor Chamber Radiator Weight . . . . .	153
5-14	Excess Area Required Versus Vapor Chamber Percent Failure (Aluminum Fins) . . . . .	153
5-15	Weight Versus Area for Vapor Chamber Fin Primary Radiator . .	156
5-16	Weight Versus Area for Conduction Fin Primary Radiator. . . . .	157
5-17	Comparison of Vapor Chamber Fin to Conduction Fin Primary Radiators . . . . .	160
5-18	Effect of Chamber Survival Fraction on Radiator Weight . . . . .	161
5-19	Effect of Evaporator Temperature Drop on Vapor Chamber Fin Primary Radiator. . . . .	163
5-20	Effect of Condensing Film Thickness on Vapor Chamber Fin Primary Radiator. . . . .	164
5-21	Comparison of Primary Radiator Fluids for Conduction Fin Primary Radiator. . . . .	166
5-22	Effect of Tube Spacing for Vapor Chamber Fin Primary Radiator. . . . .	167
5-23	Effect of Sink Temperature on Vapor Chamber Fin Primary Radiator . . . . .	168
5-24	Comparison of Sink Temperature on Conduction Fin Primary Radiator . . . . .	169
5-25	Comparison of Working Fluids for Vapor Chamber Fin Primary Radiator . . . . .	170
5-26	Effect of Vapor Chamber Diameter for Vapor Chamber Fin Primary Radiator . . . . .	172
5-27	Effect of Tube Spacing for Vapor Chamber Fin Primary Radiator. . . . .	173
5-28	Effect of Primary Fluid Slot Width on Vapor Chamber Fin Primary Radiator . . . . .	174

# LIST OF ILLUSTRATIONS (Cont'd)

<u>Figure</u>		<u>Page</u>
5-29	Effect of Duct Fin Thickness for Vapor Chamber Fin Primary Radiator . . . . .	175
5-30	Effect of Tube Spacing for Conduction Fin Primary Radiator. . . .	176
5-31	Effect of Primary Fluid Slot Width on Conduction Fin Primary Radiator . . . . .	177
5-32	Effect of Duct Fin Thickness for Conduction Fin Primary Radiator. . . . .	178
5-33	Effect of Number of Slots Per Tube for Conduction Fin Primary Radiator . . . . .	179
5-34	Launch Loads on Radiator . . . . .	181
5-35	Failure Modes . . . . .	183
5-36	Cross Section Through Conduction Fin Radiator Duct . . . . .	186
5-37	Cross Section Through Coolant Duct of Vapor Chamber Radiator. . . . .	186
5-38a	Cross Section Through Vapor Chamber Tube and Fin . . . . .	188
5-38b	Radiator Panel Matrix . . . . .	188
5-39	Vapor Chamber Radiator Design Layout. . . . .	191
5-40	Vapor Chamber Fin Radiator Design Details. . . . .	192
5-41	Vapor Chamber Fin Radiator Assembly Sequence Step 1 . . . . .	194
5-42	Vapor Chamber Fin Radiator Assembly Sequence Step 2 . . . . .	194
5-43	Vapor Chamber Fin Radiator Assembly Sequence Step 3 . . . . .	195
5-44	Vapor Chamber Fin Radiator Assembly Sequence Step 4 . . . . .	195
5-45	Vapor Chamber Fin Radiator Assembly Sequence Step 5 . . . . .	196
5-46	Vapor Chamber Fin Radiator Assembly Sequence Step 6 . . . . .	196
5-47	Vapor Chamber Fin Radiator Assembly Sequence Step 7 . . . . .	198
5-48	Vapor Chamber Fin Radiator Assembly Sequence Step 8 . . . . .	198
5-49	Conduction Fin Radiation Design Layout. . . . .	199
5-50	Conduction Fin Radiator Design Details . . . . .	200
5-51	Conduction Fin Radiator Assembly Sequence Step 1 . . . . .	201
5-52	Conduction Fin Radiator Assembly Sequence Step 2. . . . .	202
5-53	Conduction Fin Radiator Assembly Sequence Step 3. . . . .	203
5-54	Conduction Fin Radiator Assembly Sequence Step 4. . . . .	205
5-55	Conduction Fin Radiator Assembly Sequence Step 5. . . . .	206
5-56	Conduction Fin Radiator Assembly Sequence Step 6. . . . .	207
6-1	Capsule Vapor Chamber Test Unit . . . . .	216
6-2	"C" Wick Design Vapor Chamber. . . . .	217
6-3	Flow Schematic Vapor Chamber Test Unit Brayton Cycle Radiator. . . . .	218



# LIST OF ILLUSTRATIONS (Cont'd)

<u>Figure</u>		<u>Page</u>
6-4	View of Test Loop . . . . .	219
6-5	Heat Exchanger Assembly Vapor Chamber Test Unit Brayton Cycle Radiator . . . . .	221
6-6	Disassembled Heat Exchanger and Heat Pipe. . . . .	222
6-7	Vapor Chamber Tilted Position . . . . .	225
6-8	Water Heat Pipe (Cruciform Wick Configuration) Thermal Flux Versus Evaporative $\Delta T$ . . . . .	231
6-9	n-Pentane Heat Pipe (Cruciform Wick Configuration) Thermal Flux Versus Evaporative $\Delta T$ . . . . .	231
6-10	Benzene Heat Pipe (Cruciform Wick Configuration) Thermal Flux Versus Evaporative $\Delta T$ . . . . .	232
6-11	Ammonia Heat Pipe (Cruciform Wick Configuration) Thermal Flux Versus Evaporative $\Delta T$ . . . . .	232
6-12	Test Data (Cruciform Wick Configuration) Condensing Heat Flux Versus Condensing $\Delta T$ . . . . .	234
6-13	Benzene Heat Pipe ("C" Wick Configuration) Thermal Flux Versus Overall $\Delta T$ . . . . .	234

# LIST OF TABLES

<u>Table</u>		<u>Page</u>
2-1	Basic Requirements Summary . . . . .	4
2-2	Vapor Chamber Working Fluids . . . . .	6
2-3	Fluids Selected for Compatibility Tests with Aluminum . . . . .	7
2-4	Comparison of Radiator Weight and Area . . . . .	13
3-1	Reference Conditions and Specifications for the Brayton Cycle Vapor Chamber Radiator . . . . .	17
3-2	Working Fluid Performance Parameters . . . . .	19
3-3	Aluminum Cratering Coefficients . . . . .	23
3-4	Incipient Damage Factor, a, For 2024-T6 Aluminum . . . . .	23
4-1	Pertinent Properties of Potential Working Fluids for a Vapor Chamber Operating in the 20 to 350°F Range . . . . .	39
4-2	Criteria for Selection of Aluminum Alloys . . . . .	51
4-3	Vapor Chamber Performance Parameters for Candidate "High Temperature" Working Fluids (at 250°F Temp.) . . . . .	74
4-4	Vapor Chamber Performance Parameters for Alternate "High Temperature" Working Fluids (at 150°F Temp.) . . . . .	75
4-5	Vapor Chamber Performance Parameters for Alternate "Low Temperature" Working Fluids (at 150°F Temp.) . . . . .	76
4-6	Vapor Chamber Performance Parameters for Alternate "Low Temperature" Working Fluids (at 40°F Temp.) . . . . .	77
4-7	Comparison of Radiators Using Candidate Working Fluid Combinations . . . . .	89
4-8	Capsule Filling Data . . . . .	98
4-9	Calculated and Measured Heat Loss from Capsules . . . . .	103
4-10	Summary of Capsule Test Data . . . . .	131
5-1	Survival Probability Distribution . . . . .	152
5-2	Vapor Chamber Radiator Characteristics . . . . .	158
5-3	Conduction Fin Radiator Characteristics . . . . .	159
5-4	Effect of Ground Rules on Comparison . . . . .	165
5-5	Vapor Chamber Fluid Effect . . . . .	171
5-6	Radiator Weight Summary (Lb) . . . . .	208
5-7	Ground Rules for Radiator Weight Comparison . . . . .	209

# LIST OF TABLES (Cont'd)

<u>Table</u>		<u>Page</u>
6-1	Standard Inventory Level Position Data Cruciform Wick Heat Pipes . . . . .	227
6-2	Tilted, Reduced Inventory Operating Points Cruciform Wick. . . .	228
6-3	Benzene "C" Wick Configuration Heat Pipe Performance (Tilted 1/2 Inch, 30 cc Inventory) . . . . .	229
6-4	Condensate Film Thickness . . . . .	233
7-1	Fluid Selection . . . . .	238
7-2	Design Point Summary Comparison. . . . .	240
7-3	Design Point Summary Comparison. . . . .	241

## SECTION 1

### INTRODUCTION

#### 1.1 GENERAL DISCUSSION

This work was performed by General Electric Missile and Space Division's Isotope Power Systems Operation in partial fulfillment of Contract NAS3-10615, "Vapor Chamber Radiator Study," directed by NASA Lewis Research Center. The work was directed to the Research and Development of a Brayton Cycle Vapor Chamber Fin Radiator.

It is recognized that the heat rejection systems required for the relatively large space nuclear power plants required in the future comprise a significant portion of the total spacecraft weight and area. Thermal and structural efficiencies and performance variations of radiators can therefore influence overall spacecraft configurations, weight, payload and electrical power capability. Recently, General Electric completed a study of a Separately Launched Power Module employing the Brayton cycle, under Contract NAS9-7444, for NASA/MSC. This system shown in Figure 1-1 formed the basis for the requirements of the Vapor Chamber Radiator Study and serves to illustrate the role the radiator plays in serving as structure and shell for system components. The relative size of future radiators is even more dramatically illustrated by Figure 1-2, in the study of a Low Acceleration Space Transportation System performed for NASA under Contract NAS8-11423.

Obviously, a space radiator study of nuclear power systems such as the Brayton cycle power plant identified in this contract must involve evaluation and optimization techniques directed toward radiator concepts which minimize size and weight parameters.

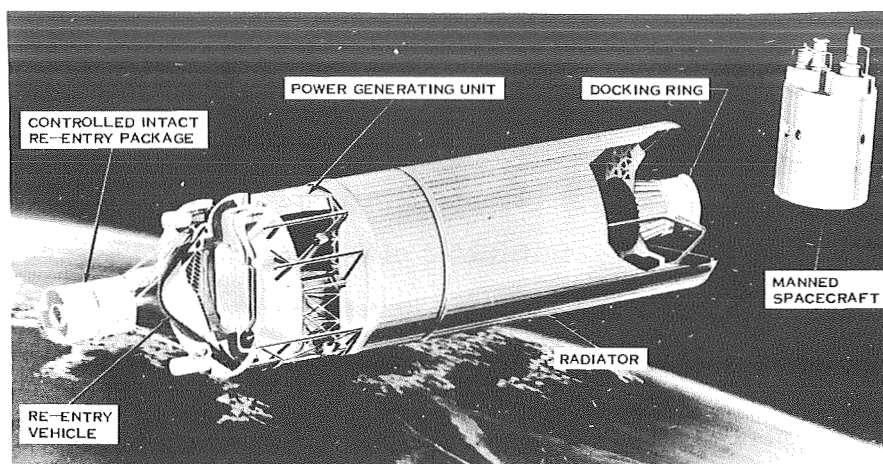


Figure 1-1. Power Module Configuration

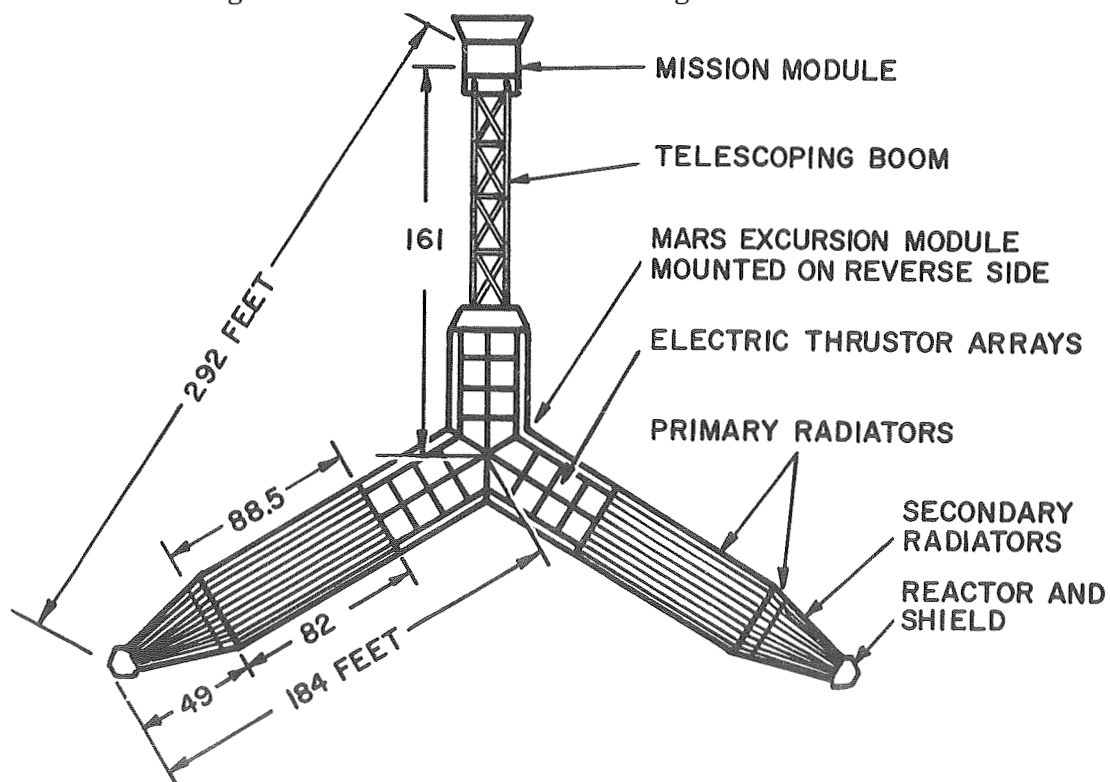


Figure 1-2. Eight MW Vehicle Concept Interplanetary Configuration

## 1.2 STUDY OBJECTIVES, GOALS AND TASKS

The purpose of this program is to evaluate, identify and design a promising Brayton cycle vapor chamber radiator for future space missions. The radiator must be capable of being tested in a one-g environment and operated in zero gravity. The heat rejection temperature range from 20<sup>0</sup>F up to 350<sup>0</sup>F is investigated. Vapor chamber working fluids are identified for use in this temperature range, their thermal characteristics and material compatibilities are determined, and preliminary radiator designs based on these characteristics are prepared. A comparison evaluation is made with a conduction fin radiator designed to the same specifications.

## 1.3 REPORT CONTENTS

Section 2 of this report contains a summary of the work performed, results obtained and conclusions to be made.

Radiator and power plant system specifications submitted by NASA Lewis were used as overall design criteria. These specifications provided the means of designing and subsequently evaluating both radiators in conformance to a single set of requirements. The requirements, specifications and study criteria used are contained in Section 3.

Section 4 describes the working fluid evaluation and material compatibility test programs performed. The radiator design, based on the requirements identified in Section 3 and the fluid, material and capsule selections of Section 4, is described in Section 5.

Section 6 presents the vapor chamber test program where representative vapor chambers were designed, fabricated and tested to evaluate and demonstrate performance compatible with requirements of the radiator design and predicted analyses.

The overall vapor chamber evaluation of results and conclusions are contained in Section 7. An appendix is provided which contains: (1) tabulated values of fluid properties, and (2) a detailed description of the atmospheric environmental criteria utilized. References are tabulated in order of appearance in Section 8.

## SECTION 2

### SUMMARY

#### 2.1 INTRODUCTION

This report contains a description and results of the work performed toward the identification of a promising Brayton Cycle vapor chamber fin (heat pipe) radiator. The specifications and requirements on which the radiator design is based were provided by NASA. A summary of reference specifications is contained in Table 2-1.

TABLE 2-1. BASIC REQUIREMENTS SUMMARY

REFERENCE CONDITIONS AND SPECIFICATIONS FOR THE BRAYTON CYCLE VAPOR CHAMBER RADIATOR	
Thermal Heat Rejection -----	12.39 kWt Primary, 2.19 kWt Secondary
Radiator Fluid Inlet Temperature -----	288 <sup>o</sup> F Primary, 118 <sup>o</sup> F Secondary
Radiator Fluid Outlet Temperature -----	64 <sup>o</sup> F Primary and Secondary
Effective Radiator Sink Temperature ---	-10 <sup>o</sup> F
Radiator Surface Thermal Emissivity ---	0.85
Radiator Fluid -----	Dow Corning 200, 2 Centistokes at 77 <sup>o</sup> F
Primary Fluid Pressure Drop -----	25 PSI maximum
Reliability -----	0.99 or 0.999 for 5 years on Vapor Chambers and on Primary Fluid Loops
Supported Load -----	6000 Pounds including Heat Rejection System

The reference Brayton cycle space powerplant uses a separate radiator loop with a heat rejection of about 15 kWt. A compact heat exchanger transfers waste heat from the power conversion loop to a liquid coolant. This coolant is then circulated through a radiator where the waste heat is rejected to space. This radiator is called the primary radiator. In addition, an auxiliary circuit and radiator reject heat lost by cooling the powerplant electrical and other components. This radiator is called the secondary radiator.

The general configuration visualized for these radiators is an array of tubes through which coolant flows and to which are attached solid, conducting fins. It was anticipated that a significant reduction in radiator weight and area might be achieved by using "vapor chamber" fins.

This study consisted of both experimental and analytical efforts. These included:

1. Vapor chamber fin fluid evaluation (compatibility testing, analytical performance predictions)
2. Vapor chamber fin radiator design
3. Conduction fin radiator design
4. Vapor chamber (heat pipe) tests
5. Comparison of vapor chamber fin and conduction fin radiators.

## 2.2 VAPOR CHAMBER FLUID EVALUATION AND SELECTION

Initially, a wide selection of fluids was considered for application in the vapor chamber fin radiator. These fluids, which are listed in Table 2-2 satisfy the following general criteria:

1. Boiling point between  $0^{\circ}\text{F}$  and  $300^{\circ}\text{F}$  (propane and ammonia are exceptions)
2. Pour point less than  $20^{\circ}\text{F}$  (except water)



3. Latent heat of vaporization greater than 100 BTU/lb (except several freons).

TABLE 2-2. VAPOR CHAMBER WORKING FLUIDS

INORGANICS	HYDROCARBONS	OTHER ORGANICS
Water	Saturated Unbranched Acyclic (Alkane Series)	Alcohols
Ammonia	Propane	Methanol (Methyl Alcohol)
Sulfur Dioxide	n-Butane	Ethanol (Ethyl Alcohol)
	n-Pentane	Isopropanol
	n-Hexane	
	n-Heptane	Amines
	n-Octane	Methylamine
	n-Nonane, etc.	Ethylamine
	Saturated Branched Acyclic	Pyridine (CP-32)
	Isobutane, etc.	CP-34
	Unsaturated Acyclic	Esters
	1-Butene, etc.	Methyl Formate
	Saturated Monocyclic	Ethers
	Cyclobutane, etc.	Anisole
	Unsaturated Monocyclic	Halogenated Hydro- carbons
	Cyclobutene, etc.	Freon F-11
	Monocyclic Aromatic	Freon F-12
	Benzene	Freon F-113, etc.
	Toluene	
	Xylene, etc.	
	etc.	

From this group, a more extensive screening process was undertaken in order to select those fluids most likely to exhibit superior vapor chamber performance. Figures of merit which were used in this analytical comparison were a capillary flow parameter, a vapor flow parameter, vapor pressure and thermal conductivity. On this basis, the thirteen fluids listed in Table 2-3 were chosen for compatibility testing with aluminum.

TABLE 2-3. FLUIDS SELECTED FOR COMPATIBILITY TESTS WITH ALUMINUM

Temperature Range		
150° to 300°F	20° to 200°F	20° to 150°F
n- Pentane	CP-32	Ammonia
n- Heptane	CP-34	Freon 11
Benzene	Ethyl Alcohol	Freon 113
Toluene	Methyl Alcohol	n- Butane
Water		

The aluminum alloy, 6-61-T6, was selected for the vapor chamber on the basis of resistance to chemical corrosion, good mechanical strength, weldability and availability. Capsules of this material were utilized in the fluid compatibility tests. Since the planned radiator lifetime is five years, compatibility testing was performed at higher temperatures than would be normally encountered so as to accelerate any corrosion processes. The actual test periods were only one percent of the mission requirements.

On the basis of these tests, benzene, n-heptane, n-pentane, freon-11, freon-113, ammonia and n-butane were judged to be compatible with 6061-T6 aluminum. The remaining fluids were found to be unacceptable for use with aluminum in the temperature ranges of interest. Water, which was known to be incompatible with aluminum, was tested in a 321 stainless steel capsule, however, appreciable amounts of hydrogen were generated.

On the basis of the analytical investigation and the compatibility testing, the following fluids were selected as prime candidates for subsequent performance testing:

Temperature Range

150 <sup>0</sup> to 300 <sup>0</sup> F	benzene, n-heptane, n-pentane
20 <sup>0</sup> to 200 <sup>0</sup> F	freon-11, freon-113
20 <sup>0</sup> to 150 <sup>0</sup> F	ammonia, n-butane

### 2.3 VAPOR CHAMBER FIN RADIATOR DESIGN

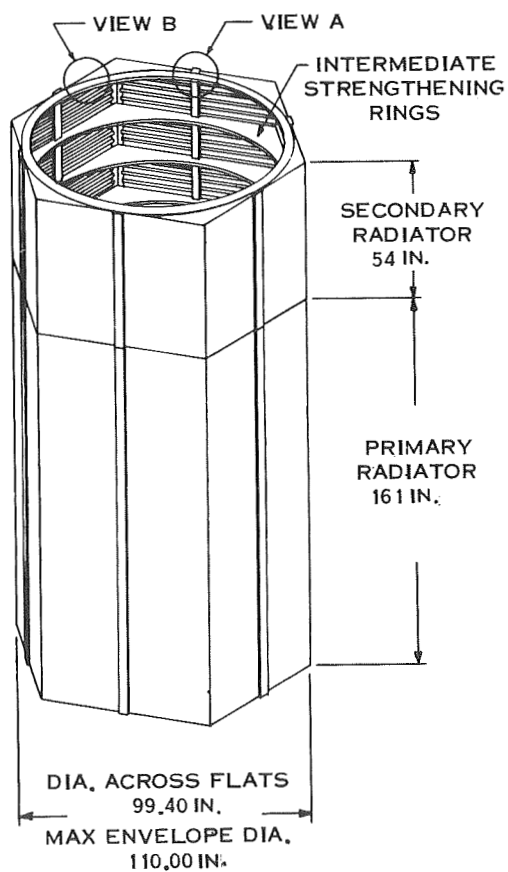
The next phase of the study concentrated on the conceptual design of a load bearing radiator. The major ground rules affecting the radiator design were:

1. Atlas-Centaur launch vehicle
2. Earth orbital mission (sink temperature = -10<sup>0</sup> F)
3. Redundant primary fluid loops (two independent loops)
4. Aluminum radiator construction
5. Primary fluid - Dow Corning 200 (Silicone liquid)

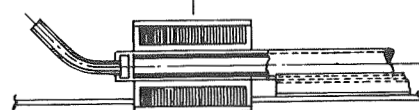
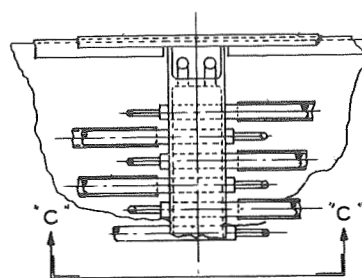
Although it was feasible to provide a circular radiator configuration by orienting the chambers longitudinally or circumferentially, a hexagonal shape was chosen. This design, shown in Figure 2-1, eliminates the fabrication problem imposed by curved vapor chambers and effectively utilizes the structural rigidity of the primary ducts to support the power system during launch.

The use of DC-200, a stable, non-corrosive, but relatively poor heat transfer fluid, required finned fluid ducts to improve the energy transfer to the vapor chamber evaporator sections. The vapor chamber design (see Figure 2-1, View B) consisted of a cylindrical tube attached to the underside of the radiating surface. This configuration formed a rigid panel in which the vapor chambers received meteoroid "bumper" protection from the hexagonal shell. This design approach resulted in reduced meteoroid armor requirements and an overall reduction in radiator weight at the higher meteoroid nonpenetration probabilities.

VAPOR CHAMBER RADIATOR  
DESIGN CHARACTERISTICS SUMMARY

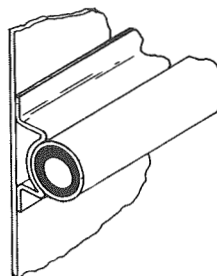


**VIEW A**  
SECTION SHOWING STAGGERED  
VAPOR CHAMBERS



**SECTION "C-C" (ENLARGED)**  
CROSS SECTION OF  
PRIMARY DUCT SHOWING  
VAPOR CHAMBER & FINNED  
DC-200 FLOW PASSAGES

**VIEW B**



**SECTION OF VAPOR CHAMBER  
SHOWING BUMPER FIN OFFSET  
FROM CHAMBER CONFIGURATION**



**CROSS SECTION OF VAPOR CHAMBER  
SHOWING CONDENSING WICK  
CONFIGURATION**

Figure 2-1. Vapor Chamber Radiator Design Characteristics Summary.

#### 2.4 CONDUCTION FIN RADIATOR DESIGN

In order to provide a reference point for the vapor chamber fin radiator evaluation, a conduction fin radiator was designed. Initial concepts utilizing a conventional round tube conduction fin radiator resulted in excessive radiator areas. This was a direct result of the radiator system conditions and the physical properties of the DC-200 coolant. The combined effects of a large fluid axial  $\Delta T$ , low radiating heat flux and low fluid heat transfer coefficient resulted in laminar film drops as high as 100<sup>o</sup>F with the round tube design.

Accordingly, the conduction fin design underwent a major alteration to the rectangular finned geometry shown in Figure 2-2. The offset tube/fin arrangement again takes advantage of the meteoroid "bumper" protection provided by the conduction fin. While more difficult to design and fabricate than the round tube radiator, this concept is on a more comparable level of sophistication with the vapor chamber fin design.

#### 2.5 VAPOR CHAMBER (HEAT PIPE) TESTS

The objectives of this phase of the program were to:

1. Demonstrate the fabrication of the vapor chamber as defined in previous studies.
2. Demonstrate the operation of the vapor chamber using the most promising candidate fluids.
3. Obtain performance data so as to verify the radiator design results as predicted by the analytical analyses.

In the low temperature range, below 150<sup>o</sup>F, ammonia and water were tested, while n-pentane and benzene were tested between 150<sup>o</sup> and 300<sup>o</sup>F. The vapor chambers were 30 inches in length, with 0.500 inch OD by 0.035 inch wall. Five vapor chambers were tested; each fluid was tested with a "c" shaped wick. All heat pipes were tested in the horizontal as well as the tilted position. Ammonia and water exhibited excellent capillary pumping capability, but the benzene and n-pentane could be tilted only to a marginal degree. The "c" shaped wick appeared to offer a superior return flow passage for the benzene.

CONDUCTION FIN RADIATOR  
DESIGN CHARACTERISTICS SUMMARY

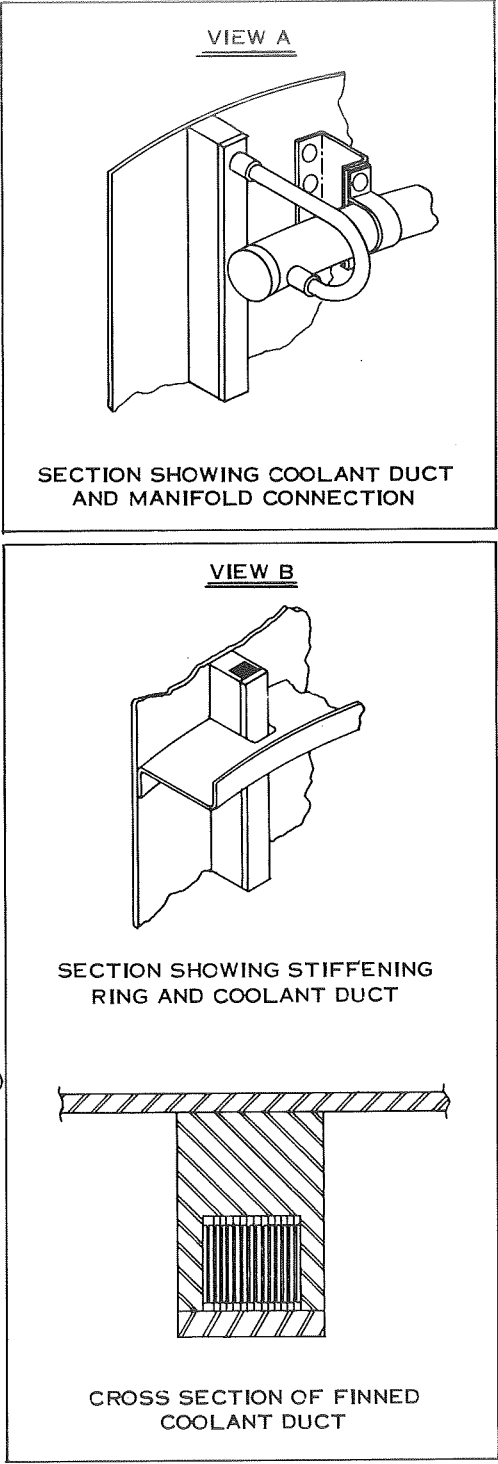
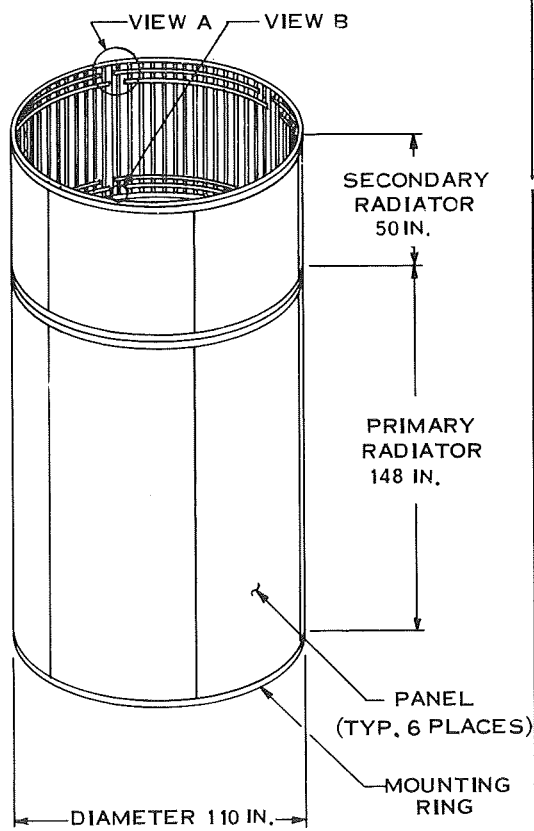


Figure 2-2. Conduction Fin Radiator Design Characteristics Summary

All four fluids demonstrated excellent thermal characteristics with ammonia and water having the lowest evaporative and condensing temperature drops. Since water is incompatible with aluminum, ammonia was judged to be the optimum fluid in the low temperature regime; n-pentane was selected as the fluid for the high temperature section.

## 2.6 RADIATOR EVALUATION AND COMPARISON

The comparison between the vapor chamber fin and conduction fin radiators was based on the weight, area requirements and fabrication considerations for each concept. The radiator weight included both the primary and secondary heat rejection systems for a Brayton cycle power system as well as associated structural members.

The weight evaluation for the vapor chamber fin and conduction fin radiators was performed with digital computer optimization codes. Area constraints, with appropriate weight penalties, were factored into the analysis. Each of these codes modeled the respective design concepts in detail; included in this analysis were heat transfer, fluid flow and meteoroid protection considerations. Structural requirements were determined by means of a computer code designed to analyze the properties of a load bearing, stiffened cylindrical shell. The structural investigation indicated that the conduction fin radiator was a more suitable load bearing structure than the vapor chamber fin radiator. However, in either case the weight of additional stiffening material required is less than the weight required for a separate load bearing structure.

A comparison of radiator weight and area is shown in Table 2-4 and Figure 2-3 for meteoroid survival probabilities of 0.99 and 0.999. The vapor chamber fin radiator shows a distinct weight advantage at the higher meteoroid survival probability.

Neither radiator exhibited a large fabrication advantage over the other. The fluid passages specified in the conduction fin radiator consist of very thin fins and narrow fluid passages, making their fabrication difficult. Candidate methods of the duct fin

TABLE 2-4. COMPARISON OF RADIATOR WEIGHT AND AREA

	PRIMARY		SECONDARY	
	WT. (LB)	AREA (FT)	WT. (LB)	AREA (FT)
<u>Survival Probability 0.999</u>				
Vapor Chamber Radiator (n-Pentane and Ammonia)	457	379	150	127
Conduction Fin Radiator	559	355	160	122
<u>Survival Probability 0.99</u>				
Vapor Chamber Radiator (n-Pentane and Ammonia)	455	377	145	127
Conduction Fin Radiator	441	344	136	122

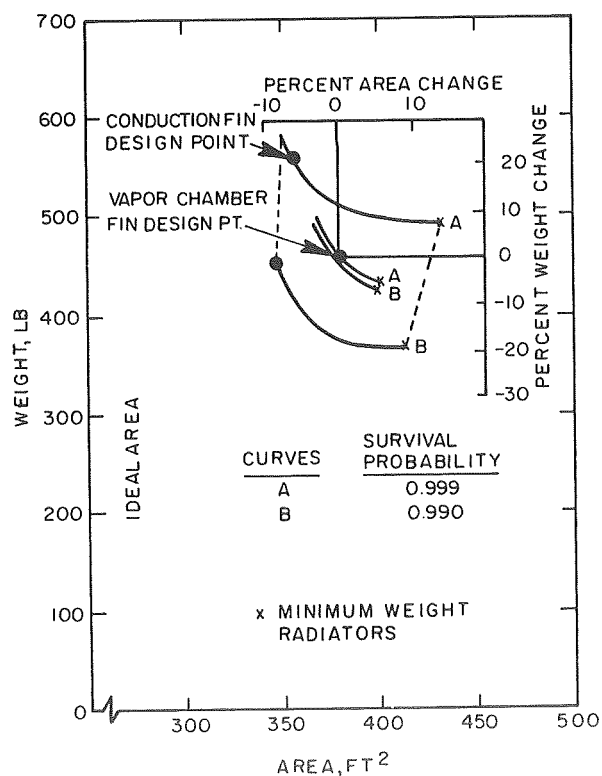


Figure 2-3. Comparison of Vapor Chamber Fin to Conduction Fin Primary Radiators



fabrication would be chemical milling, machined slots or a corrugated sheet. The vapor chamber fin radiator also utilizes finned primary fluid ducts, however, a departure from the optimum fin thickness and spacing is not as critical as in the conduction fin radiator. Fabrication of the vapor chambers and subsequent thermal interfacing of the evaporator sections with the primary fluid ducts will also require special methods and close quality control procedures.

## 2.7 CONCLUSIONS

A vapor chamber fin radiator concept has been evaluated and compared with a conduction fin radiator for the Brayton cycle space powerplant specified in Table 2-1. The following conclusions have been reached:

1. Of the fluids tested, ammonia is the best working fluid for vapor chambers operating at temperatures below 150°F.
2. At operating temperatures above 150°F, water is the best working fluid on the basis of performance calculations. However, since water is incompatible with aluminum and a liner was not considered, n-pentane was selected as the working fluid in this temperature range.
3. The vapor chamber radiator weight is insensitive to the meteoroid survival probability when compared to the influence of this parameter on the conduction fin radiator weight.
4. The specific weight for both radiator types ranges between 1.0 and 1.5 lbs/ft<sup>2</sup>.
5. Both radiators were calculated to be about equal in weight and area at a survival probability of 0.998. At higher probabilities, the vapor chamber radiator seems to be lighter and smaller, while at lower probabilities the conduction fin radiator is lighter and smaller. However, the differences in weight and area are less than 20 percent over the range of probabilities from 0.990 to 0.999.

## SECTION 3

### RADIATOR REQUIREMENTS

#### 3.1 GENERAL DISCUSSION

The Brayton cycle powerplant, under development at NASA Lewis Research Center, transfers waste heat from the gaseous working fluid to a liquid coolant, herein called the primary radiator fluid. The primary radiator fluid is then pumped to the radiator to dissipate the waste heat to space. Presently, the radiator is conceived to be an array of tubes through which the primary fluid flows and to which are attached solid, conducting fins (conduction fin radiator). This array may be cylindrical or flat in shape. Heat may be radiated from either both sides or from one side only. An aluminum alloy would be employed.

It was considered possible that significant radiator weight and/or area reduction could be achieved through the use of "vapor chamber" fins. This concept transfers the waste heat from the primary radiator fluid to the radiating surfaces under nearly isothermal conditions by the evaporation and condensing of a second fluid. Recirculation of this second fluid is accomplished by capillary forces.

Since the vapor chamber radiator is evaluated as an alternate to the conduction fin design, it must be competitive in all categories significant for evaluation. These include: reliability, performance, fabrication and operation. It is difficult to formulate a single figure-of-merit function appropriate for comparison on a combination of the above categories. Consequently, the vapor chamber radiator must compete favorably on all counts. The approach to be used is to match the reliability, operations and powerplant requirements and make the comparison on the performance parameters yielding mass and radiator area characteristics.

The requirements and criteria for the design, comparison and selection of the radiator systems are presented below.

### 3.2 POWERPLANT AND CONFIGURATION SPECIFICATIONS

Both radiator system concepts associated with the Brayton cycle powerplant have the following characteristics as listed in Table 3-1. These requirements were specified by NASA Lewis and are considered representative of current Brayton cycle concepts.

### 3.3 PERFORMANCE CRITERIA

The major criteria for comparative evaluation of the vapor chamber fin with the conducting fin is radiator mass and area while maintaining the equivalent reliability and operational characteristics.

The radiator mass is comprised of the vapor chamber fins plus the primary fluid circuit and structure. The vapor chamber mass includes container, meteoroid armor, wick, fluid inventory and any conducting fin as provided. The primary fluid circuit and structure can also represent a sizable mass; it is comprised of container, extended heat transfer surfaces, fluid inventory, meteoroid armor and support structure.

In order to reduce the radiator area the temperature drop between the primary fluid and radiating surfaces must be minimized. These temperature drops occur in the following elements:

1. Primary radiator fluid boundary layer
2. Primary radiator fluid wall to evaporator
3. Evaporator liquid to vapor interface
4. Vapor flow passage
5. Condenser liquid layer
6. Condenser wall
7. Radiator fin structure

TABLE 3-1. REFERENCE CONDITIONS AND SPECIFICATIONS FOR THE BRAYTON  
CYCLE VAPOR CHAMBER RADIATOR

Thermal Heat Rejection - Primary Radiator Secondary Radiator	12.39 kWt (6 kWe) 2.19 kWt
Radiator Fluid - Primary and Secondary	Dow Corning 200 2 Centistokes at 77°F
Radiator Fluid Flow Rate - Primary Secondary	6.9 lb/min 5.64 lb/min
Radiator Fluid Inlet Temp. - Primary Secondary	288°F (320°F peak) 118°F (150°F peak)
*Radiator Fluid Outlet Temp. - Primary Secondary	64°F maximum 64°F maximum
Primary Radiator Fluid Pressure Drop	25 psi maximum
Effective Radiator Sink Temperature	-10°F (450°R)
Radiator Thermal Emissivity	0.85
Radiator Surface Solar Absorptivity	0.25
Radiator Survival Probability (1 of 2 loops for 5 years)	0.99 and 0.999 (5 years)
Radiator Structural Material	Aluminum Alloy 6061-T6
Radiator Supported Load	5000 lb plus 1000 lb for radiator
Radiator Diameter - Primary Secondary	9 feet (max dimension dependent on shroud)
Radiator/Payload Shroud	OA0 115 in. ID nom. across flats 110 in. ID

\*Sufficient vapor chamber fin redundancy is to be provided for maintaining 64°F radiator primary fluid after 5 years of operation with a probability of 0.99 and 0.999 in each of two evaluations.

The radiator optimization process involves the minimization of these temperature losses without incurring significant mass penalties. The radiator design was optimized on a system weight parameter which includes: radiator weight, additional launch vehicle structural weight and interface penalties for excessive area, and additional powerplant weight due to the heat rejection loop parasitic power requirements. For purposes of performing this optimization a performance parameter, equivalent mass, was utilized. This equivalent mass is the following:

$$(\bar{W}_{\text{equiv.}}) = (\bar{W}_{\text{actual}}) + (K) (A_{\text{EFF.}}) + (PW) (SW) \quad (3-1)$$

where

$$(\bar{W}_{\text{equiv.}}) = \text{Equivalent mass}$$

$$(\bar{W}_{\text{actual}}) = \text{Actual Radiator Mass}$$

$$(A_{\text{EFF.}}) = \text{Effective Radiator Area}$$

$$(K) = \text{Tradeoff factor - pounds of additional structural and auxiliary weight per square foot of radiator area}$$

$$PW = \text{radiator loop electrical pump work requirements (kWe)}$$

$$SW = \text{system powerplant weight per kWe}$$

This equation provides a reasonable approach to achieve the proper compromise between minimal radiator weight and area, within the system constraint. The tradeoff factor, K, can be used in the parametric evaluation of radiator characteristics. For the nominal radiator optimization, a radiator mass/area tradeoff factor of 0 to 5 lb/ft<sup>2</sup> was used. For presentation of results, the actual mass and areas were used.

### 3.4 VAPOR CHAMBER WORKING FLUID CRITERIA

The first study task is directed at the identification of vapor chamber working fluids and their range of operating temperatures suitable for use in Brayton cycle radiators dissipating heat at temperatures between 20° and 350° F. The criteria established for the selection of candidate fluids consider life expectancy, performance and operational factors. The working fluid characteristics and critical parameters considered desirable are listed in Table 3-2. A more detailed discussion of these parameters and their influence on the vapor chamber performance is included in Section 4.

TABLE 3-2. WORKING FLUID PERFORMANCE PARAMETERS

Evaporative Heat Transfer (high)
● Vapor Pressure (moderate)
Vapor Flow Parameter $-\rho_v \lambda$ (high)
● $\rho_v$ - Vapor Density (high)
● $\lambda$ - Heat of Vaporization (high)
Condensing Heat Transfer (high)
● Liquid Thermal Conductivity (high)
● Good Wettability with Wick & Containment Vessel
Capillary Pumping Parameter - $\frac{\sigma \rho \lambda}{\mu}$ (high)
● $\sigma$ - Liquid Surface Tension (high)
● $\rho$ - Liquid Density (high)
● $\lambda$ - Heat of Vaporization (high)
● $\mu$ - Liquid Viscosity (low)
Fluid Freezing Point (low)
Thermal Stability (high)
Radiation Stability (high)
Chemical Inertness with Containment Vessel/Wick (high)

### 3.5 LIFE EXPECTANCY CONSIDERATIONS

The reliability requirements specified for the vapor chamber radiator, reference Table 3-1, are the following:

1. Sufficient vapor chamber redundancy is to be provided for maintaining 64°F radiator primary fluid after five years of operation with a probability of 0.99 and 0.999 in each of two evaluations.
2. Protection of the primary radiator fluid circuit is to be based on the probability that at least one of two independent primary radiator fluid loops will survive the threat of meteoroid damage after five years of operation for manned missions at 0.99 and 0.999 in each of two cases.

The five-year life requirement places an increased emphasis on the long life design and reliability of the system. A number of critical design features of importance are discussed below.

A potential advantage of employing vapor chambers in a radiator is that the vulnerable area of the primary radiator fluid loop can be substantially reduced. In turn, this reduces the meteoroid armor requirements. The individual vapor chambers are also vulnerable to failure by meteoroid puncture; the failure of one, however, is independent of the failure of any other parts of the radiator. Tradeoffs of redundancy of components or panels versus distribution of additional meteoroid armor are required to provide best performance within the five-year life expectancy criteria.

Meteoroid criteria used in the study is contained in Subsection 3.6.

A second failure mechanism to be considered is residual gas buildup within the vapor chamber which reduces the working volume and useful radiating surface area. Gases can be generated by any of the following processes:

1. Thermal decomposition of the working fluid
2. Radiation decomposition of the working fluid
3. Outgassing of the containment structure
4. Chemical reaction of fluid with wick and containment vessel.

The chemical reaction between the working fluid and the vapor chamber or wick causes corrosion. Some corrosion is expected to occur over the five year period, but it is

desired that this phenomena be self-limiting where the corrosion layer becomes a barrier inhibiting further corrosion. Uninhibited corrosion will eventually violate the integrity of the vapor chamber and cause leakage of the working fluid. The requirement for the five year space application is that corrosion does not cause leakage nor should the residual gas buildup be significant so as to reduce operational performance below specifications. The proper selection and sizing of materials and fluids are required. Additional design considerations involving the structural integrity of the chamber include:

1. Radiation damage causing reformation of chamber grain structure
2. Locked in stresses caused by improper annealing
3. Unaccounted for vapor pressures at design operating conditions.

### 3.6 METEOROID CRITERIA

The meteoroid criteria used in this study reflected current recommendations of NASA Lewis at that time. The meteoroid environment assumed is the Whipple 1963A flux density model (Ref. 1) with an average meteoroid velocity of 20 km/sec and a meteoroid density of 0.5g/cc. Many of the previous radiator studies at GE-SD assumed an average velocity of 30 km/sec and a meteoroid density of 0.44g/cc. The estimates specified for this study result in a 22 percent reduction in armor thickness. The use of estimates of near Earth environment may be conservative for an outward interplanetary probe mission, since the flux is generally considered to decrease with heliocentric distance. Loeffler, Lieblein and Clough (Ref. 2), suggest a flux density decreasing at the rate  $(R)^{-1.5}$ , where R is the heliocentric distance. If the flux is integrated between Earth and Jupiter, assuming a constant velocity and an  $(R)^{-1.5}$  relation, the average flux is only 29 percent of the near Earth flux. However, the flux intensities in the asteroid belt and near Jupiter are anomalous, possibly comparable in intensity to the near Earth environment. Estimates of the flux in traversing the asteroid belt vary by an order of magnitude on either side of the near Earth environment, and the near Jupiter environment is as yet unexplored. A study of Jupiter fly-by missions (Ref 3) assumes a Jupiter environment three times more severe than Earth's. Volkoff, (Ref. 4) estimates



a protection requirement ratio relative to near Earth of 0.432 for a Jupiter orbit mission based on a time integrated environment. In the absence of reliable experimental data, the more conservative estimates of near Earth environment are used in this study. The damage criteria used in determining meteoroid protection requirements is that proposed by Loeffler (Ref. 2),

$$t_a = K a \gamma \rho_p^{1/6} \rho_t^{-1/6} V^{2/3} E_t^{-1/3} \left( \frac{a A_v \tau}{-\log_e P(o)} \right)^{1/3} \beta \left( \frac{1}{\beta + 1} \right)^{1/3} \beta \quad (3-2)$$

where

$t_a$  = required armor thickness in inches

$K$  =  $0.231 \text{ in.}^{1/3} \text{ cm}^{1/2} \text{ ft}^{-7/6} \text{ lb}^{1/2} \text{ gm}^{-1/2} \text{ sec}^{2/3}$

$a$  = damage thickness factor

$\gamma$  = materials cratering coefficient

$\rho_p$  = meteoroid density in  $\text{gm/cm}^3$  (0.5)

$\rho_t$  = armor material density in  $\text{lb/ft}^3$

$V$  = meteoroid velocity in feet per second (65,500)

$E_t$  = Young's Modulus of Elasticity at operating temperature in  $\text{lb/in}^2$

$\alpha$  =  $5.3 \times 10^{-11} \frac{\text{gm}^\beta \text{ particles}}{\text{ft}^2 \text{ - day}}$

$\beta$  = 1.34

$A_v$  = vulnerable (external surface) area of armor in  $\text{ft}^2$

$\tau$  = mission time in days

$P(o)$  = design probability of no critical damage

The constants  $a$  and  $\gamma$  vary from material to material and with damage mode. The cratering coefficient  $\gamma$  for a wide range of materials has been determined experimentally. Summarized in Table 3-3 are values of the cratering coefficient determined for various aluminum alloys at room temperature and  $700^\circ\text{F}$  (Ref. 5)

TABLE 3-3. ALUMINUM CRATERING COEFFICIENTS

MATERIAL	CRATERING COEFFICIENT	
	ROOM TEMP.	700 <sup>0</sup> F
7075-T6 A1	1.93	1.68
2024-T6 A1	1.97	2.06
6061-T6 A1	1.80	---
356-T51 A1	2.58	2.31

The damage thickness factors for incipient dimple, spall, and perforation have been determined for unlined aluminum tubes.

Unlined tube investigations of 2024-T6 aluminum have shown the effect of the magnitude of tube inside diameter on inner surface dimple, spall and perforation. According to Reference 5, it was found that in general, a slight decrease in a (damage thickness) factor was observed with a decrease in tube ID. Summarized in Table 3-4 are values of the incipient damage thickness factors determined for 2024-T6 aluminum at room temperature and 700<sup>0</sup>F.

TABLE 3-4. INCIPIENT DAMAGE FACTOR, a, FOR 2024-T6 ALUMINUM

	Room Temp.	700 <sup>0</sup> F
Perforation	1.7	1.7
Spall	2.3	2.1
Dimple	2.5	2.5

The damage factors given do not represent values sufficient to prevent damage. An increase in these values is necessary to prevent the occurrence of the chosen damage.

### 3.7 STRUCTURAL CRITERIA

The reference launch vehicle to be utilized with the Brayton cycle radiator in this study is the Atlas Centaur employing an Orbiting-Astronomical Observatory Satellite shroud. The 10-foot diameter Centaur stage and shroud allows a nominal 9-foot diameter cylindrical radiator with no allowance for heat rejection through the ends of the cylinder.

The supported load of the radiator is specified to be 6,000 pounds. The spacecraft weight is based on an allowance of 1,000 pounds for the radiator and 5,000 pounds of equipment mounted above and supported by the upper radiator interface.

The maximum loads occurring on the radiator will result from launch conditions. During launch, maximum " $q\alpha$ " and maximum axial acceleration conditions exist. Maximum bending loads occur when the product of dynamic pressure and angle of attack " $q\alpha$ " reach a maximum, and the maximum axial loads occur at the instant of first stage engine cut-off. If the launch structure were designed to an axial load condition only, an unrealistic result would be obtained, since it is obvious that the structure must also have some lateral stiffness. A difficulty arises in attempting to specify a realistic load condition for lateral stiffness since it is known that static lateral accelerations during launch are generally low. One approach is to design to an artificial but conservative condition such as 12 g axial combined with 5 g lateral. This approach may be reasonable for small payloads, but excessively conservative and possibly prohibitive for a payload whose size and mass are no longer insignificant compared with the launch vehicle. The load factors must decrease as the payload size increases, as evidenced by the trend shown in Figure 3-1.

Based on existing Atlas Centaur data, (Ref. 6) the maximum axial acceleration loads are 6.2 g axial and 0.3 g lateral. Maximum lateral acceleration conditions are 2.3 g axial and 1.56 g lateral. These conditions are to be utilized in the study along with the additional environmental requirements which follow.

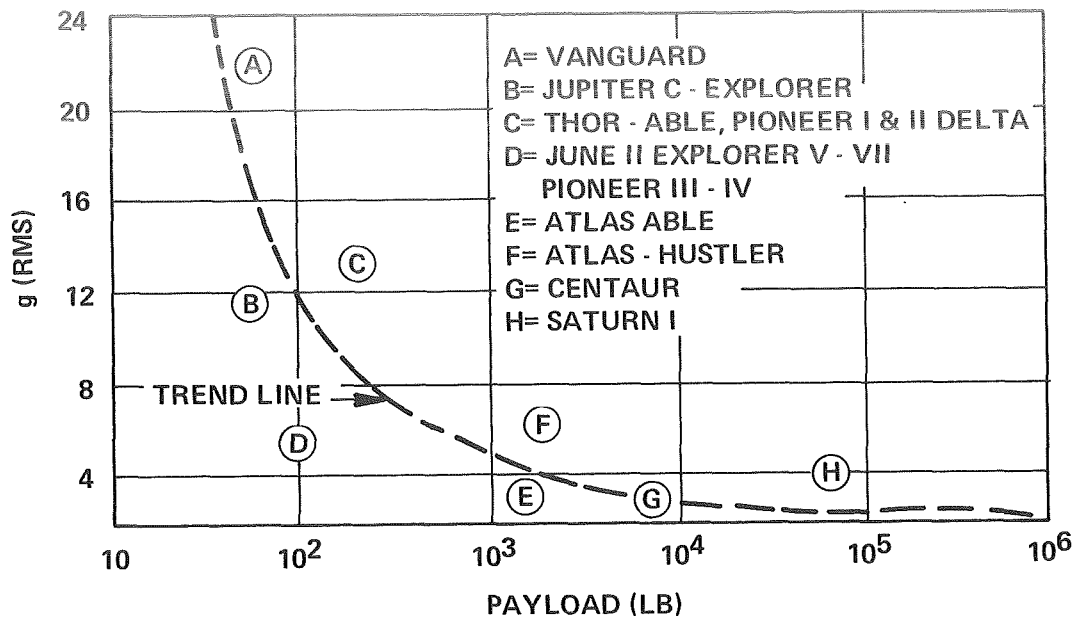


Figure 3-1. Trend in Launch Vehicle Dynamic Loads

### 3.8 STRUCTURAL ENVIRONMENTAL CRITERIA

The requirements for the vapor chamber radiator relating to the environment include the phases of ground handling, launch, and orbital operations. The vapor chamber radiator and conduction fin radiator shall be designed to withstand the anticipated environmental conditions as specified in Reference 7, and defined below, without malfunction or performance degradation.

#### 3.8.1 GROUND HANDLING CRITERIA

##### 3.8.1.1 Gravity

The vapor chamber shall be capable of operating in a one-g environment for purposes of establishing ground test performance prediction. Consideration should be given to devising a vapor chamber fin and radiator geometry capable of operating in any orientation in one-g as well as zero-g. The penalty for accomplishing this should be determined. With this requirement, one area of potential disadvantage relative

to the conduction fin radiator will be eliminated, and the operational flexibility will be enhanced.

#### 3.8.1.2 Manufacture

Wall thickness shall be sufficient to withstand normally expected tooling limits and handling techniques as well as transportation.

#### 3.8.1.3 Size

Geometric dimensions of the vapor chamber and wick shall be realistically selected to satisfy fabrication techniques.

### 3.8.2 LAUNCH, LIFT-OFF, BOOST CRITERIA

#### 3.8.2.1 Shock, Acceleration, Vibration, Acoustic Noise

The subsystem and components whether operating or not shall be capable of withstanding without performance impairment the following simultaneous launch loads applied at their mounting points and in the directions and magnitudes specified:

- a. Shock — Twenty g shock along each of three mutually perpendicular axes. The wave shape shall be a half-sine-pulse of 10 millisecond time duration.
- b. Vibration — Sinusoidal input applied at the mounting points along each of three mutually perpendicular axes.

5 to 33 cps at 0.14 inch double amplitude displacement  
33 to 140 cps at 8.0 g's peak  
140 to 240 cps at 0.008 inch double amplitude displacement  
240 to 2000 cps at 15.0 g's peak

- c. Acceleration — Six g's acceleration for five minutes along the longitudinal axis of the launch vehicle.

Three g's acceleration in the opposite direction.

Two g's acceleration in both directions along mutually perpendicular axes in the plane normal to the longitudinal axis.

The negative longitudinal and lateral accelerations are caused by low-frequency (1 to 10 cps) oscillations which last a few seconds.

- d. Acoustic Noise — The subsystems and components shall be capable of withstanding the induced vibrations while subjected to an acoustic noise field with an integrated level of 152 db, at a reference level of 0.0002 microbar for a period not less than five minutes, with a distribution as shown in Figure 3-2.

#### 3.8.2.2 Explosive Atmosphere

The subsystems and components shall be designed to minimize the hazard of fire, explosion and toxicity to the launch area personnel and facilities. The hazards to be avoided include accumulation or leakage of combustible gases, the hazard of spark or ignition source, including static discharge and toxicity due to spillage of system fluids. Applicable equipment shall be designed and fabricated to pass the explosive atmosphere test as specified in MIL-STD-810A (USAF), dated June 23, 1964, Method 511.1, Explosive Atmosphere.

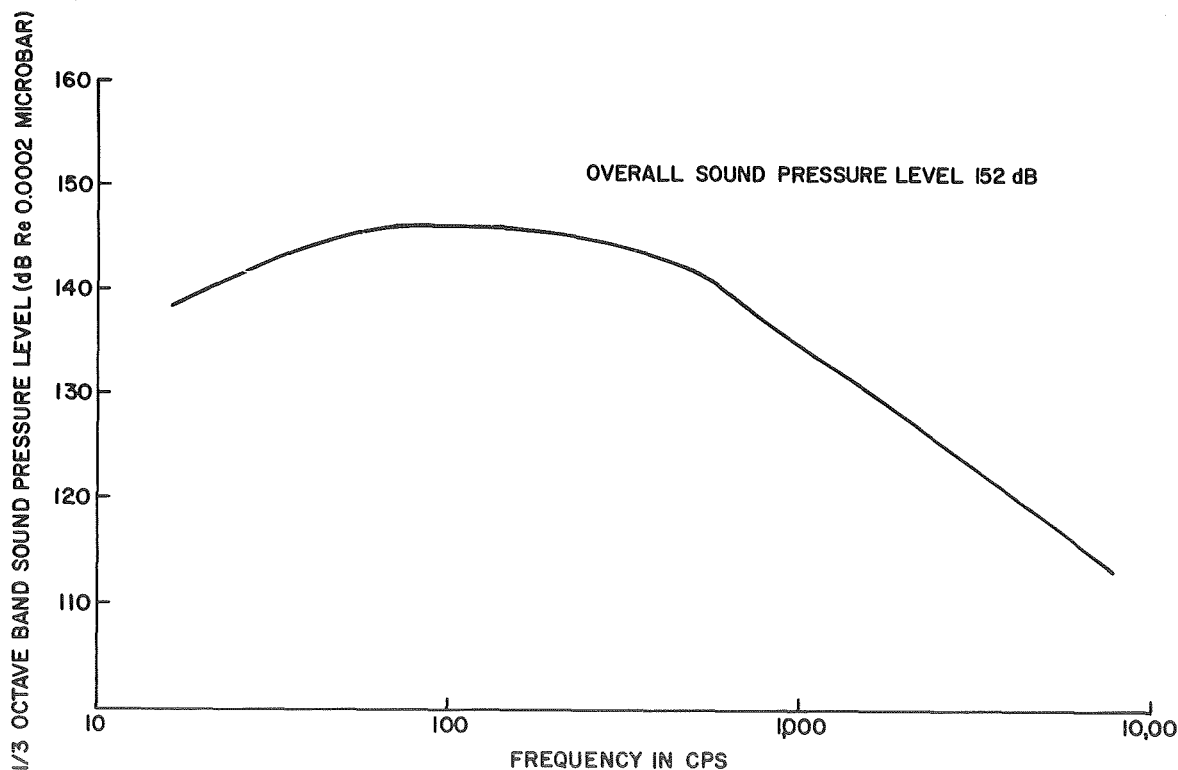


Figure 3-2. Acoustic Noise Frequency Spectrum

### 3.8.3 ORBITAL OPERATION CRITERIA

The subsystems and components shall be designed to be capable of start, shutdown, restart, and continuous operation at rated power in the natural space environment for earth orbits of from 300 to 20,000 nautical miles without malfunction or degradation for a period of five years. Space Environment Criteria Guidelines for Use in Space Vehicle Development (1965 Revision), NASA TM X-53273, dated May 27, 1965, shall be used as the space environment criteria reference.

#### 3.8.3.1 Shock

The subsystems and components shall be capable of withstanding up to 3 g's shock (course correction) having a half-sine pulse of 10 millisecond duration on each of three mutually perpendicular axes.

#### 3.8.3.2 Vibration

The subsystems and components while operating or not operating shall withstand vibrations in orbit of 0.25 g peak over a frequency range of 5 to 2000 cps for a time period of five minutes for each occurrence.

#### 3.8.3.3 Acceleration

##### 3.8.3.3.1 Short Duration

The subsystems and components shall withstand accelerations of 3.5 g in one direction along the lift-off axis, and plus or minus 1 g in all directions in the plane normal to the lift-off axis. These accelerations will be withstood individually for a period of five minutes maximum for each occurrence.

##### 3.8.3.3.2 Sustained

The subsystems and components will also be required to be capable of withstanding a continuous, unidirectional acceleration arising from a 4 rpm spin rate of the spacecraft. The g loading on the system components will be a function of their radial location with respect to the spin axis.

### 3.9 ATMOSPHERIC ENVIRONMENTAL CRITERIA

The vapor chamber and conduction fin radiators shall be designed to withstand the anticipated atmospheric environmental conditions as specified in Appendix B. The scope of this study does not allow for specific design details utilizing significant portions of this specification and therefore its detailed definition has been included in Appendix B of this report.



## SECTION 4

### WORKING FLUID SELECTION

#### 4.1 GENERAL DISCUSSION

##### 4.1.1 SPECIFIC WORK REQUIREMENTS

The first program goal was to identify suitable working fluids for the vapor chamber and to determine their range of operating temperatures. Those fluids considered were to be suitable for use in Brayton cycle radiators which dissipate heat at temperatures between 20<sup>o</sup> F and 350<sup>o</sup> F. General requirements for these fluids include:

1. High thermal conductivity, heat of vaporization and surface tension.
2. Good wettability with aluminum alloys.
3. Moderate vapor pressures.
4. Low freezing point and viscosity.
5. Thermal stability and inert chemically with aluminum alloys.

Estimates were made of the relative weights and areas of radiators employing the candidate working fluids. Based on these results plus evidence of thermal stability and corrosion resistance with aluminum alloys, the best two combinations of working fluids were selected for use in the single vapor chamber fin experiment. This work is described in the subsequent sections.

The approach formulated at the inception of the study to select the working fluid for the vapor chamber fin was:

1. Compile physical properties of candidate working fluids.
2. Perform an analytical comparative evaluation of these fluids.
3. Conduct a compatibility test program.

Vapor chamber principles were reviewed (Paragraph 4.1.2), and likely fluids were surveyed. A list of fluid properties is contained in Appendix A. Fluids which exhibited desirable characteristics (see Subsection 4.2) were selected as candidates. An analytical model for a vapor chamber fin design was formulated to perform a comparative evaluation of fluids (see Subsection 4.3). Compatibility tests were performed in parallel with the fluid evaluation using heated refluxing capsules to determine any possible gas generation or corrosion which would make the fluid unsuitable (see Subsection 4.4). Based on this comprehensive investigation, fluids were selected for the vapor chamber fin which offer the best performance potential for the Brayton cycle application.

#### 4.1.2 VAPOR CHAMBER FIN PRINCIPLES

The vapor chamber fin is a sealed duct enclosing a two-phase (vapor-liquid) working fluid. Heat is applied to the outside wall of the duct at one end, and heat is removed from the outside wall over most of the length of the duct on one or two sides. The heat transfer is accomplished internally through the actions of boiling and condensing of the working fluid on the heated and cooled sections of the duct wall, and through countercurrent mass flows of vapor and liquid within the duct. Design requirements for low temperature drop and stable heat transfer in this device include:

1. Effective distribution of liquid in a thin film over the heat input surface, and evaporative heat flux within stable limits for the fluid.
2. Maintenance of a steady, stable reflux stream of liquid, adequate to support the vaporization.
3. Vapor velocity sufficiently low to avoid entrainment of refluxing condensate in the countercurrent vapor flow and also sufficiently low to avoid flow instabilities associated with compressibility and other dynamic effects.

4. Free access of condensing vapor to the cooled wall so as to minimize thermal resistance to condensing heat transfer.

The fluid dynamics of vapor chamber fin operation are indicated schematically in Figure 4-1. Liquid is vaporized in the evaporative surface capillary structure. In the process of vaporization, a pressure rise occurs across the curved surface film interface between the liquid and vapor phases. The energy required to move the mass flow of vapor across the interface against the evaporative surface film pressure differential is supplied by the heat input. It is this energy which sustains the circulation of vapor and liquid within the duct. The effective radius of curvature of the evaporative surface film interface is necessarily smaller than that of the condensing interface, in order that a net driving pressure differential be maintained. As vapor flow takes place down the length of the duct away from the evaporation surface, the velocity is diffused as a result of condensation on the side walls. In this diffusion a rise in static pressure occurs, although this rise is reduced by the effects of wall friction. The refluxing liquid flow takes place in the opposite direction to the vapor stream within a suitable capillary structure. To sustain this flow against the frictional drag of the refluxing capillary duct, a pressure gradient is required along the length of this capillary. Since at any axial station the vapor stream and liquid stream static pressures are in general different, a curvature of the vapor-liquid interface between the liquid and vapor streams is required.

The flow phenomena in a heat pipe can be approximated to be one dimensional. For any axial position in the condenser the vapor velocity can be evaluated from the following expression

$$V = V_{\ell} \left[ 1 - X/L \right] \quad (4-1)$$

This assumes a uniform duct cross section and a uniform distribution of condensing heat transfer along the length of the duct.  $V_{\ell}$ , the vapor velocity at the evaporator/condenser interface, can be expressed in terms of the total heat transfer,  $Q$ , the heat of vaporization,  $\lambda$ , and the vapor density,  $\rho_v$ :

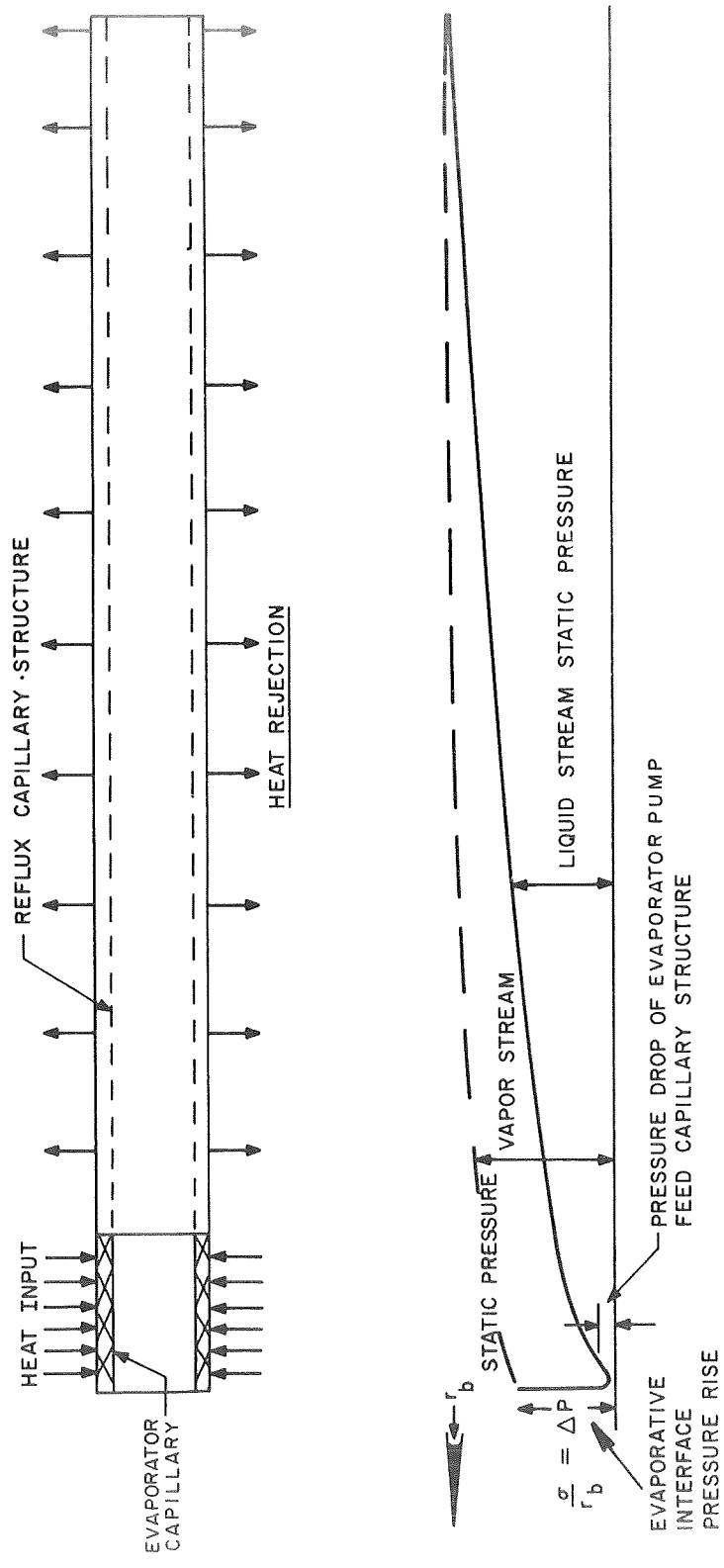


Figure 4-1. Vapor Chamber Flow Dynamics.

$$V_\ell = Q / \left( \rho_v A_v \lambda \right) \quad (4-2)$$

where  $A_v$  is the vapor flow cross-section.

The differential momentum flow equation for the vapor flow, with wall friction is

$$\frac{1}{\rho_v} \frac{dP}{dx} = \frac{2V_1 V}{g_c} \left[ \frac{1}{L} - \frac{f}{D} \frac{V}{V_1} \right] \quad (4-3)$$

where  $L$  is the vapor fin length,  
 $D$  is the hydraulic diameter,  
 $f$  is the friction factor.

In almost all cases of engineering interest, including the presently considered application,  $\rho_v$  may be treated as constant along the pipe length. When Equation (4-3) is integrated, the pressure distribution along the vapor stream is found to be like that shown in Figure 4-1. The integrated equation is:

$$P = \frac{2 \rho_v V_1^2}{g_c L} \left[ x - \frac{x^2}{2L} \right] - \frac{2f \rho_v V_1^2}{g_c D} \left[ x - \frac{x^2}{L} + \frac{x^3}{3L^2} \right] \quad (4-4)$$

Substituting  $x = L$  the pressure difference between ends is obtained:

$$\Delta P_{\text{end to end}} = \frac{\rho_v V_1^2}{g_c} \left[ 1 - \frac{2fL}{3D} \right] \quad (4-5)$$

If a refluxing capillary structure is provided which has a length  $L$ , an effective inter-layer spacing of  $d$ , and a total effective flow passage width  $W$  (including all layers), the pressure drop of the liquid flow in this capillary structure is given by:

$$\Delta P = \frac{fL}{dg_c} \left( \frac{1}{3} \rho_\ell V^2 \right) \quad (4-6)$$

(The  $1/3$  factor accounts for the linear variation of return fluid velocity along the fin length.)

For laminar two-dimensional flow between layers

$$f = \frac{24 \mu}{2 \rho_l V d} \quad (4-7)$$

$V_1$  can be expressed in terms of the total heat transfer  $Q$ ,  $W$ ,  $d$ , and the heat of vaporization  $\lambda$ .

$$V_1 = \frac{Q}{\lambda \rho W d} \quad (4-8)$$

$$\Delta P_1 = \frac{4 Q \mu}{\rho_l g_c \lambda} \left( \frac{L}{W d^3} \right) \quad (4-9)$$

In equation (4-9) the parameter  $L/W d^3$  is a function only of the refluxing capillary geometry.

To maintain the mass flow circulation needed to support the heat transfer  $Q$ , the net pressure rise in the evaporative wick structure attached to the heating surface is approximately equal to the viscous drag pressure drop in the condenser wick. The difference between these differential pressures is the pressure rise in the vapor stream.

For zero gravity operation, if the viscous drag resistance of the evaporative surface capillary flow structure is small compared to the drag resistance of the refluxing capillary, the main effect of the evaporative capillary structure upon the liquid flow will be to raise the fluid pressure. This rise occurs at the phase interface. If the effective radius of curvature of the evaporative interface surface film is  $r_b$  and  $\sigma$  the surface tension of the fluid this pressure rise is given by

$$2 \sigma / r_b = \Delta P \text{ (evaporative interface)} \quad (4-10)$$

Subject to the assumption of neglecting the vapor phase pressure drop, the overall vapor chamber pressure balance equation is:

$$\frac{\sigma}{r_b} = \frac{2 Q \mu}{g_c \rho \lambda} \frac{L}{Wd^3} \quad (4-11)$$

Equation (4-11) can be rearranged as follows:

$$Q = \frac{g_c}{2} \left[ \frac{\sigma \rho \lambda}{\mu} \right] \left[ \frac{1}{r_b} \right] \left[ \frac{Wd^3}{L} \right] \quad (4-12)$$

Equation (4-12) expresses the total heat transfer in terms of the product of three parameters:

a.  $\frac{\sigma \rho \lambda}{\mu}$

This is a function only of the working fluid properties.

b.  $\frac{Wd^3}{L}$

This is a function of the reflux capillary structure geometry.

c.  $\frac{1}{r_b}$

This is a function of the evaporative surface capillary structure geometry.

## 4.2 PHYSICAL PROPERTIES OF WORKING FLUIDS

### 4.2.1 FLUID REQUIREMENTS

A variety of physical, chemical, and thermodynamic properties of a particular working fluid must be considered in determining whether or not that fluid is suitable for the vapor chamber fin. The vapor pressure at a particular temperature is an important property. Low vapor pressure could limit the evaporative heat flux and necessitate excessive vapor velocity for a given heat flux. High vapor pressures are thus desirable to minimize the temperature difference between the evaporative and condensing sections. On the other hand, if increased wall thicknesses are required to accommodate the high internal pressure, an overall radiator weight increase may result.

The latent heat of vaporization is an important factor for vapor chambers requiring high heat fluxes. A high latent heat of vaporization reduces the mass of fluid to be pumped through the wick and vapor passages. The unusually high latent heat of

vaporization of water makes it attractive for operation in the temperature range of tolerable vapor pressures.

The temperature limits for operation of a vapor chamber with a particular fluid are determined by the melting point of the fluid on the low temperature side. The upper temperature limit is generally due to a reduced surface tension or excessive vapor pressures.

The capillary pumping ability of the working fluid is best described by the parameter  $\frac{\sigma \rho \lambda}{\mu}$ . The highest performance of a vapor chamber is thus obtained with a fluid with high surface tension, high liquid density, high latent heat of vaporization and low viscosity. In addition, however, the capillary pumping ability is also dependent on wetting of the capillary material by the fluid. If the fluid does not wet the capillary material (that is, if the contact angle is greater than  $90^\circ$ ), no pumping will occur. In general, however, most fluids will wet most solids provided the fluid is pure and the solid surface clean. In fact, in certain operations, the ability of water to wet a metal surface is taken as a measure of the cleanliness of the surface.

One important requirement of the working fluid will be the necessity for virtually complete absence of any corrosion or thermal degradation in the heat pipe for the life of the radiator. In contrast to most corrosion problems, the structural integrity of the tube wall is not the primary consideration. Rather, it is the quantity of noncondensable gas generated in the thermal decomposition or corrosion reaction that must be avoided, since such gas collects in the condensing region and effectively prevents the flow of working fluid vapor into this region.

#### 4.2.2 IDENTIFICATION OF CANDIDATE FLUIDS

On the basis of the fluid requirements discussed in the previous section, a large number of fluids have been screened for potential application in a vapor chamber radiator operating between 20 and 350<sup>o</sup> F and constructed of an aluminum alloy. The pertinent



properties of candidate fluids are listed in Table 4-1. A complete compilation of physical properties for these fluids is presented in Appendix A. The list is arranged in the order of increasing boiling points. The general criteria for the selection of fluids were:

1. Boiling point between 0 and 300<sup>o</sup>F (propane and ammonia are exceptions)
2. Pour point less than 20<sup>o</sup>F (except water)
3. Latent heat of vaporization greater than 100 BTU/lb (except several Freons)

Along with the physical properties, Table 4-1 also lists the toxicity and flammability of the candidate fluids. While these properties might not be of primary concern, it is certainly well to consider what possible complications to experimental apparatus would be involved in the handling of noxious or extremely flammable fluids. As a general rule, a fluid with maximum allowable concentration rating of 25 ppm or less represents a serious health hazard, especially if systemic effects are possible and the liquid is volatile at normal room temperature. Similarly, propane and normal butane have low flammability limits in air, and since they are normally in the gaseous state, they represent a definite fire hazard.

Note that, in Table 4-1, ammonia, water, and the alcohols have high latent heat and high surface tension; this combination of properties is quite favorable for vapor chamber fluids operating at high heat fluxes.

Corrosion and thermal stability entries are based on the best available information in the literature, but these are tentative ratings. Actual evaluation of corrosion and thermal stability will be the subject of careful investigation on this program, as discussed in a subsequent section.

TABLE 4-1. PERTINENT PROPERTIES OF POTENTIAL WORKING FLUIDS FOR A VAPOR CHAMBER OPERATING IN THE 20 TO 350°F RANGE\*

Name	Formula	°F Boiling Point	°F Melting Point	Btu/lb Latent Heat @ B. P.	Dyne/CM Surface Tension @ B. P.	Psia Critical Pressure	°F Critical Temp.	Note 1 Toxicity	Note 2 Flammability	Note 3 Thermal Stability	Note 3 Corrosion Resistance With Al
Propane	C <sub>3</sub> H <sub>8</sub>	-43.8	-305.9	183.2	7	618	206.2	None	2.2 - 9.5%	A	A
Ammonia	NH <sub>3</sub>	-28.	-107.9	589.4	35	1636	271.2	100 PPM	15 - 28%	A	A
n-Butane	C <sub>4</sub> H <sub>10</sub>	31.1	-216.9	165.8	15	552	305.6	None	1.9 - 8.5%	B	A
Freon 11	CCl <sub>3</sub> F	74.9	-168	78.3	19	635	388.4	Slight	None	A	A
n-Pentane	C <sub>5</sub> H <sub>12</sub>	96.9	-201.5	152.6	14	489.5	385.9	None	1.40 - 7.8%	A	A
Freon 113	CCl <sub>2</sub> F - CClF <sub>2</sub>	117.6	-31	63.0	18	495	417.4	Slight	None	A	A
Methyl Alcohol	CH <sub>3</sub> OH	148.4	-144.0	473.0	19	1155	464.0	200 PPM	6 - 36%	A	D
Ethyl Alcohol	CH <sub>3</sub> CH <sub>2</sub> OH	173	-174.1	367.7	18	927	469.0	1000 PPM	3.7 - 13.7%	A	D
Benzene	C <sub>6</sub> H <sub>6</sub>	176	42.	169	22	714	553.	25 PPM	1.4 - 7.10%	A	A
Isopropyl Alcohol	C <sub>3</sub> H <sub>7</sub> OH	180.3	-127.8	287	21	779	462.5	400 PPM	2.02 - 11.8%	A	D
n-Heptane	C <sub>7</sub> H <sub>16</sub>	209.1	-131	138	13	396	512.6	None	1.10 - 6.7%	A	A
Water	H <sub>2</sub> O	212.	32.	970	59	3211	705.6	None	None	A	D
Toluene	C <sub>6</sub> H <sub>5</sub> CH <sub>3</sub>	231	-139	156	18.3	590	609	200 PPM	1.27 - 6.75%	B	A
Pyridine	N:CHCH:CHCH:CH	241.	-43.6	193	28	817	657	5 PPM	1.81 - 12.4%	B	A
o-Xylene	C <sub>6</sub> H <sub>4</sub> (CH <sub>3</sub> ) <sub>2</sub>	291.9	-13.3	149	17	530	678	200 PPM	1.00 - 6.00%	?	A
n-Nonane	C <sub>9</sub> H <sub>20</sub>	302.4	-64.6	126	11	362	565	None	0.83% - ...	A	A

\*Fluids are arranged in order of increasing boiling point.

NOTES:

1. Toxicity column shows maximum allowable concentration in air for 8-hour exposure
2. Flammability column shows flammability limits in air by volume. EXPL denotes explosion limits (by volume) in air
3. Tentative thermal stability and corrosion ratings with Al: A - excellent, B - good, C - fair, D - poor

#### 4.2.3 PRELIMINARY FLUID PERFORMANCE ANALYSIS

Four processes are involved in the circulation of working fluid in a vapor chamber which result in net heat transfer from the heated end to the radiating end. These processes are:

1. Evaporation of the fluid at the heat input surface
2. Flow of vapor through the tube to the surface cooled by radiation
3. Condensation of the vapor at the surface cooled by radiation
4. Capillary pumping of the condensate back to the heated surface and distribution on the heated surface.

Any one (or more) of these processes may make up the principal thermal resistance at typical low rates of heat flux. However, it is unlikely that condensation is a limiting mechanism in the present application due to the inherent efficiency of this process and the relatively large area available for condensation.

In the following discussion, a comparison is made of the calculated performance of selected fluids chosen from Table 4-1. These fluids were selected primarily on the basis of their expected high performance and partly on the basis of readily available fluid properties. The performance parameters are evaluated at temperatures corresponding to vapor pressures between 1 and 300 psia. These limits do not, of course, represent absolute cut-off points but rather represent the range of probable application of the fluid. The fluids may be conveniently grouped into three categories; namely,

1. The relatively low boiling point refrigerant fluids (ammonia, n-butane and propane)
2. Mid-range boiling fluids (Freon 113, methyl alcohol, ethyl alcohol and water) which could possibly prove useful over nearly the entire temperature range
3. The relatively high boiling point fluids (pyridine and xylene) which could provide lower vapor pressures and thus lower stresses on the tube at temperatures

above 300°F, where deterioration in strength of aluminum alloys becomes rather appreciable.

#### 4.2.3.1 Capillary Flow Comparison of Fluids

As described in Paragraph 4.1.2 (Equation 4-12), the capillary pumping performance of fluids may be compared on the basis of a parameter,  $g_c \frac{\sigma \rho_\ell \lambda}{\mu}$  where  $\sigma$  is the surface tension of the fluid,  $\rho_\ell$  the liquid density,  $\lambda$  the heat of vaporization, and  $\mu$  the liquid viscosity. This parameter is a function only of the working fluid properties. In Figure 4-2, the capillary flow parameter is plotted against temperature for the selected fluids between 20 and 350°F. A rather arbitrary vapor pressure cutoff has been imposed also; namely, 1 psia on the low temperature side and 300 psia on the high pressure side. It is interesting to note that each curve contains a rather broad maximum near the normal boiling point of the particular fluid. The increase in the capillary flow parameter on the low temperature side of the boiling point is due to the increase in surface tension with temperature with relatively small changes in the other physical properties involved in this parameter. The decrease in the parameter on the high temperature side of the maximum occurs when the decrease in latent heat, liquid density and surface tension is more rapid than the decrease in viscosity. The parameter, of course, decreases to zero at the critical temperature where both the latent heat and surface tension become zero. In Figure 4-2, the superiority of water, ammonia and methyl alcohol in terms of capillary pumping in this temperature range is apparent.

As vapor chamber fluid temperature increases, the heat rejection capacity of the condenser section also increases according to the Stephan-Boltzmann relationship for radiant heat transfer. A greater demand is thus placed upon the capillary forces to return more condensate to the evaporator. Dividing the parameter  $\lambda \rho_\ell \sigma g_c / \mu$  by  $\sigma_B (T_f^4 - T_S^4)$ , where the radiating temperature  $T_f$  is assumed to be the condensing temperature and  $T_S$  the sink temperature, a dimensionless parameter is obtained. This parameter, shown in Figure 4-3, can be regarded as a figure of merit for the condenser operation for each fluid which must be large enough to match the evaporator capability of the vapor chamber.

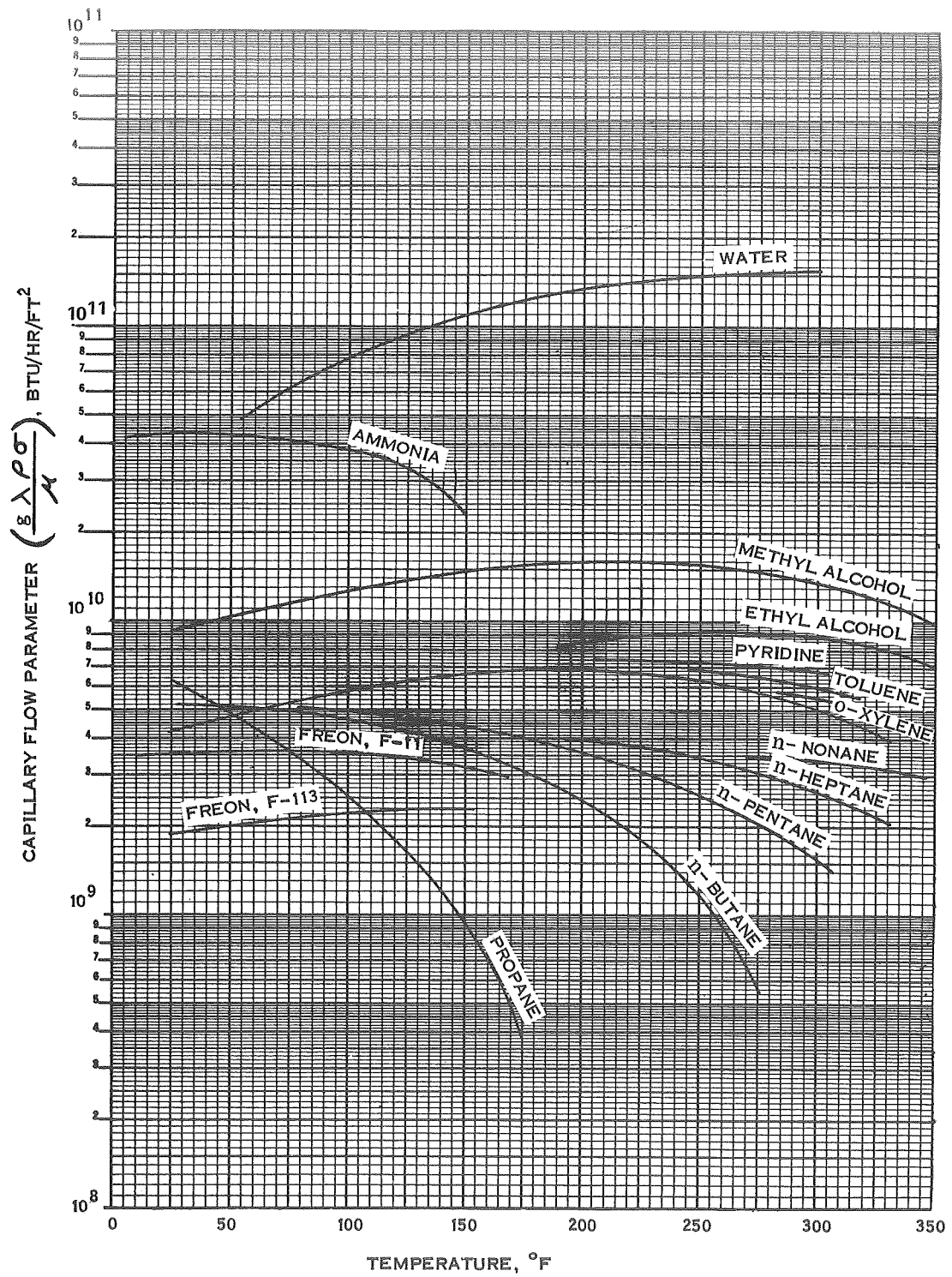


Figure 4-2. Capillary Flow Parameters vs Temperature for Vapor Chamber Working Fluids

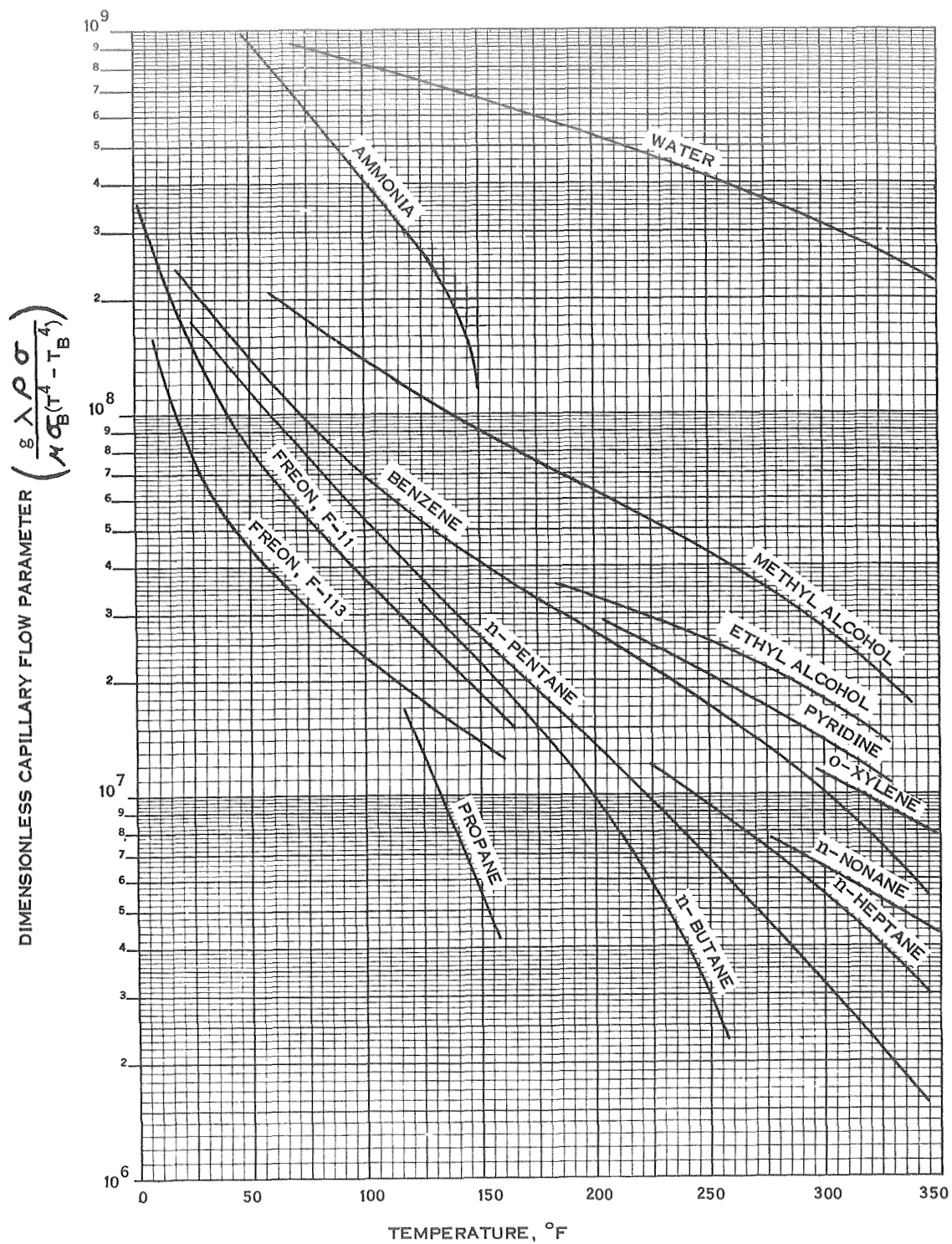


Figure 4-3. Dimensionless Capillary Flow Parameter vs Temperature for Various Fluids

#### 4.2.3.2 Vapor Flow Comparison of Fluids

The problem of excess thermal resistance due to vapor flow may be generally avoided by minimizing the vapor velocity for a given heat flux. In an earlier section, the vapor velocity at the evaporative surface was shown to be inversely proportional to the product  $\rho_v \lambda$ , where  $\rho_v$  is the vapor density. The vapor flow parameter  $\rho_v \lambda$  is plotted against temperature in Figure 4-4. Note that by maximizing this parameter, the vapor velocity is minimized. In Figure 4-4, the high and low temperature cutoff points again correspond to vapor pressures of 1 and 300 psia. It can be shown from the ideal gas law that vapor density is directly related to vapor pressure. Therefore, maximizing  $\rho_v \lambda$  generally means selecting a fluid with a high vapor density (and vapor pressure) at the temperature of interest.

#### 4.2.3.3 Boiling Heat Flux Comparison of Fluids

The fundamental limitation on heat transfer by boiling is the critical heat flux. Considerable information is available on the values of critical heat fluxes for various fluids under a variety of operating conditions. The values of the critical heat flux for a number of organic liquids boiling at pressures up to 95 percent of the critical pressure were correlated by Cichelli and Bonilla (Ref. 8) by plotting the critical heat flux  $(q/A)_c$  divided by the critical pressure as ordinate versus reduced pressure as abscissa (Figure 4-5). This is a convenient basis for comparison of the various fluids since it involves only the vapor pressure and critical pressure. A similar comparison is made for the fluids under consideration in Figure 4-6, where the critical heat flux (BTU/hr ft<sup>2</sup>) is plotted against temperature for vapor pressures in the range 1 to 300 psia. In Figure 4-5, the maximum in the curves reflects the maximum in the correlation which occurs at a reduced pressure of 0.35. It is estimated that the water and ammonia curves maximize at very high critical heat fluxes due to their very high critical pressures.

#### 4.2.3.4 Vapor Pressure Comparison of Fluids

In Figure 4-7, the vapor pressures of the fluids are plotted against temperature for vapor pressures in the range from 1 to 300 psia. The general similarity between this curve and Figure 4-4 is obvious.

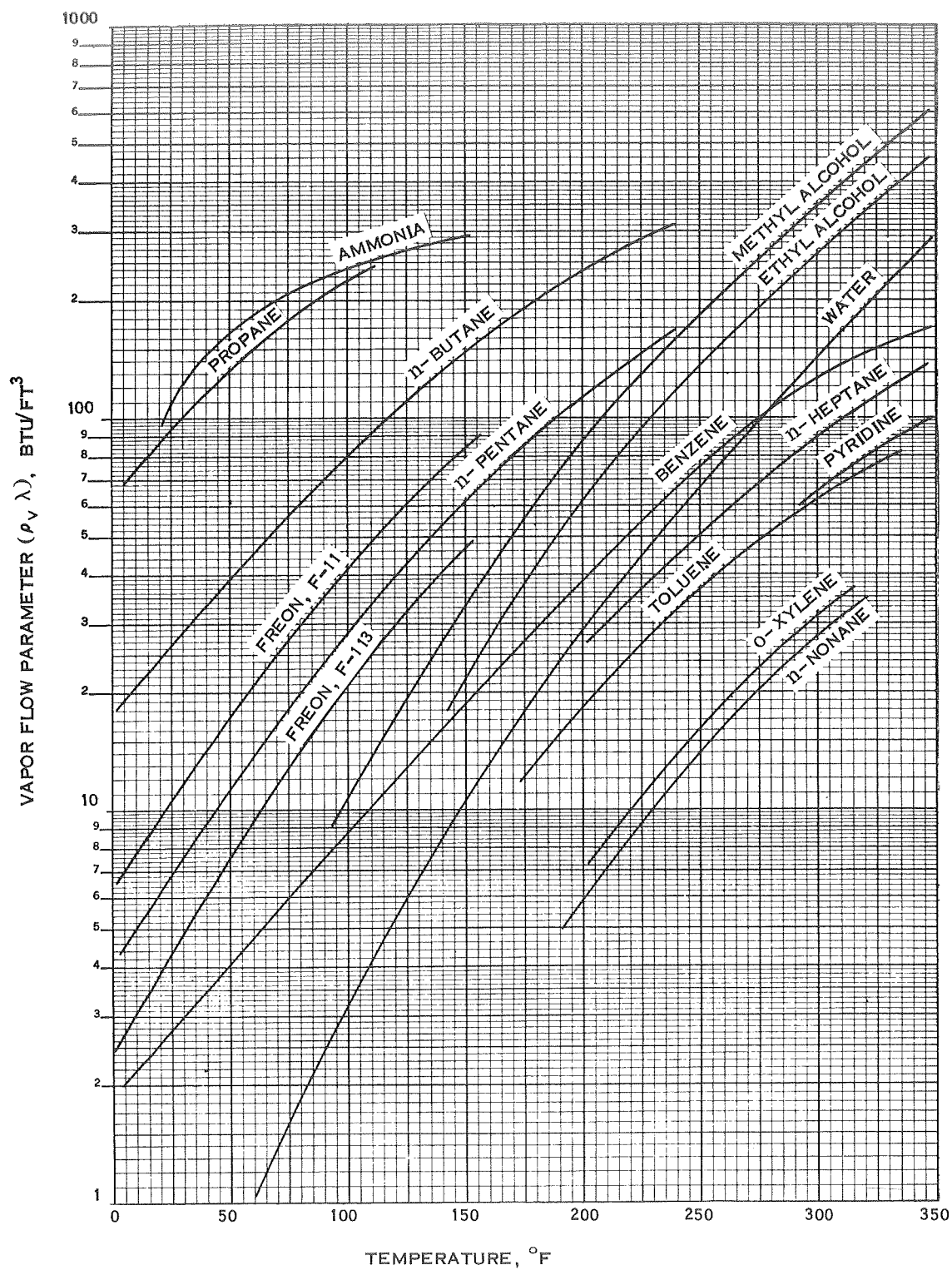
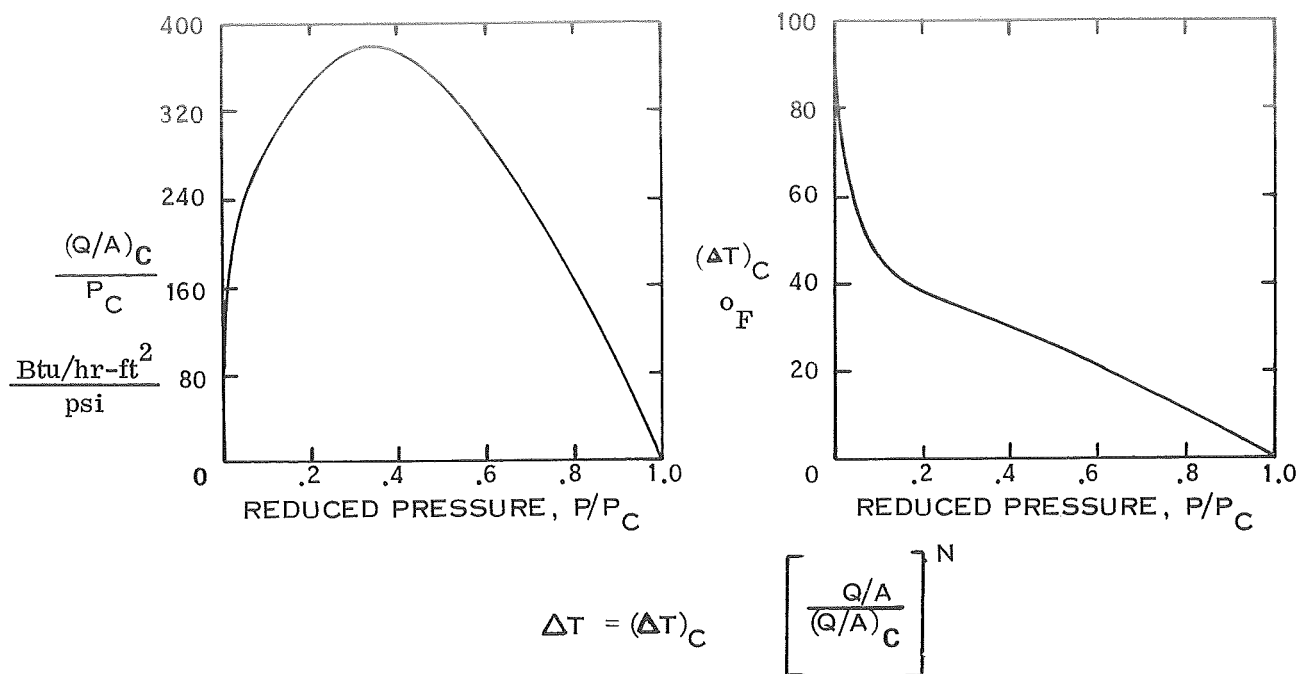


Figure 4-4. Vapor Flow Parameter vs Temperature for Various Fluids





WHERE  $N = 1/4$  TO  $1/3$

Figure 4-5. Cichelli and Bonilla Correlation

#### 4.2.3.5 Radiation Sensitivity of Vapor Chamber Working Fluids

The working fluid in the vapor chamber must have predictable properties to insure the continuous transfer and dissipation of waste heat by the systems radiator.

The effects of radiation on these fluids must be ascertained and subsequently taken into consideration during materials selection and radiator design in order to insure the successful performance of the system throughout the intended mission. The effects of ionizing radiation on liquids generally results in decomposition of the liquid with gaseous liberation and variations in their viscous properties.

Although experimental data is lacking for the majority of candidate working fluids, data is available concerning radiolysis of ammonia and freon which indicates that the threshold for significant decomposition (0.5 mol %) of these liquids may occur at an absorbed dose of approximately  $10^6$ - $10^7$  Rad.

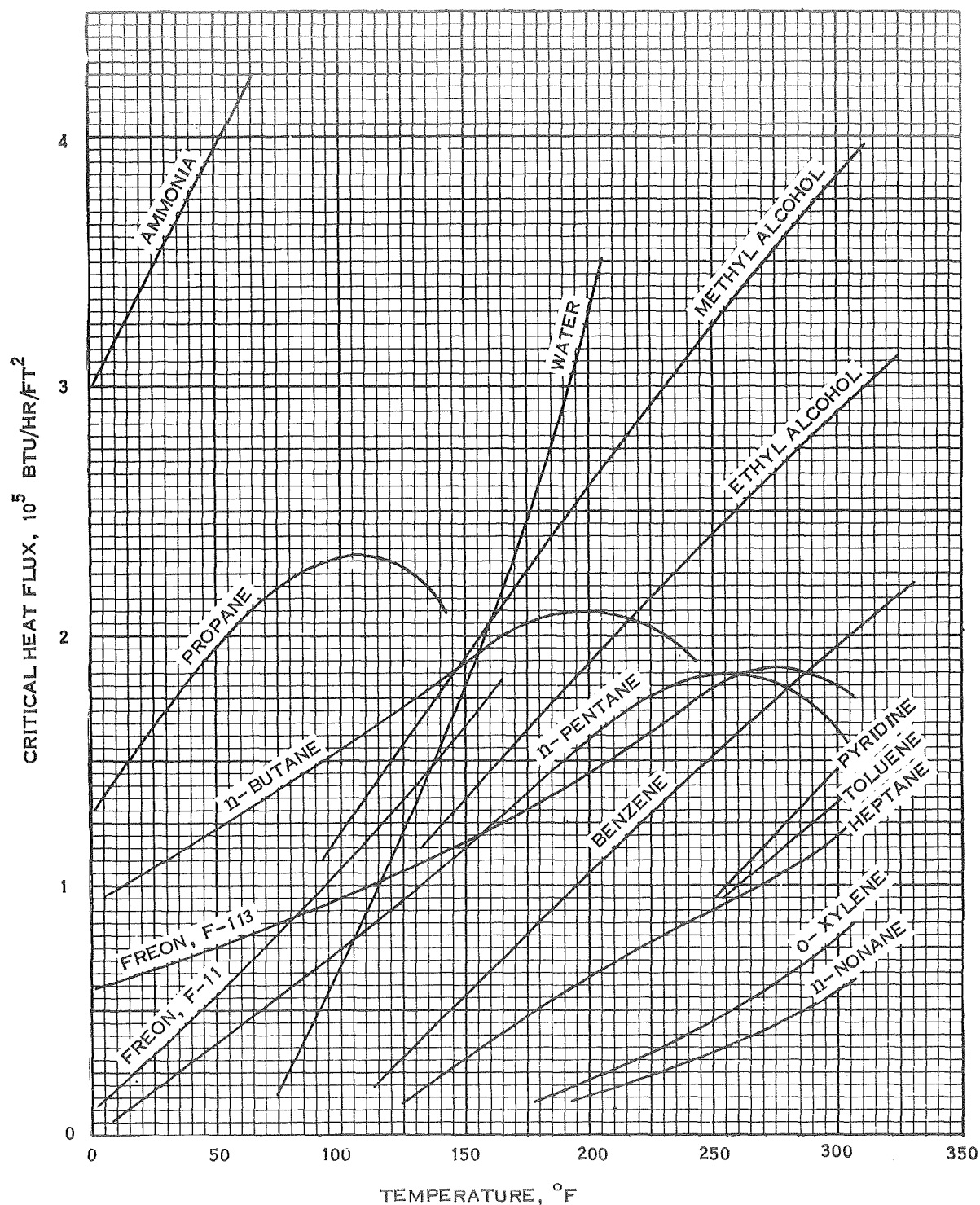


Figure 4-6. Critical Heat Flux vs Temperature for Various Fluids

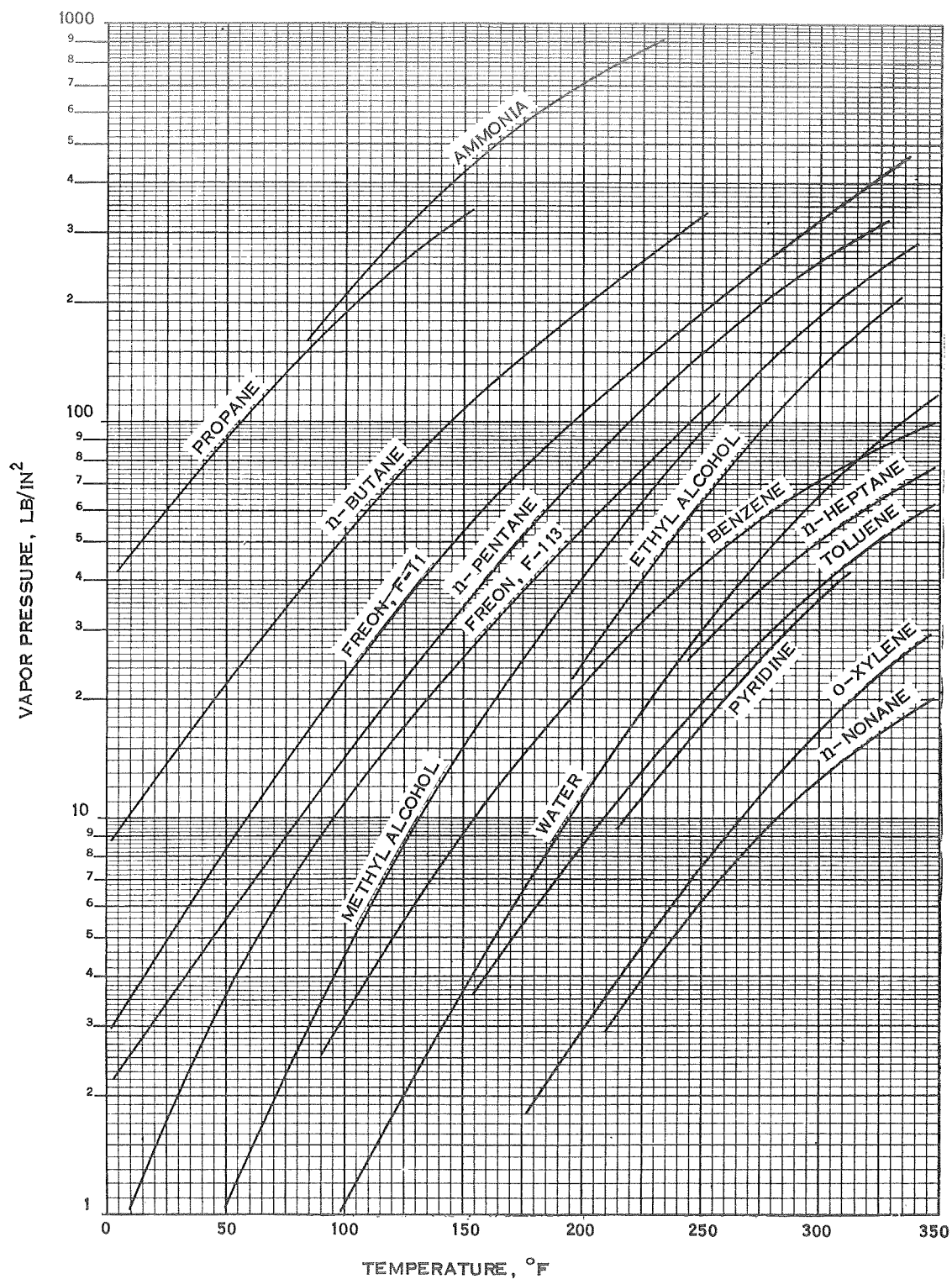


Figure 4-7. Vapor Pressure vs Temperature for Various Fluids

Further, it has been noted that the radiation-induced decomposition of organic liquid appears to increase linearly with the absorbed dose (Ref. 9).

It has been observed that a considerable reduction in the efficiency of a refrigeration system using freon was caused by an absorbed dose of  $2.5 \times 10^8$  Rad gamma (Ref. 10). In addition, viscosity changes in these fluids, particularly the benzene mixtures, appear to begin at absorbed doses of approximately  $10^7 - 10^8$  Rad (Ref. 9).

In order to assess the sensitivity of the working fluids to a variety of radiations, an estimate of the vapor chamber radiation environment after passage through  $1 \text{ gm/cm}^2$  of aluminum has been made, and is shown as a function of altitude in Figure 4-8. If the fluid is contained within a thickness at least of aluminum, there appears to be little damage from environmental radiation. However, weight competitive systems will very likely use thicknesses on the order of  $0.2$  to  $0.3 \text{ gm/cm}^2$ . Therefore, significant radiation doses will result and some form of radiation screening of the candidate fluids will be required.

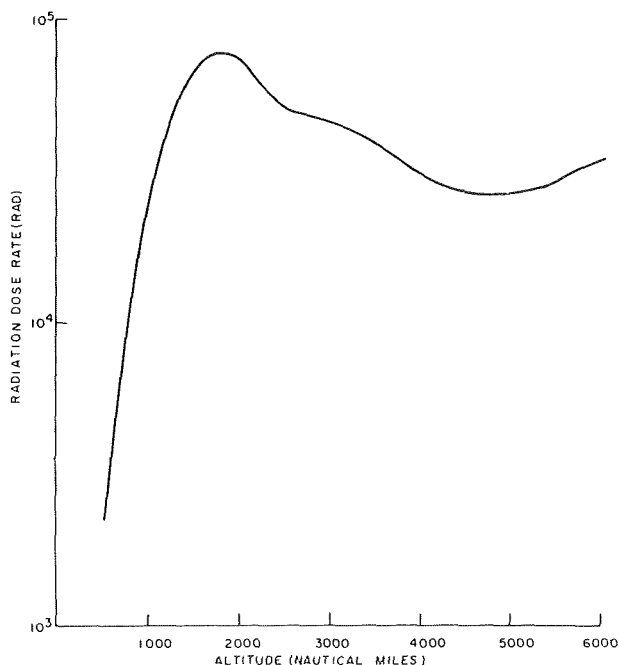


Figure 4-8. Total Yearly Ionization Dose ( $1 \text{ gm/cm}^2$  Aluminum Shielding, Polar Orbits)

In addition to the dose received from the environment, the radio isotope source may possibly contribute a significant dose to the vapor chamber working fluid. However, this dose can be effectively controlled by the spacing between the radioactive source and the radiator. Previous Brayton cycle studies (Ref. 11) show that separations of 10 feet are adequate to limit the dose to the order of 100 Rad/yr gamma radiation and  $10^{11}$  neutrons per  $\text{cm}^2$ . These doses are not expected to represent a significant problem.

#### 4.2.4 COMPATIBILITY OF CANDIDATE WORKING FLUIDS WITH ALUMINUM

The criteria for the selection of the best suited aluminum alloy to be used with the vapor chamber is shown in Table 4-2. Aluminum is a very reactive metal. Its resistance to corrosion and chemical attack is due to a thin film of aluminum oxide,  $\text{Al}_2\text{O}_3$ , which forms on the surface immediately upon exposure to the atmosphere. Such films are normally 30 to 100 Angstroms thick. A potential difference exists across this film because the metal is positive and the outer surface of the oxide is negative. This potential difference is due to the great tendency for electrons to be transferred from aluminum atoms to oxygen atoms, as indicated by the very negative free energy of formation of  $\text{Al}_2\text{O}_3$ ; that is, -150 kcal per gram-atom of oxygen. Once established, this potential difference results in an extremely high electric intensity within the film due to the fact that it is so thin. The electric intensity is, in fact, high enough to cause migration of  $\text{Al}^{+3}$  ions through the film, making them available for reaction with oxygen at the  $\text{Al}_2\text{O}_3$  - air interface. The film thus grows in thickness until the electric intensity within it is no longer high enough to cause  $\text{Al}^{+3}$  ion migration.

The film may be increased in thickness by applying an external potential difference by immersing the aluminum in an aqueous solution and making the aluminum the anode. The thickness is directly proportional to the applied potential at a given temperature and current density.

TABLE 4-2. CRITERIA FOR SELECTION OF ALUMINUM ALLOYS

Chemical Compatibility With Working Fluid
- NO gas generation
- Negligible corrosion
- Working fluid selection is quite limited
Mechanical Strength
- 50,000 hour life at 300° F
- 1% creep strength of at least 4,000 psi
Weldability
- All commercial alloys considered weldable by tungsten-electrode, inert-gas technique
- Leak tightness required
Availability
- Many alloys limited in small quantities

The  $Al_2O_3$  film is not a simple structure. It consists of several layers. The layer adjacent to the aluminum is composed of an amorphous alumina; the outer layer is crystalline in nature. Furthermore, the film has a honeycomb structure composed of adjacent pores with their axes perpendicular to the surface.

According to MacLennan, McMillan, and Greenblatt, (Ref. 10) the amorphous film adjacent to the aluminum is the most protective layer, and the outer crystalline layer is less resistant to attack; it is the rate of conversion of the amorphous form to the crystalline form which controls the rate of corrosion. They also found that nickel and iron alloying elements act cathodically and result in the formation of the amorphous barrier film during the early stages of the process. This most protective layer reaches its maximum resistance during the first 10 to 12 hours of exposure, and after this the corrosion rate is controlled by the conversion of amorphous alumina to crystalline alumina, a relatively slow process. During this early stage, the corrosion rates of pure aluminum and the corrosion resistant alloys are essentially the same. After this, the self-healing effects of the nickel and iron inclusions give the alloy a much greater resistance to attack.

The resistant alloys studied by MacLennan et. al. (Ref. 10) were two experimental alloys developed by Atomic Energy of Canada, Ltd. The composition of these alloys is given below:

<u>Alloy</u>	<u>% Ni</u>	<u>% Fe</u>	<u>% Si</u>
10155	0.5	0.5	0.2
10157	2.0	0.5	0.2

Draley and Ruther (Ref. 11) found the same sort of protective behavior for an alloy produced by the addition of 1 percent nickel to the commercial pure aluminum, 1100. This alloy is now known as X8001. These investigators also found that coupling pure aluminum (1100) with nickel markedly reduced the corrosion rate in high temperature water. Small additions (50 ppm) of easily reducible cations, such as cobalt, cadmium, and nickel to the water, also provided protection to corrosion by high temperature water (570<sup>o</sup> F). These metals are characterized by a low hydrogen over-voltage.

The water temperatures involved in the above investigations were above 500<sup>o</sup> F. In all cases, it was noted that corrosion proceeded normally for the resultant alloys during the first stages of exposure (12 to 24 hours), then decreased to very low rates. At the much lower temperatures indicated for the vapor chamber radiator under consideration, one may anticipate still lower corrosion rates and consequently much lower hydrogen production. Such alloys should therefore be investigated as possible materials of construction. It is apparent that preconditioning with 350<sup>o</sup> F water for several days before final closure of the tubes would be desirable.

The corrosion resistance of aluminum to materials other than water is generally very good and has resulted in the use of aluminum in the handling of many substances. Here again, this reactive metal depends upon its alumina surface film for its resistance to chemical attack, and any material which degrades or removes this film may result in increased corrosion.

Liquids have been selected on the basis of their physical and thermal properties as candidates for use in vapor chamber radiators. These liquids have been classified as follows:

Inorganic Materials:	water ammonia ammonia - water solutions
Alcohols:	methyl alcohol ethyl alcohol isopropyl alcohol
Amine:	pyridine
Aromatic Hydrocarbons:	benzene toluene o-xylene
Alkanes:	propane n-butane n-pentane n-heptane n-nonane
Halogenated Hydrocarbons:	freon F-11 freon F-113

That water is thermally stable in the temperature range 20<sup>o</sup> to 350<sup>o</sup> F is well known, and its corrosive behavior with aluminum at these temperatures has already been discussed. Regarding aqueous corrosion, it should also be pointed out that the use of copper as an alloying agent with aluminum increases corrosion rates with water (Ref. 12). The presence of copper ions in solution has a similar effect (Ref. 12). Mercury and mercury ions also promote corrosion (Ref. 12 and 13).

For the vapor chamber application, the production of non-condensable gases as a by-product of corrosion is a serious problem. Aluminum alloy 6061-T6 was selected as best meeting the criteria as established in Table 4-2. Experience at General Electric



with 6061 aluminum alloy vapor chambers containing water as the working fluid indicated that hydrogen evolution occurred at temperatures above 250<sup>0</sup>F. For short-term performance testing, total time 30 hours, corrosion and therefore hydrogen evolution could be effectively minimized by addition of an inhibiting agent. Although this procedure proved to be suitable for these tests, it is evident that more basic corrosion compatibilities will be required to provide the five-year life required for the proposed application. Because this information is generally not available in the literature, basic corrosion data, as it applies to the vapor chamber application, was generated by the capsule testing described in Subsection 4.4.

It is reported that anhydrous ammonia does not react with aluminum at temperatures below that at which ammonia decomposes to produce nascent hydrogen (Ref. 12, 14 and 15). Aqueous ammonia, however, does attack aluminum and its alloys (Ref. 12 and 13). According to Alcoa, the presence of iron or magnetic iron oxides can lead to pitting of aluminum when used with anhydrous ammonia. Alcoa therefore recommends that such materials be removed with a 10% HNO<sub>3</sub> rinse for 15 minutes followed by a rinse with distilled water to remove residual HNO<sub>3</sub>. The aluminum should then be preconditioned with 28 percent ammonium hydroxide for three to four hours until gas evolution ceases, followed by careful washing with distilled water and drying.

Methanol and ethanol are both reported to corrode aluminum and aluminum alloys at their boiling points when anhydrous (Ref. 16). However, the addition of a trace of water, <0.2% by weight, greatly reduces the rate (<0.001 cu in./sq.in./yr). The rate for n-propanol containing 0.2 percent water is 0.0001 cu in./sq.in./yr. The alcohols are thermally stable at temperatures of 300<sup>0</sup>F or higher. The mode of decomposition at higher temperatures is dehydrogenation (Ref. 17).

It is reported that propane and n-butane do not attack aluminum (Ref. 12). However, it is known that AlCl<sub>3</sub> catalyzes the conversion of straight-chain hydrocarbons to branched-chain hydrocarbons; a trace of chloride could therefore result in the conversion of

n-butane to isobutane (Ref. 18). The alkanes are stable in the temperature range 20<sup>0</sup> to 350<sup>0</sup> F.

The freons indicated in the foregoing tables are all stable and non-corrosive in aluminum within the indicated temperature range (Ref. 12, 14, 19 and 20). However, the water vapor content should be maintained below 20 ppm (Ref. 13).

### 4.3 ANALYTICAL COMPARATIVE EVALUATION

#### 4.3.1 ANALYTICAL MODEL OF VAPOR CHAMBER FIN

Although the major vapor chamber fin radiator design effort was performed at a later time, a preliminary design of the radiator was developed in conjunction with the fluid evaluation. The analytical model resulting from the concept illustrated in Figures 4-9 and 4-10, was helpful in comparing the performance characteristics of the various fluids. Later designs stressed the more practical aspects of developing a reliable and fabricable system.

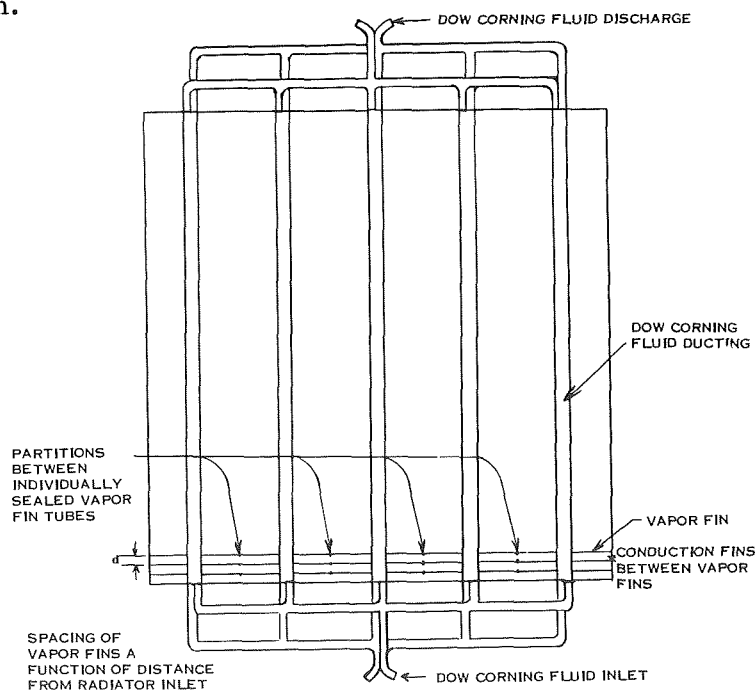
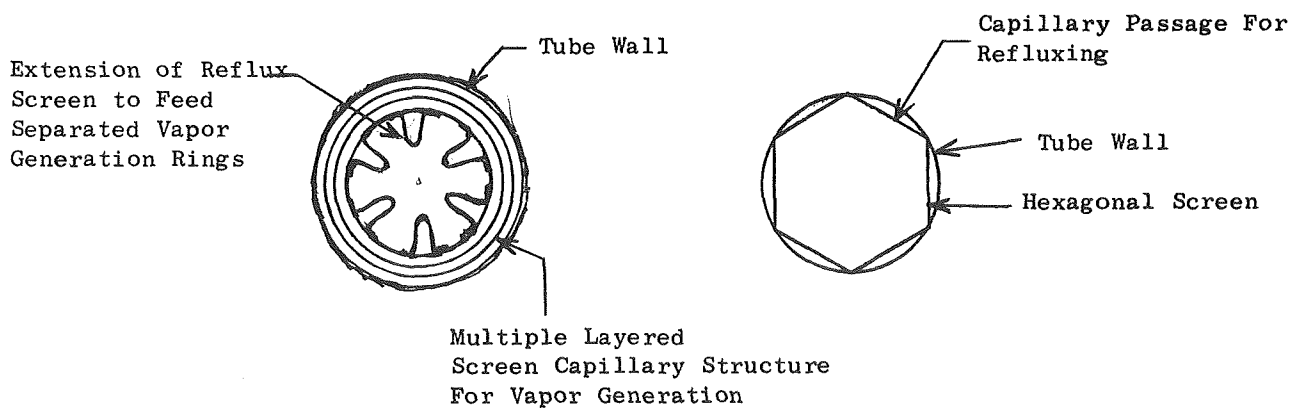
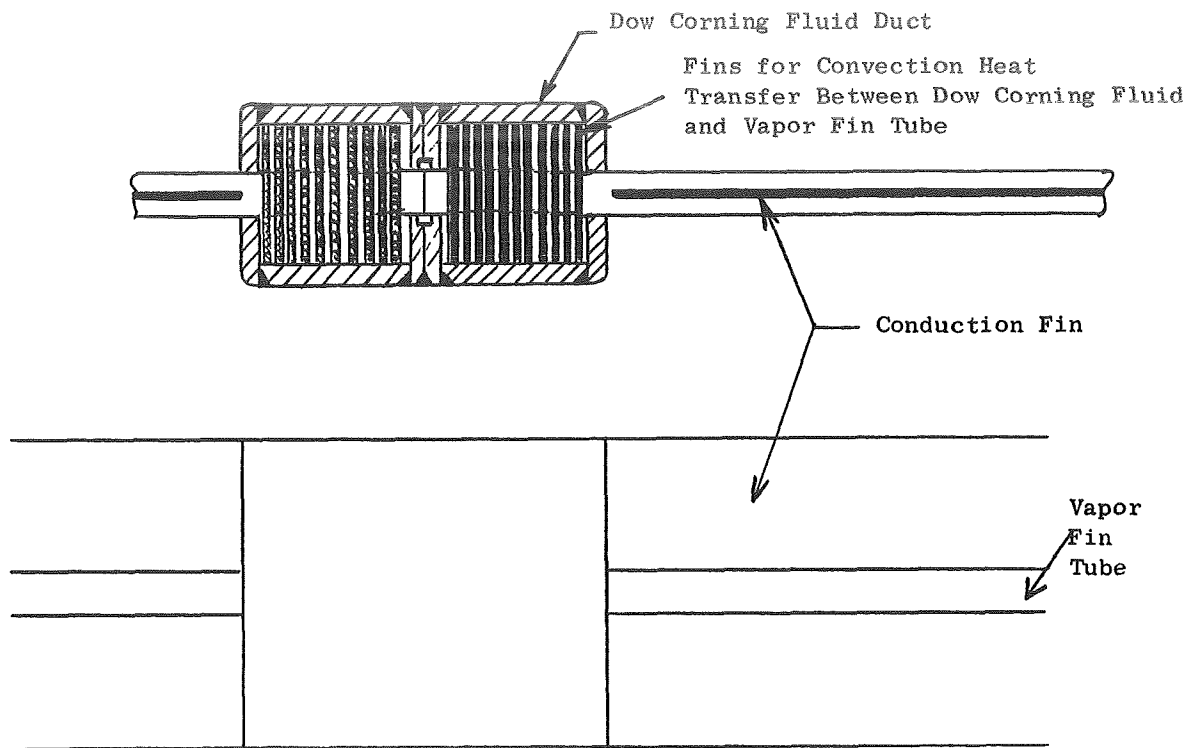


Figure 4-9. Vapor Chamber Radiator Panel



Section Thru Vapor Fin  
In Vapor Generation Section

Section Thru Vapor Fin  
In Refluxing Section

Figure 4-10. Individual Vapor Chamber Element

Three major elements comprise the radiator; these are the primary radiator fluid duct, the vapor chamber fins, and the conduction fins. The radiator arrangement is in the form of a flat panel radiating to space from both sides. Heat rejected by the Brayton cycle power conversion system is transported from a compact cooler to the radiator by a circulating primary radiator fluid loop employing Dow Corning 200 liquid. Heat from this fluid is transmitted to the vapor chambers, which in turn transmit the heat to conduction fins for final dissipation to space via thermal radiation. A typical vapor chamber radiator thermal schematic is shown in Figure 4-11.

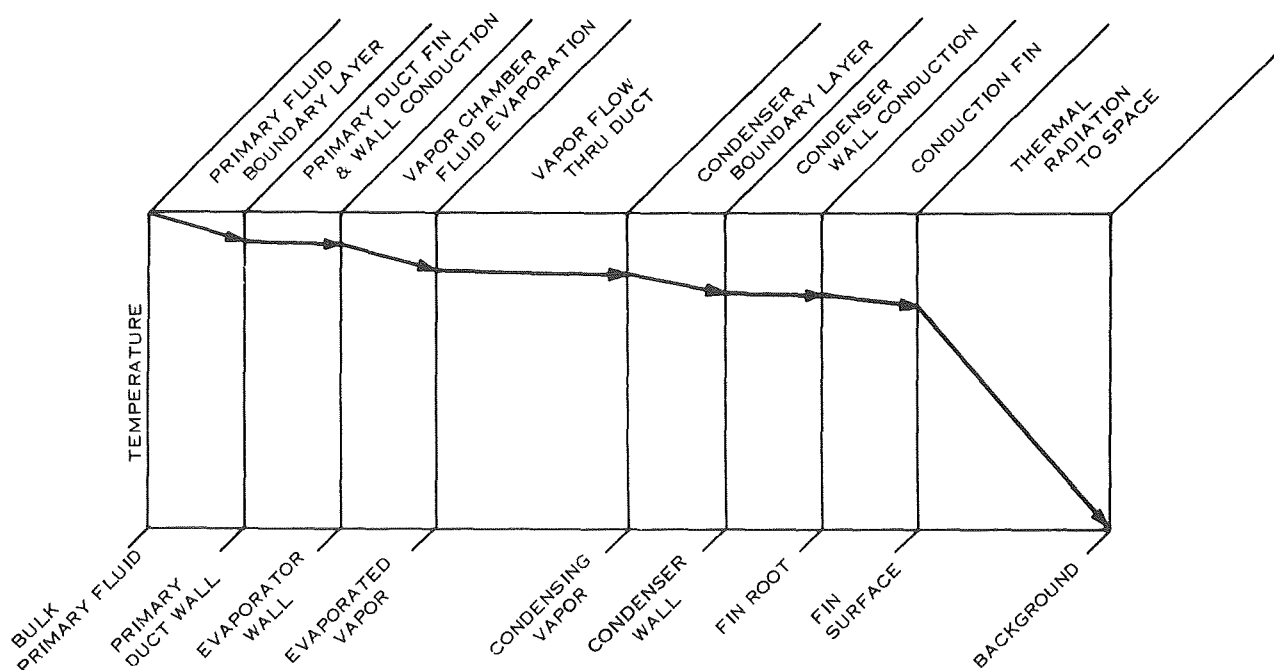


Figure 4-11. Vapor Chamber Thermal Schematic

Two independent sets of primary radiator fluid ducts are incorporated into the design. Either of these fluid ducts are capable of handling the full heat rejection load. The ducts are rectangular in cross-section and run in parallel across the radiator panel. They enclose the evaporator portion of the vapor chamber fins.

Component parts of the vapor chamber are the evaporator section, vapor flow passage, condenser section, and fluid return passage. The vapor chamber is a cylindrically shaped pressure vessel, with one end buried in the primary radiator fluid duct, and the axis of the vapor chamber running perpendicular to the direction of the primary radiator fluid ducts. The evaporator, which is buried in the duct, is externally finned to improve the heat transmission characteristics between the primary radiator fluid and vapor chamber. A special wick design is used internally to provide desirable evaporative heat transmission characteristics. Vapor flow is through the vapor chamber to the locale for condensation. Capillary structures comprised of layers of metal cloth are used on the condensate fluid return passage from the condenser to the evaporator.

The capillary wick structure is the major novelty of the vapor chamber fin concept. It includes a single layer hexagonal screen in the condenser, or reflux section, and a number of multiple (three) layer wire cloth rings spaced at short intervals along the length of the vapor generation, or evaporator, section of the vapor chamber. The outer layers of these rings fit closely to the inside wall of the vapor chamber tube. Inserted inside the inner layer are crimped extensions of the reflux screen which, in the manner indicated, feed the refluxing liquid into the three-layer wire cloth rings. Liquid is fed circumferentially through the inner two annular spaces of the three-layer ring structure and evaporation takes place between the outer ring and the heated wall. Vapor escapes into the center vapor chamber section through the spaces between the axially spaced rings.

Certain radiator characteristics and design limits have been identified for use as a basis for comparison of candidate vapor chamber working fluids; these include the following:

1. MAXIMUM LENGTH OF A  $\frac{1}{4}$ -INCH ID VAPOR CHAMBER-

Maximum length of a  $\frac{1}{4}$ -inch ID vapor chamber is determined by the capability of the reflux and vapor generation capillary structures. (One-quarter-inch diameter represents a practical minimum diameter for a vapor chamber. It is shown later that minimum weight of the radiator is attained with minimum diameter vapor chambers.)

2. VAPOR PHASE PRESSURE DROP-

Vapor phase pressure drop in a 4-foot long,  $\frac{1}{4}$ -inch diameter vapor chamber as determined by heating the middle of the tube. (Such a chamber length represents a reasonable upper limit design selection for an actual radiator. Chambers of substantially longer length are not desirable from considerations of Dow Corning fluid duct and chamber design as well as from considerations of individual vapor chamber vulnerable area and resulting meteorite armor weight.)

3. VAPOR GENERATION TEMPERATURE DROP AND HEAT FLUX RATIO-

The vapor generation temperature drop and ratio of heat flux to critical heat flux. (This measurement has been based upon a constant vapor generation length in the vapor chambers, which represents a reasonable compromise between vapor chamber temperature drop and the vulnerable area and weight of the Dow Corning duct structure.)

4. VAPOR CHAMBER CONDENSING TEMPERATURE DROP-

The vapor chamber condensing temperature drop measurement is made across the condensing interface. (This measurement is based on a condensing surface heat flux which is constant at a given chamber operating temperature level for all working fluids.)

The thermodynamic and fluid flow equations and their development for making these comparisons, presented in the subsequent subsections, are based on the following steps:

1. The conduction fin length is optimized for a particular vapor chamber fin diameter, tube weight per unit length, and temperature level. After the conduction fin length is determined, the total heat transfer per unit length of vapor chamber fin can be calculated for a given temperature level.
2. Capillary flow pressure drop calculations are made for a particular vapor chamber fin tube diameter, length, total heat transfer, and set of fluid properties.
3. Calculations are made of maximum vaporization surface net pumping heat capability for a given set of fluid properties, a given ratio of vaporization capillary feed length to width ratio ( $L/W$ ), and an optimum spacing between layers of the vaporization surface capillary.
4. The limiting value of  $L/W$  is determined as a function of fluid properties and length and diameter of vapor chamber.
5. The vapor phase pressure drop in the vapor chamber is calculated.

6. Approximate calculations are made of vaporization surface  $\Delta T$  and ratio of design heat flux to critical heat flux.
7. Approximate calculations are made of condensation surface  $\Delta T$ .

#### 4.3.1.1 Conduction Fin Analysis

The effectiveness  $n_f$  of a radiation cooled conduction fin is a function of a radiation modulus  $\lambda$  and the temperature ratio of  $T_s/T$  (Ref. 21), where

$$\lambda = \frac{2 \sigma \epsilon \ell^2 T^3}{K t} \quad (4-14)$$

$\ell$  = fin length, ft

$\sigma$  = Stefan Boltzmann constant,  
 $0.173 \times 10^{-8}$  Btu/sq. ft. hr  $(^{\circ}\text{R})^4$

$\epsilon$  = radiating surface emissivity

$T$  = fin base temperature,  $^{\circ}\text{R}$

$K$  = fin thermal conductivity,  
 Btu/hr-ft- $^{\circ}\text{F}$

$t$  = fin thickness, ft

$T_s$  = radiation sink temperature,  $^{\circ}\text{R}$

The relationship between  $\lambda$ ,  $n_f$ , and  $T_s/T$  is plotted in Figure 4-12. If a value of  $n_f$  is selected,  $\lambda$  may be determined. For the present purposes,  $n_f$  has been chosen 0.9, which yields  $\lambda = 0.1$  for essentially the entire range of  $T_s/T$  (see Figure 4-10).

The following parameter describes the conduction fin performance characteristics:

$$Q/W = \frac{2 Q_{\text{FIN}} + Q_{\text{TUBE}}}{2 W_{\text{FIN}} + W_{\text{TUBE}}} \quad (4-15)$$

where  $Q$  = total heat radiated to space by the vapor chamber tubes with conduction fins per unit length of vapor chamber tube

and  $W$  = combined weight of vapor chamber tube plus conduction fin per unit length of vapor chamber tube

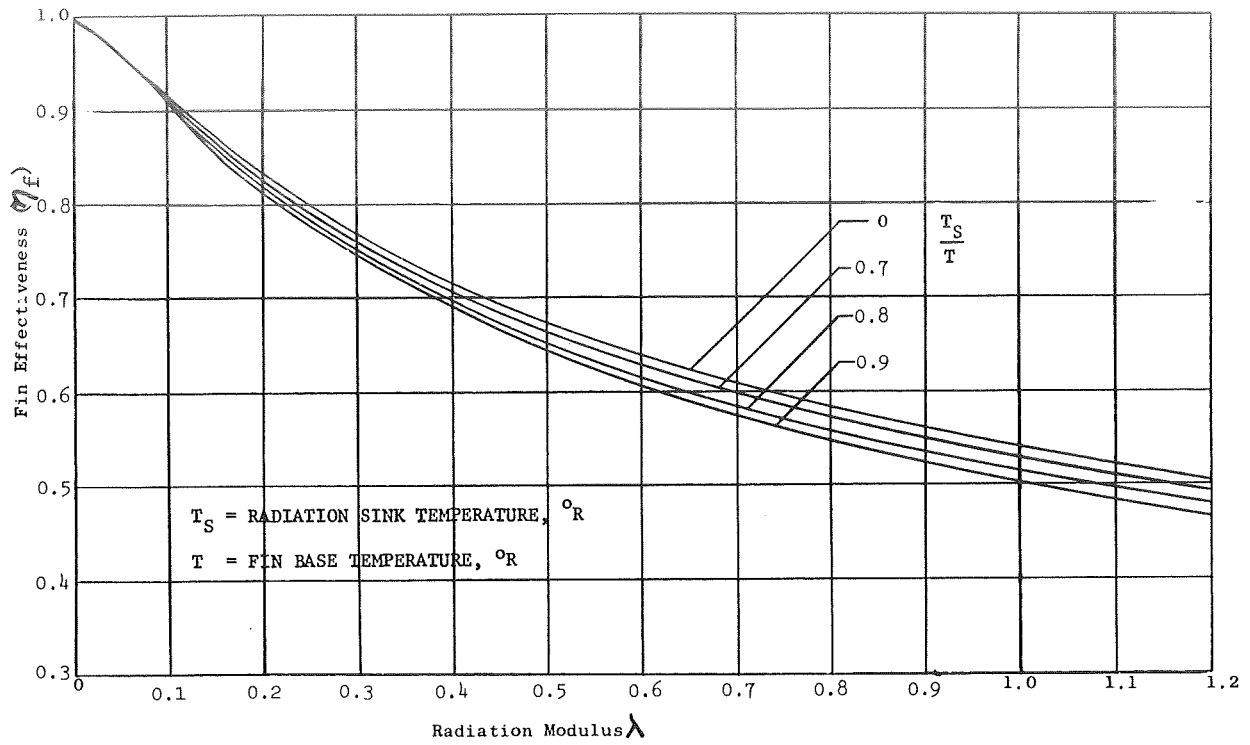


Figure 4-12. Variation of Fin Effectiveness with Radiation Modulus for Fin Radiating from Two Sides

The heat rejection and weights of the conduction fin and vapor chamber are as follows:

$$Q_{\text{FIN}} = 2 \sigma \epsilon \ell (T^4 - T_s^4) n_f \quad (4-16)$$

$$W_{\text{FIN}} = \ell t \rho \quad (4-17)$$

$$\text{where } t = \frac{2 \sigma \epsilon \lambda^2 T^3}{\lambda K}$$

and  $\rho$  = fin and tube material density

$$Q_{\text{TUBE}} = 2.5 D \sigma \epsilon (T^4 - T_s^4) \quad (4-18)$$

where  $D$  = vapor chamber tube diameter



The 2.5 factor includes a view factor between the tube and space (Ref. 22).

$$W_{\text{TUBE}} = \pi D t_{se} \rho \quad (4-19)$$

where  $t_{se}$  = effective tube thickness with allowance for wicks and working fluid inventory.

Combining Equations (4-15) through (4-19) yields the following:

$$Q/W = \frac{4 \sigma \epsilon \ell (T^4 - T_s^4) n_f + 2.5 D \sigma \epsilon (T^4 - T_s^4)}{\frac{4 \sigma \epsilon T_o^3 \ell \rho}{K \lambda} + \pi D t_{se} \rho} \quad (4-20)$$

For optimum conduction fin length  $\ell$ ,  $Q/W$  is a maximum. Differentiating Equation (4-20) with respect to  $\ell$  yields the following:

$$\begin{aligned} \frac{d(Q/W)}{d\ell} = 0 = & \left[ \frac{8 \sigma \epsilon \rho}{K \lambda} \right]^3 + \left[ \frac{7.5 \rho D \sigma \epsilon}{K \lambda n_f} \right] \ell^2 \\ & + \frac{\pi D t_{se} \rho}{T^3} \end{aligned} \quad (4-21)$$

This cubic equation must be solved to determine the optimum value of  $\ell$ . When  $\ell$  is known, the total vapor chamber heat transfer  $Q_T$  per unit length,  $\mathcal{L}$ , can be determined. The result is as follows:

$$Q_T/\mathcal{L} = 4 \ell_{\text{opt.}} (T^4 - T_s^4) n_f + 2.5 D \sigma \epsilon (T^4 - T_s^4) \quad (4-22)$$

Using Equation (4-20) the parameter  $Q/W$  for the vapor chamber fin element can be calculated. For  $\mathcal{L} = 4$  ft, the total vapor chamber fin heat transfer ( $Q_T$ ) has been calculated using Equation (4-22), substituting values of  $\ell$  obtained for solution of Equation (4-21). These values are plotted in Figure 4-13.  $Q/W$  for Equation (4-20) is plotted in Figure 4-14, and  $t$  and  $\ell$  for Equations (4-17) and (4-20) are plotted in Figures 4-15 and 4-16.

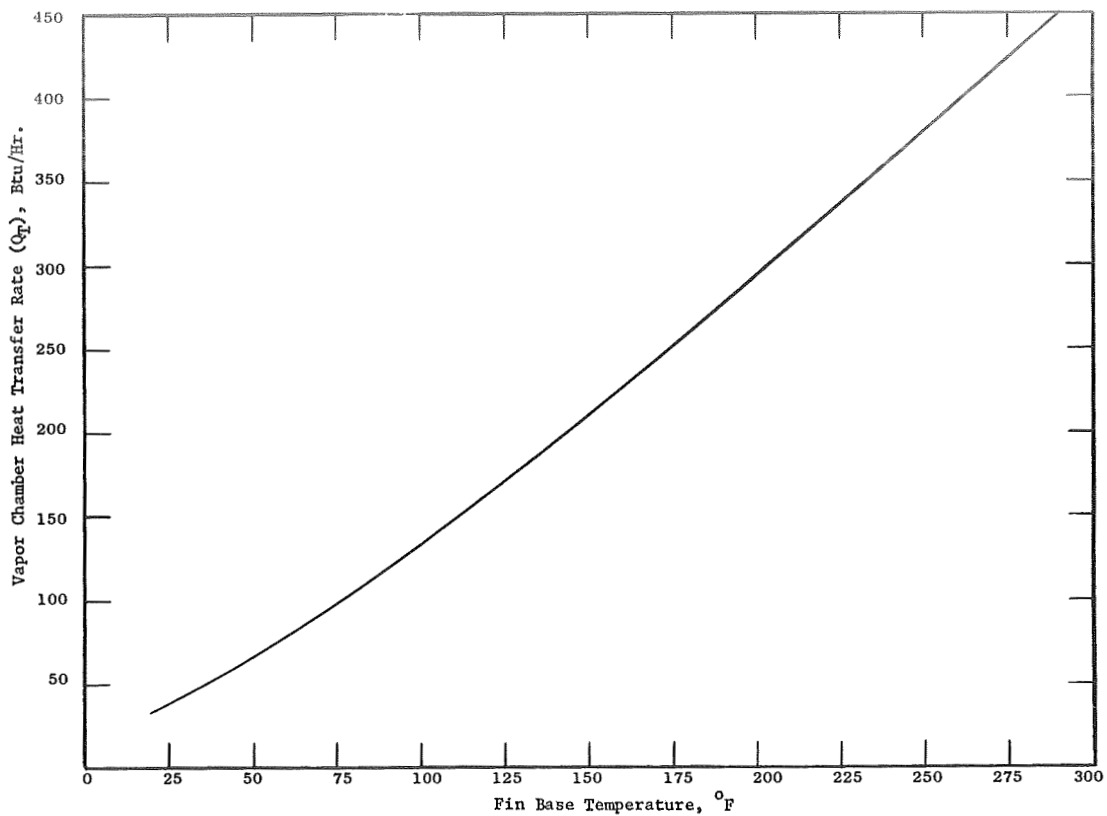


Figure 4-13. Heat Transfer Rate vs Temperature of A Single Vapor Chamber

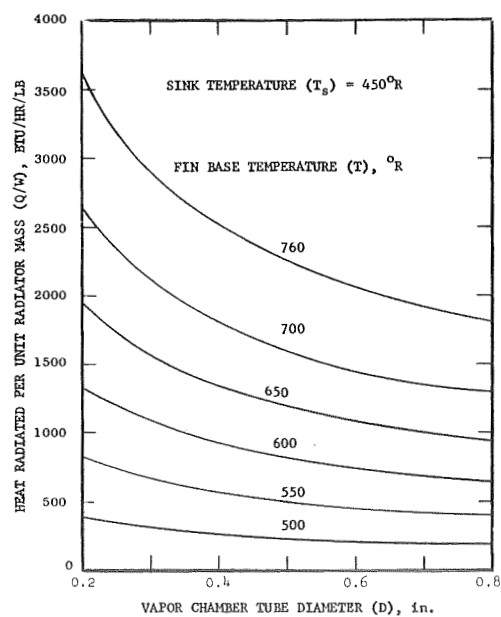


Figure 4-14. Vapor Chamber Heat Radiated Per Unit Radiator Mass

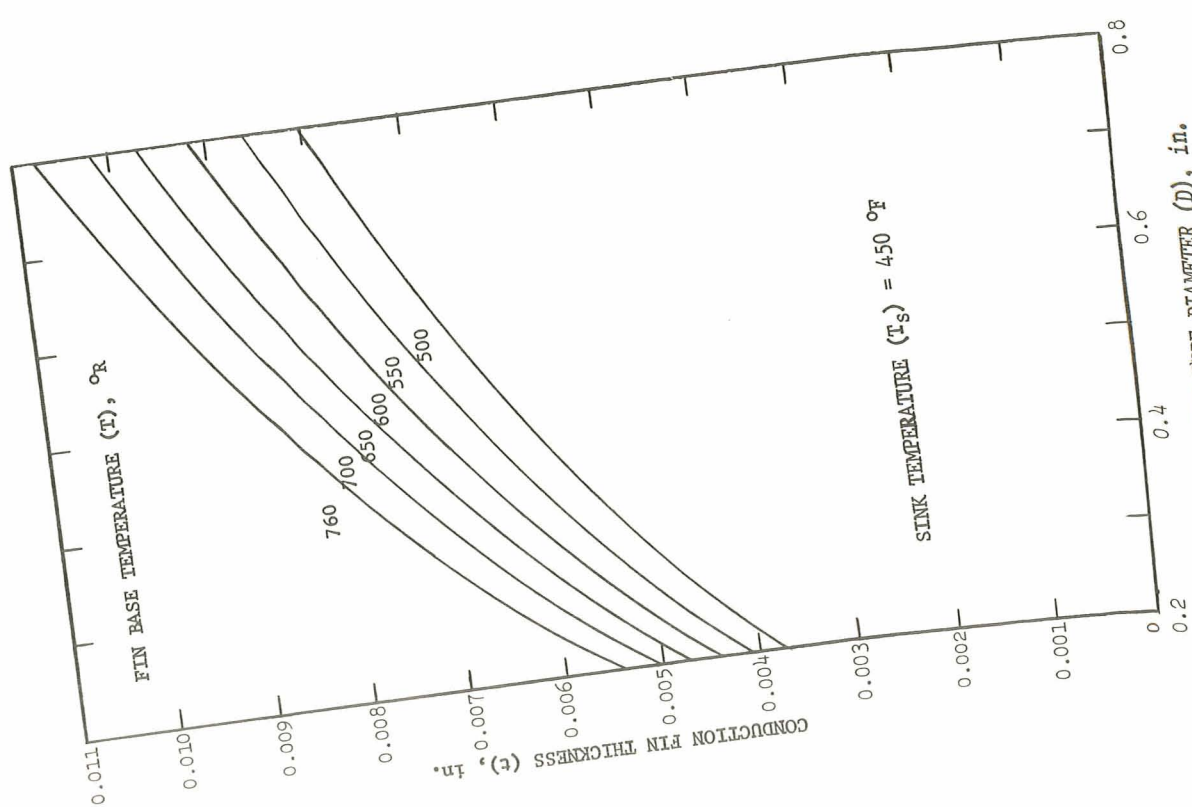


Figure 4-15. Conduction Fin Thickness vs Vapor Chamber Tube Diameter and Temperature

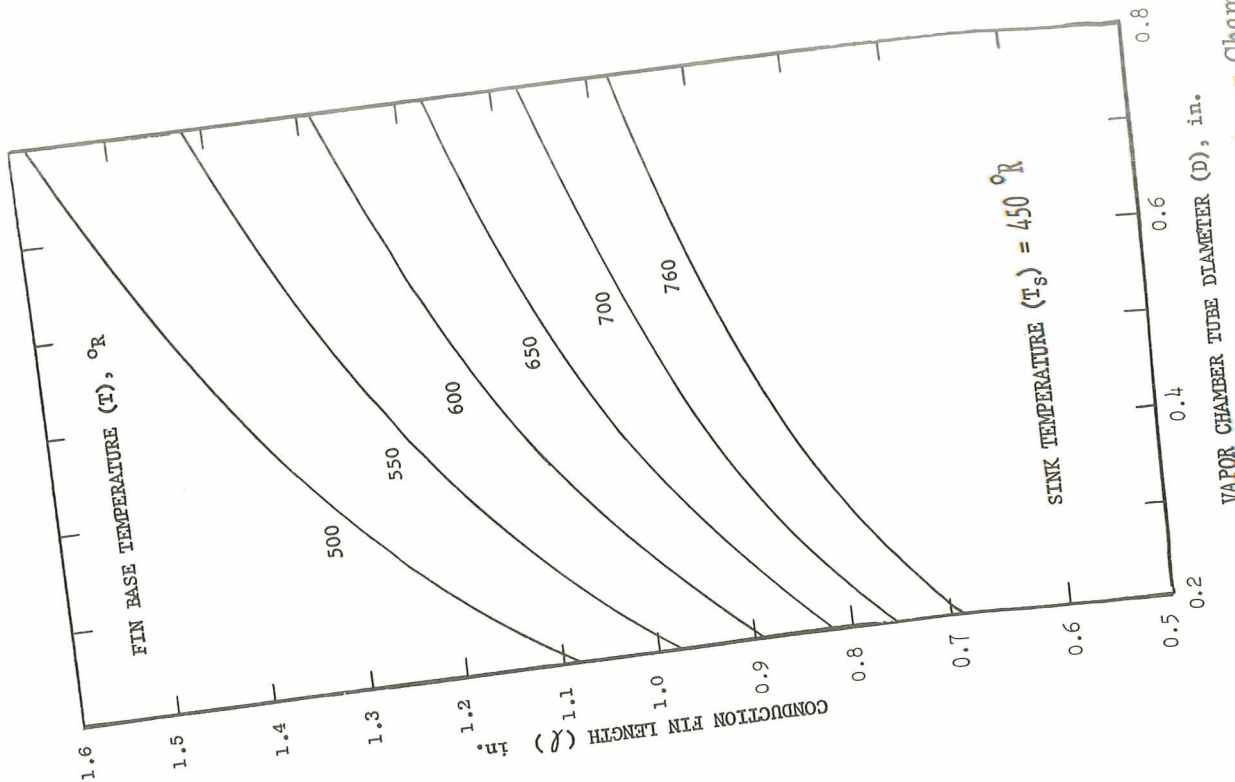


Figure 4-16. Conduction Fin Length vs Vapor Chamber Tube Diameter and Temperature

#### 4.3.1.2 Reflux Capillary Analysis

The reflux capillary is the liquid condensate return passage for the vapor chamber.

The pressure drop, generated in the reflux capillary, which must be overcome by the evaporator capillary pump pressure rise is given by the following equation:

$$\frac{dP}{dx} = -4 \frac{f}{D_h} \frac{\rho_\ell V^2}{2 g_c} = - \frac{48 \mu_\ell V}{D_h^2 g_c}$$

where  $P$  = liquid pressure

$x$  = liquid passage length

$f$  = laminar flow friction factor  $\frac{24 \mu_\ell}{D_h V \rho_\ell}$

$D_h$  = reflux passage hydraulic diameter  $0.13 D$

$D$  = vapor chamber tube diameter

$V$  = flow velocity

$\rho_\ell$  = liquid density

$\mu_\ell$  = liquid viscosity

$g_c$  = force/mass conversion factor  $\frac{1 \text{bm ft}}{1 \text{b}_f \text{sec}^2}$

The liquid velocity can be expressed as the following function of location along the vapor chamber:

$$V = V_o (1 - x/\mathcal{L}) \quad (4-23)$$

where  $\mathcal{L}$  = vapor chamber length

At the evaporator end of the vapor chamber, the liquid velocity is a maximum, and it is as follows:

$$V_o = \frac{Q_T}{\rho_\ell A_{XL} \lambda} \quad (4-24)$$

where:  $A_{XL}$  = liquid flow cross section  $\approx 0.14 D^2$

$\lambda$  = fluid heat of vaporization

Total pressure drop over the length  $\mathcal{L}$  is given by

$$\Delta P = \int_0^{\mathcal{L}} \left( \frac{dP}{dx} \right) dx = - \frac{24 \mathcal{L} \mu_{\ell} Q_T}{D_h^2 g_c A_{XL} \rho_{\ell} \lambda} \quad (4-25)$$

The reflux passage friction head is,

$$h_o = - \frac{\Delta P}{\rho_{\ell}} = \frac{24 \mathcal{L} \mu_{\ell} Q_T}{D_h^2 g_c A_{XL} \rho_{\ell} \lambda} \quad (4-26)$$

#### 4.3.1.3 Evaporator Capillary Analysis

The evaporator capillary pump structure used in the evaluation consists of a series of three layer wire cloth rings, which are spaced at short intervals along the axis of the heated portion of the vapor chamber tube. In practice, the layers of these rings are spot-welded together and to the tube by a central circumferential row of spot welds, thus forming wedge shaped feeding spaces between the layers, and between the outer layer and the tube wall. For simplicity in this comparative analysis, it is assumed that a constant spacing  $y$  is maintained between the layers and also between the outer layer and the heated vapor chamber wall. Vaporization is assumed to occur in the space between the outer layer and the heated wall, and a curved liquid-vapor interface surface of radius  $y/2$  is assumed to exist in this space. Surface tension on this curved interface maintains a pressure difference (capillary pumping pressure rise) of

$$\frac{2 \sigma_s \cos \theta}{y}$$

across the interface, where  $\sigma_s$  is the liquid surface tension and  $\theta$  is the wetting contact angle. The two interlayer spaces are used for feeding liquid circumferentially from

the points of contact (six in number) between the reflux capillary liquid flow spaces and the vaporization rings. Movement of liquid from the reflux capillaries into the ring feed spaces and from the ring feed spaces into the vaporization space occurs by radial flow through the wire cloth. The effective pumping length along feed capillaries of interlayer spacing  $y$  is designated by  $L$ .

The frictional pressure drop in the feed length  $L$  is given by

$$\frac{dP}{d\ell} = \frac{4 f^{\rho} \ell V^2}{4 y g_c} \quad (4-27)$$

since the hydraulic diameter of the feed channel is  $2 y$ .

The friction factor for laminar flow is

$$f = \frac{24 \mu \ell}{2 y V \rho_{\ell}}$$

Thus,

$$\frac{dP}{d\ell} = - \frac{12 \mu \ell V}{y^2 g_c} \quad (4-28)$$

If the average vaporization surface heat flux is  $F_{AV}$  and the axial width of the total ring surface is  $W$ ,

$$F_{AV} L V = 2 W y \rho_{\ell} V_o \lambda \quad (4-29)$$

since there are three layers and two feed spaces superimposed in the vaporization space.

$$V = V_o (1 - \ell/L)$$

$$\frac{dP}{d\ell} = \frac{-12 \mu_L F_{AV} L (1 - \ell/L)}{2 y^3 g_c \rho_\ell \lambda}$$

Integrating from  $\ell = 0$  to  $\ell = L$ , the total vaporization capillary pressure drop over the length  $L$  is

$$\Delta P_{va} = \frac{-3 \mu_\ell F_{AV} L^2}{y^3 g_c \rho_\ell \lambda} \quad (4-30)$$

$\Delta P_{va}$  adds to the reflux capillary pressure drop. The sum of the reflux and vapor passage pressure drops must be overcome by the capillary pumping pressure rise across the interface meniscus. (This assumes that the vapor phase pressure change is negligible compared to the liquid phase changes - an assumption which is justified by subsequent calculations.) Both  $\Delta P_{va}$  and the capillary pumping pressure rise depend on the spacing  $y$ . One way of determining the optimum value of  $y$  for a given  $L$  is to assume a ratio  $r$  between the reflux capillary pressure drop and the interfacial pressure rise:

$$r \frac{2 \sigma_s \cos \theta}{y} = \rho_\ell h_o \quad (4-31)$$

$$\Delta P_{va} = \frac{2 \sigma_s \cos \theta}{y} - \rho_\ell h_o = \frac{1-r}{r} \rho_\ell h_o \quad (4-32)$$

$$y = \frac{2 \sigma_s \cos \theta}{\rho_\ell h_o} \quad \text{substituting (4-32) into (4-30)}$$

$$\Delta P_{va} = \frac{3}{8} \frac{\mu_\ell F_{AV} L^2 \rho_\ell^2 h_o^3}{\sigma_s^3 r^3 g \lambda \cos^3 \theta} = \frac{1-r}{r} \rho_\ell h_o \quad (4-33)$$

solving (4-33) for  $h_o^2$

$$h_o^2 = \frac{8 \sigma_s^3 g_c \lambda \cos^3 \theta r^2 (1-r)}{3 \mu_\ell F_{AV} L^2 \rho_\ell} \quad (4-34)$$

Equation (4-34) shows that  $h_o$  is zero for  $r = 0$  and for  $r = 1$ . For optimum  $r$ ,  $h_o$  is a maximum.

$$\frac{d(h_o^2)}{dr} = 0 = \frac{8 \sigma_s^3 g_c \lambda \cos^3 \theta}{3 \mu_L F_{AV} L^2 \rho_L} (2r - 3r^2) \quad (4-35)$$

$$\text{from which } r = 2/3 \quad (4-36)$$

substituting  $r = 2/3$  in equation (4-34)

$$h_{o \max} = 0.63 \left[ \frac{\sigma_s^3 g_c \lambda \cos^3 \theta}{\mu_\ell F_{AV} L^2 \rho_\ell} \right]^{0.5} \quad (4-37)$$

Since the reflux liquid stream, corresponding to  $Q_T$ , the total vapor chamber heat transfer, is fed to the vaporization ring structure at six points.

$$F_{AV} = \frac{Q_T}{6 WL} \quad (4-38)$$

$$h_{o \max} = 1.54 \left[ \frac{\sigma_s^3 g_c \lambda \cos^3 \theta}{\mu_L Q_T \rho_\ell} \right]^{0.5} \left( \frac{W}{L} \right) \quad (4-39)$$

substituting (4-38) into (4-37)

By equating expressions (4-26) and (4-39) for  $h_o$ , an equation for the limiting (maximum) value of  $\left(\frac{L}{W}\right)$  in terms of the reflux capillary geometry, total vapor chamber heat transfer  $Q_T$ , and fluid properties can be obtained:



$$h_o = \frac{24 \mu_L Q_T \mathcal{L}}{D_h^2 g_c A_{XL} \rho_\ell^2 \lambda} = 1.54 \left[ \frac{\sigma_s^3 g_c \lambda \cos^3 \theta}{\mu_\ell Q_T \rho_\ell} \right]^{0.5} \left( \frac{W}{L} \right)$$

Solving this equation for L/W yields:

$$\frac{L}{W} = 0.00413 g_c^3 \left( \frac{\sigma_s \cos \theta \rho_\ell \lambda}{\mu_\ell Q_T} \right)^3 \frac{D_h^4 A_{XL}^2}{2} \quad (4-40)$$

For liquids making a wetting contact with a wire cloth surface, the value of  $\theta$  is essentially zero, since there is a liquid film attached to the individual wire surfaces. In this respect a wire cloth surface differs from, say, a sheet metal surface.

Equation (4-40) provides the basis for comparing alternate working fluids with respect to liquid refluxing performance. For different fluids at a given temperature level with fixed geometry, the quantities  $g_c$ ,  $Q_T$ ,  $D_h$ ,  $A_{XL}$  and  $\mathcal{L}$  are constant, leaving the expression  $\sigma_s \rho_\ell \lambda / \mu_\ell$  to account for the effect of fluid properties. Desired, with reference to fluid selection, for a given geometry and total heat transfer  $Q_T$ , is the largest possible limiting value of L/W. In order for a vapor chamber to operate at the stated  $Q_T$ , the physical value of L/W must be at least as large as the limiting value given by Equation (4-40). A positive difference between the value given by Equation (4-40) and the physical value represents a safety margin of excess of performance capability over the requirement. Alternatively, for an arbitrarily selected  $Q_T$ , tube diameter and limiting value of L/W, the maximum permissible length  $\mathcal{L}$  can be determined for various working fluids; or for a given fluid,  $Q_T$ , limiting L/W, and specified length, the minimum operable tube diameter can be found.

#### 4.3.1.4 Evaporative Temperature Drop

A major factor in the determination of required radiator area is the magnitude of the temperature drop between the Dow Corning 200 fluid and the radiating surface. This overall temperature drop has three principal components (reference Figure 4-11):

1. Convection-conduction temperature drop between the DC-200 fluid and the vapor chamber tube heated surface.
2. Evaporative surface temperature drop.
3. The condensing surface temperature drop.

A fourth possible temperature drop is between the evaporative and condensing surfaces of the vapor chamber. However, for all cases of interest in this analysis, this drop is negligible. The radiation cooled conduction fin temperature drop has already been accounted for by assigning a fixed value to the conduction fin effectiveness.

In order to estimate the temperature drop across the liquid film at the heat input section, it is necessary to know the thickness of the liquid layer and the mechanism for energy transfer. The mass transfer in a heat pipe is generally believed to be evaporative as distinguished from boiling. In fact, if the fluid in the entire heat input section were boiling, it is impossible to formulate a model in which the capillary forces draw the fluid to the interior portions of the evaporator. The onset of boiling for any particular fluid, however, is not easily predictable since it is controlled by the surface conditions of the container as well as temperature sensitive fluid properties. The presence of a fine pore wick further complicates the analytical model.

Over the expected radiator design evaporator heat fluxes it is probable that the mass transfer is due to a combination of local nucleate boiling and evaporation. This view was later supported by the experimental test data as explained in Subsection 6.5. In order to examine the vapor chamber fin radiator in its most favorable light, it was assumed that the evaporator  $\Delta T$  could be predicted by a pool boiling heat transfer correlation.

The data correlation of Cichelli and Bonilla is used (Ref. 8). In this correlation, the ratio of critical heat flux to critical pressure is plotted against the reduced pressure  $P/P_c$  (Figure 4-8). Also, the evaporative surface  $\Delta T$  at the critical flux is plotted against the reduced pressure. The ratio of critical heat flux to critical pressure peaks at a reduced pressure of approximately 1/3 and falls off to zero at reduced pressures of zero and 1. The critical  $\Delta T$  is very high (over 100<sup>o</sup>F) at values of  $P/P_c$  near zero, falls rapidly for reduced pressures between 0 and 1 and then falls less rapidly to zero at a reduced pressure of 1. At particular vapor chamber operating temperatures, the reduced pressure and critical flux was determined. From the selected fin geometry and  $Q_T$ , the vapor chamber evaporative flux was calculated. The cube root of the ratio of design flux to critical flux was taken and this factor multiplied by the critical  $\Delta T$  to get the estimated operating  $\Delta T$ . This follows from Reference 8 which states that  $q/A$  is proportional to a power of  $\Delta T$  ranging from three to four. By using the value 3 the most optimistic estimate of  $\Delta T$  is obtained. The assumption is made that the laws governing critical heat flux and  $\Delta T$  are similar in the case of the vapor chamber to the case of pool boiling. This assumption should be adequate to compare fluids, although it is entirely not accurate. In Figure 4-17, design levels of vapor chamber evaporative flux are plotted against temperature. This held for all working fluids.

#### 4.3.1.5 Condensing Temperature Drop

The condensing surface temperature drop is calculated as the temperature difference required to transfer the condensing heat flux across the mean radial thickness of the reflux capillary passage through the condensate layer by conduction.

#### 4.3.1.6 Vapor Phase Pressure Drop

Using the vapor density and viscosity, the vapor chamber cross sectional area for vapor flow, and the vapor chamber mass flow required to support the heat transfer  $Q_T$ , the vapor velocity and Reynolds number were calculated as a function of distance down the condensing section of the vapor chamber tube. In the turbulent range of Reynolds numbers an average friction factor was used, and the pressure drop calculated assuming a

linearly varying velocity and constant friction factor. In the laminar range, the Poiseville pressure drop formula was used. In all cases, using the assumed design conditions, the vapor phase pressure drop was very low, in fact, for practical purposes, negligible.

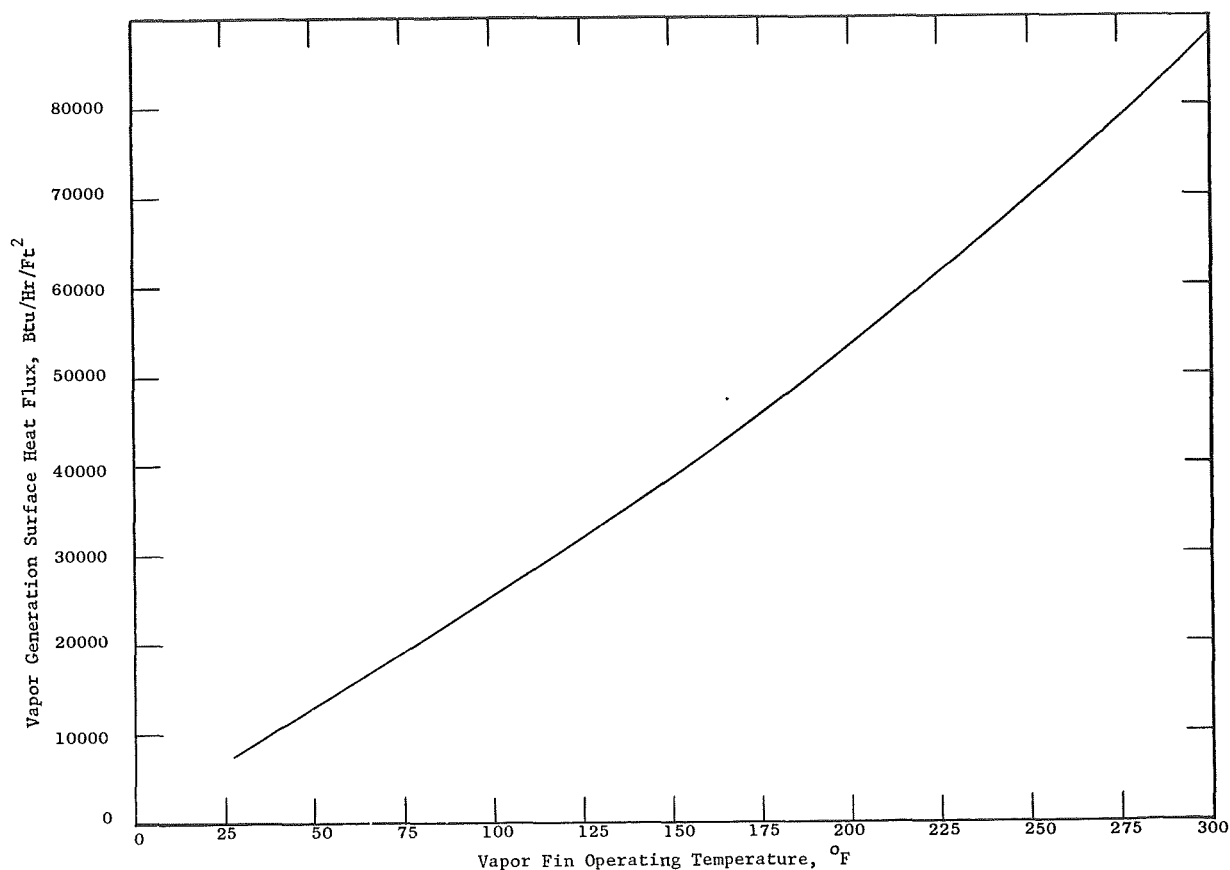


Figure 4-17. Individual Vapor Fin Evaporation Surface Thermal Flux vs Temperature

#### 4.3.2 COMPARISON OF VAPOR CHAMBER PERFORMANCE USING CANDIDATE WORKING FLUIDS

A summary of results of a comparison of the refluxing and vapor chamber total temperature drop performance for candidate working fluids is shown in Tables 4-3, 4-4, 4-5 and 4-6. Comparison parameters listed are the following:

TABLE 4-3. VAPOR CHAMBER PERFORMANCE PARAMETERS FOR CANDIDATE "HIGH TEMPERATURE" WORKING FLUIDS (AT 250°F TEMP.)

Fluid	Max. Length of 1/4 in. dia. Vapor Chamber (L/W = 1)	Req'd dia. of 4 ft. Vapor Chamber (1/4 in. assumed to be a practical minimum)	$\frac{\Delta P_v}{P_v}$ (For 1/4 in. dia. 4 ft. long Vapor Chamber)	P/P <sub>c</sub>	$\frac{(q/A)_D}{(q/A)_c}$	$\Delta T_v$ Evaporative Temperature Drop	$\Delta T_c$ Condensing Temperature Drop	Remarks
Methyl Alcohol	10.2 ft	1/4 in.	Negligible	0.08	0.22	28°F	17°F	Refluxing performance excellent; vapor flow OK, moderately high vapor fin $\Delta T$ ; good margin on critical evaporative flux
Ethyl Alcohol	7.5 ft			0.07	0.29	34°F	19°F	Similar to methyl alcohol except vapor chamber $\Delta T$ higher.
n-Pentane	5.3 ft			0.30	0.38	25°F	27°F	Similar to ethyl alcohol
Benzene	5.7 ft			0.06	0.39	40°F	27°F	Similar to ethyl alcohol except for high vapor chamber $\Delta T$
n-Heptane	4.1 ft			0.07	0.70	46°F	24°F	Similar to benzene except evapora- tive flux margin is minimal.
Pyridine (CP-32)	6.2 ft			0.02	0.43	54°F	22°F	Similar to benzene but higher vapor chamber $\Delta T$ .
Toluene	6.0 ft			0.03	0.52	52°F	32°F	Similar to pyridine — very high vapor chamber $\Delta T$ .
o-Xylene	5.7 ft			0.015	0.63	60°F	33°F	Similar to toluene but lower vapor pressure and higher vapor cham- ber $\Delta T$ .
Water	40.6 ft			0.009	0.14	23°F	5°F	By far the best on all counts. However, stainless steel tube liner is required. This results in approx. 3% radiator wt. penalty over best alternative organic fluid.
Isopropyl Alcohol	3.4 ft	.3 in.		0.06	0.35	38°F	24°F	High liquid viscosity results in poor refluxing performance.
n-Nonane	4.1 ft	1/4 in.	.003	0.017	1.0	77°F	32°F	No margin on evaporative flux and also very high vapor chamber $\Delta T$ .
Anisole	5.3 ft		.007	0.009	1.0	85°F	22°F	Similar to n-nonane.

TABLE 4-4. VAPOR CHAMBER PERFORMANCE PARAMETERS FOR ALTERNATE "HIGH TEMPERATURE" WORKING FLUIDS (AT 150°F TEMP.)

Fluid	Max. Length of 1/4 in. dia. Vapor Chamber (L/W = 1)	Req'd dia. of 4 ft. Vapor Chamber (1/4 in. assumed to be a practical minimum)	$\frac{\Delta P_v}{P_v}$ (For 1/4 in. dia. 4 ft. long Vapor Chamber)	P/P <sub>c</sub>	$\frac{(q/A)_D}{(q/A)_c}$	$\Delta T_v$ Evaporative Temperature Drop	$\Delta T_c$ Condensing Temperature Drop	Remarks
Methyl Alcohol	14.1 ft.	1/4 in.	Negligible	0.01	0.20	43°F	9°F	Relative performance of these fluids are approximately the same at 150°F.
Ethyl Alcohol	8.9 ft.			0.009	0.26	50°F	10°F	
n-Pentane	6.7 ft.			0.073	0.30	30°F	14°F	
Benzene	8.7 ft.			0.012	0.34	53°F	14°F	
n-Heptane	6.5 ft.			0.012	0.55	65°F	13°F	
Pyridine (CP-32)	6.1 ft.			0.003	0.40	65°F	12°F	
Toluene	8.7 ft.			0.005	0.55	70°F	15°F	
o-Xylene	7.8 ft.			0.001	0.61	70°F	15°F	
Water	46.5 ft.		.02	0.001	0.075	20°F	3°F	
Isopropyl Alcohol	2.9 ft.	.3 in.		0.009	0.33	52°F	12°F	
n-Nonane	5.7 ft.			0.002	0.93	85°F	18°F	
Anisole	6.6 ft.			0.001	1.65	78°F	12°F	

TABLE 4-5. VAPOR CHAMBER PERFORMANCE PARAMETERS FOR ALTERNATE "LOW TEMPERATURE" WORKING FLUIDS (AT 150°F TEMP.)

Fluid	Max. Length of 1/4 in. dia. Vapor Chamber (L/W = 1)	Req'd dia. of 4 ft. Vapor Chamber (1/4 in. assumed to be a practical minimum)	$\frac{\Delta P_v}{P_v}$ (For 1/4 in. dia. 4 ft. long Vapor Chamber)	P/P <sub>c</sub>	$\frac{(q/A)_D}{(q/A)_C}$	$\Delta T_v$ Evaporative Temperature Drop (°F)	$\Delta T_c$ Condensing Temperature Drop (°F)	Remarks
Ammonia	10.3 ft.	1/4 in.	Negligible	0.263	0.07	14	5	Best low temperature fluid. Most important point of superiority is the vapor chamber heat transfer $\Delta T$ .
Freon 11	5.4 ft.	1/4 in.	Negligible	0.08	0.23	30	21	
Freon 113	7.1 ft.	1/4 in.	Negligible	0.05	0.32	39	27	

TABLE 4-6. VAPOR CHAMBER PERFORMANCE PARAMETERS FOR ALTERNATE "LOW TEMPERATURE"  
WORKING FLUIDS (AT 40°F TEMP.)

Fluid	Max. Length of 1/4 in. dia. Vapor Chamber (L/W = 1)	Req'd dia. of 4 ft. Vapor Chamber (1/4 in. assumed to be a practical minimum)	$\frac{\Delta P_v}{P_v}$ (For 1/4 in. dia. 4 ft. long Vapor Chamber)	$P/P_c$	$\frac{(q/A)_D}{(q/A)_c}$	$\Delta T_v$ Evaporative Temperature Drop (°F)	$\Delta T_c$ Condensing Temperature Drop (°F)	Remarks
Ammonia	43.2 ft.	1/4 in.	Negligible	0.04	0.034	20	1.4	Same relative advantages as at 150°F.
Freon 11	16.3 ft.	1/4 in.	Negligible	0.011	0.12	33	3	
Freon 113	10.9	1/4 in.	Negligible	0.0035	0.16	37	4	



1. Maximum Length of a  $\frac{1}{4}$ -inch Diameter Vapor Chamber Which Will Provide a Reflux Parameter  $L/W$  (see Equation 4-40) of Greater Than One. The value 1 is a "safe" design value, inherently providing margin for vapor chamber overloading due to adjacent chamber failure, and also for departure of the interlayer clearances and other details of the vaporization surface capillary structure from the assumed optimum geometry.
2. Required Diameter of a 4-foot Long Vapor Chamber Heated at the Middle. This is believed to be a parameter of greater practical significance than (a) above, because various design considerations, mentioned above, indicate that the vapor chamber length in an optimized radiator panel will be of the order of 4 feet or less.
3. Percentage of Vapor Phase Pressure Drop Along The Vapor Chamber Length- These calculations apply to a 4-foot long,  $\frac{1}{4}$ -inch diameter vapor chamber heated in the middle.
4. Reduced pressure  $P/P_c$ . This parameter is important because it governs the limiting peak thermal flux attainable and also the  $\Delta T$  at the limiting flux, and thereby strongly influences the  $\Delta T$  at the design flux. It is desirable for maximum margin on thermal flux and minimum vaporization  $\Delta T$  that  $P/P_c$  be above 0.1 and below 0.7 (0.33 is optimum).
5. Ratio of Design Evaporative Thermal Flux to Limiting Critical Thermal Flux- This is an index of the degree of margin for overloading the vapor chamber as a result of failure of an adjacent chamber. A margin of 100 percent is desirable.
6. Evaporative Temperature Drop.
7. Condensing Temperature Drop.

Table 4-3 and 4-4 includes fluids appropriate for the high temperature end of the radiator ( $350^{\circ}\text{F}$  to  $150^{\circ}\text{F}$ ). Table 4-5 includes fluids suited for use in the low temperature end of the radiator ( $150^{\circ}\text{F}$  to  $20^{\circ}\text{F}$ ). A graphical comparison of the evaporative and condensing temperature losses obtained with each candidate working fluid is shown in Figures 4-18 and 4-19. Of the high temperature fluids indicated, water is eminently superior in all respects. The evaporative  $\Delta T$  for water was determined. The  $\Delta T$  of water is not governed by the correlation used to estimate  $\Delta T$  in the organic fluids. Next to water comes the alcohols, methanol and ethanol followed closely by the

hydrocarbon n-pentane. Pentane seems to be superior to other hydrocarbons because of the favorable value of  $P/P_c$  which reduces the evaporative  $\Delta T$ . Of the low temperature fluids compared, ammonia is markedly superior to the freons. This is due to its lower evaporative  $\Delta T$  resulting from a relatively favorable value of  $P/P_c$  and also to its comparatively high liquid phase thermal conductivity. Ammonia also has refluxing superiority but the refluxing performance of freons 11 and 113 is good enough that this difference is probably not of much practical significance for design. A comparison of the maximum condenser length obtainable within safety limits for the candidate working fluids is shown in Figure 4-20. Ammonia and water are clearly superior to other fluids indicating excellent refluxing potential for the temperature range specified.

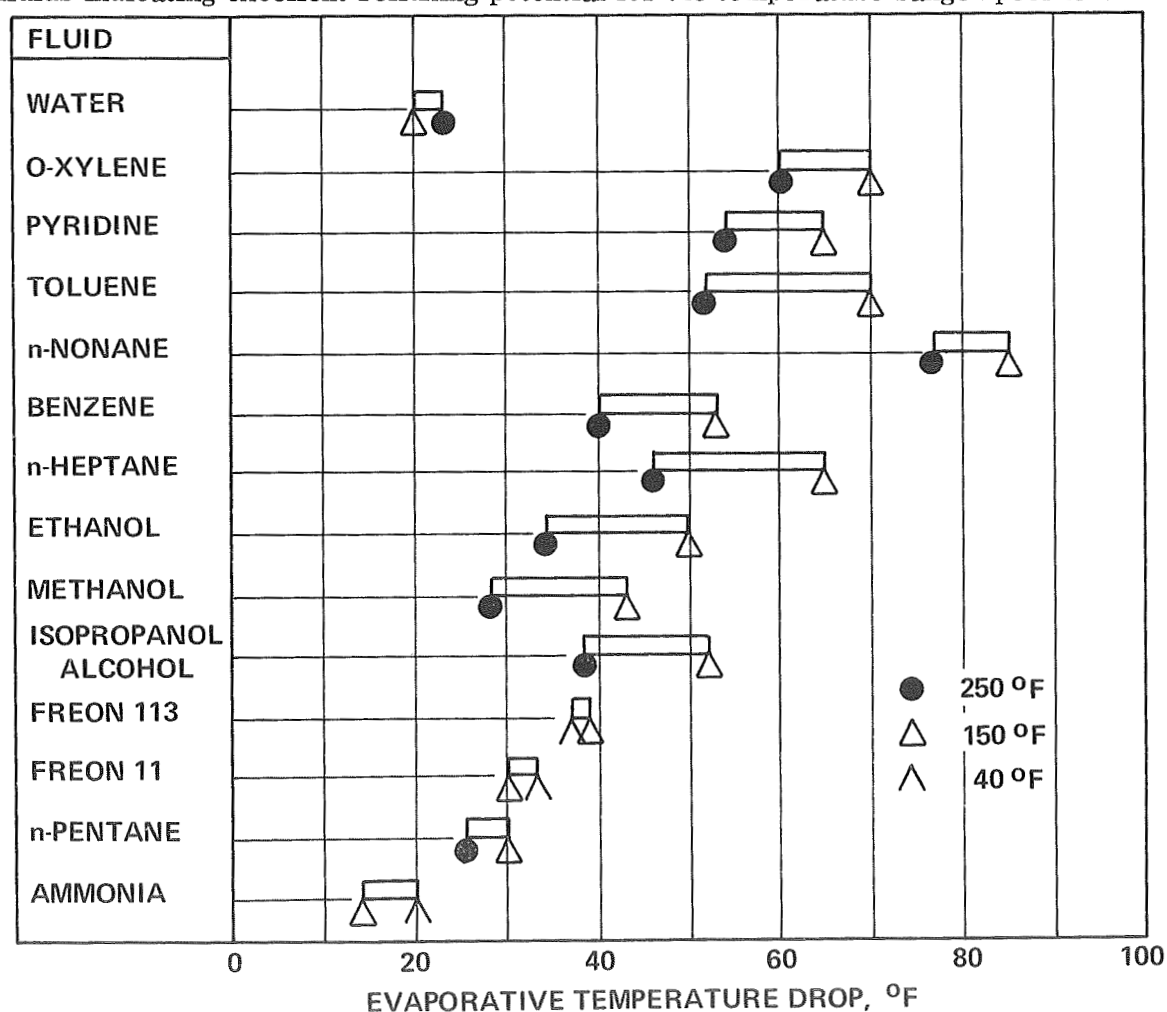


Figure 4-18. Evaporative Vapor  $\Delta T$  Comparison

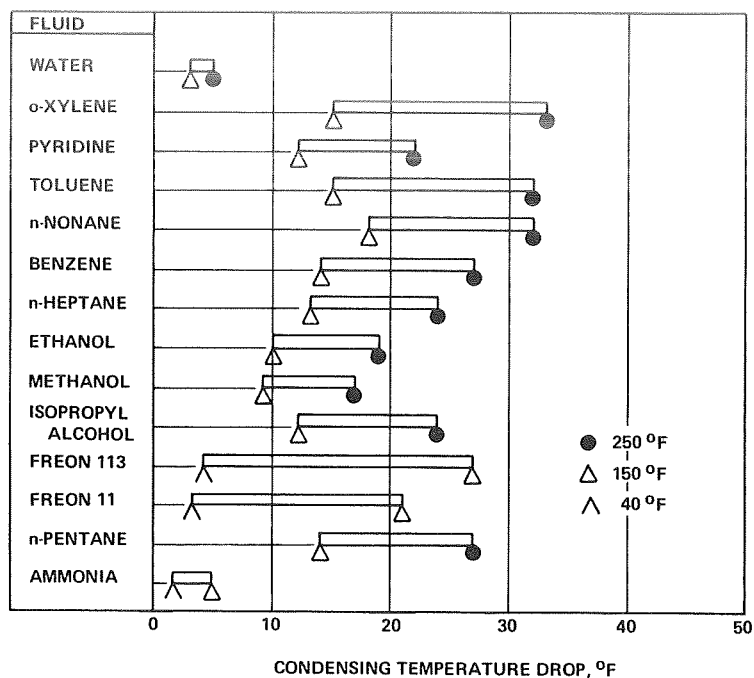


Figure 4-19. Condensing Temperature Loss

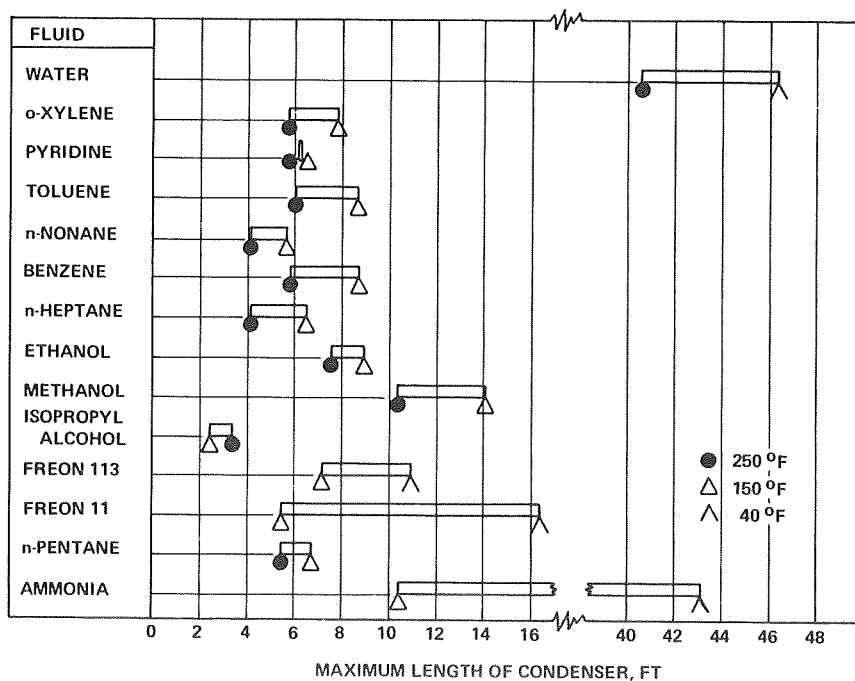


Figure 4-20. Condenser Length Limit

#### 4.3.2.1 Comparative Procedure

In order to further evaluate the design significance of the differences identified in Tables 4-3 to 4-6 between alternate working fluids, approximate calculations of radiator areas and weights have been carried out. The procedure for doing this is outlined as follows:

1. Following the method discussed above for conduction fin optimization, vapor chamber-conduction fin element dimensions were determined for a range of operating temperatures and for a range of vapor chamber wall thicknesses. Corresponding values of total vapor chamber heat transfer per unit length and of the parameter  $Q/W$  were determined.

$Q$  - Heat transfer per unit length

$W$  Weight of vapor chamber - conduction fin element per unit length

For  $\frac{1}{4}$ -inch vapor chamber tubes having several wall thicknesses  $Q/W$  is plotted against temperature on Figure 4-21.

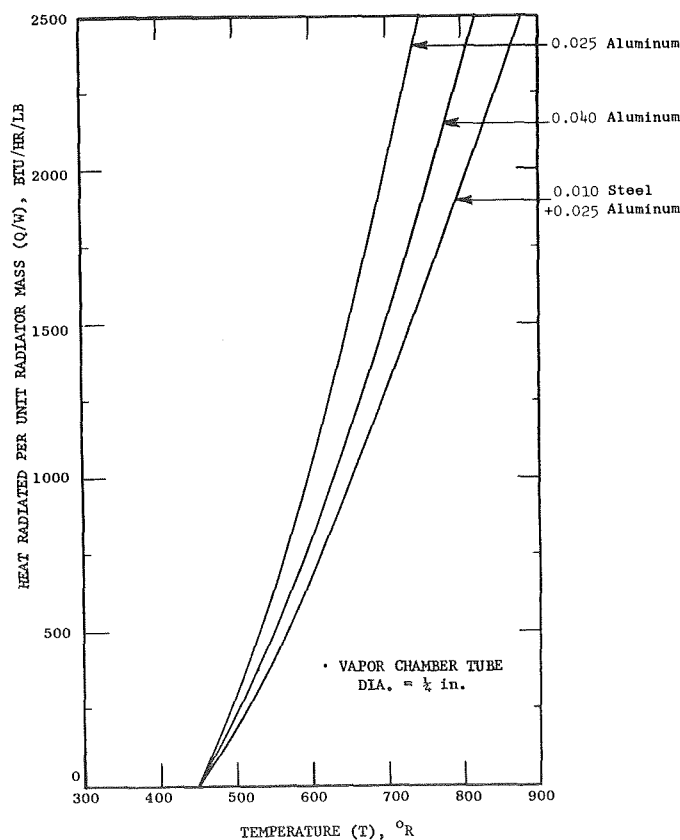


Figure 4-21. Effect of Tube Wall Thickness and Temperature on Vapor Chamber Fin Heat Radiated Per Unit Radiator Mass

2. Using the radiator configuration shown in Figures 4-9 and 4-10 as a basis, various numbers, sizes, and proportions of Dow Corning fluid ducts were investigated with consideration for the following factors:
  - a. Fin area, fin spacing, fin effectiveness (thickness and size) of fins required in Dow Corning fluid duct
  - b. Pressure drop in Dow Corning duct flow
  - c. Vulnerable area of Dow Corning fluid ducts
  - d. Vulnerable area of individual vapor chamber tubes
  - e. Thermal flux level on heat input section of vapor chamber tubes
  - f. Length of heat input section of vapor chamber, considering requirement for two independent Dow Corning duct systems.
3. As a result of these investigations the following generalizations were reached for establishing comparative designs:
  - a. Five Dow Corning fluid ducts (or, actually duct pairs) are used on all radiator panels, these being located at the centers of five end-to-end vapor chambers each approximately four feet long extending across the width of the panel (Figure 4-9).
  - b. Each duct is 1-inch wide by  $\frac{3}{4}$ -inch deep. The two ducts of each pair are side by side with a common partition wall.
  - c. Four-foot long vapor chambers are  $\frac{1}{4}$ -inch in diameter. Longer vapor chambers result in thicker required armor on the vapor chambers and save very little vulnerable area of Dow Corning ducts.
  - d. Spacing of the vapor chambers in the direction of the ducts is variable in accordance with the requirements of maximum  $Q/W$  for the vapor chamber - conduction fin element (see Figure 4-16).
  - e. The correlation of Equation (4-41) below was used to establish meteoroid armor thicknesses on the Dow Corning fluid ducts and on the vapor chambers.

$$t_a = \frac{0.448}{\rho_t^{1/6} E^{1/3}} \left[ \frac{A T}{- \ln P_o} \right]^{0.249} \quad (4-41)$$

$t_a$  = armor thickness (inches)

$\rho_t$  = density of vulnerable material (lbs/in<sup>3</sup>)

$E$  = Young's modulus of vulnerable material (psi)

$A$  = vulnerable area (ft<sup>2</sup>)

$T$  = time (hours)

$P_o$  = probability of no puncture

- f. Individual no puncture probability of the Dow Corning fluid ducts was selected at 0.9 which corresponds to a probability of 0.99 for survival of at least one duct in the paired duct system.
- g. The initial value of the individual no puncture probability of the vapor chambers was selected at 0.75. This corresponds closely to a 0.99 probability that 72 percent of the vapor chambers will survive. This value was later changed to 0.85. (Punctured chambers retain partial effectiveness as conducting fins.)
- h. Weight of the radiating surface was calculated by using incremental areas of the radiator as weighting factors to be applied to the calculated values of  $Q/W$  for various temperature levels in order to obtain a mean effective value of  $Q/W$  for the entire radiator. The radiator area, (both on an incremental basis to get weighting factors for average  $Q/W$  calculation, and on an overall basis was calculated from Equation (4-42).

$$A = \frac{1}{n_f} \frac{\frac{W}{2} C_p}{T_s^3 \epsilon \sigma} \left\{ \frac{1}{2} \ln \left[ \frac{(T_H - T_s)(T_c + T_s)}{(T_H + T_s)(T_c - T_s)} \right] - \left[ \tan^{-1} \left( \frac{T_H}{T_s} \right) + \tan^{-1} \left( \frac{T_c}{T_s} \right) \right] \right\} \quad (4-42)$$

where

$A$  = radiator area

$n_f$  = mean effectiveness of the radiating surface

$\underline{w}$  = Dow Corning fluid weight flow

$C_p$  = Dow Corning fluid specific heat

$T_s$  = Radiation sink temperature

$T_H$  = Radiating surface temp. at high temp. end of radiator

$T_c$  = Radiating surface temp. at low temp. end of radiator

$\epsilon$  = emmissivity

$\sigma$  = Stephen Boltzmann constant

- i. Weight penalty to be applied to the water tube liner portion of a water-ammonia radiator was calculated on the basis of using a 0.010-inch thick stainless steel tube inside of aluminum meteoroid armor. Armor value of the steel tube was allowed for.

#### 4.3.2.2 Allowance for Punctured Vapor Chambers

Depending upon the vapor chamber wall thickness and the vulnerable area of each tube, there is a definite survival probability for an individual vapor chamber. This relationship is given by Equation (4-41) above. For a given wall thickness, the survival probability of the individual tube increases as the vulnerable area decreases. This fact represents the reason for limiting the length of the vapor chambers, in some cases, substantially below values permitted by refluxing performance (see Tables 4-3 to 4-6). If there is a large number of vapor chambers, the probability that a specified fraction of these will survive is related to the number of chambers and to the probability that one individual tube in the large group will survive. For a particular number of chamber units (1000), the relationship between survival fraction and individual tube survival probability for a stated probability of achieving the survival fraction is summarized in Figure 4-22. This relationship holds closely for any large number of units, such as 1000 or more. From Figure 4-23 it can be determined that if the individual vapor

chamber survival probability is 0.75, 72 percent of the vapor chambers in the entire radiator (a number larger than 1000 tubes) can be expected to survive with a probability of 0.99. The puncture of 28 percent of the vapor chambers does not result in a loss of 28 percent of the radiator capacity. The reason for this is that the vapor chamber elements are short enough in lateral dimension, that punctured tubes lying between unpunctured tubes have a significant conduction fin effectiveness, thus increasing the effective length of the conduction fins attached to the surviving vapor chambers. A margin of refluxing and evaporative surface thermal flux performance adequate to handle a 100 percent overload has been purposely provided to take care of vapor chamber overloading resulting from puncturing of adjacent tubes. The heat transfer area provided by the fins in the primary fluid duct are also designed to accommodate a higher heat load per vapor chamber.

In order to calculate the effectiveness of the portion of the radiator represented by the 28 percent punctured vapor chambers, it is necessary to determine the probable distribution of the punctures in the radiator vapor chambers. The probability of a puncture pattern involving K filled tubes in a row is given by:

$$P_K = \frac{S}{N} \times \frac{N-S}{N-1} \times \frac{N-S-1}{N-2} \times \frac{N-S-2}{N-3} \dots \frac{N-S+1-K}{(N-K)} \frac{(S-1)}{N-K-1} \quad (4-43)$$

where N = total number of vapor chambers

S = number of tubes surviving (unpunctured)

The probable number of such failures is given by

$$N_K = N P_K \quad (\text{This equation is an approximation which has been verified by detailed calculations to be slightly conservative.})$$

The probability of multiple tube failures has been illustrated for a typical radiator where N = 1300 and the tubes are  $\frac{1}{4}$ -inch diameter and are approximately 4 feet long. For five years, 0.75 probability of survival, approximately 0.040-inch aluminum tube



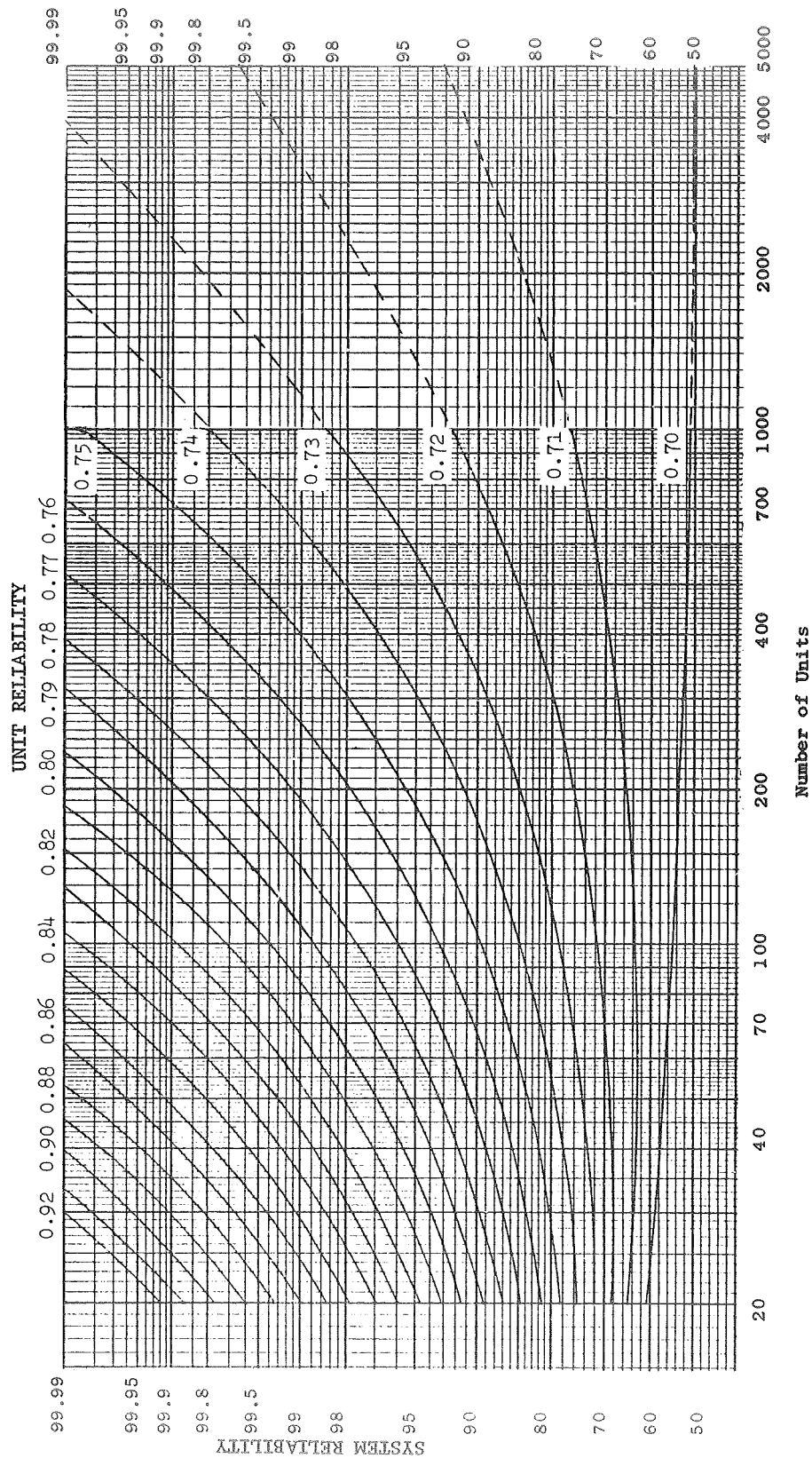


Figure 4-22. Probability That 70 Percent or More Units Survive as a Function of Unit Reliability

thickness is required, or, for the case of a water vapor chamber, 0.010-inch stainless steel plus 0.025-inch aluminum (Equation 4-42). From Figure 4-23, a 72 percent survival fraction can be achieved with a probability of 0.99 if the individual vapor chamber survival probability is 0.75. Therefore:

$$\begin{aligned}
 N &= 1300 \text{ tubes} \\
 S &= 0.72 \times 1300 = 940 \text{ tubes} \\
 N-S &= 360 = \text{max. no. failed} \\
 P_1 &= \frac{(940)}{(1300)} \frac{(939)}{(1299)} \frac{(360)}{(1298)} = 0.145 \\
 N_1 &= 1300 \times 0.145 = 188 \text{ failures involving 1 punctured tube bracketed by} \\
 &\quad \text{by two good tubes.} \\
 N_2 &= 188 \frac{(1300 - 940 - 1)}{(1300 - 1 - 2)} = 52 \text{ failures involving two punc-} \\
 &\quad \text{tured tubes in series.} \\
 N_3 &= 52 \frac{(358)}{(1296)} = 14 \text{ failures involving three punctured tubes} \\
 &\quad \text{in series.}
 \end{aligned}$$

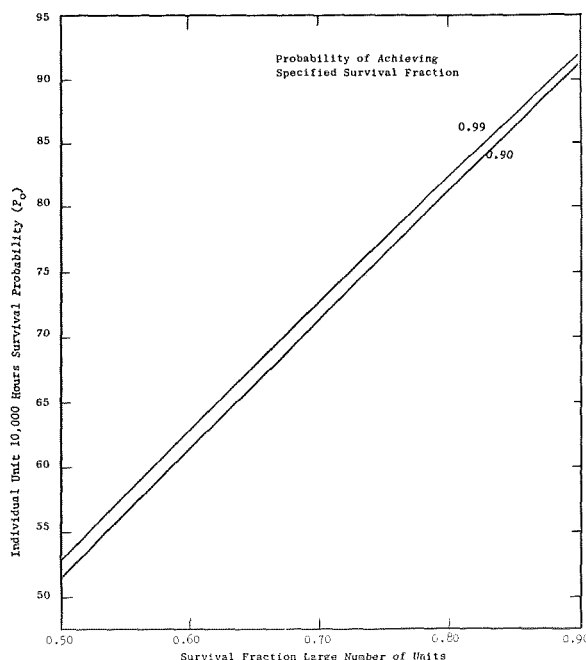


Figure 4-23. Correlation of Individual Vapor Chamber Survival Probability Required to Achieve Fixed Overall Radiator Success Probability Against Vapor Chamber Survival Fraction

From Figure 4-24 it can be determined that, if  $n_f = 0.9$  for the basic radiator surface with no punctured tubes, the radiating surface effectiveness for the portion of the radiator involving one tube failure bracketed by two good tubes is approximately 0.70; the effectiveness for the portion with two failed tubes in series is 0.55; and the effectiveness of the portion with three failed tubes in series is 0.4. Using these numbers, and neglecting the portion of the radiator involving more than three failures in series, the resultant effectiveness of the 28 percent of the radiator involving punctured tubes can be calculated as follows:

$$\begin{aligned} \epsilon_F &= \frac{188 (0.70) + 52 \times 2 (0.55) + 14 \times 3 (0.4)}{360} \\ &= 0.57 \end{aligned}$$

Therefore, the excess area required to compensate for the 28 percent punctured tubes can be estimated as follows:

$$\begin{aligned} \frac{\text{Area Initially Provided}}{\text{Effective Area at End of Mission}} &= \frac{1}{0.72 + 0.57 \times 0.28} \\ &= 1.14 \end{aligned}$$

Thus, 14 percent excess area is required to compensate for the loss of 28 percent of the vapor chambers. This factor has been used in the preparation of Table 4-7.

#### 4.3.2.3 Results of Comparative Radiator Calculations

In Table 4-7 is shown a summary of the results of the approximate radiator design calculations. Eight possible working fluid combinations have been compared. Other combinations are possible but all of these are either very similar in characteristics to one or another of the indicated combinations, or are markedly inferior to any shown. Similar, but slightly inferior to methanol as a high temperature fluid, is ethanol. Similar, but inferior to benzene are n-heptane and pyridine. Similar but inferior to toluene is

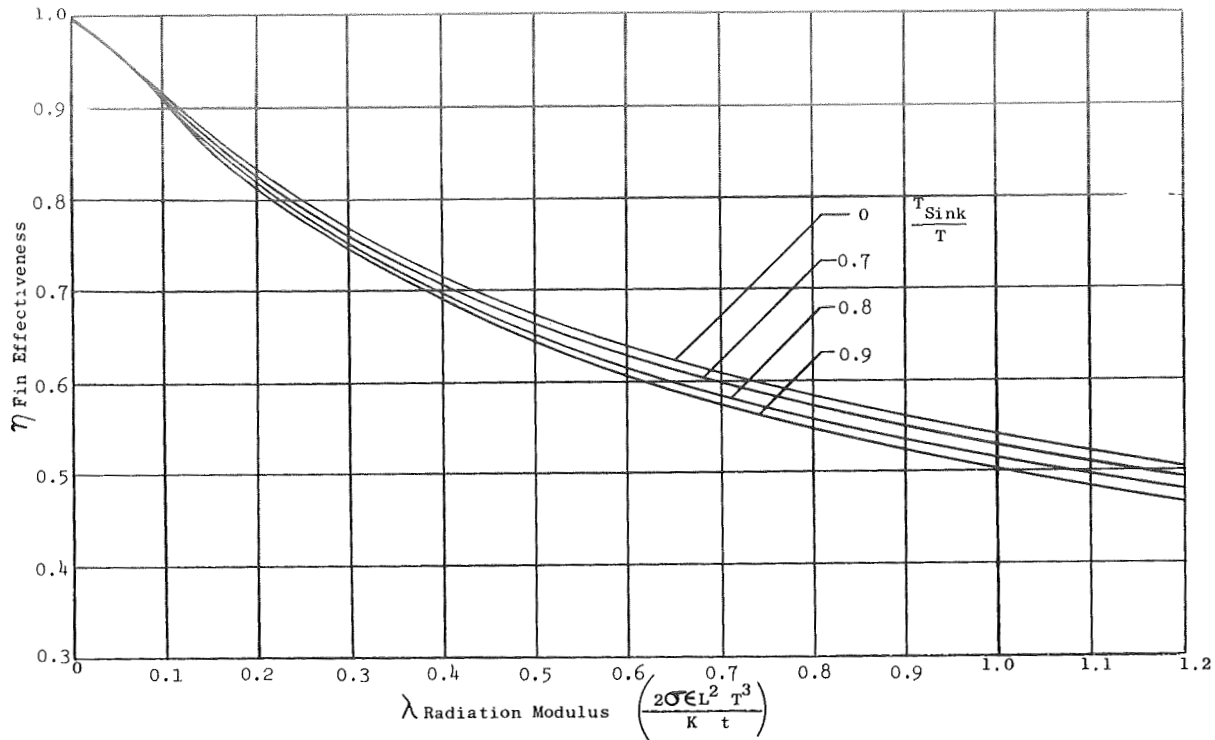


Figure 4-24. Fin Effectiveness vs  $\lambda$  Radiation Modulus  $\left(\frac{2 \sigma \epsilon L^2 T^3}{K_t}\right)$  for Fin Radiating from Two Sides

o-xylene. Isopropyl alcohol, n-nonane, and anisole are markedly inferior high temperature fluids for reasons indicated in Table 4-3. Freon 113 is similar but inferior to Freon 11 as a low temperature working fluid.

The use of water and ammonia is approximately 4 percent heavier than the most attractive alternative, methanol and ammonia. It is only 2.5 percent heavier than n-pentane and ammonia, which may be the closest feasible alternative, because of anticipated corrosion problems with methanol and ethanol. Also, the combination, using a stainless steel tube inside the enclosing aluminum fin structure must be seriously considered as a preferred choice. On the basis of available data, it may be said that the heat transfer performance of this combination can be predicted from present knowledge with greater certainty than that of any of the other combinations.

TABLE 4-7. COMPARISON OF RADIATORS USING CANDIDATE WORKING FLUID COMBINATIONS

Working Fluids	Oil Bath Temperature, $T_{Hr}$ ( $^{\circ}F$ )	Condensing Surface Temperature, $T_{cr}$ ( $^{\circ}F$ )	Radiator Area ( $ft^2$ )	Radiating Surface Weight (lb)	Liquid Coolant Duct Weight (lb) (includes duct fins)	Total Weight (lb)
Water and Ammonia	243	20	1280	228	145	373
Methanol and Ammonia	223	20	1370	210	149	359
n-Pentane and Ammonia	218	20	1390	216	150	366
Benzene and Ammonia	200	20	1490	222	153	375
Toluene and Ammonia	188	20	1550	232	156	388
Methanol and Freon 11	233	0	2100	294	170	464
n-Pentane and Freon 11	218	0	2140	304	173	477
Benzene and Freon 11	200	0	2290	336	185	521

Conclusions which can be drawn from the data summarized in Tables 4-3 to 4-6 are the following:

1. From the standpoint of calculated performance as vapor chamber working fluids and of calculated radiator weight and area a number of possible working fluids for the high temperature ( $150^{\circ}\text{F}$  to  $350^{\circ}\text{F}$ ) end of the Brayton cycle radiator have been identified. These are, listed in order of preference (based on calculated performance, without regard to possible chemical stability and interaction problems) the following:

Methanol (Methyl Alcohol)  
Ethanol (Ethyl Alcohol)  
n-Pentane  
Water  
Benzene  
Isopropanol  
n-Heptane  
Pyridine  
Toluene  
o-Xylene  
Anisole  
n-Nonane

2. Similarly, the following low temperature ( $20^{\circ}\text{F}$  -  $150^{\circ}\text{F}$ ) vapor chamber radiator working fluids have been identified. These are, in order of preference:

Ammonia  
Freon 11  
Freon 113

3. The principal criterion which has been found to be of major significance in the comparative evaluation of vapor chamber radiator working fluids is the sum of the evaporative and condensing temperature drops within the vapor chamber. The exception to this is found in the case of water. The weight penalty assigned to water results from the known need for a stainless steel tube liner. This represents a fabrication difficulty as well as a small (4%) weight penalty.

Final selection of working fluid combinations to be used in a test vapor chamber were based on the results of the above calculations and the reflux capsule tests. These tests discussed in Section 4.4 define the all important question of the existence of chemical stability and compatibility with the containment material.

#### 4.4 TESTS FOR COMPATIBILITY OF MATERIALS

##### 4.4.1 TECHNICAL APPROACH

The objective of the materials compatibility test program was to determine the existence and quantity of any noncondensable gas formed when the working fluid of the vapor chamber fin was in direct contact with the wicking and structural containment materials within the expected operating temperature range. Noncondensable gas, if formed, would arise from either a corrosion or a thermal degradation type reaction. Since noncondensable gas is detrimental to the operating performance of the vapor chamber fin, the lack of any measurable gas generation provided reasonable acceptability of the materials combination. If a measurable rate of gas formation was detected, the feasibility of the materials combination was in doubt.

Structural containment materials considered for the vapor chamber fin were restricted to alloys of aluminum. In particular, the aluminum alloy 6061-T6 was selected as the structural material on the basis of its strength, fabricability, corrosion resistance, stability, and availability in the required shapes and sizes. Commercial purity aluminum (99% A1-designation 1100) was selected as the wicking material for the vapor chamber because of the unavailability of 6061-T6 screens.

A preliminary screening of working fluids was made, and a number of classes of fluids were identified as being likely candidates for working fluids in a vapor chamber radiator in the temperature range 20<sup>o</sup> to 350<sup>o</sup> F. This preliminary selection was made primarily on the basis of expected fluid thermal stability, compatibility with aluminum alloys, and equilibrium vapor pressure, with the performance of the fluid in the vapor chamber being a secondary consideration. Promising classes of fluids identified were Freon-type refrigerants and solvents, alkanes, alcohols, aromatic hydrocarbons, inorganic fluids (especially water and ammonia) and several organic fluids which had previously been used for high-temperature, vapor-phase heat transfer applications. In addition, various chemical companies were contacted for information concerning available proprietary compounds which may not yet be in general commercial use. These

inquiries produced two other classes of fluids: the Freon E Series fluorocarbons (E.I. DuPont De Nemours & Co.) and a group of experimental thermodynamic fluids under investigation by the Monsanto Company.

It was finally decided that fluid-material compatibility tests would be performed on the following thirteen fluids: n-pentane, n-heptane, benzene, toluene, water, CP-32, CP-34 (Monsanto thermodynamic fluids), ethyl alcohol, methyl alcohol, ammonia, Freon 11, Freon 113, and n-butane. In view of the known corrosion of aluminum by water, the water tests were conducted in stainless steel. This single test, was performed because water as a vapor chamber working fluid is highly advantageous.

In order to simulate as nearly as possible the actual radiator operating conditions, the fluids were placed in a gravity refluxing capsule fabricated of 6061-T6 aluminum alloy, except water which was tested in a type 321 stainless steel capsule. Heat was supplied at one end of the capsule by immersion in an oil bath operating at constant temperature. Heat rejection at the upper end of the capsule was accomplished by flow of ambient temperature air. Three thermocouples were located near the upper end of the capsule, and the temperatures were monitored for at least 500 hours at the selected test temperature. The accumulation of noncondensable gas in the capsule was indicated by the development of an axial temperature gradient near the upper end of the capsule.

#### 4.4.2 CAPSULE DESIGN AND FABRICATION

The aluminum reflux capsules were approximately 23.5 inches long and 0.5 inch in outside diameter. The capsule design is shown in Figure 4-25. In constructing the capsules, all parts were first cut to the required size and then thoroughly cleaned. The cleaning procedure involved an initial soak in hot alkaline cleaner followed by deoxidation in a solution of 112 gm. sodium sulfate and 150 ml concentrated nitric acid in 850 ml water for 20 minutes at 140<sup>0</sup> F. In addition, the aluminum was either machined or abraded in the area of the welds. A single layer wick of aluminum screen (1100-aluminum alloy, 120-mesh twill) was then inserted in the tube and pressed against the



inside wall by rolling over a 3/8 inch rod inserted down the axis of the tube. The capsules were then TIG welded under helium in a vacuum purged inert gas welding chamber. After welding, the capsules were leak checked with a helium mass spectrometer leak detector and pressure checked with argon at 900 psig after which the leak check was repeated.

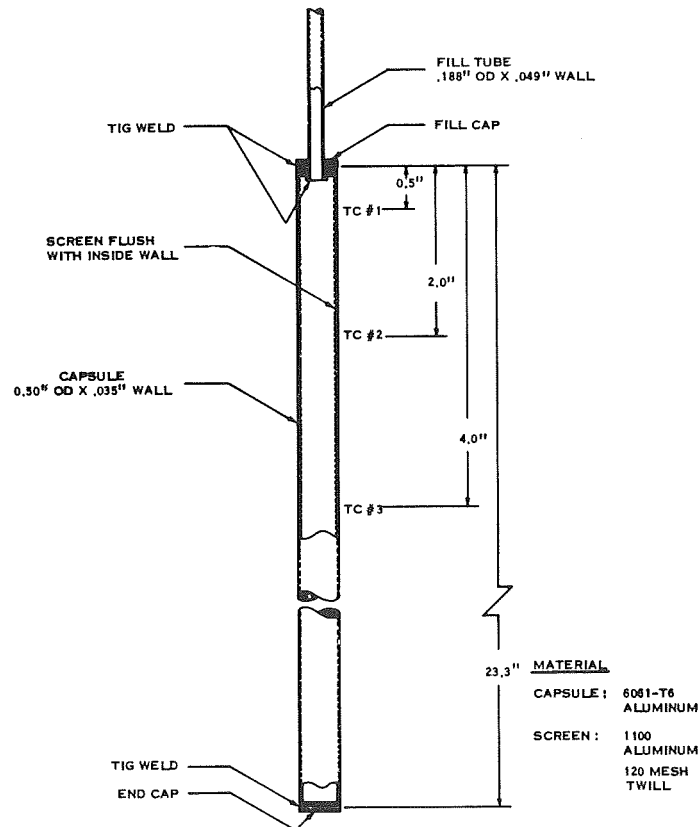


Figure 4-25. Aluminum Capsule

The type 321 stainless steel capsule for the water test was similar to the aluminum capsule except that the fill tube was 0.25 inch OD by 0.035 inch wall. The stainless capsule was cleaned before fabrication by soaking in hot alkaline cleaner and pickling for 15 minutes at 135<sup>o</sup> F in a solution of 15% by volume concentrated nitric acid, 5% by volume concentrated hydrochloric acid, and 80% water. In addition, the stainless steel was passivated by soaking for 15 minutes at 150<sup>o</sup> F in a 15% by volume nitric acid solution. The wick material consisted of a single layer of 150-mesh, type 316 stainless

steel screen pressed against the inner wall. The stainless steel capsule was TIG welded in air with argon purging.

Three thermocouples were located on each capsule at 0.5 inch, 2.0 inches, and 4.0 inches from the upper (filling) end as shown in Figure 4-25. The couples were cemented to the wall with epoxy cement. The thermocouples were 24-gauge copper versus constantan with fiberglass insulation. Following attachment of the thermocouples and curing of the epoxy, each capsule was again leak checked.

Two trial capsules of aluminum were proof tested to further check the weld integrity. These capsules burst at 3400 and 3500 psig. respectively, in good agreement with the ultimate tensile strength of welded 6061-T6 Aluminum.

#### 4.4.3 CAPSULE FILLING AND SEALING

The procedure adopted for filling the capsules involved filling the capsule completely with fluid and then distilling the fluid from the capsule until the desired quantity remained. This procedure served to remove residual air from the capsule, absorbed gases from the interior surfaces, and dissolved gases from the fluid. In addition, the more volatile impurities were removed from the fluid during the distilling operation.

For the fluids with boiling points above ambient temperature, the capsule was filled completely with fluid from a hypodermic syringe using a 6-inch, No. 20 hypodermic needle. The total capsule volume was approximately 54 cc. A valve was then attached to the fill tube and to a water-cooled glass condenser and volumetric collector. A photograph of the filling system is shown in Figure 4-26. The bubbler serves to prevent evaporation of the more volatile liquids.

After filling the capsule completely with liquid, a heating tape was wound around the exterior of the capsule and heat was supplied to boil the fluid. It was found that the heat had to be applied near the surface of the liquid to prevent eruptive boiling and

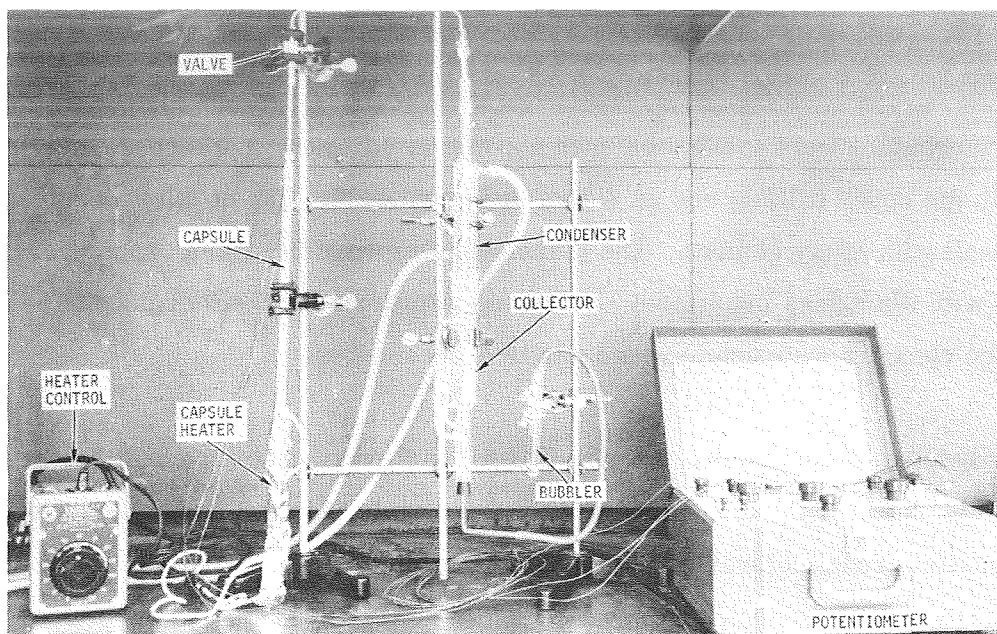


Figure 4-26. Capsule Filling System

subsequent sudden flow of a large liquid volume. The distilling process continued until the capsule was approximately half full at which point the valve was closed, and the capsule temperature was increased to approximately  $30^{\circ}\text{F}$  above the normal boiling point. The capsule was heated at this temperature for several hours with occasional venting of the capsule to remove noncondensable gas accumulating at the upper end of the capsule. The temperature of the three thermocouples was monitored during this time to indicate the quantity of noncondensable gas. When the capsule thermocouples indicated an isothermal condition and the desired quantity of liquid remained within the capsule, the fill valve was finally closed, and the capsule was allowed to cool to ambient temperature.

In filling capsules with fluids boiling at or below ambient temperature, (that is Freon 11, ammonia, and n-butane), a somewhat different procedure was employed. In each case, the capsule was weighed before and after the filling operation to determine the

quantity of fluid in the capsule. The initial charge of Freon 11 was inserted into the capsule with a hypodermic syringe as with the higher boiling liquids. In filling the n-butane capsule, the capsule was first evacuated and then attached to a cylinder containing liquid n-butane. After thoroughly flushing the connecting lines, the n-butane was distilled into the capsule which was maintained at 32<sup>o</sup> F in an ice bath, while the n-butane cylinder was at ambient temperature. In filling the ammonia capsule, the capsule was first evacuated and then attached to a reservoir containing liquid ammonia. After thoroughly flushing the connecting lines, the ammonia reservoir was tilted so that the liquid ammonia drained by gravity into the capsule.

The final fluid inventory was approximately 12 cc at normal room temperature in each capsule. This value was calculated to give a liquid level inside the capsule which was near the oil level of the bath when the capsule was on test. Table 4-8 gives the capsule identification, the fluid supplied for all of the capsules tested, the final fluid inventory, and the capsule test temperature. In the case of methyl alcohol, the capsule was not put on test since reaction with the aluminum capsule was noted during the filling operation. This is discussed further in a later section of this report. It should be noted that Freon 11 was available as the solvent, Freon MF. Similarly, Freon 113 was available as TF solvent and as PCA (precision cleaning agent). In each case, the highest purity grade was used.

After the capsule was filled with the desired quantity of fluid, a permanent seal of the fill tube on the aluminum capsules was made. To accomplish this, the fill tube was sealed with a pinch-off tool. After the pinch-off operation, an aluminum cup, which had been placed around the fill tube before the valve was attached, was pulled up so that it surrounded the pinch-off, and the cup was then filled with epoxy cement. This "potting" of the pinch-off effectively reinforced it against high internal pressures encountered during the capsule tests. The epoxy used for reinforcement of the pinch-off was especially suited for this purpose since it is stable at 350<sup>o</sup> F; it readily flows around the pinch-off, and it cures within one hour at 150<sup>o</sup> F or overnight at room temperature. Figure 4-27 is a photograph of a cross section of the fill tube pinch-off after "potting" in epoxy cement.

TABLE 4-8. CAPSULE FILLING DATA

Capsule Identification	Fluid	Supplier	Grade	Fluid Quantity (grams) (~ 12cc)	Capsule Test Temp. (°F)
C-1	Methyl Alcohol	Baker	Spectro.	Not filled completely	Not completely tested due to heavy evolution of gas.
C-2	n-Pentane	Eastman	Practical	7.5	316
C-3	Benzene	Eastman	Spectro.	10.5	316
D-1	Ammonia	Matheson	Anhydrous	8.0	159
SS-1	Water	-	Distilled	11.0	328
D-2	Freon 11	duPont	MF Solvent	16.6	156
D-3	Freon 113	duPont	PCA	18.4	155
D-4	Toluene	Eastman	Sulfur-free	10.4	322
D-5	n-Heptane	Eastman	Spectro.	8.2	321
D-6	CP-32 (Pyridine)	Monsanto	Thermodynamic Fluid	10.8	320
D-7	CP-34	Monsanto	Thermodynamic Fluid	12.7	319
D-8	Freon 113	duPont	PCA	18.8	225
D-9	Freon 11	duPont	MF Solvent	16.9	223
D-10	n-Butane	Matheson	Instrument	7.2	156

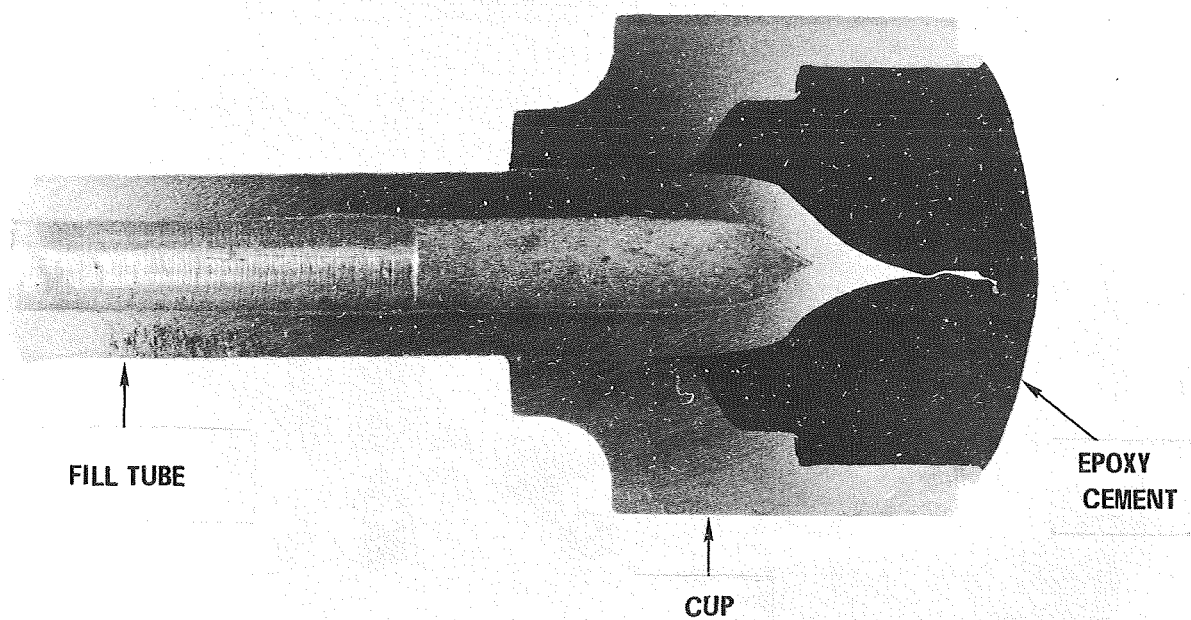


Figure 4-27. Cross Section of Fill Tube Pinch-off Potted in Epoxy Cement (C67112007)

The stainless steel capsule containing water was not permanently sealed. All tests were conducted with the filling valve in place.

#### 4.4.4 CAPSULE TEST APPARATUS

Heat was supplied to the capsules from oil baths operating at constant temperature. Heat was dissipated at the upper end of the capsules by a flow of ambient temperature air. This type of system was chosen for this test in order to accommodate the number of capsules to be tested, and to eliminate, as far as possible, overheating of the capsules during the long-term tests. Each bath was provided with overtemperature protection which automatically shut down the bath in case of a malfunction in the bath temperature control.

Figure 4-28 is a photograph of the capsule test apparatus. The capsules in the high-temperature bath were insulated between the air duct and the bath to decrease the heat loss in this area. The three oil baths were operated at temperatures of 362, 260, and 183<sup>o</sup>F, respectively.

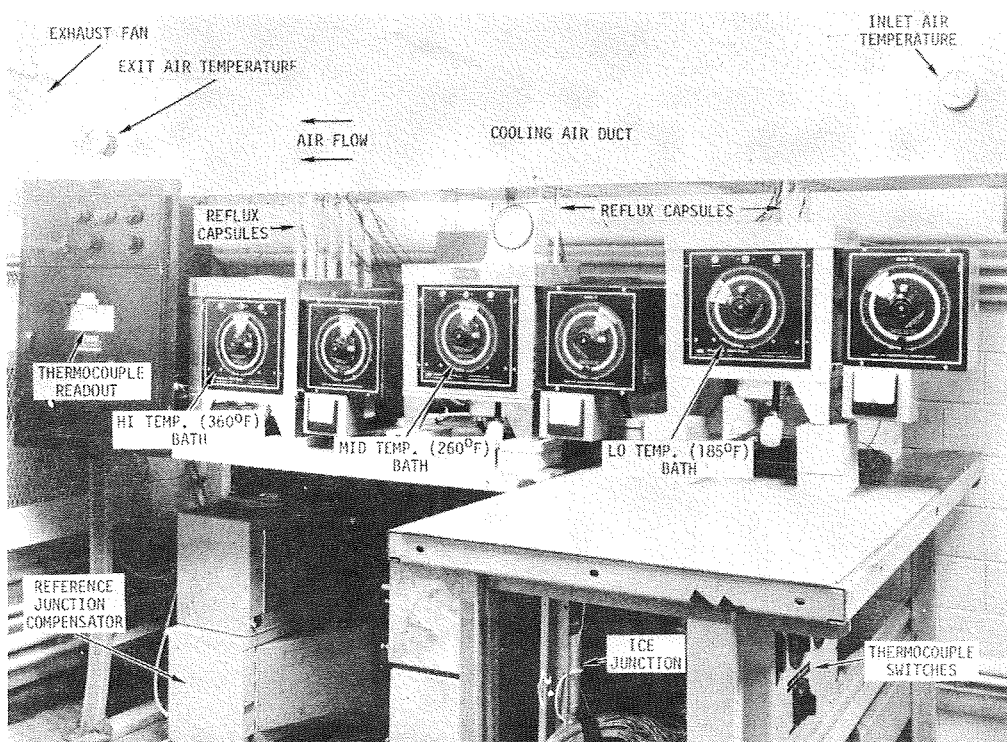


Figure 4-28. Capsule Test Apparatus (C67101205)

Air flow was provided by a fan rated at 225 cfm which was mounted in the exit end of the 12-inch by 12-inch air duct. The air velocity was measured with a velometer and averaged 4.2 ft/sec. In the high-temperature bath, the capsules extended 4.4 inches into the air duct, in the mid-temperature bath, 6.3 inches; and in the low-temperature bath, 10.9 inches. The immersion in the air duct was calculated so that each capsule would dissipate approximately 20 watts (68 BTU/hr) within the duct. The lower end of each capsule extended approximately 6 inches below the oil level in the bath.

Figure 4-29 is a schematic of the thermocouple circuit. Each capsule thermocouple was connected to an isothermal block where connections to copper leads were made. The isothermal block was a Model 4081 thermocouple reference junction compensator which was at ambient temperature. The copper leads went to a 40-position switch and then back to the isothermal block where a connection was made to the thermocouple wire which, in turn, was connected to an ice junction and then to the thermocouple readout. The thermocouple readout was a precision millivolt indicator which gave thermocouple EMF to one microvolt. The purpose of the isothermal block was to maintain the copper lead wire to thermocouple wire connections at the same temperature and thus avoid spurious emf's in the circuit.

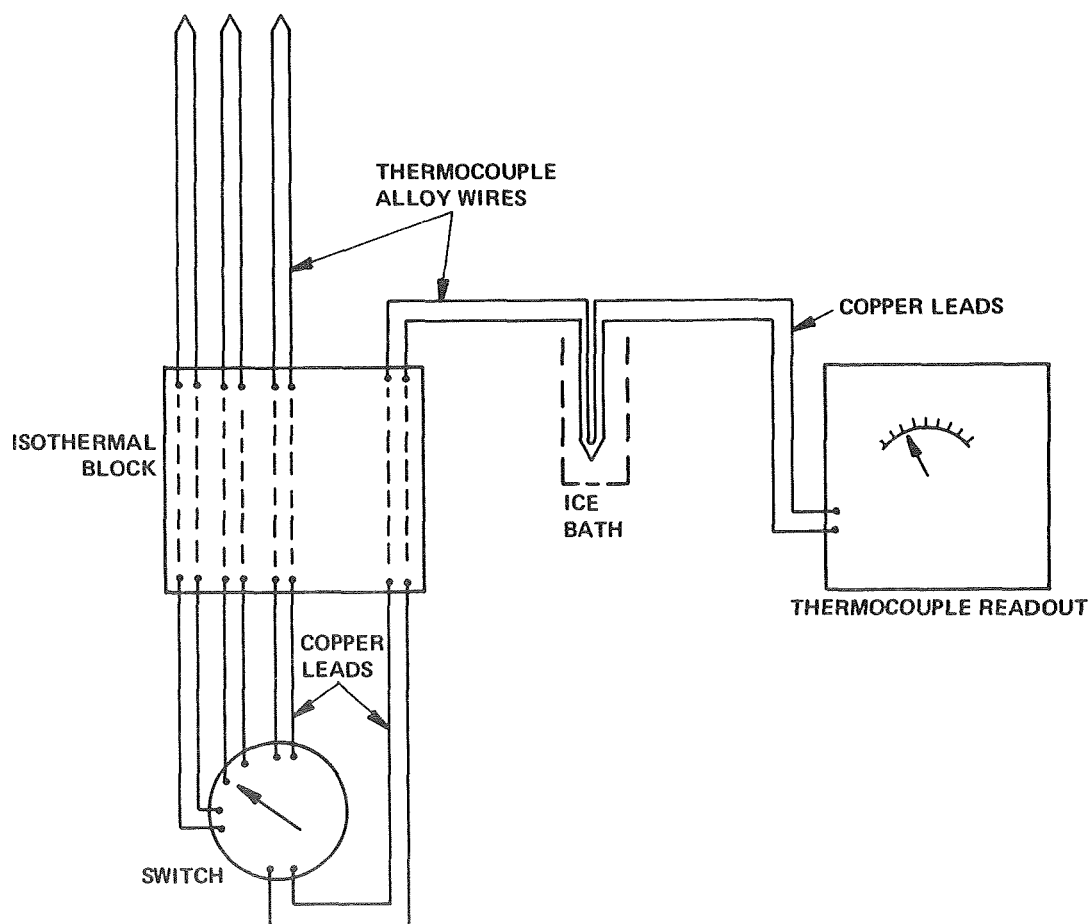


Figure 4-29. Schematic of Thermocouple Circuit



It should be noted that the primary test measurements were the differences between the three thermocouple readings on each capsule, and that no particular effort was made to obtain accurate absolute temperature readings. In order to assure that no spurious temperature differences were being introduced in the thermocouple circuit, the thermocouple output of the three thermocouples on each capsule was compared at the conclusion of the test. The section of capsule wall to which the thermocouple was attached was cut from the capsule and the three thermocouple sections from a particular capsule were placed in intimate contact at the bottom of a heavy-walled, brass-well placed in one of the baths. When the three thermocouple outputs were compared under these conditions, no differences greater than 2 microvolts ( $0.08^{\circ}\text{F}$ ) were detected.

Several measurements were made of the total heat dissipation from the capsules in each bath. These heat dissipation values were obtained by measurement of the electrical power to the bath heaters with the capsules at operating temperature, and subtracting from this the power input to the bath with no capsules in the bath and with the bath at the same temperature. Average values of heat losses have also been calculated, and the results are shown in Table 4-9, where comparison is made with the measured value. Radiation losses have been included by assuming an emissivity of 0.1 for the aluminum. Very good agreement between calculated and measured heat loss was obtained for the low temperature and mid-temperature baths. Measured heat loss in the high temperature bath exceeds the calculated value by 5% even though the calculations were made assuming no insulation on the capsules between the bath and the air duct.

It can be shown from the heat loss values in Table 4-9 that the heat flux from the capsules within the air duct approximates the heat flux from a vapor chamber in a radiating panel when the vapor chamber spacing is 2.4 inches, and radiation is from both sides. Since this is quite a reasonable value, the condensing heat flux in these capsule tests is quite representative of values to be expected in a typical vapor chamber radiator panel. The evaporative heat fluxes, however, range from 1000 to 3000 BTU/hr ft<sup>2</sup> and thus are considerably lower than those to be expected in a typical vapor chamber radiator operating at the specified reference conditions.

TABLE 4-9. CALCULATED AND MEASURED HEAT LOSS FROM CAPSULES

Bath Temperature (°F)	Capsule Temperature (°F)	Capsule Length in Air Duct (inches)	Calculated Heat Loss per Capsule (Btu/hr)			Measured Total Heat Loss per Capsule (Btu/hr)
			In Air Duct	Between Bath & Duct	Total	
Hi Temp. Bath 363	320	4.4	74.8	71.7*	147	155
Mid Temp. Bath 260	225	6.3	65.2	32.5*	98	102
Low Temp. Bath 184	156	10.9	59.8	9.3*	69	68

\*Assuming no insulation on the capsules.

#### 4.4.5 CAPSULE TEST RESULTS

The primary test measurement was the difference in temperature readings of the three thermocouples on each capsule. As was mentioned above, the three thermocouple readings were compared under isothermal conditions and were found to agree within  $0.08^{\circ}\text{F}$ , which shows that only extremely small temperature differences might be accounted for by spurious emf's in the thermocouple circuit. There are, however, several other explanations for temperature differences between the thermocouples. One is, of course, that non-condensable vapor has formed in the capsule and causes the upper thermocouple to read lower than the other two. If noncondensable vapor formation continues, then the temperature of the upper thermocouple would continue to decrease with time. In addition, there is appreciable thermal resistance between each thermocouple and the vapor within the capsule due to the rather low thermal conductivity of the liquid film on the interior and the rather uncertain thermal contact of the thermocouple with the wall. Thus, if the screen does not make good contact with the wall in the region of the thermocouple or if the thermocouple does not make good contact with the wall, then a particular thermocouple might read lower than the other two on the capsule by several degrees. In order to aid in determining the cause of the temperature differences, the capsule temperatures were decreased at various times during the tests. If the temperature of a particular thermocouple increased with respect to the other two when the capsule temperature decreased, this is an indication that there is high thermal resistance in the region of the thermocouple in question. If the upper thermocouple indicates a low temperature and the temperature decreases with respect to the other two couples when the capsule temperature decreases, this indicates non-condensable vapor within the tube has accumulated at the top of the capsule.

A description of the test and test results for each of the selected working fluids is contained in the following paragraphs.

#### 4.4.5.1 Methyl Alcohol (Capsule C-1)

No capsule tests were made with methyl alcohol since relatively large quantities of gas were evolved during the filling operation. The capsule was first filled completely with methyl alcohol and then, with the filling valve open, approximately half of the liquid was distilled out of the capsule at the boiling point, 148.5°F. The filling valve was then closed, and the capsule temperature was increased while the temperature of the three thermocouples was monitored. Some gas evolution was noted at a capsule temperature of 158°F where the upper thermocouple was about 5°F cooler than the lower thermocouple. At a capsule temperature of 172°F rather rapid gas evolution was observed, and the difference between the upper and lower thermocouples was 41°F. The gas was vented several times and continued reaction was observed. Finally, a small quantity of evolved gas was collected with air and ignited to determine if it was combustible. The gas was probably hydrogen since it readily exploded on ignition with air. The capsule was then cooled to room temperature, the fill valve was removed, and the fill tube was closed with a rubber cap. The rubber cap blew off after a few hours indicating that, once started, the reaction proceeded even at room temperature.

The capsule was sectioned and the interior was examined. Extensive corrosion was noted, especially on the screen near the upper end of the capsule. A photograph of the sectioned capsule is shown in Figure 4-30. The powdered material in the lower left of the photograph is the residue after evaporation of the alcohol.

The evidence thus shows rapid attack of aluminum by methyl alcohol with the reaction beginning at about 160°F. The product is, presumably aluminum methoxide formed by the reaction:  $3 \text{CH}_3\text{OH} + \text{Al} \rightarrow \text{Al}(\text{OCH}_3)_3 + \frac{3}{2}\text{H}_2$ . The solid reaction products gave a weight gain, upon ignition in air, which was consistent with the above reaction.

#### 4.4.5.2 n-Pentane (Capsule C-2)

The capsule containing n-pentane was tested for about 750 hours at temperatures above 300°F. About 570 hours of this test were at 316°F. At 316°F, the capsule temperature

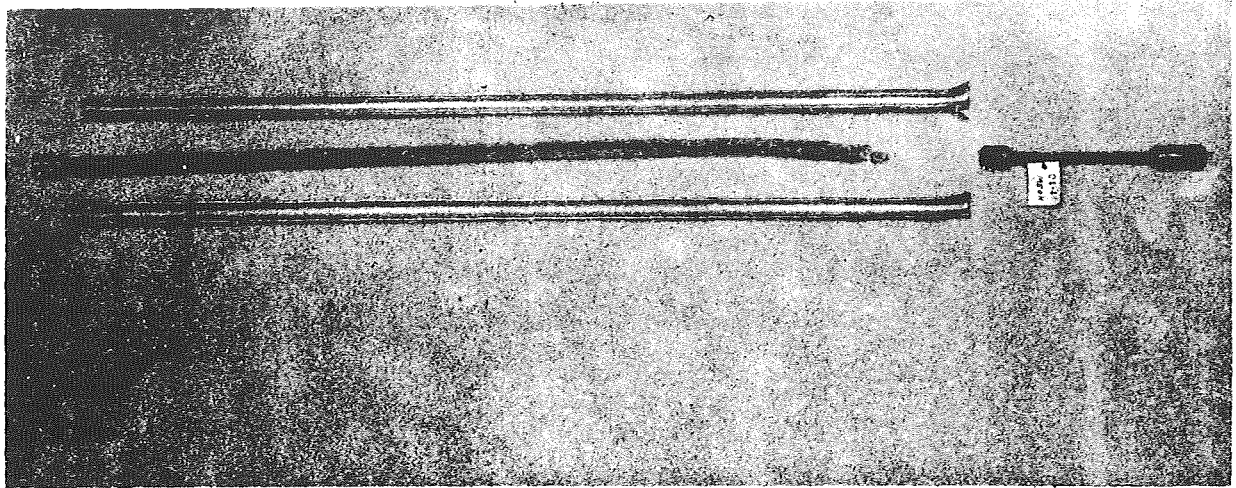


Figure 4-30. Sectioned Aluminum Capsule Following Heating to 170° F with Methyl Alcohol (C67100450)

was typically 46° F lower than the bath temperature. Internal capsule pressure was 270 psia and calculated vapor velocities were 0.15 ft/sec near the evaporating liquid surface and 0.064 ft/sec at the level of the lower thermocouple. The results of this test are shown in Figure 4-33 where  $T_1 - T_3$  and  $T_2 - T_3$  are plotted against test hours.  $T_1$  is the temperature of the upper thermocouple (0.5 inch from top of capsule);  $T_2$  is the temperature 2.0 inches from the top of the capsule and  $T_3$  is the temperature 4.0 inches from the top of the capsule. The data shown in Figure 4-31 are particularly erratic in comparison to some of the other capsules tested. There was definite indication of excess thermal resistance near the lower thermocouple ( $T_3$ ) since  $T_2$  was always greater than  $T_3$  but became very nearly equal to  $T_3$  when the temperature was lowered to about 250° F. The fact that  $T_1$  was from 3 to 8° F less than  $T_3$  could be taken as an indication that there was some noncondensable vapor in this capsule.

However, at the conclusion of the test when the temperature was decreased to 252°F there was an increase in  $T_1$  with respect to both  $T_2$  and  $T_3$ , which is not consistent with the assumption of noncondensable vapor in the capsule. The constant temperature differences noted over the last 450 hours of test indicate that no continued gas formation occurred during this period.

It should be noted that variations in the individual temperature occurred throughout the test. Short-term (fraction of a second) instabilities were especially noticeable on the capsules in the high-temperature bath where the apparent random fluctuations had amplitudes of roughly 0.3°F. These fluctuations were visually averaged in an individual reading. Periodic changes occurred as the bath heaters cycled with periods ranging from 35 seconds in the high-temperature bath to about 60 seconds in the low-temperature bath. In addition, long-term variations occurred mainly as a result of changes in ambient temperature.

At the conclusion of tests on the n-pentane capsule, the capsule was sectioned and the interior examined visually and microscopically. Very light, brownish areas of discoloration were noted on the interior wall, but the screen appeared clean. No evidence of corrosion of the aluminum was found. The liquid removed from the capsule also had a very faint brownish coloration.

#### 4.4.5.3 Benzene (Capsule C-3)

The benzene capsule was also run for a total of 750 hours at temperatures above 300°F, of which 570 hours were at 316°F. At this temperature, the vapor pressure of benzene is 100 psia. Calculated vapor velocity was 0.32 ft/sec near the evaporating surface and 0.14 ft/sec at the level of the lower thermocouple. Temperature differences are plotted against test hours in Figure 4-32.

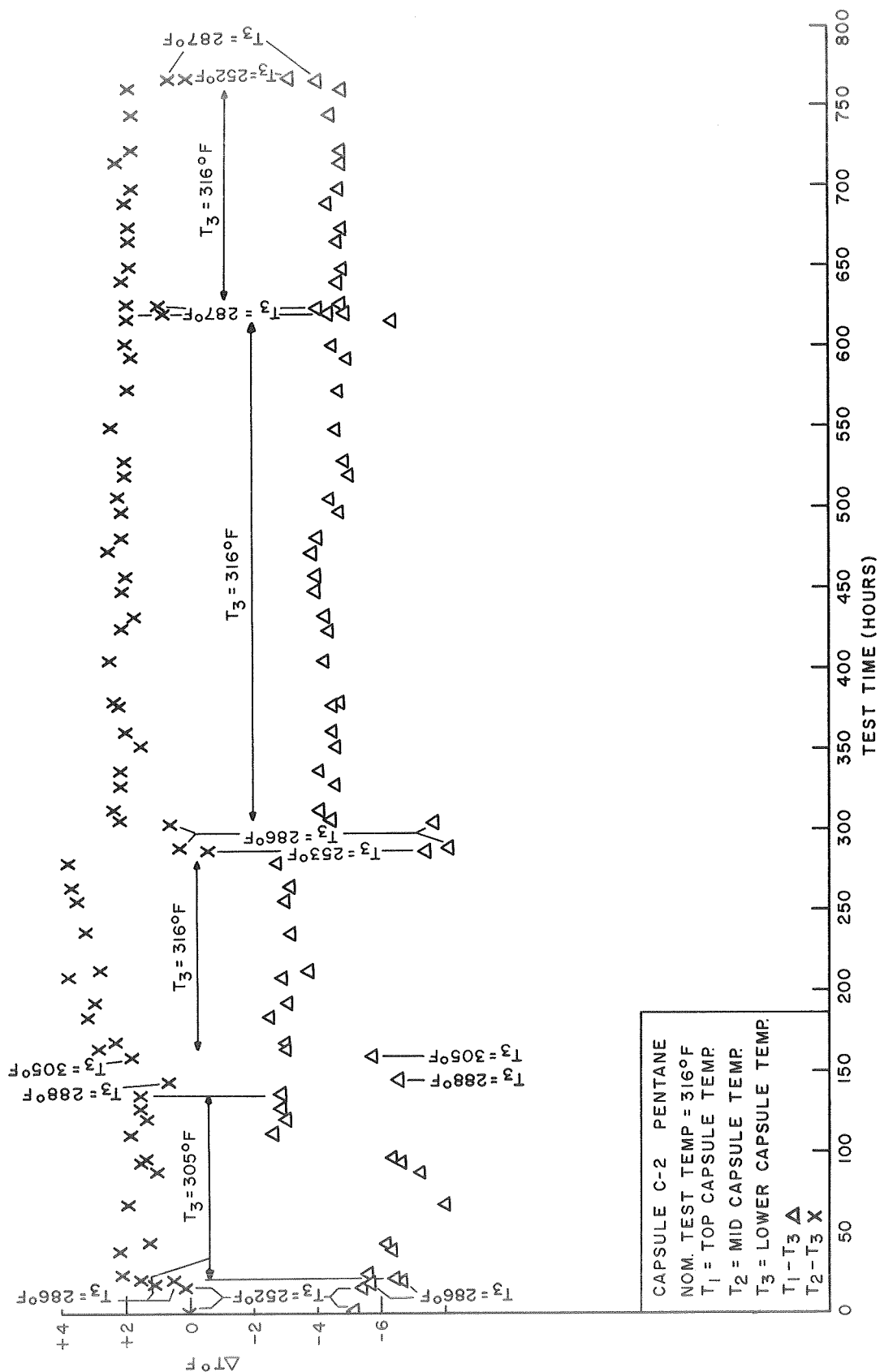


Figure 4-31. Capsule Test Data for n-Pentane

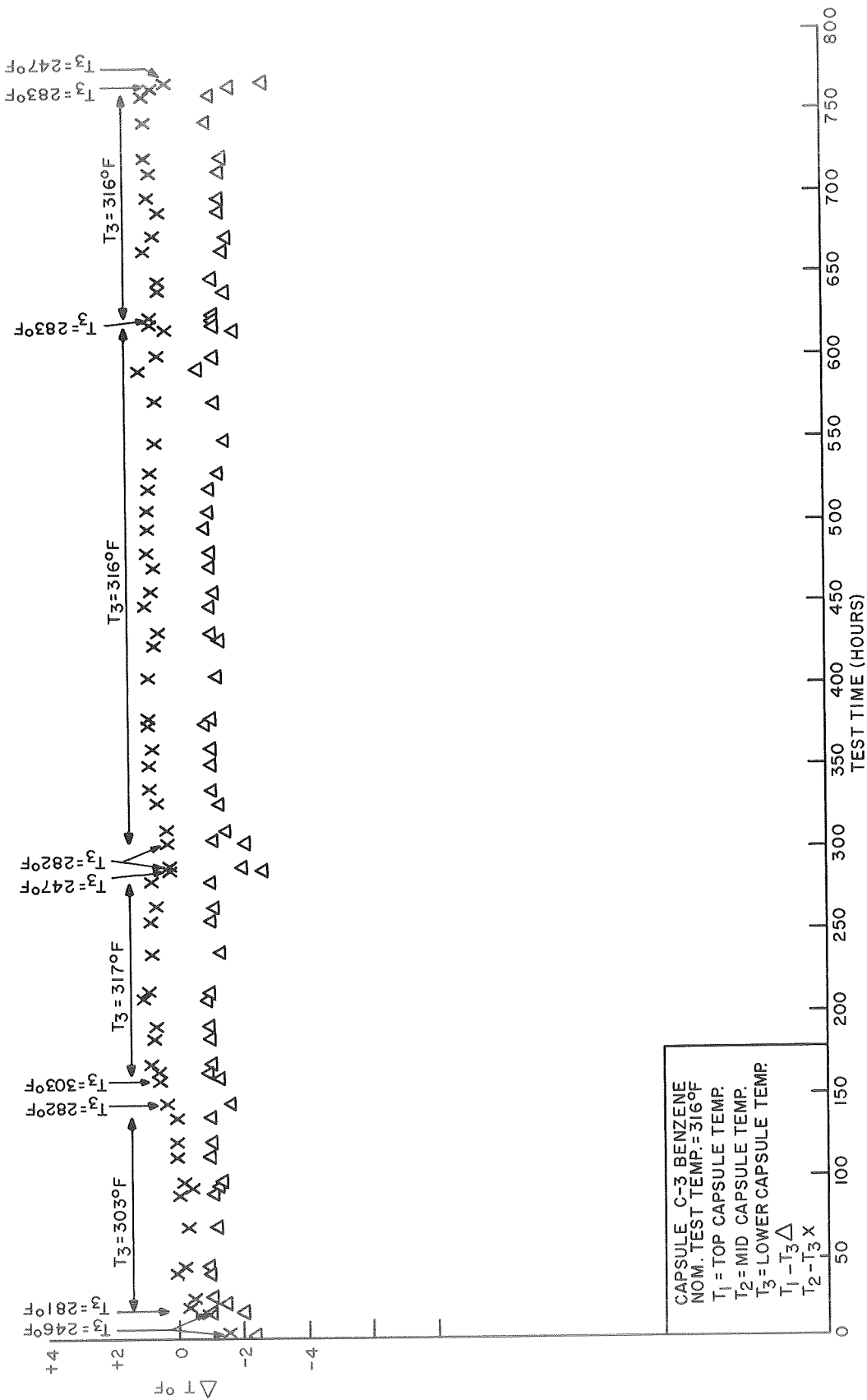


Figure 4-32. Capsule Test Data for Benzene



Measured temperature differences were quite small throughout the test and were constant with time. A slight decrease in both  $T_1 - T_3$  and  $T_2 - T_3$  was noted when the capsule temperature was lowered. This indicates some slight excess thermal resistance in the area of the No. 3 thermocouple; that is, the  $T_3$  temperature increases with respect to the other two when the heat flux is decreased.

The capsule was sectioned after the test, and very slight, local areas of discoloration were noted on the interior with no evidence of corrosion. The screen material was clean, and the liquid was clear. On the basis of this test, benzene appears to be exceptionally stable in contact with 6061-T6 aluminum at temperatures near 300°F.

#### 4.4.5.4 Water in Type 321 Stainless Steel (Capsule SS-1)

Distilled water in type 321 stainless steel was exposed to temperatures in excess of 300°F for 750 hours, of which 570 hours were at 327°F. At this temperature, the vapor pressure of water is 99 psia. Calculated vapor velocity was 0.24 ft/sec at the evaporating liquid surface and 0.11 ft/sec at thermocouple No. 3. Temperature differences are plotted against test hours in Figure 4-33. A steady decrease in  $T_1 - T_3$  occurred throughout the test, until at 750 hours the upper temperature was 72°F lower than  $T_3$ . The temperature of the middle thermocouple agreed quite closely with  $T_3$  until the conclusion of the test when the temperature was decreased to 260°F at which time  $T_2$  was 10°F lower than  $T_3$ , and  $T_1$  was 117°F lower than  $T_3$ . There was thus definite evidence of considerable quantities of noncondensable gas evolved during this test. A qualitative mass spectrometric analysis of the vapor within the capsule was performed after the test and showed a large concentration of hydrogen.

Sectioning of the capsule at the conclusion of the test revealed extensive discoloration on the interior, especially in the areas of the welds. It is considered likely that the capsule was not effectively purged of air before welding and that oxidation of the capsule material thus occurred during welding. A portion of the oxidation products could have been transported into the liquid during the reflux tests and produced the black deposits

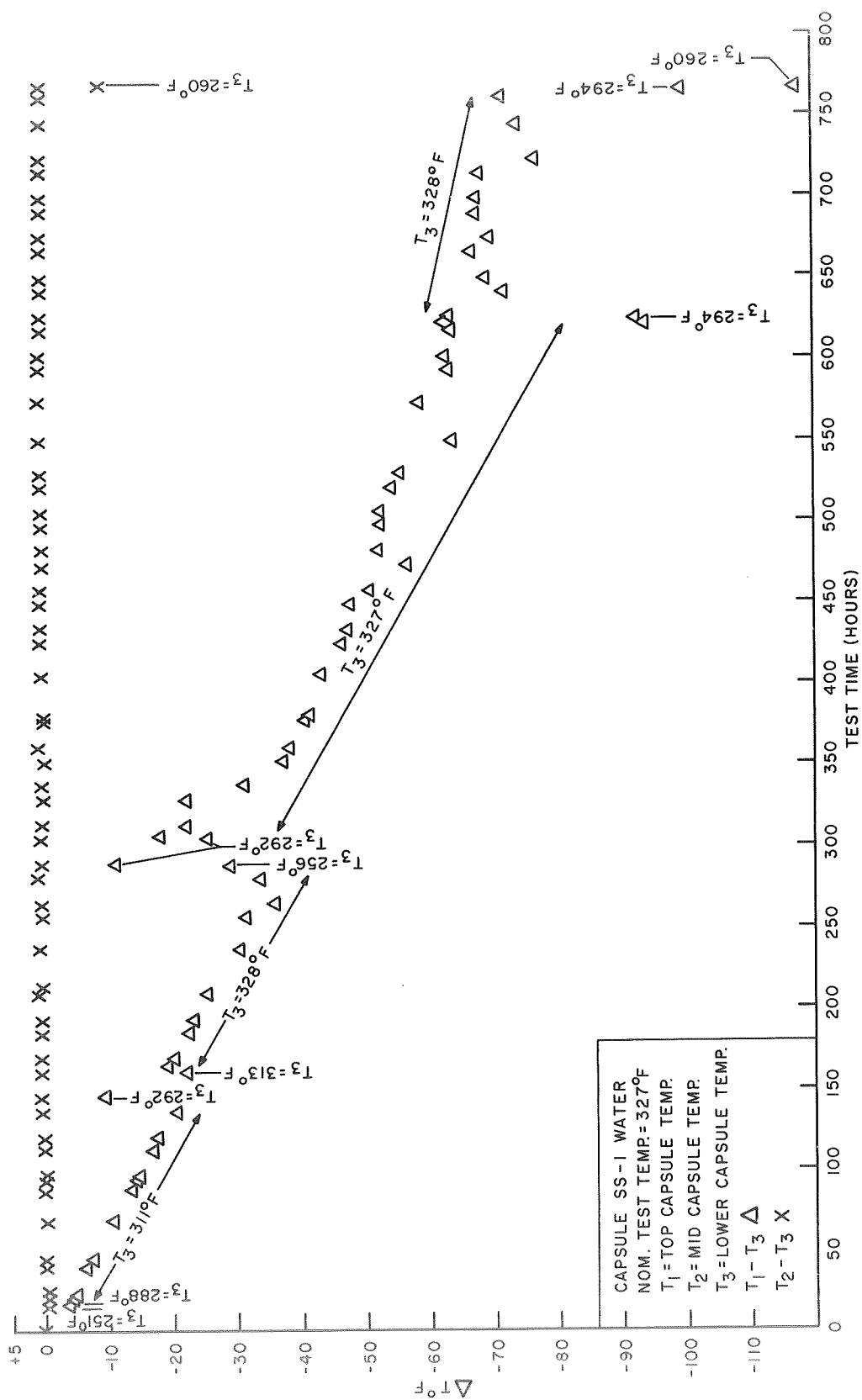


Figure 4-33. Capsule Test Data for Water in 321 Stainless Steel

which were observed in the lower (liquid) portion of the capsule. In the upper portion of the capsule there was relatively uniform brown coloration typical of light oxidation of stainless steel. In addition, the water removed from this capsule contained a small quantity of brown precipitate. It thus appears that reaction of the water with the stainless occurred during the test with subsequent evolution of hydrogen. If one assumes that the hydrogen-water vapor interface during the tests was sharp, and that, at the conclusion of the test, the interface just reached the middle thermocouple with the capsule temperature at 260<sup>o</sup> F, then the quantity of hydrogen within the capsule at the conclusion of the test was 150 std cc. Since the interface is not, in reality, sharp, the quantity of hydrogen is probably not this large.

#### 4.4.5.5 Ammonia (Capsule D-1)

The capsule containing ammonia was run for more than 500 hours at 159<sup>o</sup> F. The vapor pressure at this temperature is 480 psia, and the calculated vapor velocity is 0.031 ft/sec at the evaporating surface and 0.010 ft/sec at the level of thermocouple No. 3. These unusually low vapor velocities are the result of the high heat of vaporization of ammonia and the high vapor density at the test temperature. Temperature differences are plotted against test hours in Figure 4-34. Both  $T_1 - T_3$  and  $T_2 - T_3$  are very constant throughout the test at about +1.6 and +1.2<sup>o</sup> F, respectively. The fact that both  $T_1 - T_3$  and  $T_2 - T_3$  are positive, and decrease slightly when the capsule temperature is decreased, indicate that there is a slight excess thermal resistance near the No. 3 thermocouple which tends to cause  $T_3$  to be lower than the other two temperatures.

Sectioning of this capsule at the conclusion of the test revealed some discoloration of both the screen and the capsule wall in the liquid region. It is believed that this discoloration is due to some nonvolatile impurity in the ammonia which could have been introduced when the capsule was filled. In particular, the lubricant on the stem threads of the filling valve could have been flushed into the capsule during the filling operation. It should be noted that the ammonia capsule is the only capsule tested in which liquid was inserted into the capsule through the filling valve.

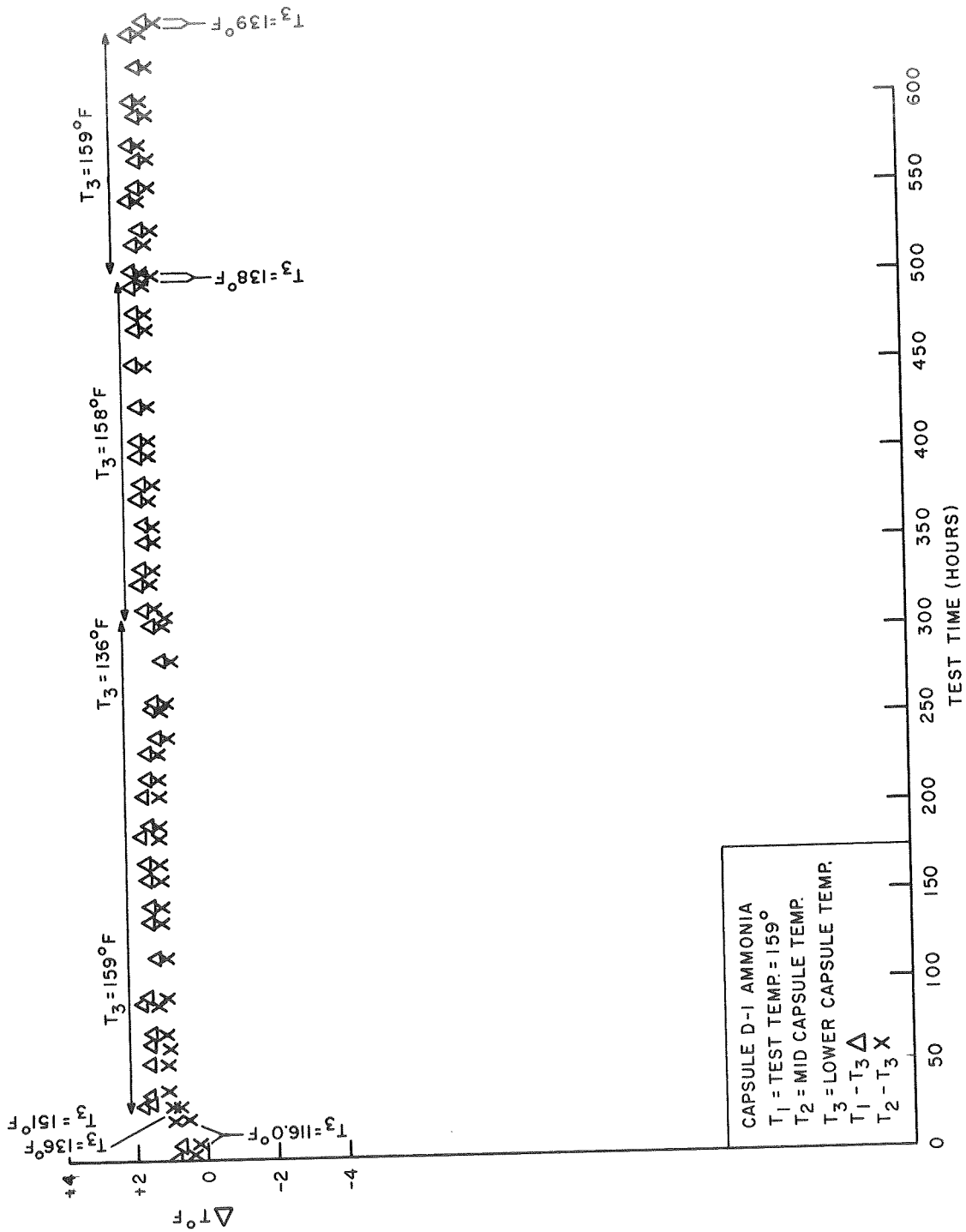


Figure No. 4-34. Capsule Test Data for Ammonia

#### 4.4.5.6 Freon 11 (Capsule D-2) (Capsule D-9)

A capsule containing Freon 11 was run for over 500 hours at 156<sup>o</sup>F, and a second capsule was run for more than 500 hours at 222<sup>o</sup>F. Results of these tests are shown in Figure 4-35 and Figure 4-36. At 156<sup>o</sup>F, the vapor pressure of Freon 11 is 57 psia and the vapor velocities in the first capsule were 0.22 and 0.071 ft/sec at the evaporating surface and at the level of thermocouple No. 3, respectively. In the second Freon 11 capsule, the vapor pressure was 119 psia and vapor velocity at the evaporating surface was 0.16 ft/sec and at thermocouple No. 3, 0.064 ft/sec.

For the first capsule, temperature differences were very constant throughout the test (Figure 4-35) and no significant changes were noted when the capsule temperature was decreased. Similarly, for the second Freon 11 capsule, Figure 4-36, the temperature differences were constant throughout the test with very small changes noted when the capsule temperature was lowered. The positive temperature differences suggest that there was excess thermal resistance in the vicinity of thermocouple No. 3 for the second capsule.

When the first Freon 11 capsule was cut open, a few, small areas of discoloration were observed on the inner wall. The screen appeared clean and the fluid was clear. The second Freon 11 capsule was clean throughout the interior following the test and the fluid was clear.

#### 4.4.5.7 Freon 113 (Capsule D-3) (Capsule D-8)

A capsule containing Freon 113 was tested for over 500 hours at 155<sup>o</sup>F and a second capsule was tested for more than 500 hours at 224<sup>o</sup>F. At 155<sup>o</sup>F the vapor pressure of Freon 113 is 28 psia and at 224<sup>o</sup>F, the vapor pressure is 74 psia. In the first capsule, vapor velocities at the evaporating surface and at thermocouple No. 3 were 0.41 and 0.13 ft/sec, respectively; in the second capsule corresponding values were 0.26 and 0.11 ft/sec. Results of these tests are shown in Figure 4-37 and Figure 4-38.

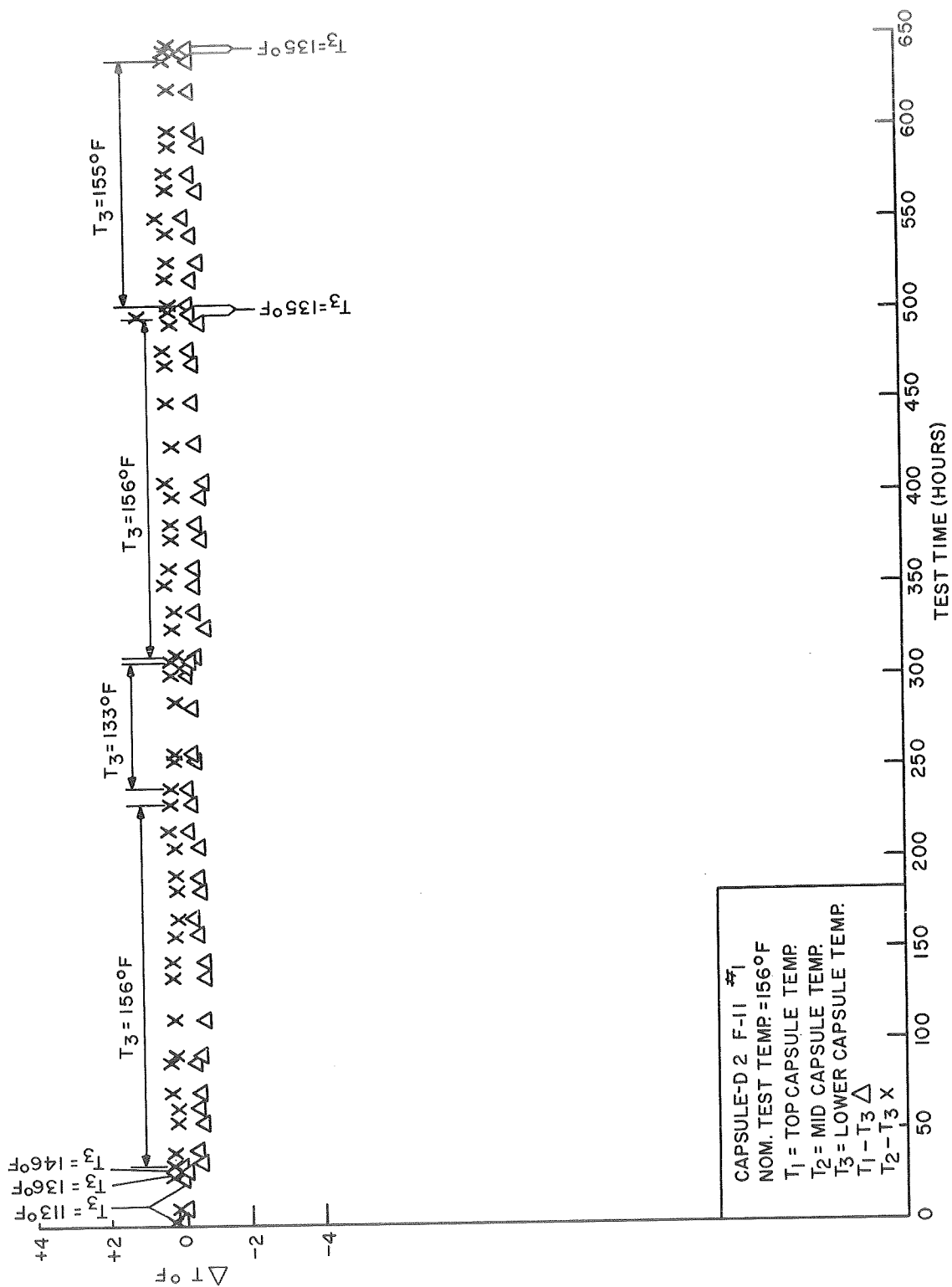


Figure 4-35. Capsule Test Data for Freon 11, Capsule No. 1 (T=156°F)

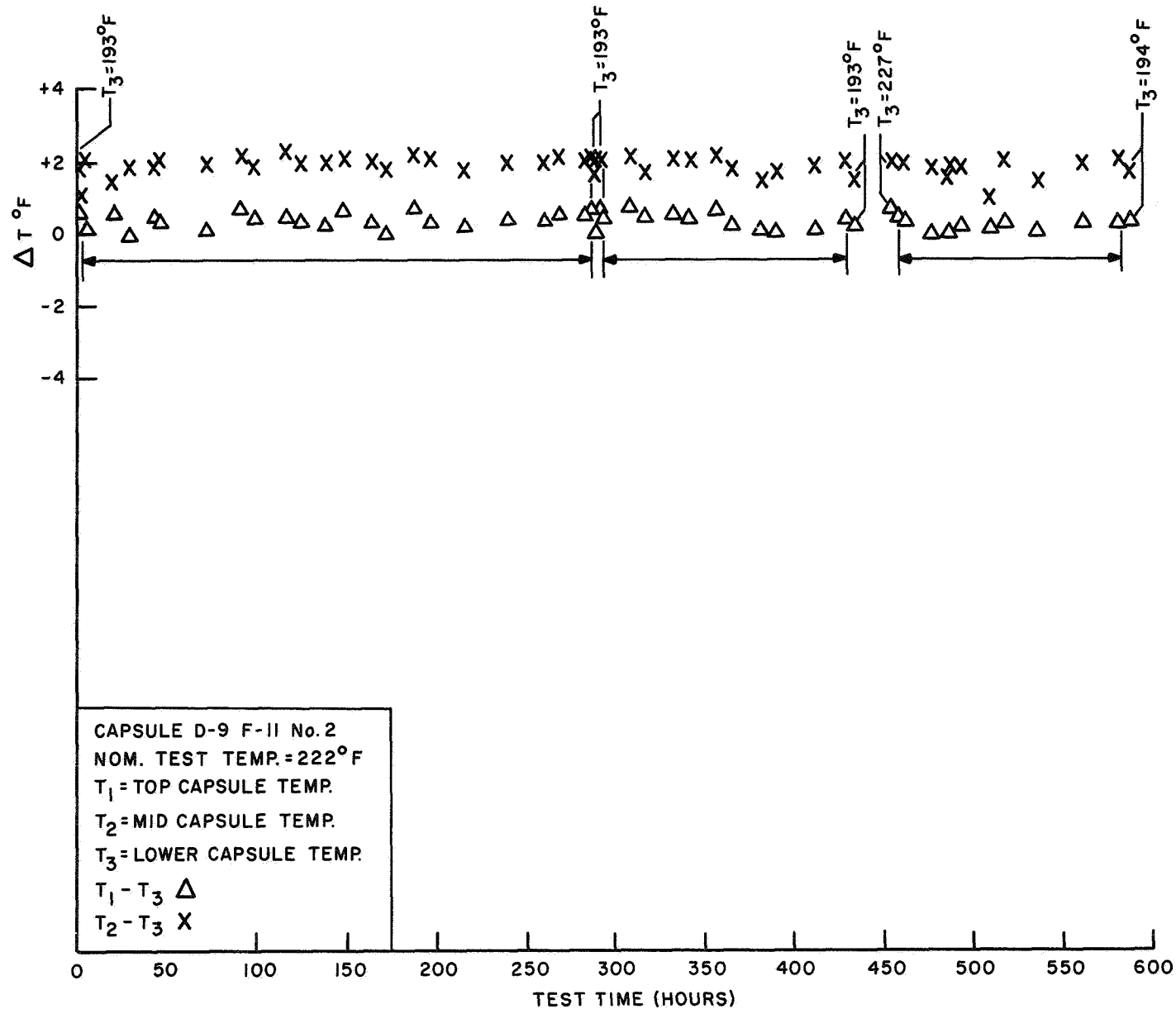


Figure 4-36. Capsule Test Data for Freon 11, Capsule No. 2 (T=222°F)

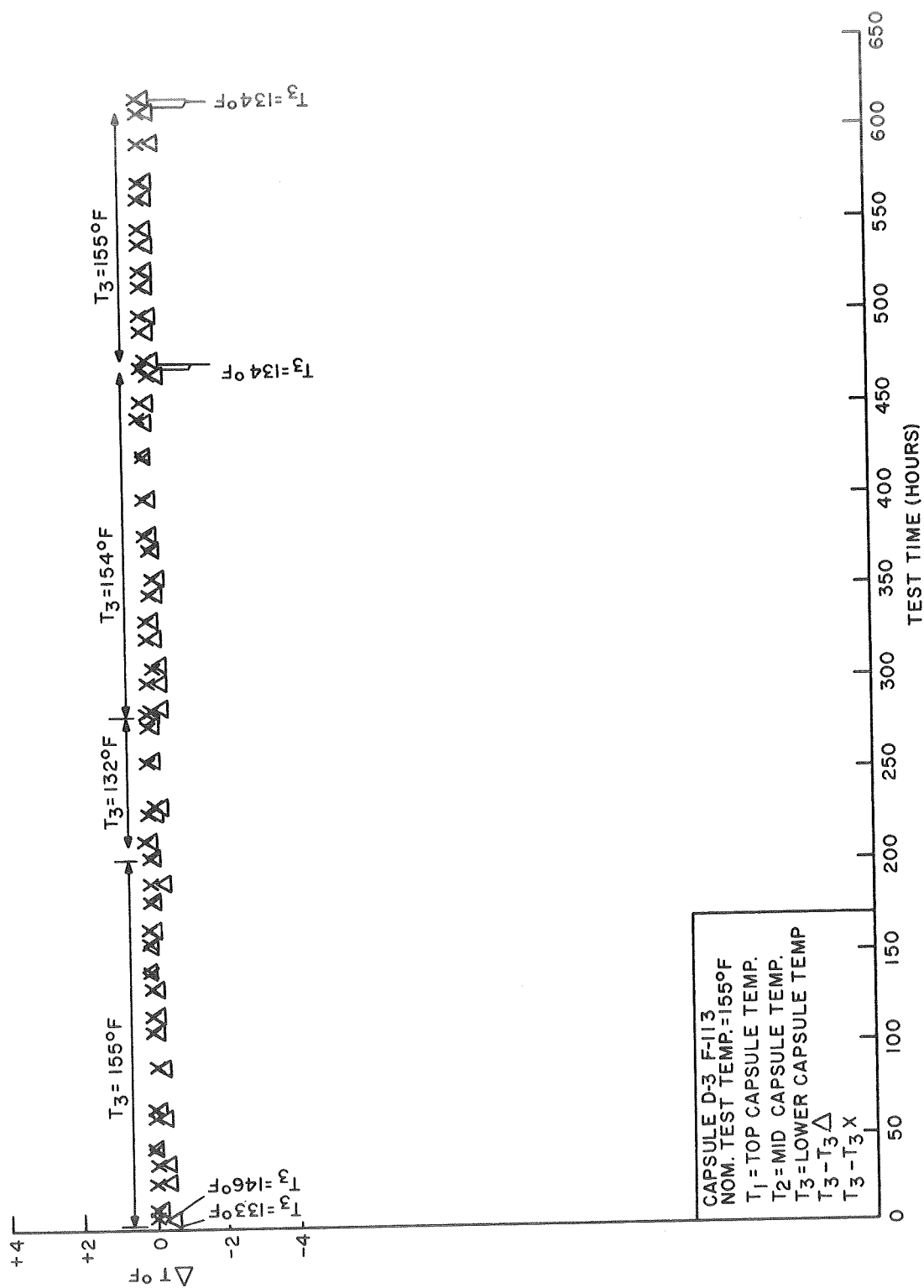


Figure 4-37. Capsule Test Data for Freon 113, Capsule No. 1 (T=155°F)



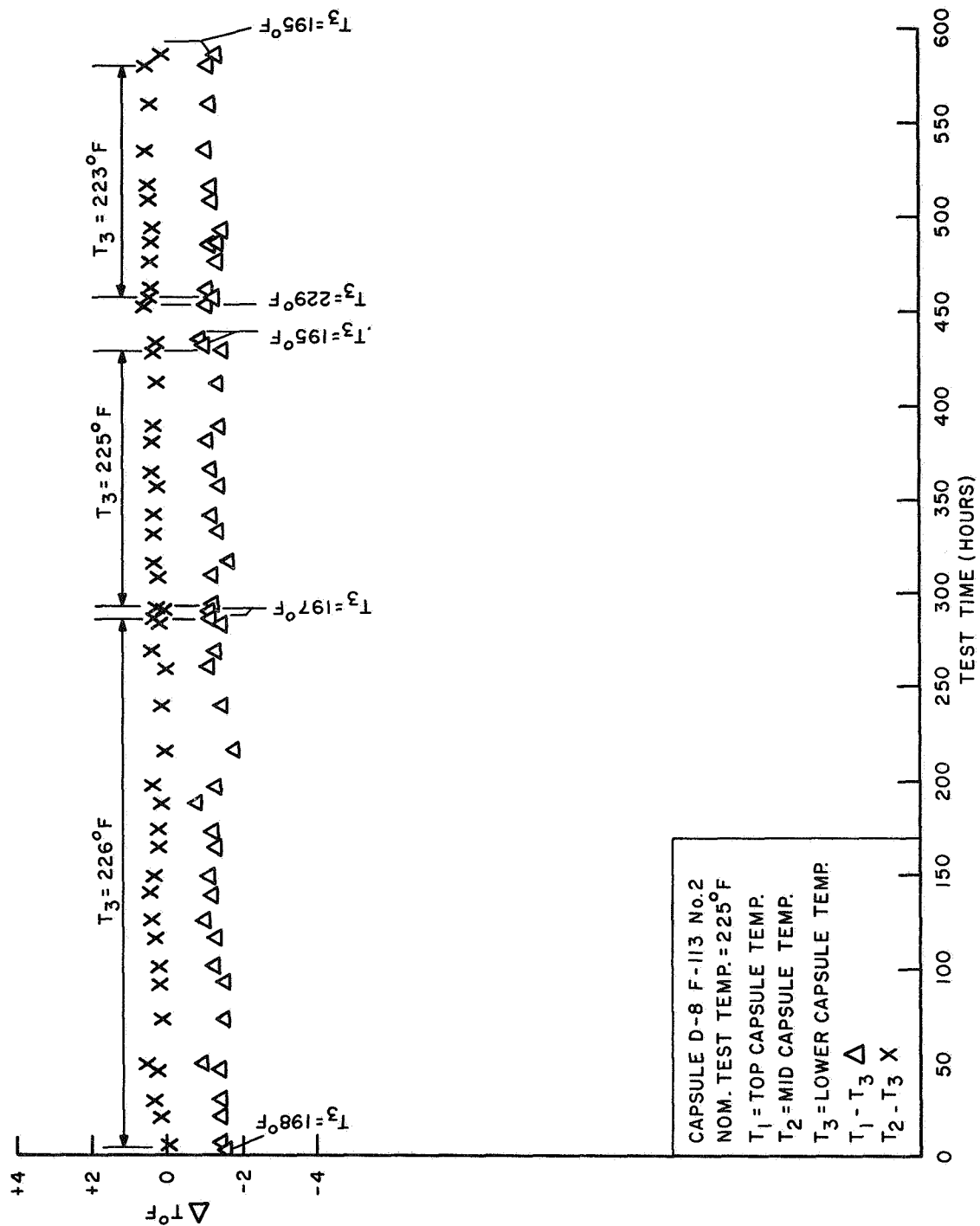


Figure 4-38. Capsule Test Data for Freon 113, Capsule No. 2 (T=225°F)

For the capsule tested at 155<sup>o</sup> F, temperature differences were very constant throughout the test and amounted to only a few tenths of a degree as shown in Figure 4-37.

For the second capsule, temperature differences were constant throughout the test with  $T_1 - T_3$  being -1.4<sup>o</sup> F and  $T_2 - T_3$ , +0.2<sup>o</sup> F (Figure 4-38).

The interiors of both capsules were clean following these tests and the fluid was clear.

#### 4.4.5.8 Toluene (Capsule D-4)

The total test time on the toluene capsule was 600 hours at 323<sup>o</sup> F, at which temperature the toluene vapor pressure is 54 psia. The calculated vapor velocity was 0.62 ft/sec at the evaporating surface and 0.27 ft/sec at thermocouple No. 3. Temperature differences are plotted against test hours in Figure 4-39. A gradual decrease in  $T_1 - T_3$  occurred for the first 200 hours of test, with rather stable readings of about -6<sup>o</sup> F obtained after this time. Very small differences between  $T_2$  and  $T_3$  were noted throughout the test. No significant changes in temperature differences occurred when the changes in temperature differences occurred when the capsule temperature was decreased.

The capsule interior appeared clean after this test with the exception of a small, localized patch of discoloration on the inner wall. This seemed to be a surface deposit with no evidence of attack of the aluminum. The screen material was clean and the fluid was clear at the conclusion of the test.

#### 4.4.5.9 n-Heptane (Capsule D-5)

The total test time on the n-heptane capsule was about 600 hours at 321<sup>o</sup> F at which temperature the vapor pressure is 66 psia. The calculated vapor velocity was 0.42 ft/sec at the evaporating surface and 0.18 ft/sec at the level of thermocouple No. 3. Temperature differences are plotted against test hours in Figure 4-40. Temperature differences were fairly constant throughout the test with  $T_1 - T_3$  being typically -3.7<sup>o</sup> F and  $T_2 - T_3$  about -3.0<sup>o</sup> F. No significant changes were noted in  $T_1 - T_3$  when the

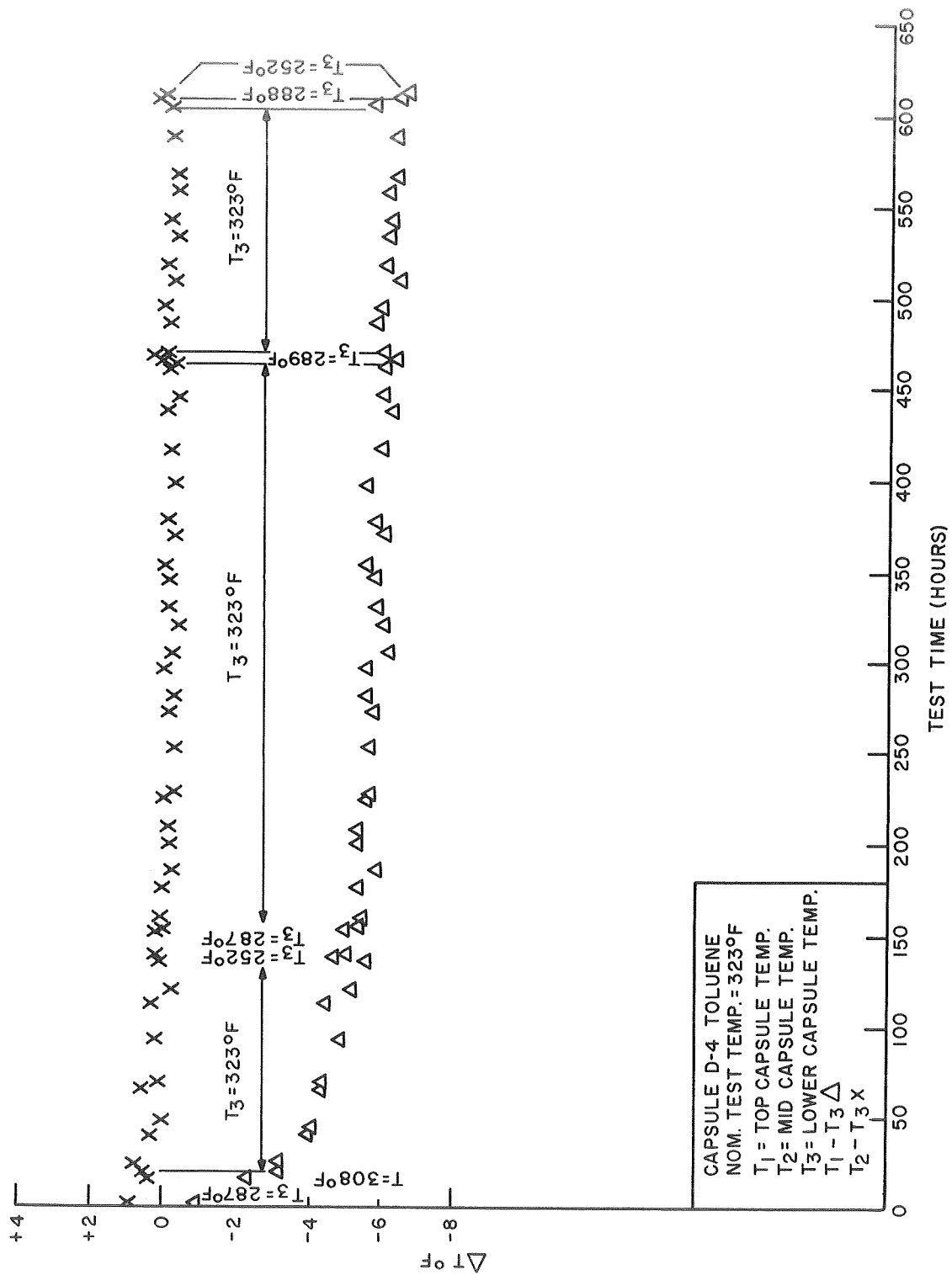


Figure 4-39. Capsule Test Data for Toluene

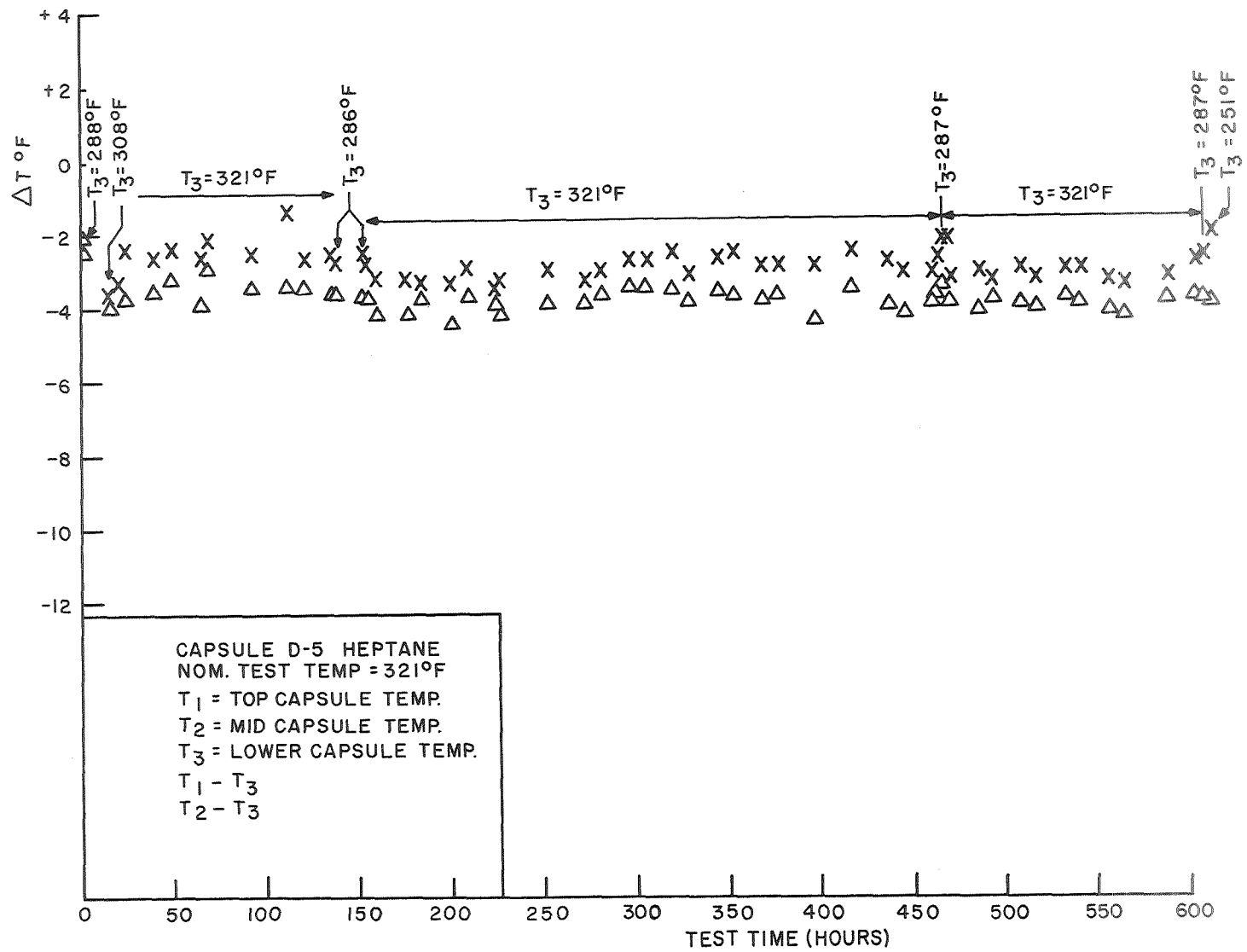


Figure 4-40. Capsule Test Data for n-Heptane

capsule temperature was lowered. However, a slight increase in  $T_2 - T_3$  was observed when the capsule temperature was lowered at 465 hours and again at 608 hours.

This indicates a slight excess thermal resistance in the area of the No. 2 thermocouple.

The entire capsule interior, including the screen, appeared clean after this test, and the fluid removed from the capsule was clear

#### 4.4.5.10 CP-32 (Monsanto Thermodynamic Fluid) Pyridine (Capsule D-6)

The Monsanto thermodynamic fluid, CP-32, was run for 550 hours at  $318^{\circ}\text{F}$ , at which temperature the vapor pressure is 45 psia. The calculated vapor velocity at the evaporation surface was 0.56 ft/sec and 0.25 ft/sec at thermocouple No. 3. Temperature differences are plotted against test hours in Figure 4-41. A gradual decrease in  $T_1 - T_3$  was observed over the initial 250 hours of test after which a constant value of about  $-5.5^{\circ}\text{F}$  was obtained. The temperature difference  $T_2 - T_3$  was more irregular. For the first 50 test hours, there was little if any difference between  $T_2$  and  $T_3$ . After the first 50 hours, a gradual increase in  $T_2 - T_3$  was observed until 200 test hours, after which time the difference became constant at  $+1.6^{\circ}\text{F}$ . After 480 test hours a sudden increase in  $T_2 - T_3$  to  $+4.6^{\circ}\text{F}$  was obtained. This behavior may be explained by assuming an excess thermal resistance in the vicinity of the No. 3 thermocouple which is not constant with time. When the capsule temperature was lowered at 335, 480 and 550 test hours, a decrease in both  $T_1 - T_3$  and  $T_2 - T_3$  was found.

Some rather localized discoloration was found on the interior of the capsule in the liquid region when this capsule was sectioned. This appeared to be a brownish deposit on the surface. The screen appeared to be clean, but the fluid removed from the capsule was slightly darkened.

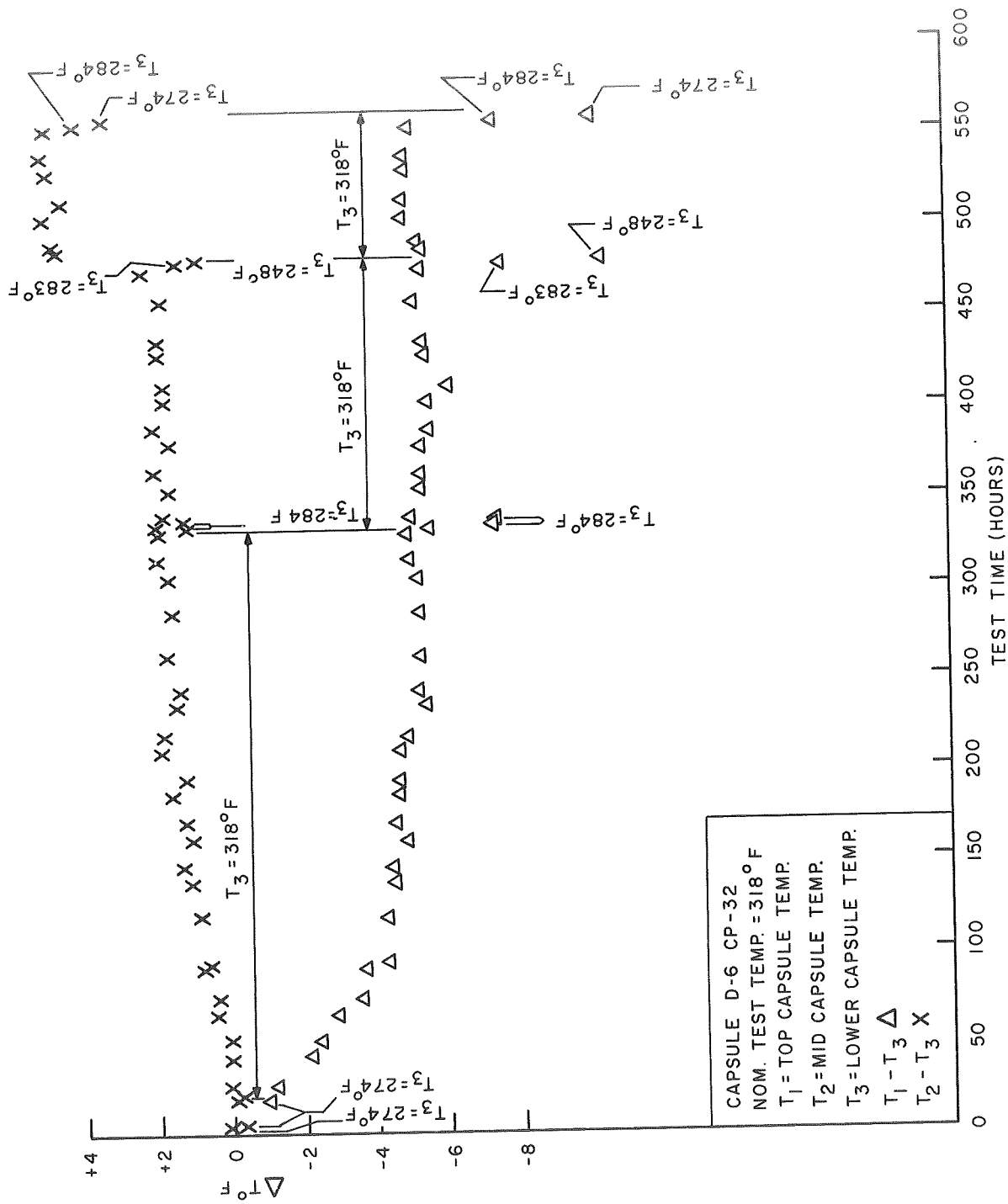


Figure 4-41. Capsule Test Data for CP-32

#### 4.4.5.11 CP-34 (Monsanto Thermodynamic Fluid) (Capsule D-7)

The Monsanto thermodynamic fluid, CP-34, was tested for 550 hours at 319<sup>o</sup>F at which temperature the vapor pressure of CP-34 is 93 psia. The calculated vapor velocity at the evaporating surface was 0.32 ft/sec and at the No. 3 thermocouple, was 0.14 ft/sec. Temperature differences are plotted against test hours in Figure 4-42. A gradual decrease in  $T_1 - T_3$  was noted for the duration of the test, with the value reaching -8.7<sup>o</sup>F at the conclusion of the test. The difference  $T_2 - T_3$  was quite stable at about -1.0<sup>o</sup>F. A decrease in  $T_1 - T_3$  was observed when the capsule temperature was lowered at 430 and again at 550 test hours.

Sectioning of the capsule at the conclusion of the test revealed a rather extensive area of local discoloration on the capsule wall near the liquid surface. No apparent discoloration was found on the screen. The fluid removed from the capsule was considerably darkened.

#### 4.4.5.12 n-Butane (Capsule D-10) (Capsule D-11)

A capsule containing n-butane was tested for over 500 hours at 155<sup>o</sup>F at which temperature, the vapor pressure is 114 psia. Calculated vapor velocities were 0.13 ft/sec at the evaporating surface and 0.043 ft/sec at the level of thermocouple No. 3. Temperature differences for this test are plotted against test hours in Figure 4-43. A gradual decrease in  $T_1 - T_3$  was observed over the first 70 hours of test at 132<sup>o</sup>F. The capsule temperature was then increased to 153<sup>o</sup>F and  $T_1 - T_3$  continued to decrease and, after about 250 test hours, leveled off at -18.5<sup>o</sup>F. There was no significant difference between  $T_2$  and  $T_3$  when  $T_3$  was 155<sup>o</sup>F, but with  $T_3$  at about 133<sup>o</sup>F,  $T_2 - T_3$  was about -1.0<sup>o</sup>F. There was, however, no significant change in  $T_1 - T_3$  when the capsule temperature decreased to 133<sup>o</sup>F.

One might be inclined to attribute this behavior to evolution of non-condensable gas within the capsule, except for the fact that  $T_1 - T_3$  did not change appreciably when the capsule temperature was decreased. A more likely explanation seems to be

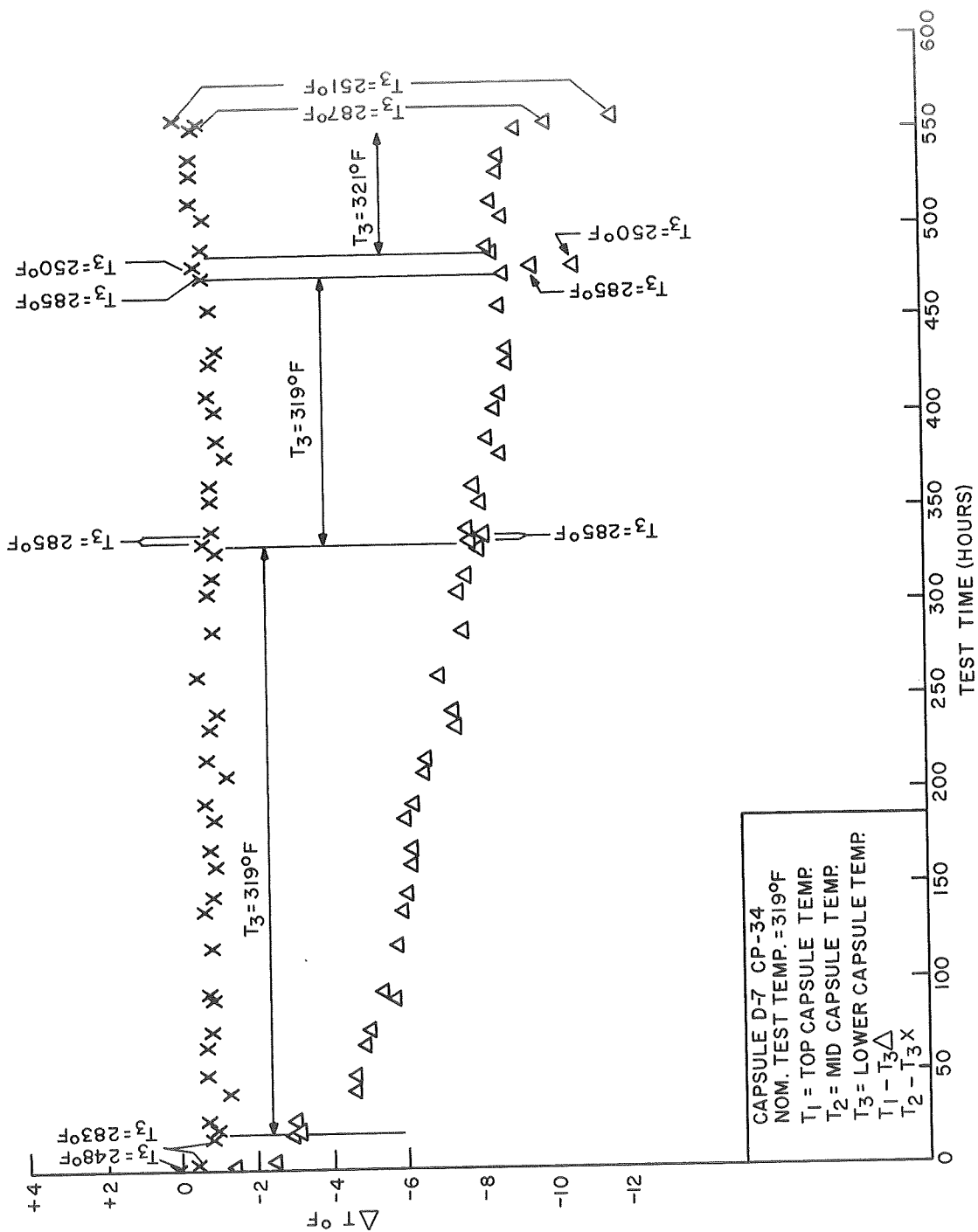


Figure 4-42. Capsule Test Data for CP-34



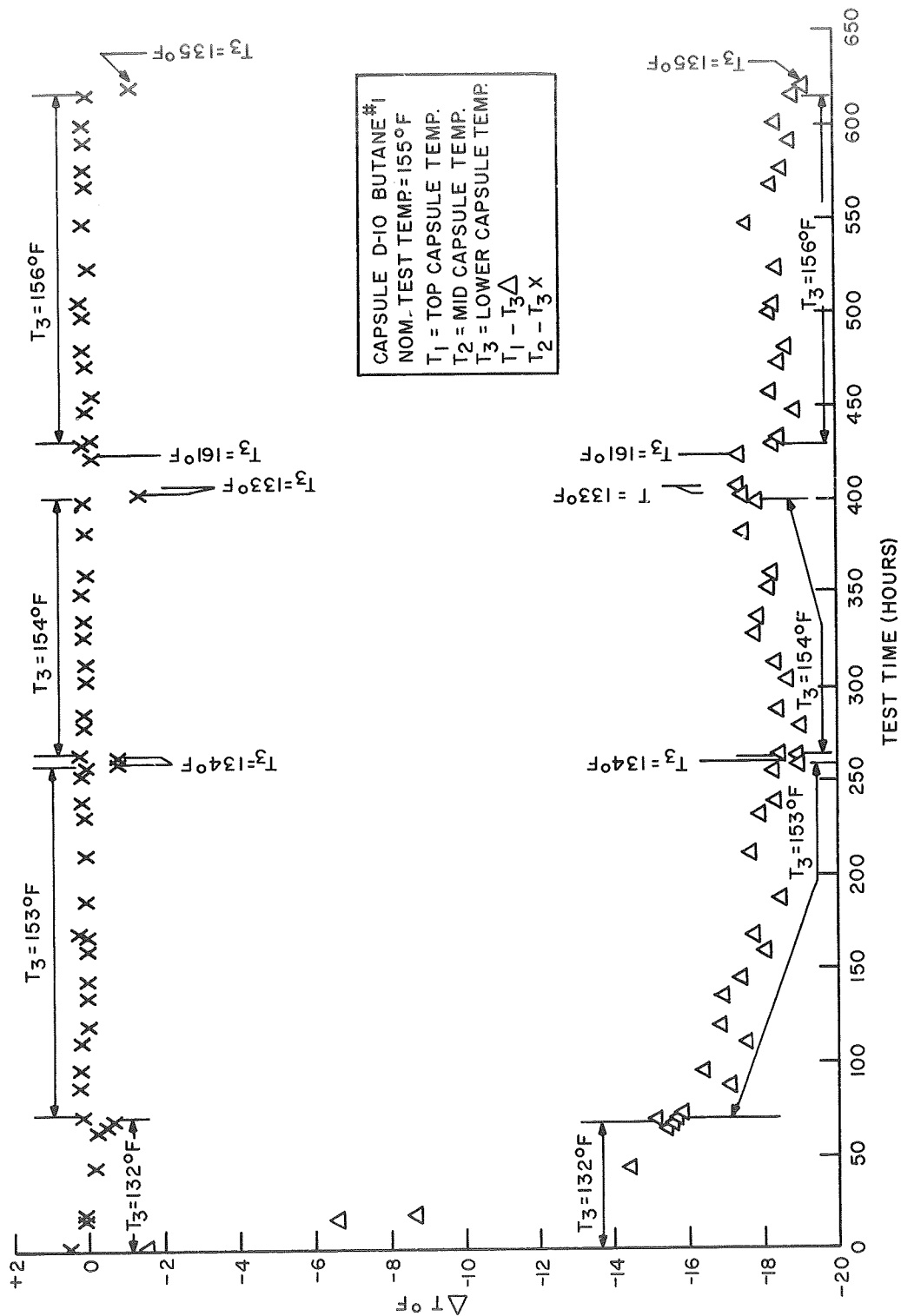


Figure 4-43. Capsule Test Data for n-Butane, Capsule No. 1

that some impurity was present in the initial charge of n-butane and that this impurity gradually concentrated in the heat rejection end of the capsule. The behavior of heat pipes with multicomponent fluids has been described in detail by Cotter (Ref. 23).

Cotter has shown that due to the requirements of conservation of mass, local vapor-liquid equilibrium, and essentially isobaric conditions throughout the pipe, the more volatile component of a two-component fluid must separate and reflux independently at the heat rejection end of the pipe. The pressure in the pipe is determined by the equilibrium vapor pressure of the less volatile component at the temperature attained near the heat input section, while the temperature in the zone containing the more volatile component is a temperature at which the equilibrium vapor pressure is the same as that of the less volatile component.

A major impurity in the instrument grade n-butane is isobutane (Ref. 19). A small quantity of isobutane in the initial n-butane charge would cause a temperature difference of  $-22^{\circ}\text{F}$  based on available vapor pressure data, which is in good agreement with the observed value of  $-18.5^{\circ}\text{F}$ . The data of Figure 4-43 can thus be explained by the assumption of a condensable impurity, probably isobutane, in the initial n-butane charge.

In order to further investigate the behavior of n-butane in the reflux capsule, a second capsule was filled with n-butane. In an attempt to eliminate impurities from this second capsule, the capsule was heated at about  $140^{\circ}\text{F}$  for 40 hours before finally venting and sealing the capsule. The capsule was then heated in the oil bath at  $150^{\circ}\text{F}$  for more than 500 hours. Temperature differences during this time are plotted in Figure 4-44. In this test,  $T_1 - T_3$  decreased and leveled off at about  $-6.2^{\circ}\text{F}$  compared to  $-18.5^{\circ}\text{F}$  for the first butane capsule. These results indicate that the treatment given the second capsule served to diminish the temperature differences developed during the test but apparently did not completely purge the capsule of isobutane. The interiors of both the first and second n-butane capsules were clean at the conclusion of the tests and the fluid was clear.



#### 4.4.6 EVALUATION AND CONCLUSIONS FOR THE SELECTION OF VAPOR CHAMBER WORKING FLUIDS

As stated previously, the selection of working fluids was based upon thermal performance as well as material compatibility. The effort as discussed in this section was devoted to identifying fluids with suitable thermal performance characteristics and then subjecting the candidate fluids to a controlled material compatibility test.

The primary indicator of the overall stability of a particular fluid-material combination in the capsule tests was the change in temperature of the top thermocouple with respect to the other two. This is, apparently, a very sensitive indication of the homogeneity of the vapor within the capsule. Non-homogeneity of the vapor, however, can arise from thermal decomposition of the fluid, reaction of the fluid with the capsule material, separation of volatile impurities, or simply outgassing of the fluid. In an attempt to determine the source of the foreign vapor, the change in  $T_1 - T_3$  was noted when the capsule temperature was decreased, as was the appearance of the capsule interior and the fluid following the test.

It should be emphasized that the present tests were planned to investigate the compatibility of a particular fluid-material combination for long-term (5-year) use in a vapor chamber radiator under specified conditions. The reference conditions call for a steady state temperature of 288° F for the primary radiator fluid at the inlet to the radiator and a 320° F short-term peak temperature. The actual temperature to which the vapor chamber working fluid is exposed must be somewhat less than the primary radiator fluid temperature, since some temperature drop occurs from the primary radiator fluid to the evaporative surface within the vapor chamber. It is estimated that, in these capsule tests, the high-temperature fluids were exposed to temperatures at least 20° F higher than the peak temperature and at least 50° F greater than long-term steady state temperature that the fluids would experience in the actual radiator. In addition, the fluid inventory in these capsule tests was considerably in excess of that to be employed in the actual radiator. Thus, while the time of exposure in these capsule tests is only about 1% of the planned radiator lifetime, the conditions of exposure

were much more severe. It seems reasonable, then, to assume that if the fluid-material combination completed the capsule tests with no adverse effects, it is a likely candidate for a radiator with a 5-year lifetime.

A summary of the test results is shown in Table 4-10.

#### 4.4.6.1 Acceptable Fluids

On the basis of the capsule compatibility tests, the following fluids are judged to be acceptable for long-term use in a vapor chamber radiator, constructed of 6061 aluminum for a working fluid temperature not exceeding 300° F:

1. Benzene
2. n-Heptane
3. n-Pentane

Benzene and n-heptane showed no indication of adverse effects throughout the capsule tests. The n-pentane showed stable temperatures but some discoloration of both the fluid and the interior of the capsule occurred. This discoloration could have resulted from a nonvolatile residue in the initial fluid charge.

The following fluids are judged to be suitable for long-term use in 6061 aluminum for fluid temperatures not exceeding 200° F:

1. Freon 11
2. Freon 113

Neither fluid showed indication of deterioration in 500-hour tests at 155° F and at 225° F. Data from Dupont (Ref. 24) indicates a corrosion rate of Freon 11 with aluminum of  $0.7 \times 10^{-6}$  inch per month at 130° F and  $0.5 \times 10^{-6}$  inch per month at 250° F. The DuPont data also shows a decomposition rate of 0.1 per cent per year at 192° F. Other tests with Freon 113 (Ref. 25) showed no corrosion with aluminum in 100 hours at the boiling point. Freon 113 has also been stored with various metals at 300° F for two years with 0.3 to 0.4 per cent decomposition.

TABLE 4-10. SUMMARY OF CAPSULE TEST DATA

Capsule Identification	Fluid	Bath Temp. ( $^{\circ}$ F)	Test Temp. ( $^{\circ}$ F)	Test Hours	Test Results
C-1	Methyl Alcohol		Test not completed	-	Gas generated during fill
C-2	n-Pentane	362	316	570	No gas, no corrosion, slight fluid discoloration
C-3	Benzene	362	316	570	Showed good stability
SS-1	Water	362	327	570	Gas generation and corrosion occurred
D-1	Ammonia	183	159	500	Showed good stability
D-2	Freon 11	183	156	500	Showed good stability
D-3	Freon 113	183	155	500	Showed good stability
D-4	Toluene	362	323	600	Showed good stability
D-5	n-Heptane	362	321	600	Showed good stability
D-6	CP-32 (Pyridine)	362	318	550	No gas, but deposits and fluid discoloration occurred
D-7	CP-34	362	319	550	Slight gas and fluid discoloration
D-8	Freon 113	260	224	500	Showed good stability
D-9	Freon 11	260	222	500	Showed good stability
D-10	n-Butane	183	155	500	Gas due to impurities
D-11	n-Butane	183	150	500	Showed good stability

The following fluids are suitable for long-term use in 6061 aluminum at fluid temperatures not exceeding 150<sup>o</sup>F:

1. Ammonia
2. n-Butane

The ammonia capsule gave very stable temperature differences throughout the test. The discoloration observed in the capsule interior is thought to be due to impurities accidentally introduced when the capsule was filled. The temperature decrease observed in both n-butane capsules is consistent with the assumption of a volatile impurity, probably isobutane, contained in the initial fluid charge.

The results of capsule tests on toluene were not conclusive. Although a decrease in top capsule temperature occurred throughout the test, there was no decrease in  $T_1 - T_3$  when the capsule temperature was reduced and no fluid discoloration was noted. On the basis of the test data no acceptance or rejection of the fluid could be made.

#### 4.4.6.2 Fluids Not Suitable For Use in Vapor Chamber

On the basis of the capsule test results, the following fluids were found to be not acceptable for long-term use in vapor chambers operating at the indicated temperature:

1. Water in type 321 stainless steel at 330<sup>o</sup>F
2. CP-32 (Pyridine) in 6061 aluminum at 320<sup>o</sup>F
3. CP-34 in 6061 aluminum at 320<sup>o</sup>F
4. Methyl alcohol in 6061 aluminum at 160<sup>o</sup>F
5. Toluene in 6061 aluminum at 320<sup>o</sup>F.

The capsule tests indicate that water oxidizes type 321 stainless steel at 330<sup>o</sup> with evolution of hydrogen. It has been shown, however, in a test at Los Alamos (Ref. 26) that no noncondensable gas is evolved when water is in contact with type 347 stainless steel at about 200<sup>o</sup>F. In a heat pipe life test, the pipe has been operated for over 3000 hours with no noticeable change in the temperature pattern.

The capsules containing the two Monsanto thermodynamic fluid, CP-32 and CP-34, both showed a decrease in upper capsule temperature; and, in addition, some discoloration of the fluid occurred. Information from the Monsanto Company (Ref. 27) indicates good thermal stability for CP-34 (0.5% decomposed in 920 days at 450<sup>o</sup>F). Corrosion evaluation of CP-34 with aluminum at 300<sup>o</sup>F for 244 hours gave a corrosion rate of  $0.21 \times 10^{-3}$  inch per year in the liquid zone and less than  $0.07 \times 10^{-3}$  inch per year in the vapor zone. Similar corrosion evaluation of CP-32 with aluminum gave corrosion rates of less than  $1 \times 10^{-3}$  inch per year for both vapor and liquid.

Methyl alcohol was found to react rapidly with aluminum at temperatures above the boiling point. This reaction was accompanied by evolution of hydrogen. The attack was especially severe on the screen material (1100 alloy). Corrosion of aluminum by various anhydrous alcohols has been reported elsewhere (Ref 28). The available information, thus, indicates that the alcohols in general, and methyl alcohol in particular, are not suitable for use in aluminum vapor chambers.



## SECTION 5

### RADIATOR DESIGN

#### 5.1 DESIGN CONCEPTS

##### 5.1.1 GENERAL DISCUSSION

The prime objective of the radiator design study is to identify a promising Brayton cycle vapor chamber radiator. A secondary objective is to compare this vapor chamber radiator to the alternative conduction fin radiator. Therefore, this study formulates conceptual designs which offer the best potential performance for both the vapor chamber and conduction fin radiators. In either case, the Brayton cycle radiator requirements necessitate the use of primary and secondary radiator loops. The primary radiator system serves to cool the Brayton cycle power plant working fluid, whereas, the secondary radiator, operating at somewhat lower temperatures, cools the system rotating machining and auxiliary equipment.

The vapor chamber fin radiator is relatively complex compared to the conventional round tube conduction fin radiator. However, it was determined early in the study that the fluid mechanics and thermodynamics associated with the Dow Corning 200 (DC-200) primary radiator fluid makes a conventional round tube unsatisfactory for the alternative conduction fin radiator and a more complex fluid passage geometry must be employed. To make a fair comparison between vapor chamber and conduction fin radiators, both concepts were evolved as the performance aspects demanded. The complexity of fabrication and assembly procedures were kept consistent for both radiators throughout the design evaluation. The resulting radiator designs and comparisons are a direct function of the Brayton cycle characteristics. A high Brayton cycle system thermodynamic efficiency requires rejection of waste heat at the lowest temperature possible. Also, the Brayton cycle requires a large inlet to outlet temperature change

of the primary radiator fluid. Consequently, the radiator operates at a low average temperature.

Significant effects of the Brayton cycle power system requirements on the radiator designs are:

1. A low primary radiator fluid flow rate plus the selection of an organic fluid leads to laminar flow solutions.
2. Low heat fluxes and low operating temperatures yield high conduction fin efficiencies.
3. Required operating temperatures restrict the vapor chamber fluid selections to those with relatively poor heat transfer and flow properties compared to liquid metals.

#### 5.1.2 VAPOR CHAMBER FIN RADIATOR DESIGN

Both the vapor chamber fin and conduction fin radiator diameters were limited to the envelope restrictions of the 10-foot-diameter launch vehicle aerodynamic shroud. For the vapor chamber radiator, there are two obvious possibilities for the orientation of the primary tubes and vapor chambers (Figure 5-1).

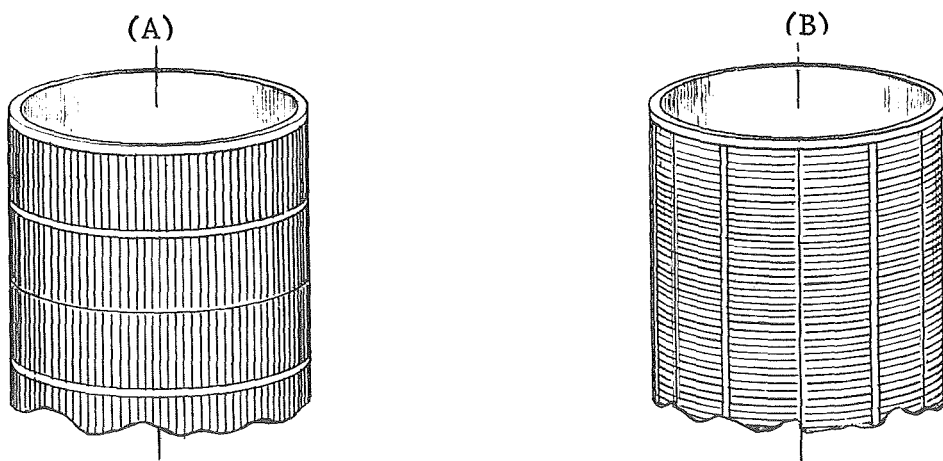


Figure 5-1. Configuration Possibilities

Each design, fabricating either curved primary tubes (A) or curved vapor chamber tubes (B), presents a fabrication difficulty.

Heat rejection is equivalent for both configurations, but the structural capabilities differ. Meteoroid protection requirements and the heat transfer characteristics associated with the primary fluid ducts concentrate a significant part of the vapor chamber fin radiator weight in the primary fluid loop. Vertical orientation (concept B) of the primary fluid ducts enables them to be utilized as supporting structures and reduces the weight by eliminating the need for purely structural longitudinal stiffeners.

Studies in working fluid selection (see Section 4.3) indicated that vapor chamber lengths somewhat greater than 2 feet were acceptable for the candidate fluids and six fluid ducts could be considered. The six primary ducts were arranged to form a hexagon, eliminating the fabrication problem of curved vapor chambers at a cost of less than 5 percent increased radiator length. This conceptual arrangement (Figure 5-2) appeared advantageous on all counts and was selected for more detailed study.

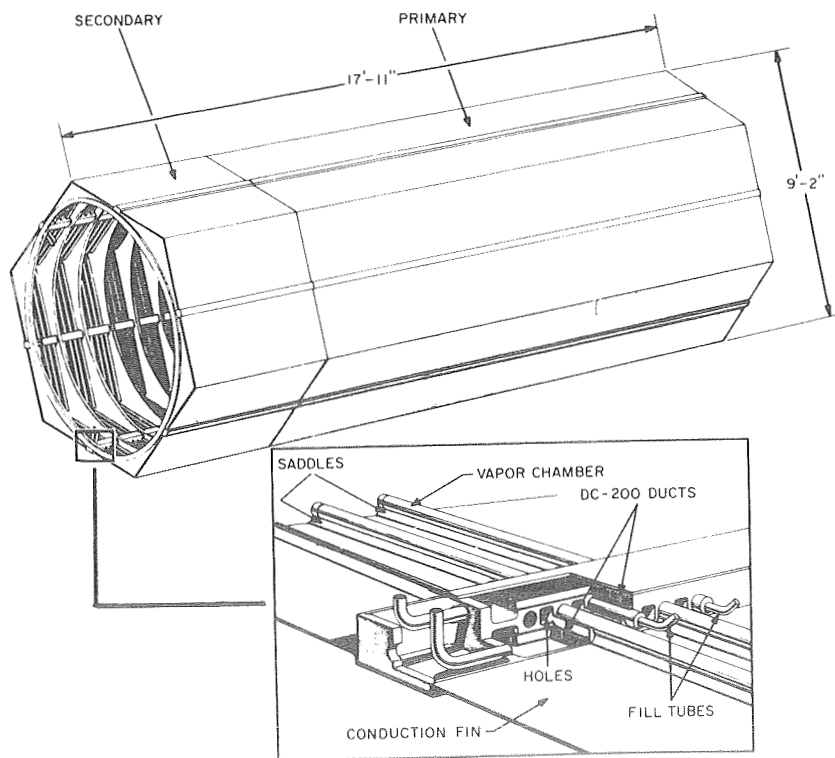


Figure 5-2. Vapor Chamber Radiator Conceptual View

The primary fluid duct and vapor chamber geometries were determined mainly by the heat transfer and meteoroid protection criteria. Three major temperature drops occur between the primary radiator fluid and the vapor chamber fin radiating surface:

1. The bulk primary fluid to the evaporator outer wall temperature drop.
2. The evaporator inner wall to the vapor stream temperature drop.
3. The vapor stream to the vapor chamber fin inner condensing wall temperature drop.

All of the other temperature drops were comparatively minor.

Since the laminar convective heat transfer coefficient is approximately inversely proportional to the hydraulic flow diameter, it is imperative to reduce the hydraulic flow diameter to obtain a reasonable heat transfer coefficient. The laminar film temperature drop can be reduced further by providing a large amount of heat transfer area. Both a small hydraulic diameter and a large heat transfer surface area are achieved by designing the primary fluid ducts with closely spaced fins. Preliminary designs without finned ducts showed the temperature drop across the DC-200 laminar film to be excessive (on the order of 100°F). The inclusion of fins reduced this  $\Delta T$  to a few degrees.

The second significant temperature drop occurs across the evaporator. As previously discussed, this temperature drop was assumed to follow the Cichelli and Bonilla relationship for organic fluids (see Sections 4.2 and 4.3). The factors which governed the design of the evaporator were the need to maintain close proximity with the primary radiator fluid and to provide a continuous flow path for the condensate from the condenser to all parts of the evaporator. Failure to keep a good heat transfer path between the primary radiator fluid and evaporator results in an added temperature drop, a lower evaporator temperature and an uneven evaporator temperature distribution. Because

the width of the primary fluid duct is constrained by the meteoroid protection requirements, it is clear that the evaporator length will be restricted. The evaporator was designed as a round tube to keep a continuous condensate flow path with the round tube vapor chamber condenser section. The round tube selected combines excellent structural integrity with ease of fabrication and, at the same time, is compatible with the numerous possibilities for the condenser wick design. The final primary duct-evaporator configuration concept is shown in Figure 5-3.

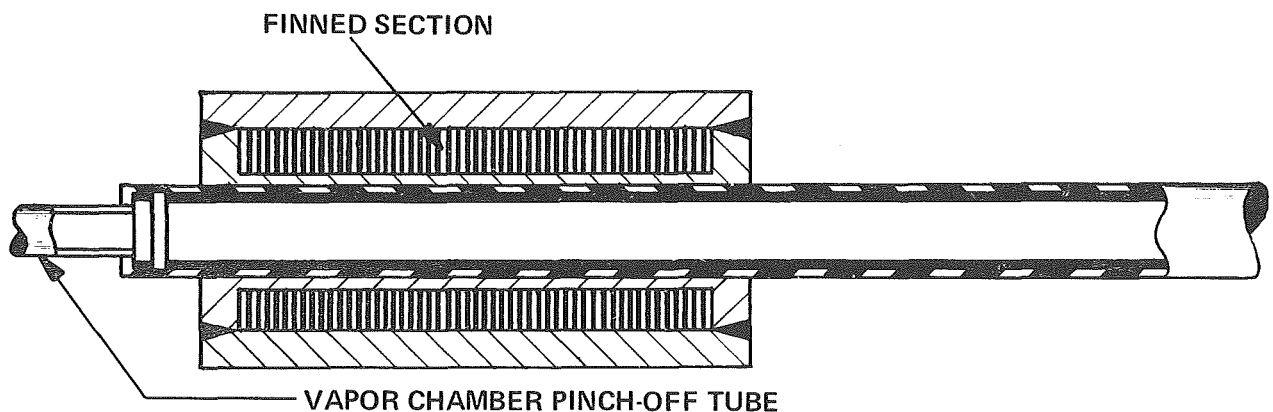


Figure 5-3. Final Primary Duct-Evaporator Configuration

Only one of the primary fluid ducts is assumed to operate at any one time. With this arrangement, the evaporator side furthest from the operating duct will operate at a lower temperature than the near side; however, this temperature difference is less than a degree because of the good heat transfer path afforded by the aluminum. The alternative would be to place each operating primary duct above and below the evaporator (Figure 5-4). This design is not as efficient because it does not utilize all of the available evaporator area at any one time.

By staggering the vapor chambers, the most effective use of the primary duct area is obtained (Figure 5-5).

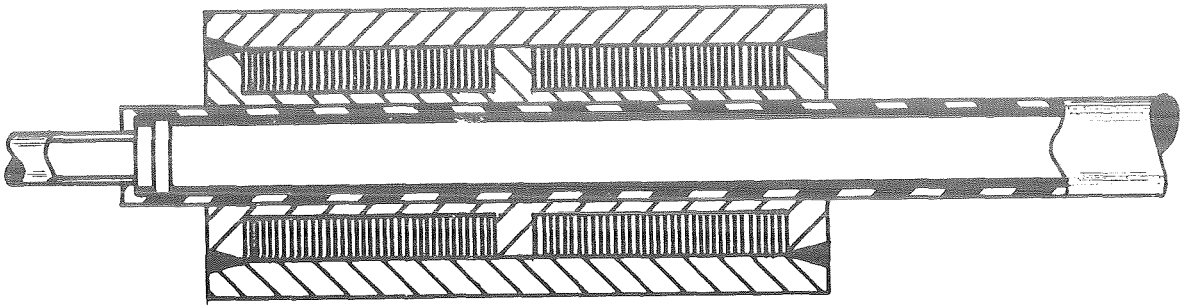


Figure 5-4. Alternative Design

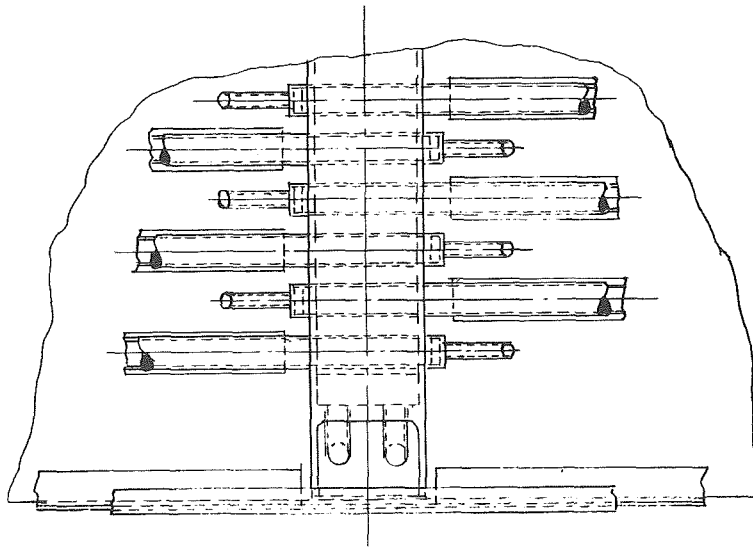


Figure 5-5. Staggered Vapor Chambers

The conduction fins separating the vapor chambers serve to prevent evaporation in the condenser section due to the axial radiator temperature gradient and yield a lighter weight design as will be shown later.

The condensing temperature drop is largely dependent upon the thickness of the condensing film. Efforts to reduce this temperature drop were directed towards finding a condensing wick design which would limit this film thickness to approximately 0.010 inch or less. At the same time, the condensing film flow area must be large enough to keep the frictional flow losses low so that capillary pumping can be effected. Both of these aims can be achieved by configuring the condensing wick as shown in Figure 5-6. The bulk of the condensation occurs on the upper portion of the wick which is closest to the radiating surface. The condensate then flows down along the wick into the reservoir provided in the lower section where it is drawn by capillary action back to the evaporator.

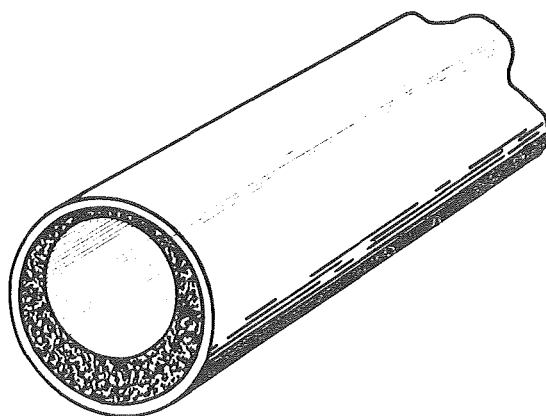


Figure 5-6. Condensing Wick

Various approaches for connecting the vapor chambers to the conduction fins were investigated. From a thermal standpoint, the central fin design (Figure 5-7) would be most advantageous. Although thermal requirements would permit extremely thin fins, fabrication and handling considerations require a fin thickness of at least 0.020 inch. Meteoroid armor protection on the chambers of at least 0.040 inch is required using this approach.

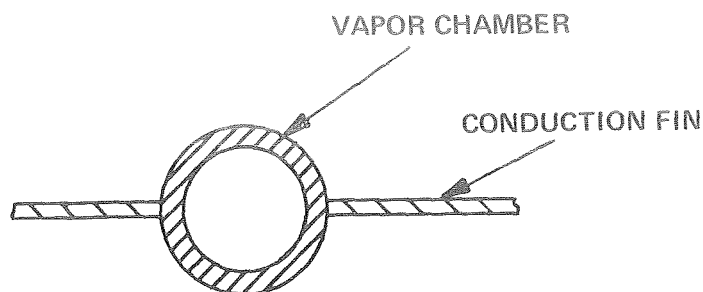


Figure 5-7. Central Fin Design

Another concept which utilizes the conduction fins as meteoroid bumper protection was found to offer a structurally superior design with increased meteoroid protection at no expense in weight. This configuration takes advantage of the fin thickness and enables the vapor chamber walls to be reduced to the minimum allowable for fabrication and handling; 0.015 inch. The offset chamber configuration (Figure 5-8) becomes exceptionally attractive as chamber diameter increases. The standoffs, which connect the vapor chambers to the conduction fin, are 2.5 times the required armor thickness in height in order to satisfy the bumper criteria for meteoroid puncture. As a result of the relatively low heat fluxes in the condenser section and the high conductivity of aluminum, the temperature drop across the standoffs is negligible.

### 5.1.3 CONDUCTION FIN RADIATOR DESIGN

The conduction fin radiator design concept was dictated by the poor heat transfer properties of the organic working fluid and, to a lesser extent, the meteoroid protection requirements. Previous radiator designs have been characterized by round flow tubes, but in this application, the radiator areas become very large because of the large liquid film temperature drop. Therefore, a different approach to the conduction fin radiator was needed, one which was consistent in comparison of complexity with the vapor chamber fin concept.



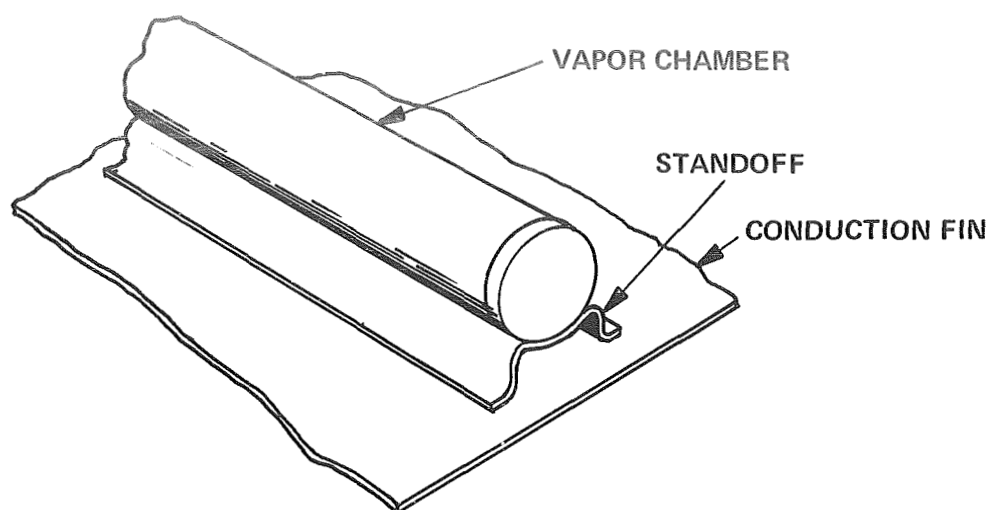


Figure 5-8. Offset Chamber Configuration

The low flow rate dictated by the Brayton cycle, coupled with the pressure drop restrictions, made operation in the turbulent flow regime impractical. The Reynolds number for round tubes can be expressed as:

$$N_{RE} = \frac{4 W_{TOT}}{\pi \mu D N_t} \quad (5-1)$$

where:

$W_{TOT}$  = total flow rate

$\mu$  = viscosity of fluid

$D$  = tube diameter

$N_t$  = number of parallel flow tubes

For DC-200 in the temperature range of interest, the above relationship can be reduced to:

$$N_{RE} = 2.04 \times 10^4 \left( \frac{W_{TOT}}{D N_t} \right) \quad (5-2)$$

Where  $W_{TOT}$  is in lb/sec and  $D$  is in inches. From Figure 5-9, it can be seen that for a reasonable pressure drop and a reasonable tube diameter, turbulent flow operation cannot occur with more than six parallel flow tubes. In order to keep the radiator dimensions reasonable with six or fewer tubes, it is necessary to arrange the flow tubes in a serpentine configuration. This consideration results in a lengthening of any one individual flow path. The pressure drop relationship for this situation can be conservatively expressed for turbulent flow as:

$$\Delta P = 2.08 \times 10^{-7} \left( \frac{N_{RE}^{1.8}}{D^3 N_t} \right) \text{ psi} \quad (5-3)$$

This equation assumes a 6-inch tube spacing and a fictitious radiator area assuming no fluid film temperature drop and a 100 percent fin efficiency. Imposing the 25 psi pressure drop restriction, Figure 5-9 shows that the number of tubes must be reduced to three for turbulent operation to be maintained within the pressure drop limit (point 1). The tube diameters necessary to reduce the pressure drop are relatively large and tend to lower the convective heat transfer coefficient and present large vulnerable areas. The convective heat transfer coefficient, calculated from a form of the Dittus-Boelter equation, (Ref. 29) can be written for DC-200 as:

$$h = 0.023 \frac{k}{D} N_{RE}^{0.8} N_{PR}^{0.333} \left( \frac{\mu}{\mu_W} \right)^{0.14} \frac{\text{Btu}}{\text{hr-ft}^2\text{-}^\circ\text{F}} \quad (5-4)$$

where:

$k$  = liquid conductivity  
(for turbulent flow)

$N_{PR}$  = Prandtl number

$\mu$  = viscosity of bulk fluid

$\mu_W$  = viscosity of fluid at the wall

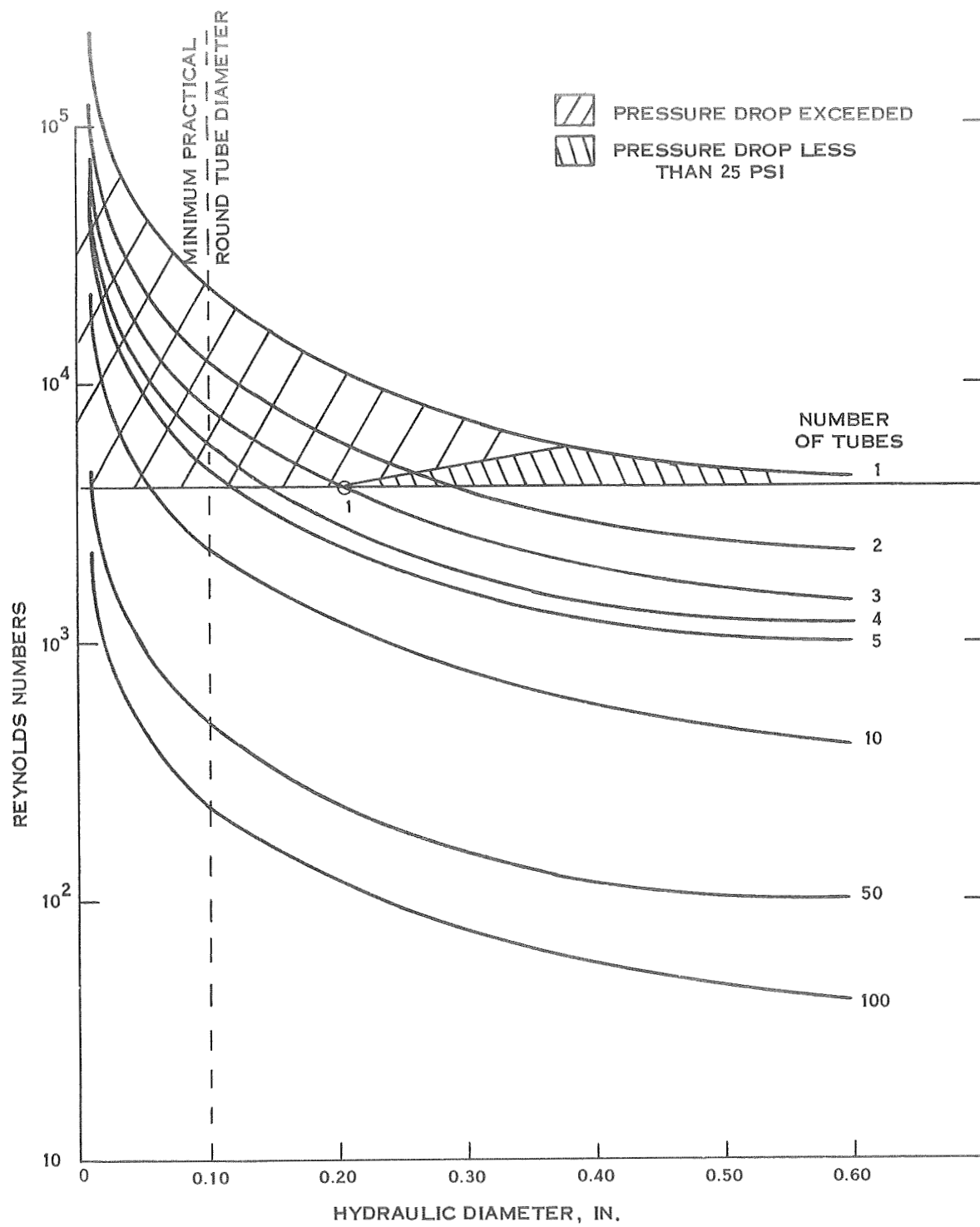


Figure 5-9. Reynolds Number Versus Hydraulic Diameter

The problem of reducing the DC-200 film temperature drop can be solved by departing from the round tube design and providing finned ducts which offer a large heat transfer area. Although fluid flow must be in the laminar regime, the heat transfer coefficient in the ducts is kept reasonably high by reducing the hydraulic diameter. The lower limit assumed for this design was a 0.010-inch spacing which corresponds to a 0.020-inch hydraulic diameter.

The model for the finned duct conduction fin radiator is shown in Figure 5-10. The offset tube design, which takes advantage of the meteoroid "bumper" protection, reduces the tube armor required by the relatively large amount of vulnerable area for this design. A redundant loop was incorporated into the design by providing additional tubes which were alternated with the operating set of tubes.

Small hydraulic diameters do not result in excessive pressure drops since the cross sectional flow area in this design is much greater than that provided by one or two round tubes.

Using the following approximate relation for laminar flow, the convective heat transfer coefficient  $h$ , can be calculated where  $D_h$  is the hydraulic diameter of the flow passage and  $k$  the fluid thermal conductivity

$$h = \frac{3.66 k}{D_h} \quad \frac{\text{Btu}}{\text{hr} - \text{ft}^2 - ^\circ\text{F}} \quad (5-5)$$

A comparison of the turbulent and convective heat transfer coefficients is shown in Figure 5-11. By going to small hydraulic diameters, reasonable laminar heat transfer coefficients can be obtained.

A more meaningful comparison between the round tube turbulent flow design and the laminar flow finned duct design is shown in Figure 5-12 where the convective conductance (product of convective heat transfer coefficient and heat transfer area) is plotted

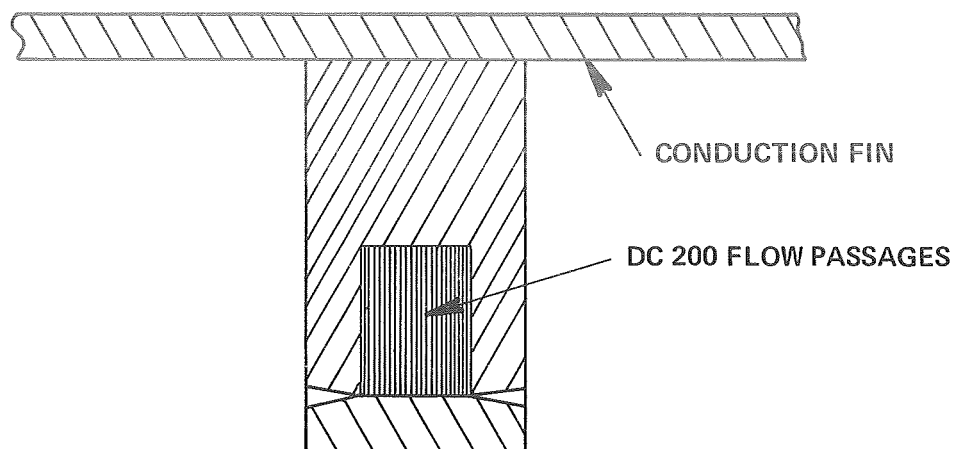


Figure 5-10. Model for Finned Duct Conduction Fin Radiator

against the primary duct or tube vulnerable area. The fluid film temperature drop is inversely proportional to the convective conductance. The values of vulnerable area per tube length are in the range corresponding to acceptable round tube diameters obtained from Figure 5-9. The heat transfer coefficient associated with the round tube diameters are given in Figure 5-11. The heat transfer area for the finned duct was obtained using a 0.250-inch-long fin, 0.010-inch flow gap and a 0.005-inch fin thickness. The corresponding laminar heat transfer coefficient was obtained from Figure 5-11. Figure 5-12 shows, for comparable vulnerable areas, the finned duct is capable of drastically lowering the fluid film temperature drop. The significance of this effect is that smaller temperature drops result in shorter radiator lengths and less total vulnerable area.

## 5.2 PERFORMANCE ANALYSIS

### 5.2.1 METHODOLOGY

The conduction fin and vapor chamber fin radiators were designed with the aid of the Spartan III and Spartan VI digital computer optimization programs. Both of these codes

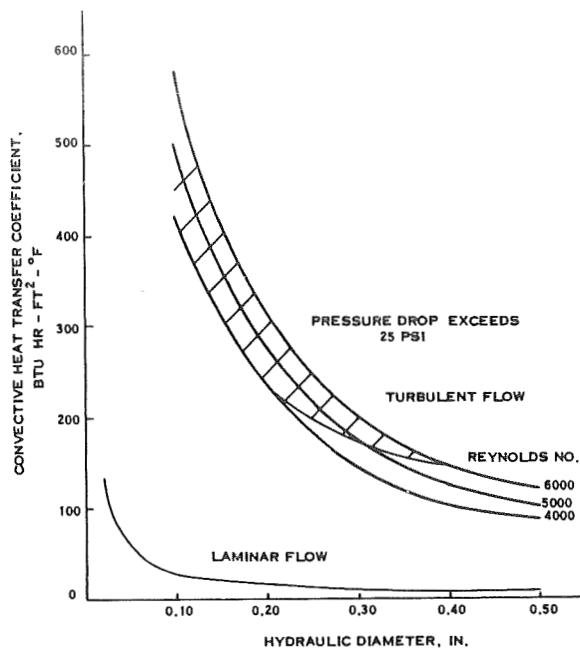


Figure 5-11. Heat Transfer Coefficients for Laminar and Turbulent Flow Versus Hydraulic Diameter

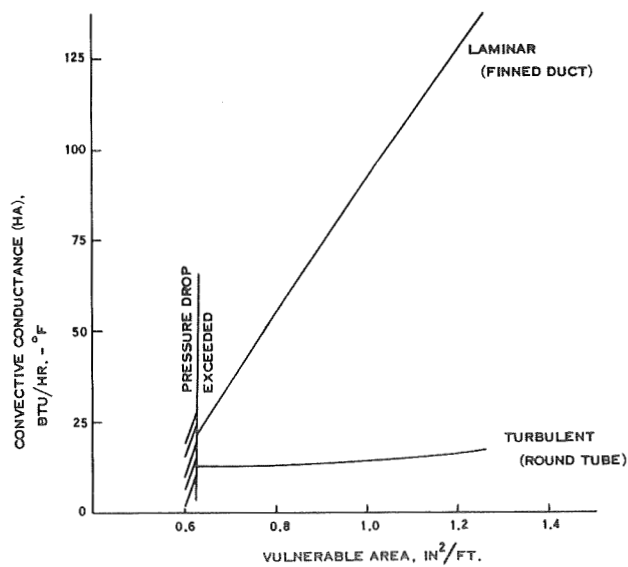


Figure 5-12. Comparison of Convective Conductance for Laminar and Turbulent Flows

provide minimum weight preliminary radiator designs by simultaneously solving the equations for meteoroid survival, heat transfer and fluid flow.

The Spartan III code, which has received extensive use in the analysis of round tube radiators, was modified to reflect the geometry of the more complex finned duct conduction fin radiator. The program was revised to optimize all radiator parameters including the dimensions of fin thickness, length and spacing in the tube ducts. It is important to note that finned primary ducts were also required with the vapor chamber radiator to increase heat transfer from the fluid to the evaporator section. Spartan VI was developed specifically by General Electric to analyze a vapor chamber fin radiator employing several vapor chamber fluids. The Spartan VI code divides the basic radiator panel into designated axial sections with the primary working fluid temperatures associated with each section. Each section may contain a different vapor chamber fluid and different geometric parameters determined by the optimization procedure. All fluid properties, including the primary working fluid, are temperature dependent. Provision is also made for calculating the optimum amount of vapor chamber redundancy for any input conditions.

#### 5.2.1.1 Heat Transfer Analysis

- (a) Vapor Chamber Radiator: The convective heat transfer coefficient for DC-200 was calculated using the Sieder-Tate equation (Ref. 30):

$$N_{NU} = 1.86 (N_{RE} N_{PR})^{1/3} \left( \frac{D_H}{L} \right)^{1/3} \left( \frac{\mu}{\mu_W} \right)^{0.14} \quad (5-6)$$

where:  $N_{NU}$  = Nusselt number,  $hD_H/k$

$N_{RE}$  = Reynolds number,  $D_H V \rho / \mu$

$N_{PR}$  = Prandtl number,  $C_P \mu / k$

$D_H$  = hydraulic diameter

$h$  = heat transfer coefficient

$L$  = flow length

$\mu$  = fluid viscosity at bulk fluid temperature

$\mu_W$  = fluid viscosity at wall temperature

For convenience the last term,  $(\mu/\mu_W)^{0.14}$  was set equal to 1.0, which is a good approximation when the driving force is small. The calculated heat transfer coefficient was used to predict the temperature drop to the primary duct fins across the fluid laminar film.

The duct fin efficiency was computed from the following relation:

$$N_{\text{eff}} = \frac{\tanh(\lambda L)}{\lambda L} \quad (5-7)$$

where:  $L$  = height of fin

$\lambda$  = fin parameter =  $\sqrt{h P/A k_f}$

$h$  = heat transfer coefficient

$P$  = fin perimeter

$A$  = heat transfer area of fin

$k_f$  = fin conductivity

This relationship is true for fins with a low width to height ratio and assumes a uniform fin conductivity, heat transfer coefficient and bulk fluid temperature. The fluid laminar film temperature drop can now be written as:

$$\Delta T = \frac{Q}{h A_{\text{FIN}} N_{\text{eff}}} \quad (5-8)$$



where:  $Q$  = heat to be transferred

$A_{\text{FIN}}$  = fin heat transfer surface area

The lack of experimental data for the many fluids investigated made the determination of the evaporator  $\Delta T$  especially difficult to predict. The phenomena of evaporation is sensitive to the evaporator surface. Consequently, the performance on a screen surface, over a period of time at various heat fluxes can only be estimated. For many organic fluids in the nucleate boiling region, the  $\Delta T$  can be calculated using the Cichelli and Bonilla correlation (presented in Sections 4.2 and 4.3):

$$\Delta T_{\text{EVAP}} = \left[ \frac{(Q/A)}{(Q/A)_p} \right]^n \Delta T_C \quad (5-9)$$

where:  $(Q/A)$  = evaporative heat flux

$(Q/A)_p$  = peak heat flux

$\Delta T_C$  = critical temperature drop

$n$  = experimental constant, 0.250 to 0.333 (0.300 used in study)

Cichelli and Bonilla also presented curves of  $(Q/A)_p$  and  $\Delta T_C$  (Figure 4-8) as a function of the reduced pressure. This correlation is directly applicable to pool boiling and represents a performance which is partially accurate for low temperature heat pipes (see Section 6.5).

The remaining significant temperature drop in the vapor chamber is across the fluid condensing film. This temperature drop is significant because of the low thermal conductivity of organic fluids. For purposes of analysis, a temperature drop was assumed not to occur in the vapor phase during the condensing process. The condensing temperature drop was expressed as:

$$\Delta T_{\text{COND}} = K \frac{Q}{2 \pi L k_{\text{film}}} \ln \left( \frac{r_o}{r_i} \right) \quad ^\circ\text{F} \quad (5-10)$$

where:  $Q$  = heat transferred

$L$  = chamber length

$k_{\text{film}}$  = thermal conductivity of film

$r_o$  = outside radius of condensing film

$r_i$  = inside radius of condensing film

$K$  = constant to account for unequal condensing distribution  
(= 3.0)

The principle uncertainty concerning the condensing  $\Delta T$  is the thickness of the condensing film. The reference design assumed a condensing film thickness of 0.010 inch; however, the effect of varying this parameter was investigated.

The temperature of the fin directly adjacent to the vapor chamber was assumed to be equal to that of the outside chamber surface. In order to account for the temperature drop along the fin between chambers, standard curves for fin efficiency (see Figure 4-24) were used.

- (b) Conduction Fin Radiator: The temperature drops considered in the conduction fin radiator were: the  $\Delta T$  from the bulk fluid to the internal tube fin root, the  $\Delta T$  across the armor and the  $\Delta T$  between tubes along the conduction fin. The fluid laminar film temperature drop and the conduction fin efficiency were calculated in the manner explained for the vapor chamber fin radiator. The temperature drop across the tube armor is calculated by the Fourier equation for heat transfer:

$$dT = \frac{Q}{k_A A} dx \quad (5-11)$$

where:  $Q$  = heat transferred

$k_A$  = conductivity of armor

$A$  = heat transfer area

$dx$  = length of heat path

#### 5.2.1.2 Meteoroid Analysis

Both the vapor chamber fin and conduction fin radiators were studied for survival probabilities ranging from 0.99 to 0.999. This survival probability is an overall requirement and includes the secondary radiators as well as the primary radiators. Additionally, the vapor chamber fin primary and secondary radiators each have two components, the ducts and heat pipe fins. These must be accounted for.

The overall survival probability of a system is equal to the multiple of the individual survival probabilities which constitute that system. Therefore, the overall survival probabilities consist of four principal components for the vapor chamber fin and two components for the conduction fin radiators. A further consideration is the distribution of the overall survival probability in the most advantageous manner. Components having small vulnerable areas or which can be easily protected due to the effect of redundancy should be given the more stringent survival requirement. The individual survival probabilities were distributed as shown in Table 5-1. The secondary radiators were given a higher survival probability than the primary radiators in such a ratio as to keep the armor requirements nearly identical. The most advantageous probability distribution between the primary ducts and vapor chambers was examined. The primary radiator weight was found to be fairly insensitive to this distribution and is shown in Figure 5-13.

TABLE 5-1. SURVIVAL PROBABILITY DISTRIBUTION

	Vapor Chamber Fin		Conduction Fin	
Overall Survival Probability	0.999	0.990	0.999	0.990
Primary Radiator				
Ducts	0.99928	0.9928	0.9992	0.992
Chambers	0.99992	0.9992		
Secondary Radiator				
Ducts	0.99982	0.9982	0.9998	0.9980
Chambers	0.99998	0.9998		

For the conditions assumed in the study, the meteoroid equation proposed by Loeffler (Section 3.6) reduces to:

$$t_a = 1.45 \rho_t^{-0.167} E_t^{-0.333} \left( \frac{A_v \tau}{-\log_e P_o} \right)^{0.249} \quad (5-13)$$

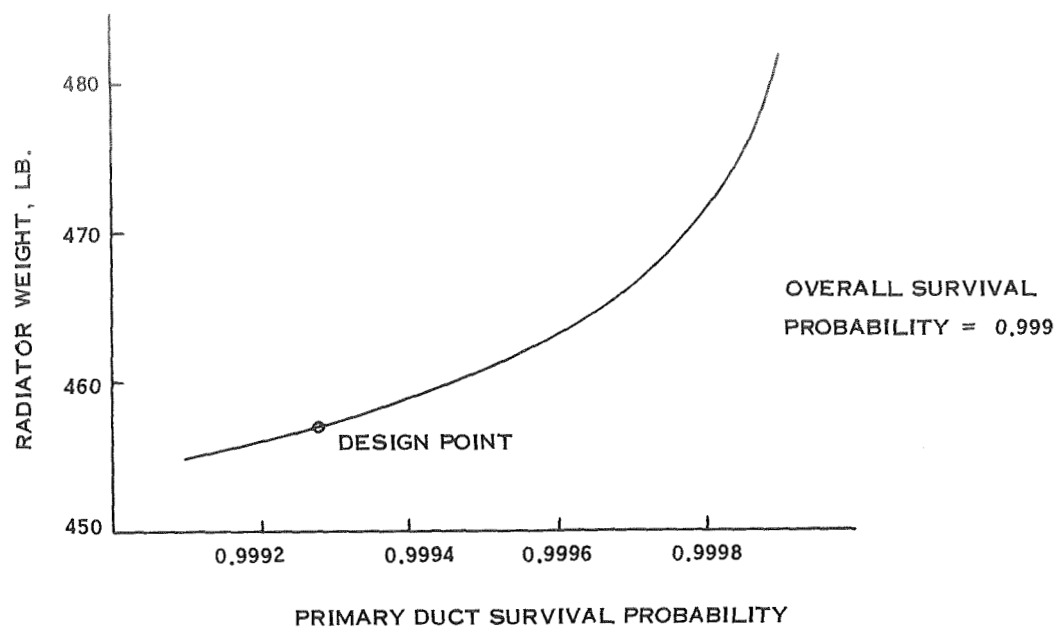


Figure 5-13. Effect of Survival Probability Distribution Between Ducts and Chambers on Vapor Chamber Radiator Weight

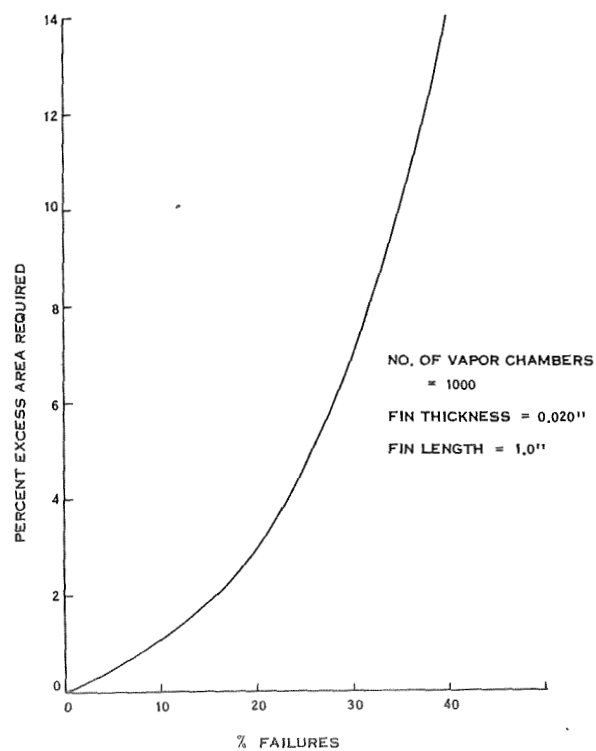


Figure 5-14. Excess Area Required Versus Vapor Chamber Percent Failure (Aluminum Fins)

where:  $t_a$  = required armor thickness

$A_v$  = vulnerable area of armor (ft<sup>2</sup>)

$\tau$  = mission time (days)

$P_o$  = design probability of no critical damage

The external area of the armor was used as the vulnerable area for both the primary fluid ducts and vapor chambers.

The armor requirements of the primary fluid ducts was decreased by providing redundant loops for both the vapor chamber fin and conduction fin radiators.

In order to keep the meteoroid armor requirements of the vapor chambers within reasonable limits, it is necessary to allow a certain percentage of failures which reduces the individual chamber survival probability. The relationship between the amount of additional radiating area and percentage failure can be calculated from the analysis shown in Section 4.3. The results are shown in Figure 5-14 for a 0.020-inch-thick fin with a 2-inch spacing between chambers.

### 5.2.2 RESULTS

The comparison between the vapor chamber fin and conduction fin radiators was made over a range of radiator areas for several meteoroid survival probabilities. These investigations drew several fundamental conclusions about the relative characteristics of each radiator type. The accuracy of the analytical comparison was tempered somewhat by two uncertainties concerning the vapor chamber fin calculations: the magnitude of the evaporator and condensing temperature drops. Consequently, the sensitivity of the vapor chamber fin radiator design to changes in these parameters was investigated and the results upon the comparison are presented.

The variation of vapor chamber fin and conduction fin radiator weights as a function of area are shown in Figure 5-15 and 5-16 for several survival probabilities. At survival probabilities higher than 0.999, the vapor chamber fin radiator shows an advantage while the conduction fin radiator is lighter at survival probabilities of 0.99 and lower.

The "ideal" area shown on these figures refers to a limiting situation in which the radiator is isothermal at any axial position around its circumference and no  $\Delta T$  exists between the primary fluid and the radiating surface. While the secondary radiator weights and areas have not been shown in Figures 5-15 and 5-16 the same conclusions would be drawn with their inclusion.

The vapor chamber fluids used in the analysis were n-pentane in the high temperature section and ammonia in the low temperature section; the dividing point corresponding to a primary fluid temperature of 180°F. Due to the decreasing surface tension of ammonia with increasing temperature, the capillary pumping requirements preclude the use of ammonia at higher temperatures. The characteristics of the reference designs at the 0.999 and 0.990 survival probabilities are presented in Tables 5-2 and 5-3.

Weight of the conduction fin radiator, with its larger primary fluid duct vulnerable area, is much more sensitive to changes in the overall survival probability. Although the vulnerable area of the vapor chambers is considerable, the redundancy incorporated into the design makes it possible to increase the overall chamber survival probability without large weight increases. This effect is shown in Figure 5-17 for an 85 percent chamber survival. The choice of an 85 percent chamber survival was based on structural requirements of the radiator shown in Figure 5-18. At chamber survival probabilities greater than 85 percent, the conduction fin thickness necessary to provide meteoroid protection exceeds the structural requirements. At lower chamber survival fractions, the conduction fin thickness is reduced and rings must be added to provide the necessary structural integrity. The minimum weight occurs at a survival fraction of approximately 0.85.

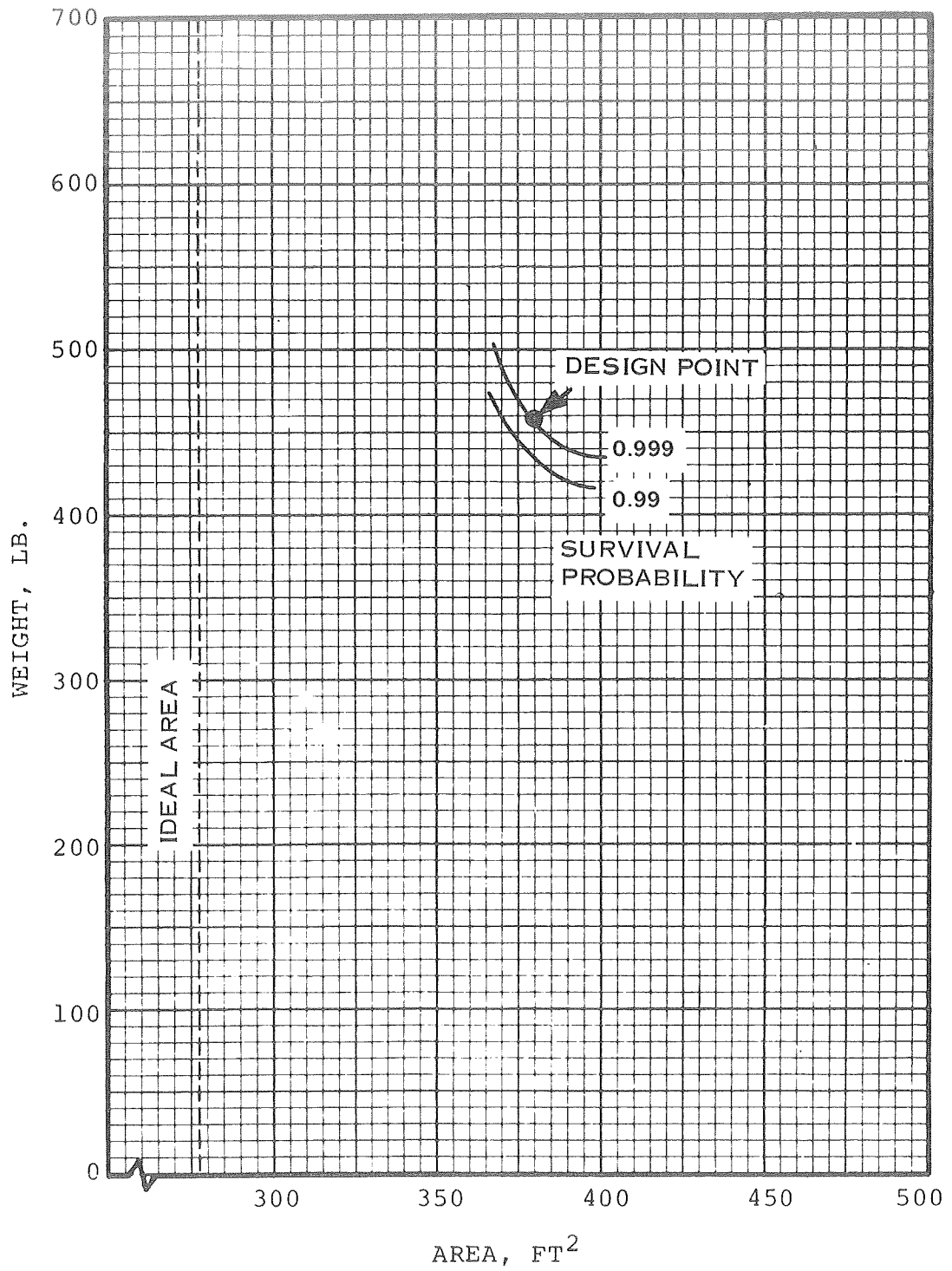


Figure 5-15. Weight Versus Area for Vapor Chamber Fin Primary Radiator

WEIGHT VS. AREA FOR  
CONDUCTION FIN PRIMARY RADIATOR

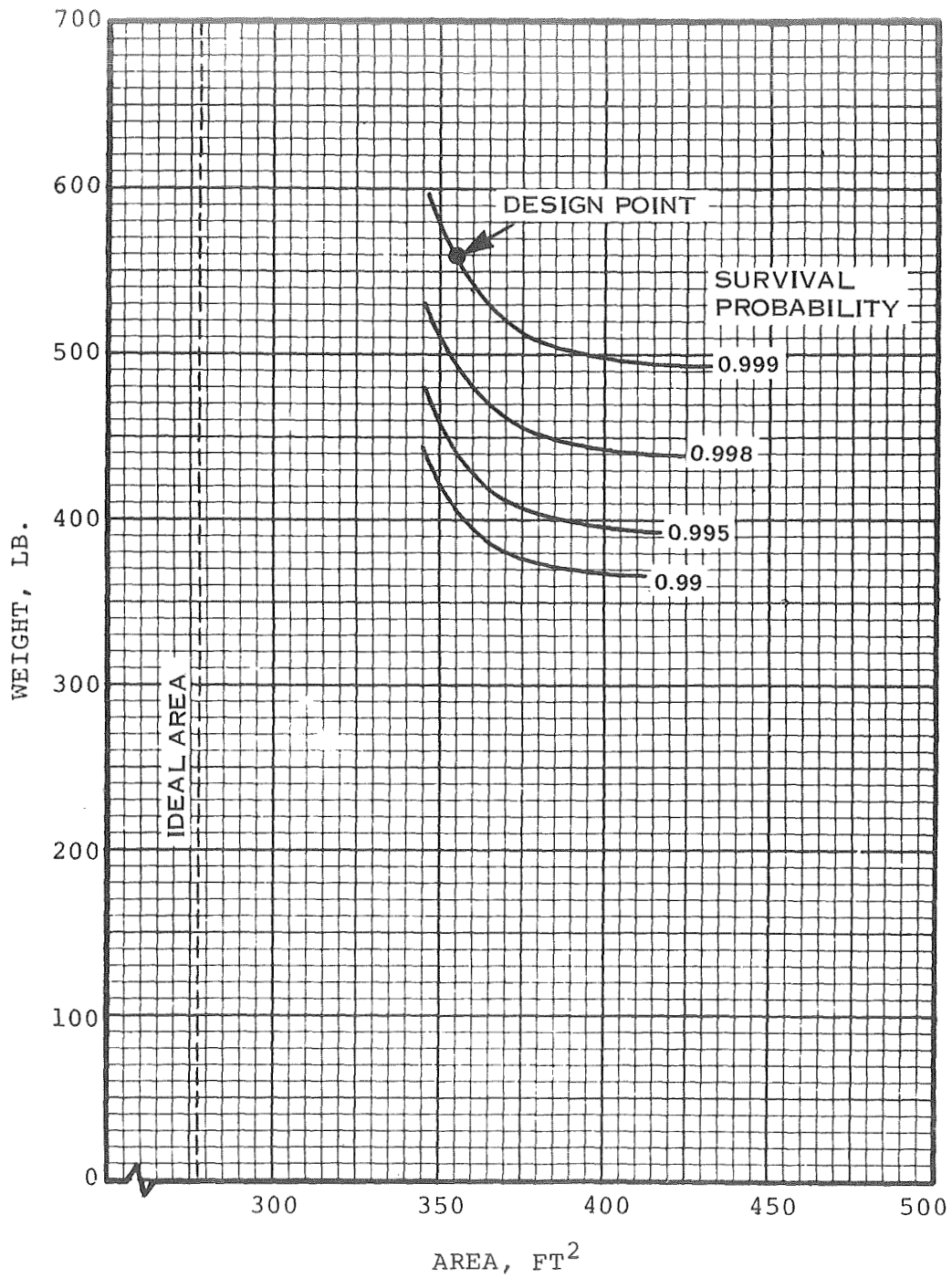


Figure 5-16. Weight Versus Area for Conduction Fin Primary Radiator



TABLE 5-2. VAPOR CHAMBER RADIATOR CHARACTERISTICS

	0.999 Survival Probability		0.99 Survival Probability	
	Primary	Secondary	Primary	Secondary
Primary Fluid Temp. Range, n-Pentane Section	288-180	--	288-180	--
Primary Fluid Temp. Range, Ammonia Section	180- 64	118- 64	180- 64	118 - 64
Average Primary Fluid $\Delta T$ , n-Pentane Section	10	--	10	--
Average Primary Fluid $\Delta T$ , Ammonia Section	3	1	3	1
Average Evaporator $\Delta T$ , n-Pentane Section	14	--	14	--
Average Evaporator $\Delta T$ , Ammonia Section	9	10	9	10
Average Condenser $\Delta T$ , n-Pentane Section	19	--	19	--
Average Condenser $\Delta T$ , Ammonia Section	3	2	3	2
Length of n-Pentane Section, ft	4.0	--	4.0	--
Length of Ammonia Section, ft	10.0	4.7	9.9	4.7
Length of Chambers, in.	26.2	26.2	26.2	26.2
Outside Diameter of Chambers, in.	0.310	0.310	0.310	0.30
Number of Chambers	1537	432	1512	437
Average Chamber Spacing, in.	1.31	1.57	1.32	1.54
Chamber Wall Thickness, in.	0.015	0.015	0.015	0.015
Required Duct Armor Thickness, in.	0.201	0.181	0.145	0.138
Bumpered Duct Armor Thickness, in.	0.104	0.0864	0.0571	0.0516
Primary Duct Outside Height, in.	1.02	0.933	0.914	0.853
Primary Duct Outside Width, in.	1.49	1.55	1.55	1.56
Duct Fin Height, in.	0.150	0.125	0.145	0.125
Duct Fin Thickness, in.	0.005	0.005	0.005	0.005
Duct Passage Width, in.	0.013	0.0125	0.0137	0.0135
Conduction Fin Thickness, in.	0.021	0.021	0.021	0.021
Average Primary Fluid Reynolds No.	60	33	60	33
Average Primary Fluid Flow Velocity, ft/sec	0.38	0.32	0.35	0.29
Primary Fluid Pressure Drop, lb/in. <sup>2</sup>	8.88	3.8	7.8	3.0
Total Weight	457	150	455	145
Total Area	379	127	377	127
Specific Weight	1.20	1.18	1.21	1.14

TABLE 5-3. CONDUCTION FIN RADIATOR CHARACTERISTICS

	0.999 Survival Probability		0.99 Survival Probability	
	Primary	Secondary	Primary	Secondary
No. of Panels	6	6	6	6
Total No. of Tubes/Panel*	14	12	20	12
No. of Passages/Tube	10	11	10	11
Height of Passage, in.	0.210	0.160	0.181	0.158
Width of Passage, in.	0.010	0.0115	0.010	0.0105
Internal Tube Fin Thickness, in.	0.005	0.0055	0.005	0.006
Conduction Fin Length, in.	4.03	4.70	2.68	4.59
Conduction Fin Thickness, in.	0.0625	0.0580	0.0470	0.0520
Fin Efficiency, %	93.5	92.0	95.4	91.8
Inside Diameter of Header, in.	0.623	0.546	0.694	0.529
Outside Diameter of Header, in.	0.743	0.666	0.814	0.649
Required Armor Thickness, in.	0.303	0.261	0.221	0.186
Bumpered Armor Thickness, in.	0.0838	0.067	0.0590	0.039
Radiator Length, ft.	12.4	4.21	12.0	4.21
Average Fluid Velocity, ft/sec.	0.36	0.34	0.29	0.36
Average Reynolds, No.	39	26	31	26
Pressure Drop, lb/in. <sup>2</sup>	13.7	5.8	10.8	7.3
Total Weight, lbs.	559	160	441	136
Total Area, ft <sup>2</sup>	355	122	344	122
Specific Weight, lbs/ft <sup>2</sup>	1.57	1.31	1.28	1.11

\*Half of these tubes are fed by each redundant loop.

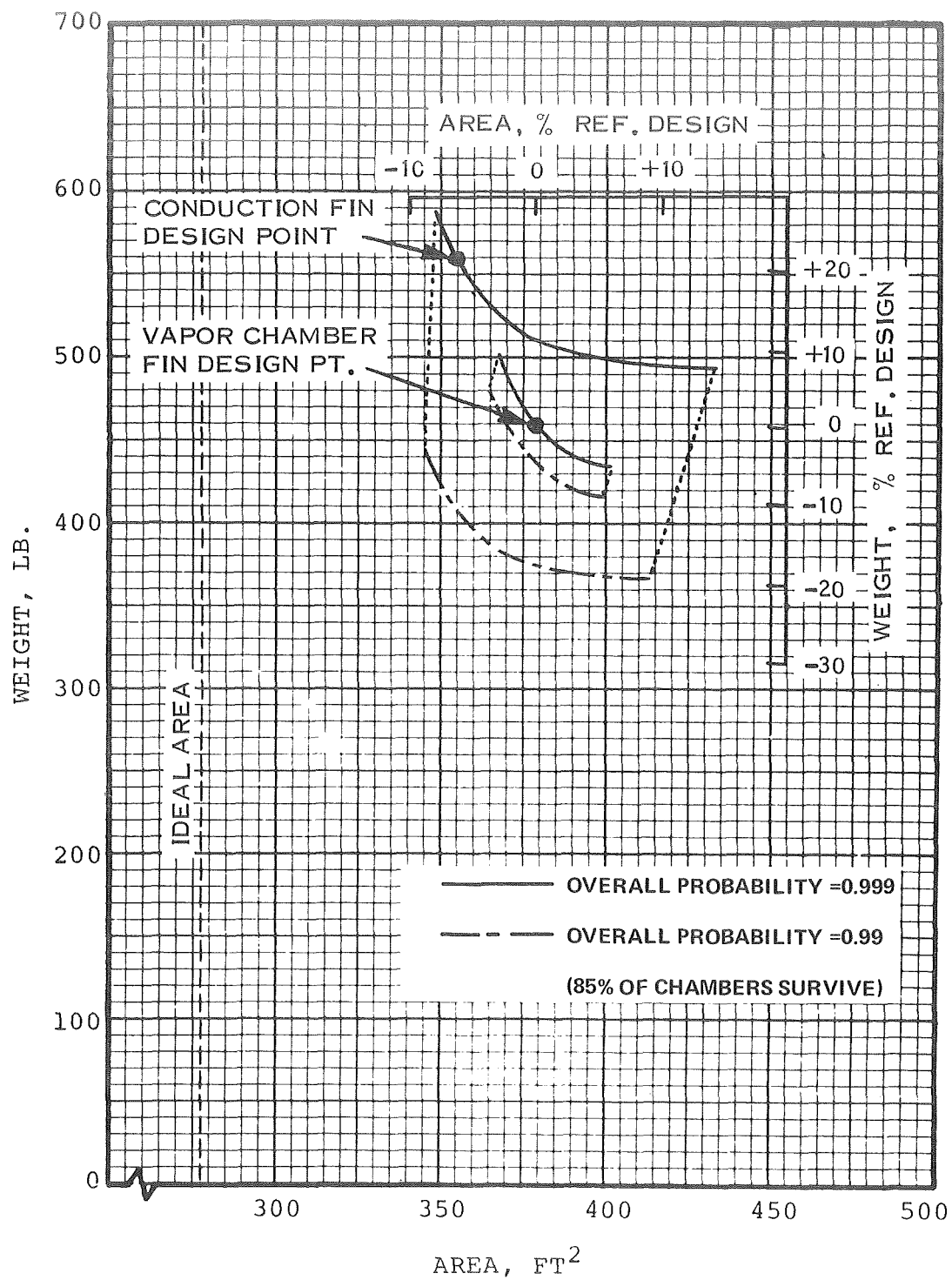


Figure 5-17. Comparison of Vapor Chamber Fin to Conduction Fin Primary Radiators

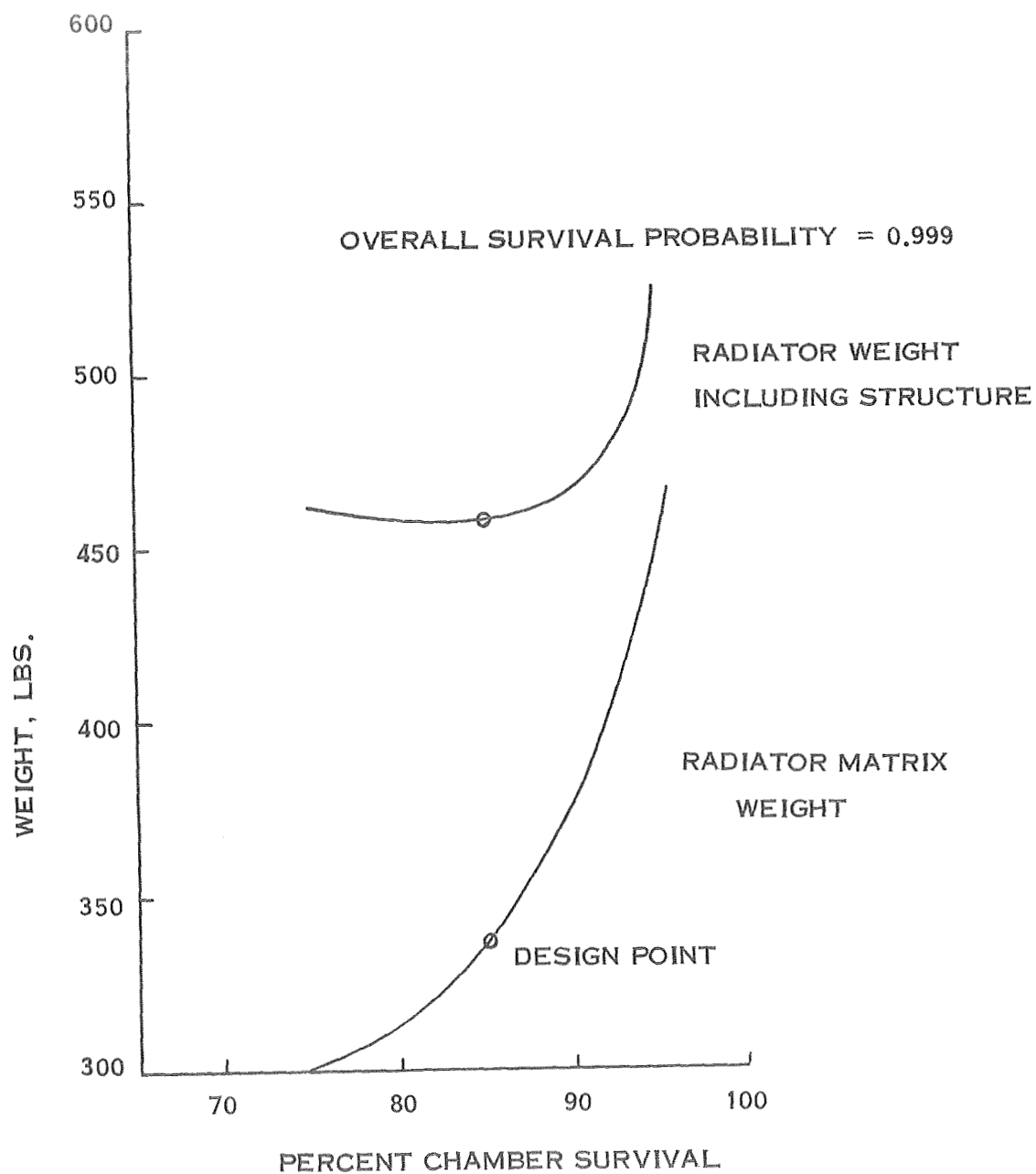


Figure 5-18. Effect of Chamber Survival Fraction on Radiator Weight

In the event that the evaporative temperature drops predicted by Cichelli and Bonilla are not achievable, the effect of temperature drops 50 and 100 percent higher are shown in Figure 5-19. Whereas the vapor chamber radiator had previously shown a slight advantage at the 0.999 survival probability design point, it rapidly becomes noncompetitive if there is a significant departure from the predicted evaporator temperature drop. Similarly, the effect of the condensing film thickness on the radiator design was found to be important. These results are shown in Figure 5-20. Clearly, the experimental evaluation of these two parameters could change the analytical comparison shown in Figure 5-17.

The importance of several of the ground rules on the radiator comparison was also examined; specifically, the sink temperature, the primary fluid choice and the pumping penalty. The results of these perturbations are shown in Table 5-4. The use of water as a primary fluid measurably improved the weight and area of the conduction fin radiator, but had a significantly smaller effect on the vapor chamber radiator as depicted by Figures 5-21 and 5-22. However, the compatibility of water with any form of aluminum is questionable. The effect of sink temperature on both radiators is shown in Figures 5-23 and 5-24.

The choice, during the working fluid selection phase of this study, of n-pentane and ammonia as vapor chamber fluids was subjected to scrutiny by using the Spartan VI optimization program to investigate other fluids. Other combinations that were studied are:

	<u>High Temp.</u>		<u>Low Temp.</u>		<u>High Temp.</u>		<u>Low Temp.</u>
	<u>Section</u>		<u>Section</u>		<u>Section</u>		<u>Section</u>
1.	Benzene	+	Ammonia	5.	n-Pentane	+	Water
2.	n-Butane	+	Ammonia	6.	Water	+	Water
3.	n-Pentane	+	Ammonia + Propane				
4.	Water	+	Ammonia				

# EFFECT OF EVAPORATOR TEMPERATURE DROP ON VAPOR CHAMBER FIN PRIMARY RADIATOR

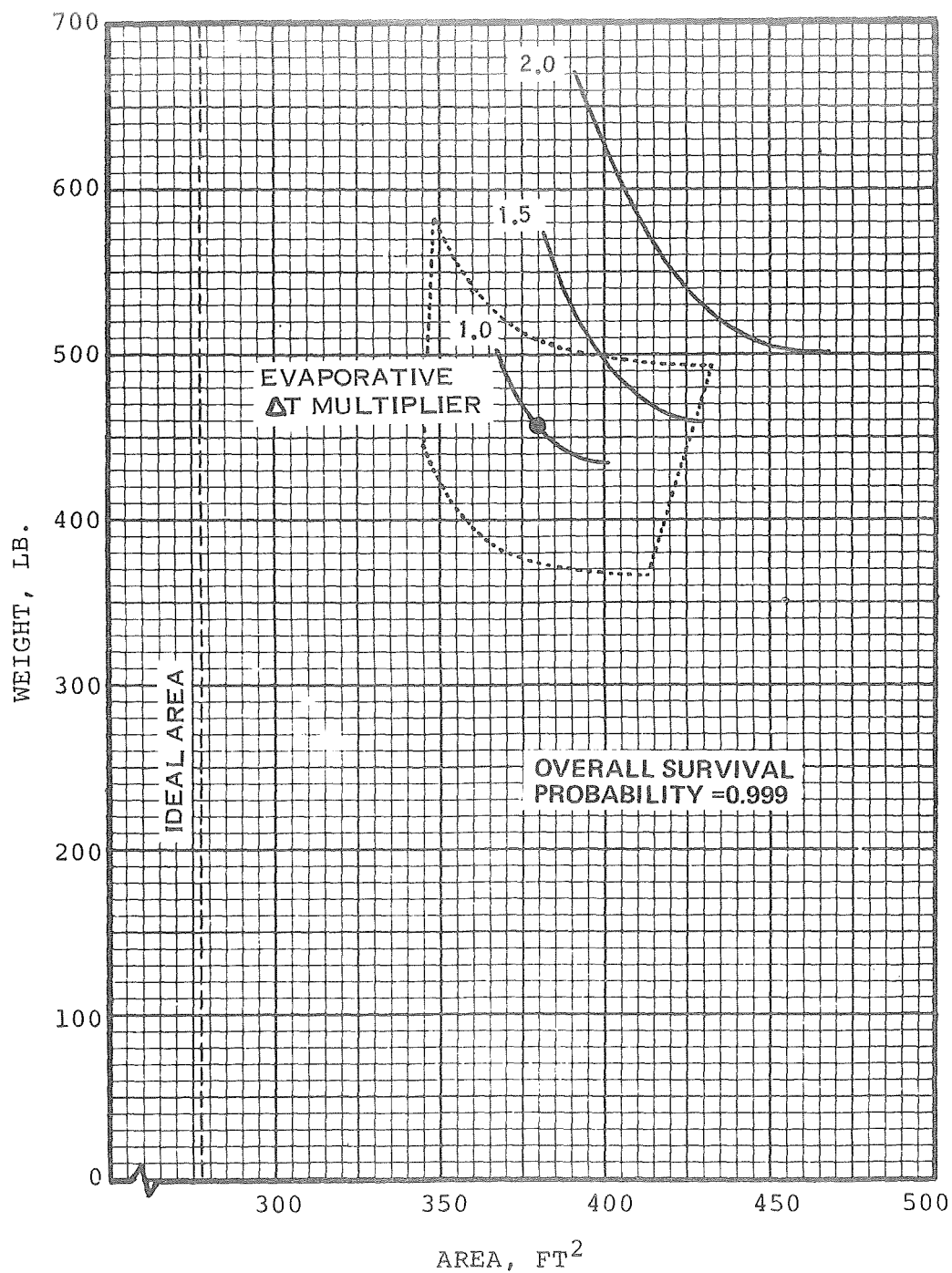


Figure 5-19. Effect of Evaporator Temperature Drop on Vapor Chamber Fin Primary Radiator

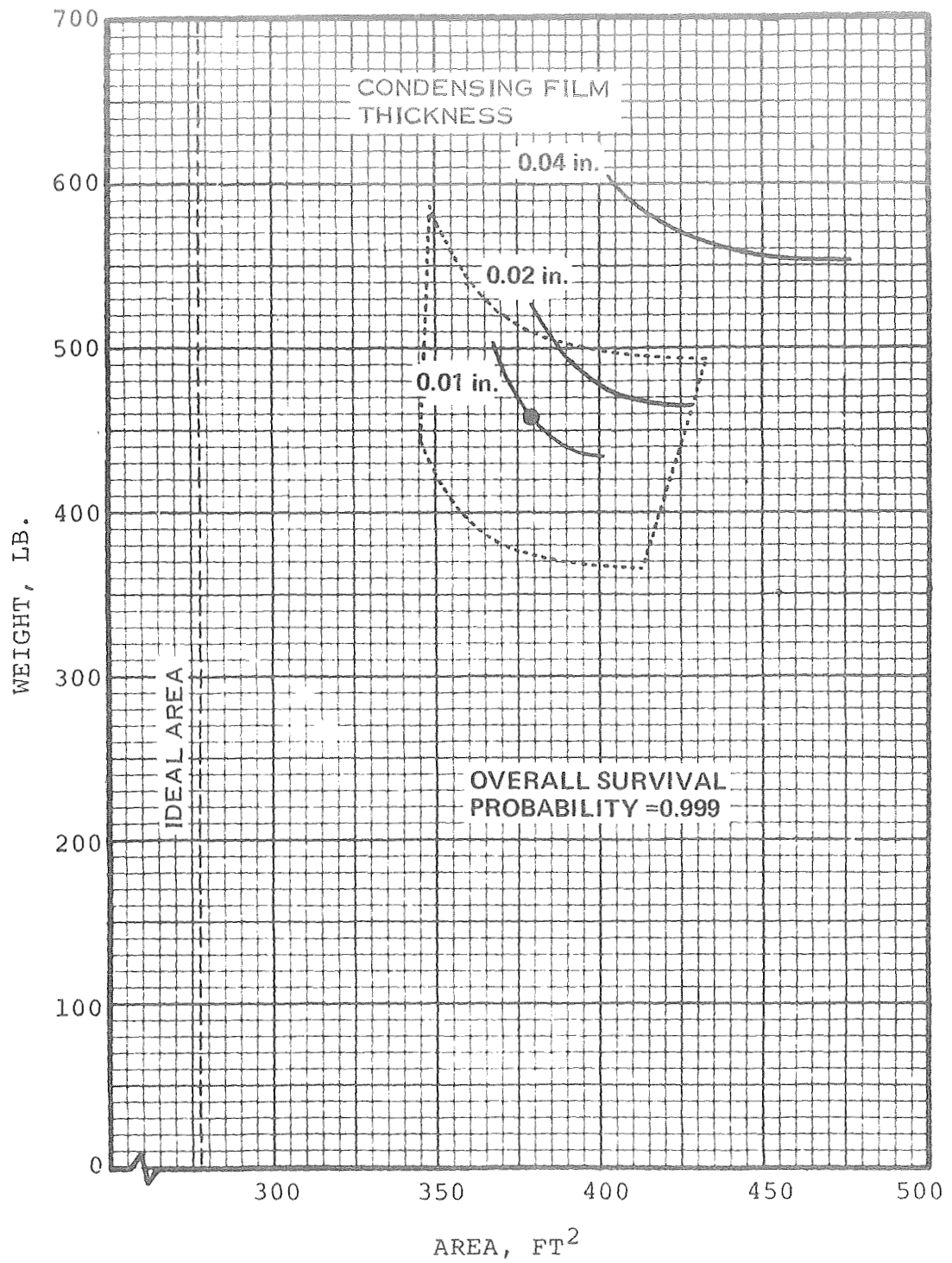


Figure 5-20. Effect of Condensing Film Thickness on Vapor Chamber Fin Primary Radiator

TABLE 5-4. EFFECT OF GROUND RULES ON COMPARISON

Ground Rule Change	Vapor Chamber Fin			Conduction Fin		
	WT	AREA	$\Delta P$	WT	AREA	$\Delta P$
Sink Temperature						
30°F	685	425	11.3	806	487	19.3
-60°F	386	309	6.4	440	293	11.6
Primary Fluid						
0.65 centistoke DC-200	450	384	8.63	560	353	7.87
WATER	447	378	2.69	519	340	1.96
Pumping Penalty						
None, 50 psi $\Delta P$ limit	449	381	34.7	521	355	38.5

Of these combinations, all showed heavier weights and larger radiator areas except for the combination of water and ammonia. The present weight advantage offered by replacing pentane with water is negated by the incompatibility of water with aluminum. Results are presented in Table 5-5 and depicted graphically by Figure 5-25.

A more complete understanding of the important parameters affecting the radiator weights was obtained by varying several of the parameters about the values specified by the optimization program. For the vapor chamber radiator, the variables which were perturbed are: duct fin thickness, fluid gap thickness, vapor chamber spacing and vapor chamber diameter. These results are presented in Figures 5-26 to 5-30. The vapor chamber diameter exerted the largest influence on both radiator area and weight (Figure 5-26). The parameters investigated for the conduction fin radiator are: the number of fins per primary tube, fluid gap thickness, internal fin thickness and the



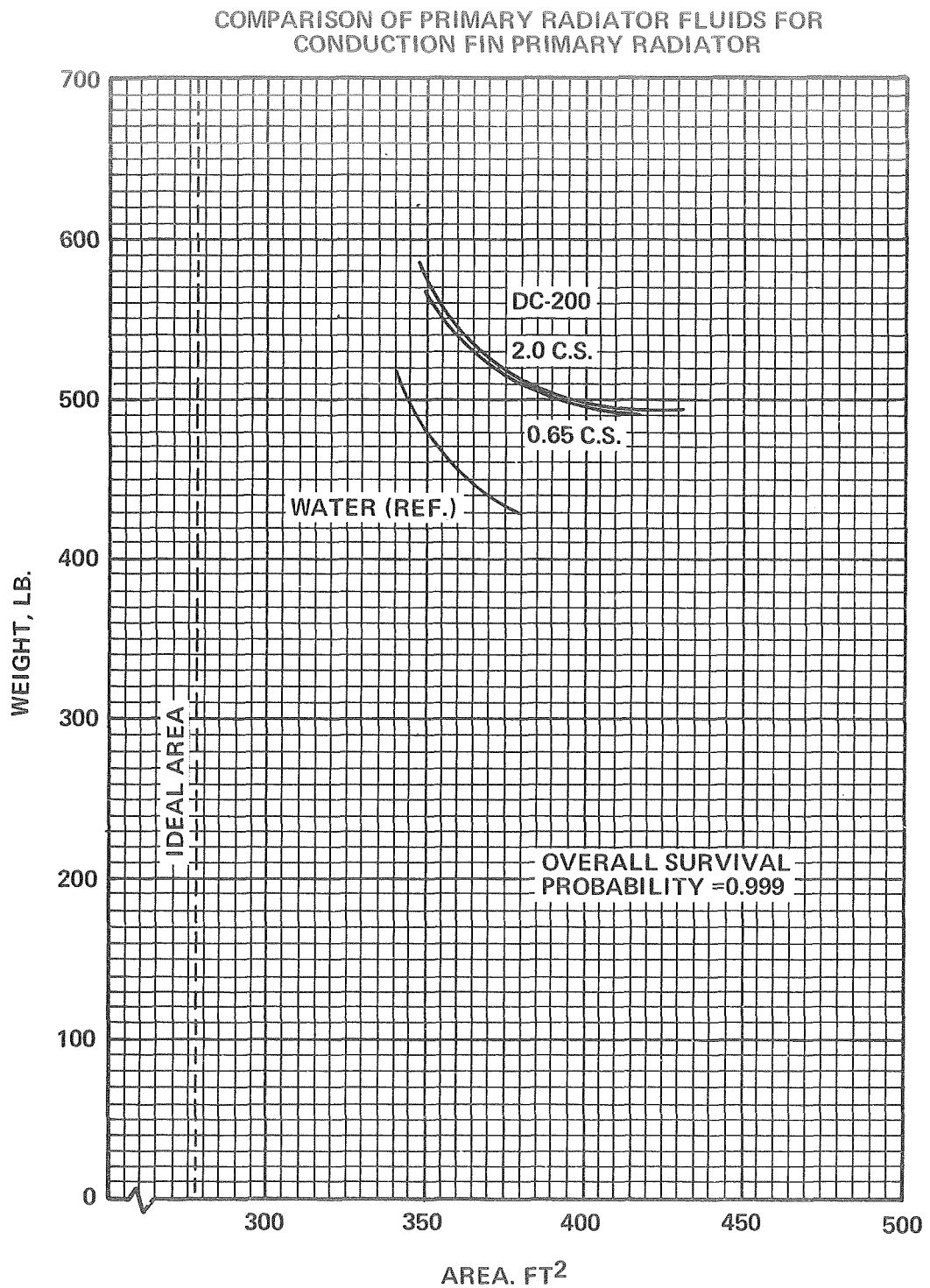


Figure 5-21. Comparison of Primary Radiator Fluids for Conduction Fin Primary Radiator

# COMPARISON OF PRIMARY RADIATOR FLUIDS FOR VAPOR CHAMBER FIN PRIMARY RADIATOR

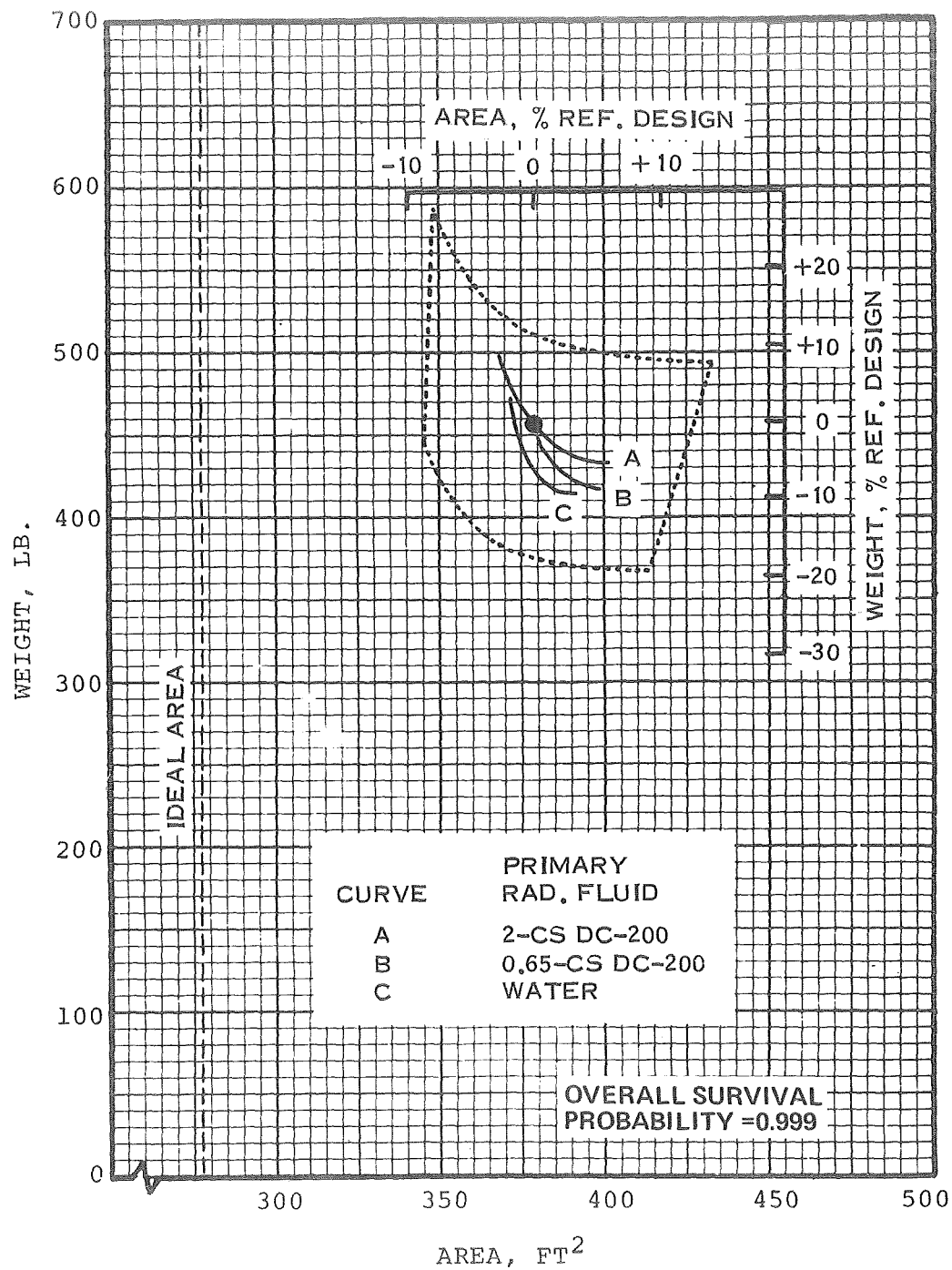


Figure 5-22. Effect of Tube Spacing for Vapor Chamber Fin Primary Radiator

# EFFECT OF SINK TEMPERATURE ON VAPOR CHAMBER FIN PRIMARY RADIATOR

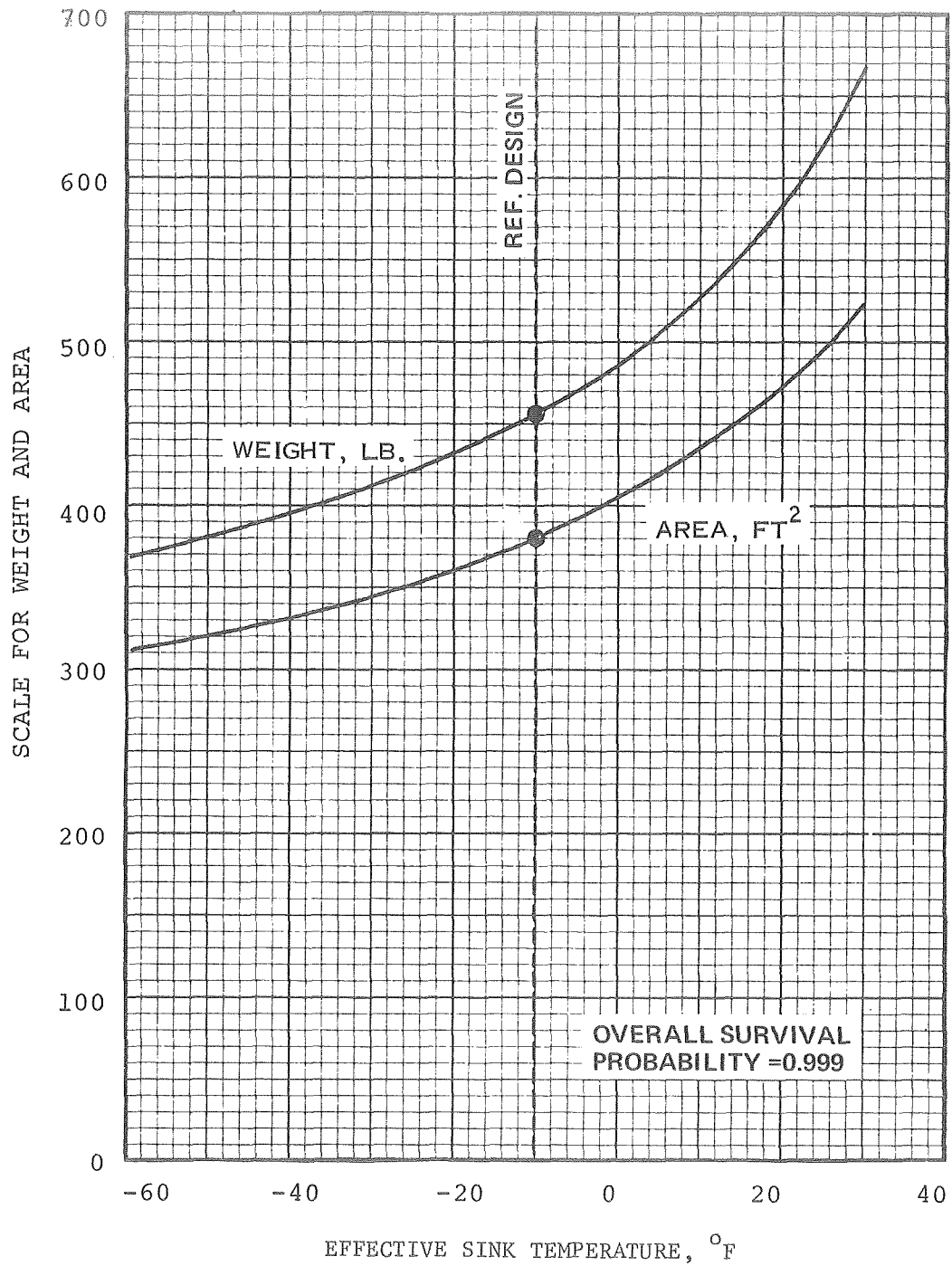


Figure 5-23. Effect of Sink Temperature on Vapor Chamber Fin Primary Radiator

# EFFECT OF SINK TEMPERATURE ON CONDUCTION FIN PRIMARY RADIATOR

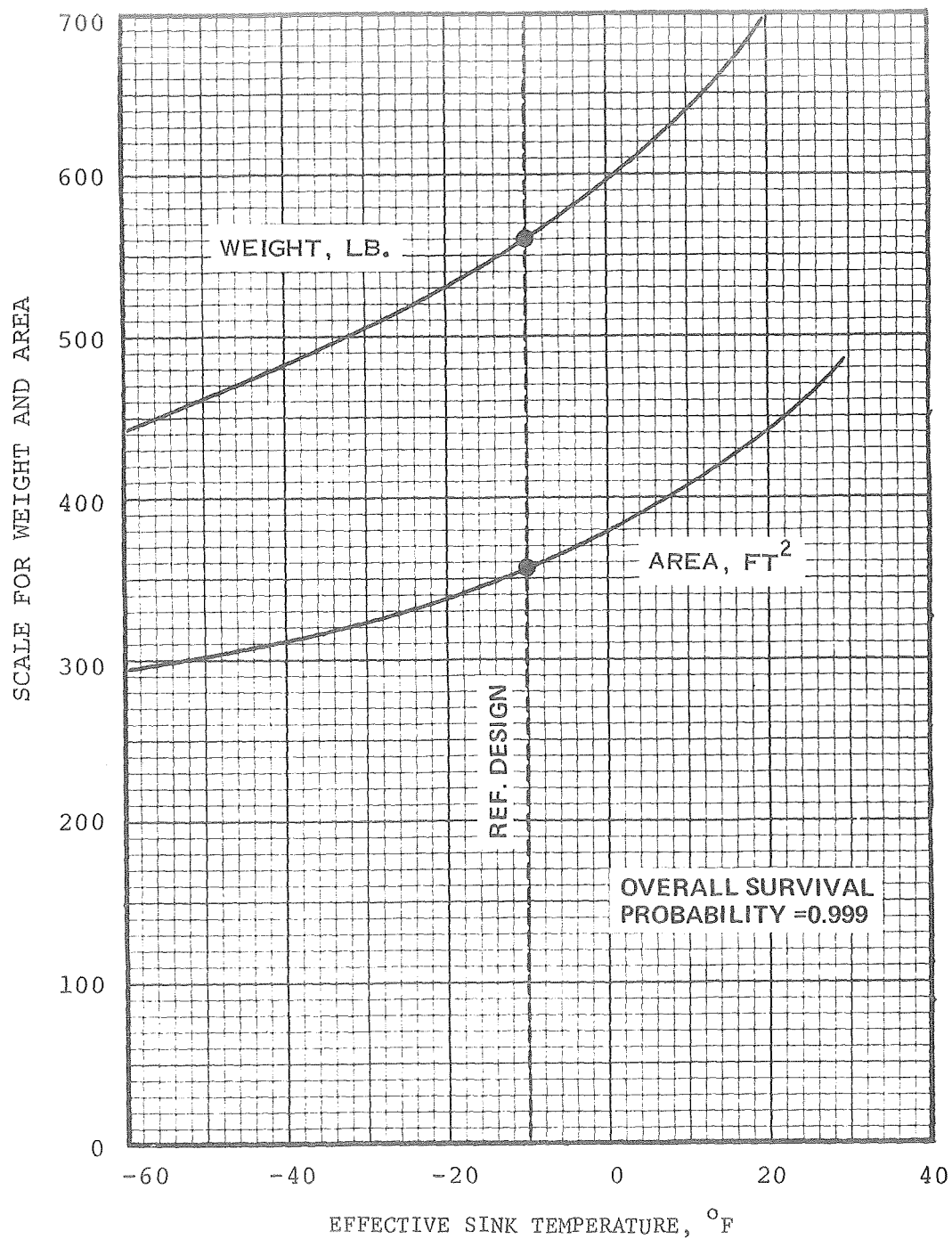


Figure 5-24. Comparison of Sink Temperature on Conduction Fin Primary Radiator

# COMPARISON OF WORKING FLUIDS FOR VAPOR CHAMBER FIN PRIMARY RADIATOR

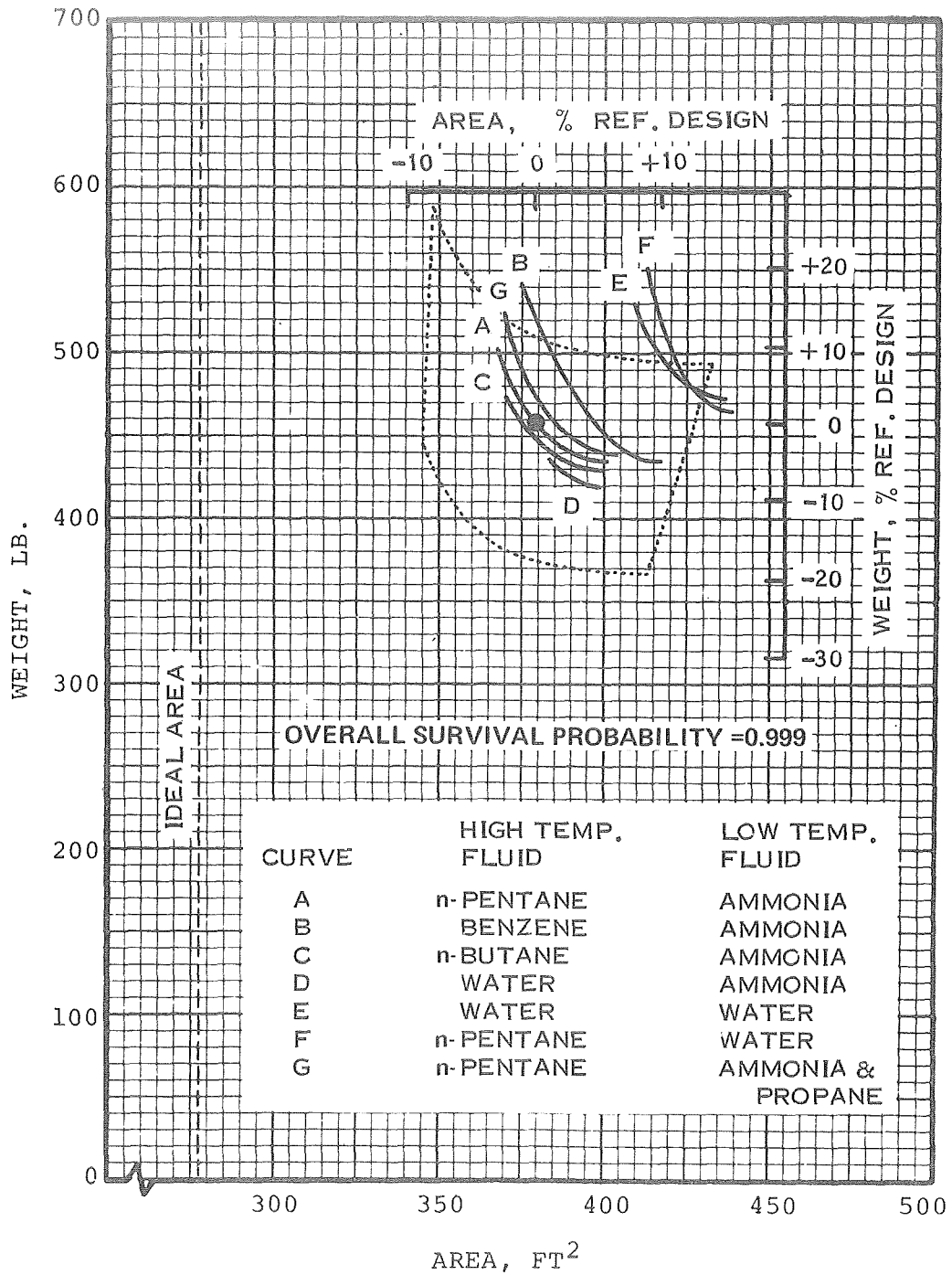


Figure 5-25. Comparison of Working Fluids for Vapor Chamber Fin Primary Radiator

TABLE 5-5. VAPOR CHAMBER FLUID EFFECT  
0.999 Overall Survival Probability

FLUIDS		PRIMARY SECTION		
High Temperature Section	Low Temperature Section	WT	AREA	$\Delta P$
Benzene	Ammonia	506	386	8.87
n-Butane	Ammonia	466	377	9.14
n-Pentane	Ammonia, Propane	476	383	7.42
Water	Ammonia	450	384	8.63
n-Pentane	Water	525	418	9.53
Water	Water	506	419	7.79
n-Pentane	Ammonia	457	379	8.88

number of tubes per panel. All of these parameters affect the primary duct heat transfer which dominates the conduction fin radiator design; consequently, changes in these parameters resulted in substantial variations in the radiator weight and area as shown in Figures 5-30 to 5-33.

### 5.3 STRUCTURAL ANALYSIS

#### 5.3.1 GENERAL DISCUSSION

A comparison was made between a vapor chamber fin radiator and a radiator with conducting fins designed to the same requirements. Both radiators were assumed to be load bearing so that the influence of structural requirements was reflected in the comparison. This section presents the structural analysis used in determining the weight increments attributable to structural requirements of both radiators.

The maximum design loads for the radiators occur during launch. The two conditions of interest during the launch trajectory are the times at which maximum lateral and maximum axial accelerations occur. The load factors for these conditions are a

# EFFECT OF VAPOR CHAMBER DIAMETER FOR VAPOR CHAMBER FIN PRIMARY RADIATOR

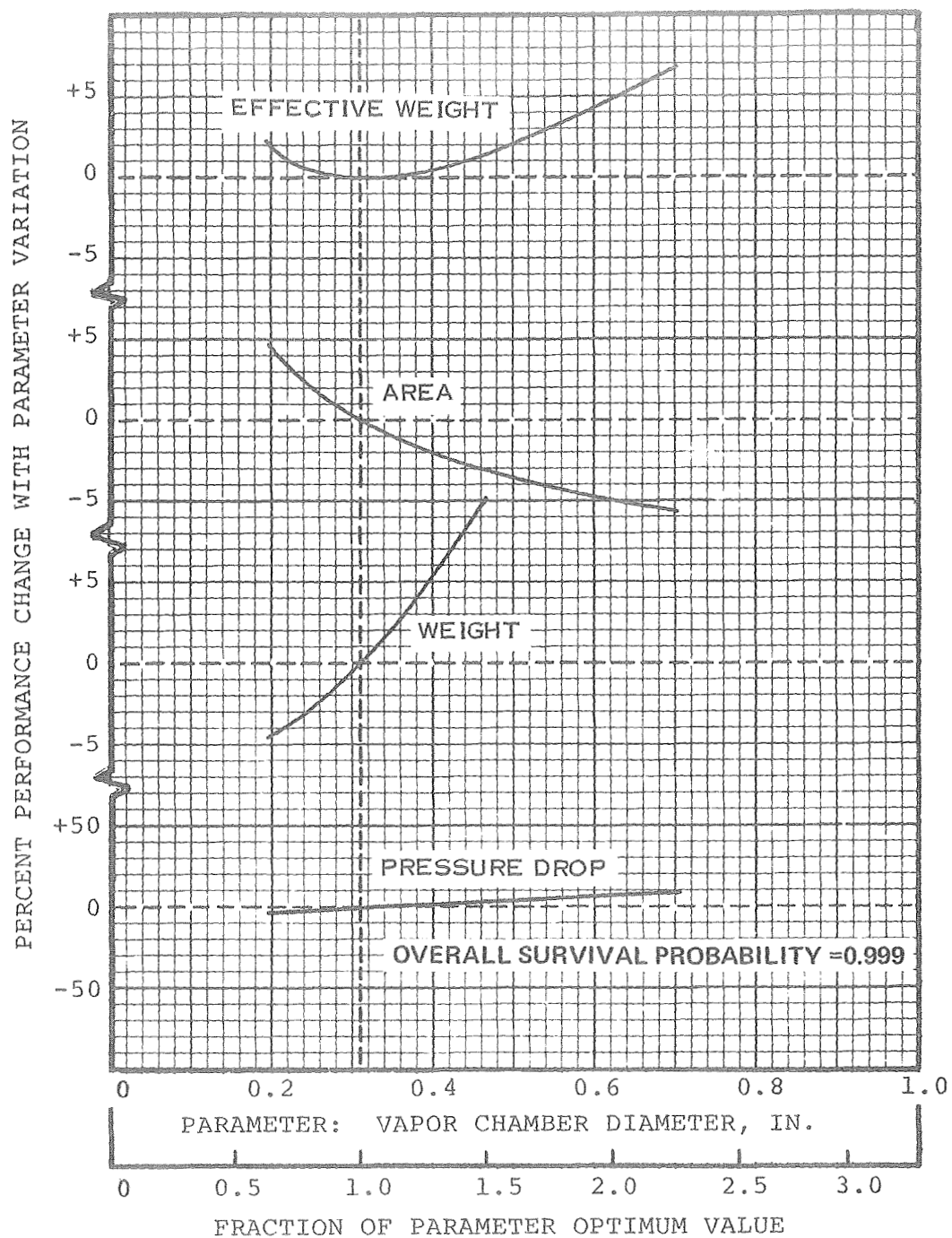


Figure 5-26. Effect of Vapor Chamber Diameter for Vapor Chamber Fin Primary Radiator

# EFFECT OF TUBE SPACING FOR VAPOR CHAMBER FIN PRIMARY RADIATOR

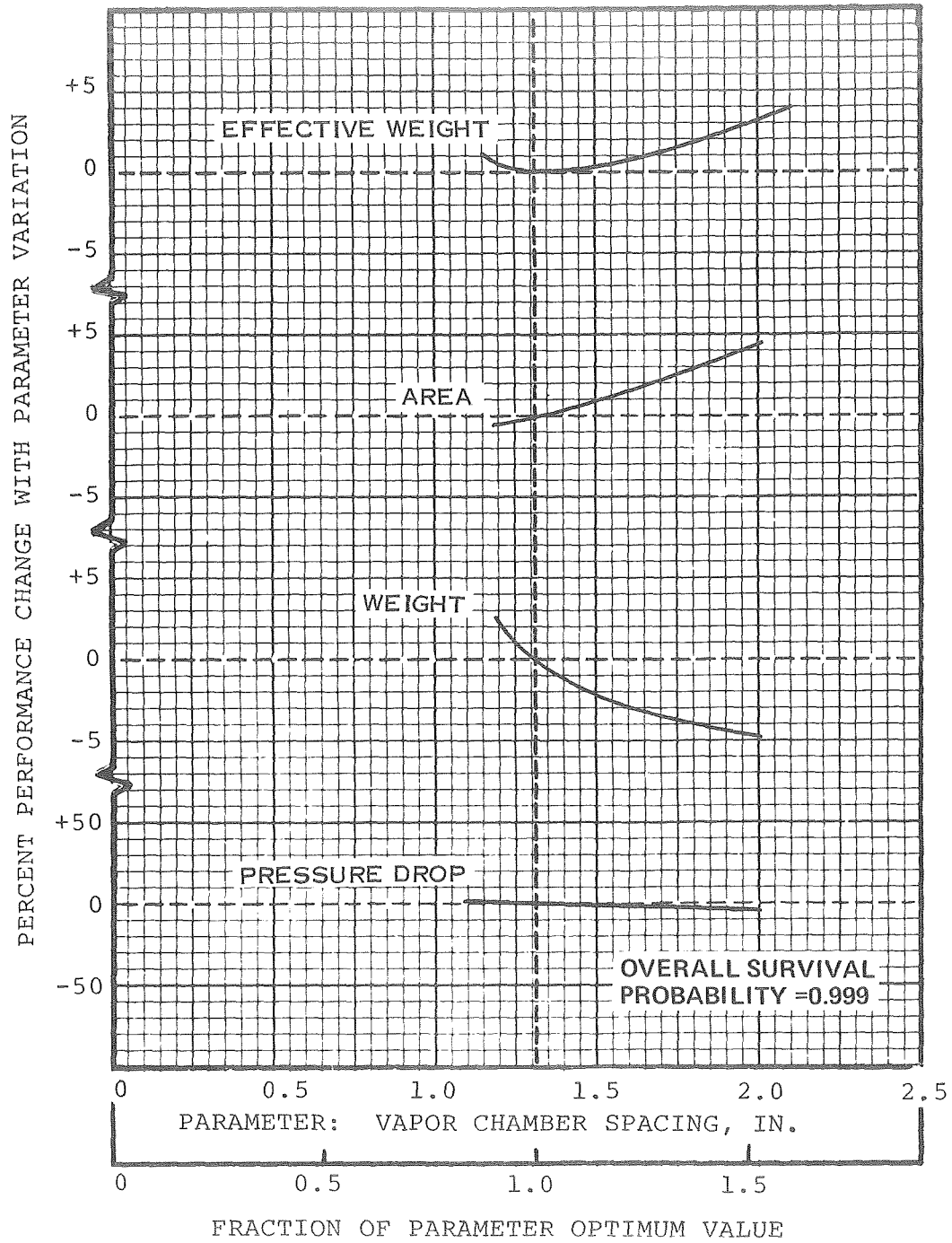


Figure 5-27. Effect of Tube Spacing for Vapor Chamber Fin Primary Radiator



# EFFECT OF PRIMARY FLUID SLOT WIDTH ON VAPOR CHAMBER FIN PRIMARY RADIATOR

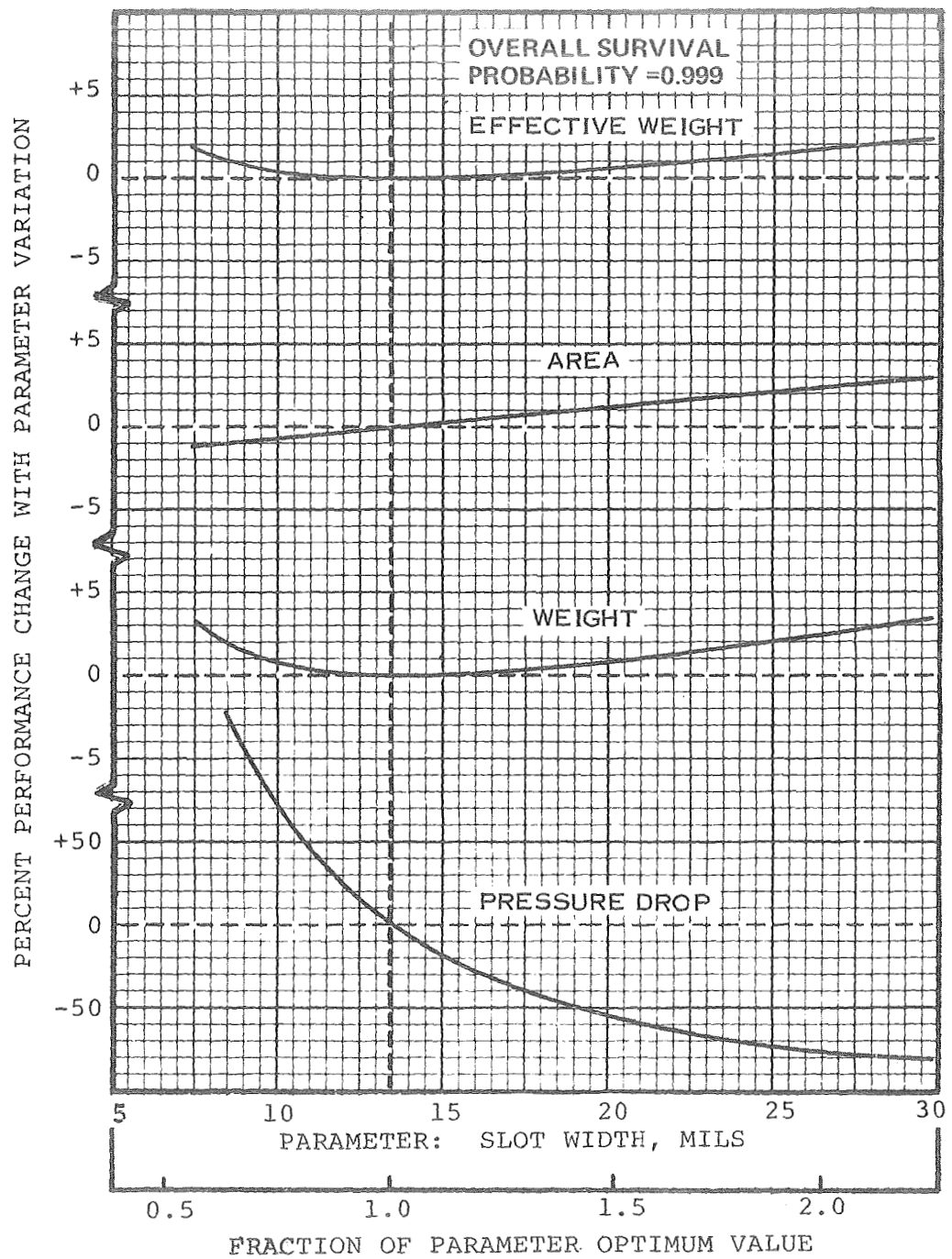


Figure 5-28. Effect of Primary Fluid Slot Width on Vapor Chamber Fin Primary Radiator

# EFFECT OF DUCT FIN THICKNESS FOR VAPOR CHAMBER FIN PRIMARY RADIATOR

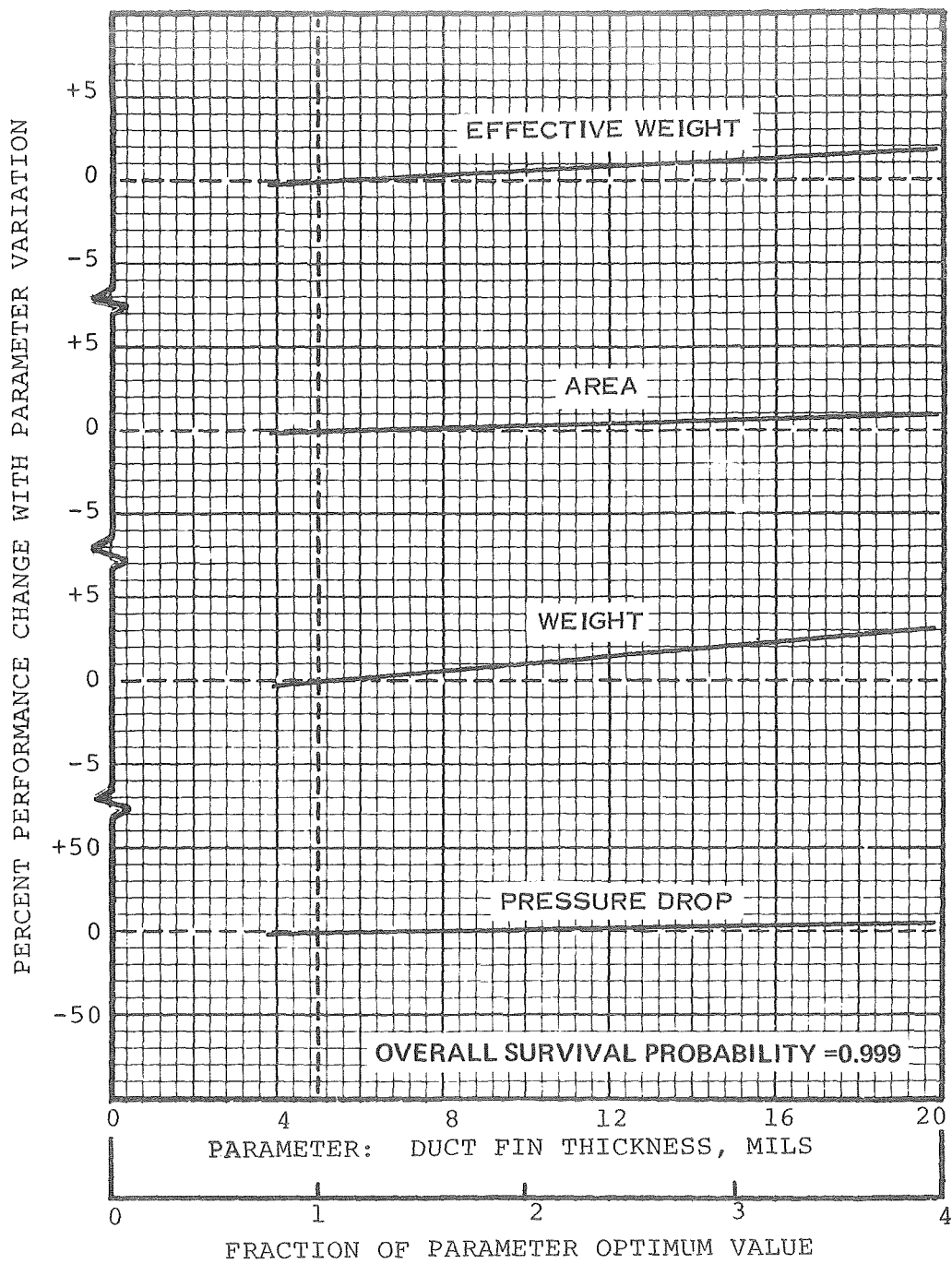


Figure 5-29. Effect of Duct Fin Thickness for Vapor Chamber Fin Primary Radiator

# EFFECT OF TUBE SPACING FOR CONDUCTION FIN PRIMARY RADIATOR

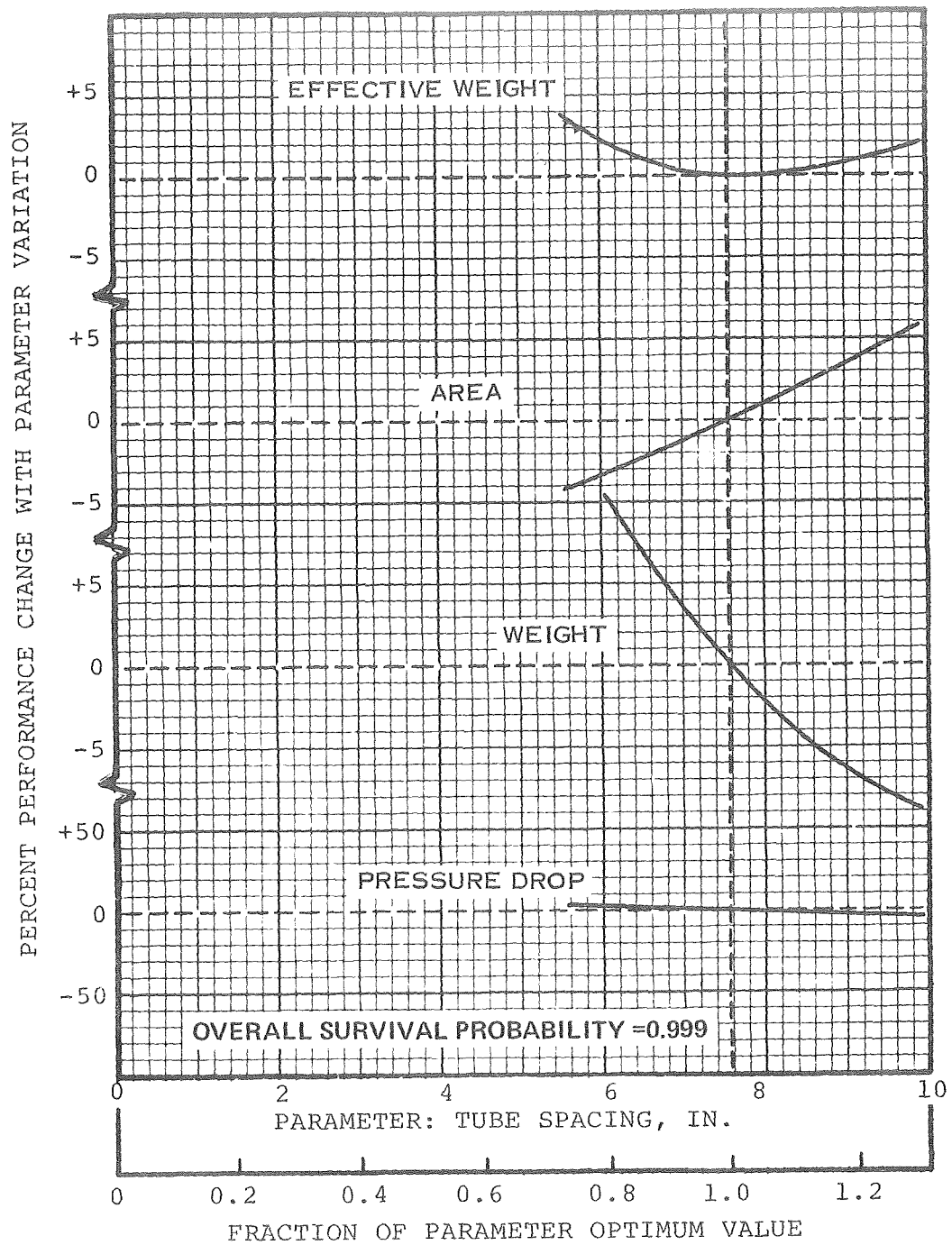


Figure 5-30. Effect of Tube Spacing for Conduction Fin Primary Radiator

# EFFECT OF PRIMARY FLUID SLOT WIDTH ON CONDUCTION FIN PRIMARY RADIATOR

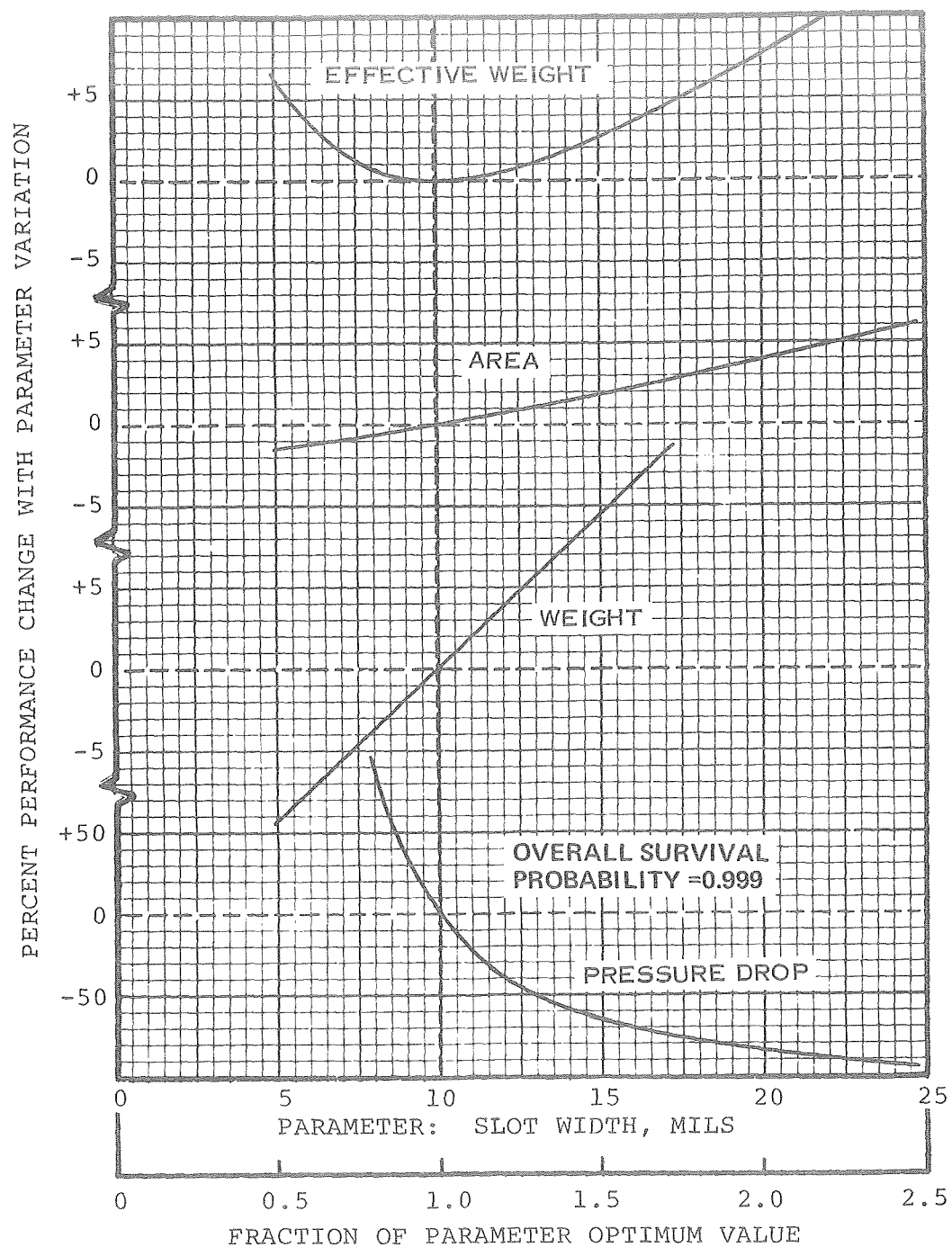


Figure 5-31. Effect of Primary Fluid Slot Width on Conduction Fin Primary Radiator

# EFFECT OF DUCT FIN THICKNESS FOR CONDUCTION FIN PRIMARY RADIATOR

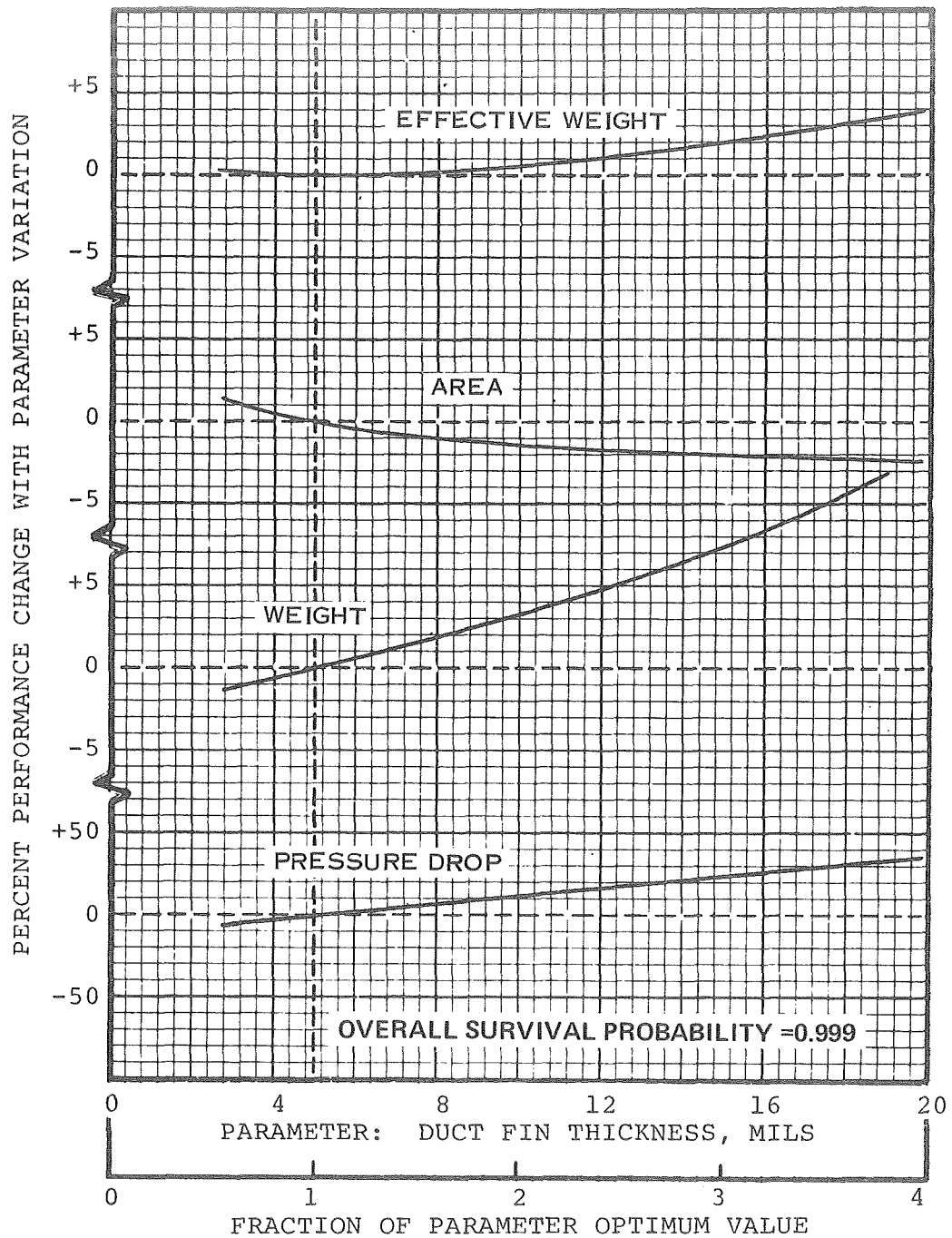


Figure 5-32. Effect of Duct Fin Thickness for Conduction Fin Primary Radiator

# EFFECT OF NUMBER OF SLOTS PER TUBE FOR CONDUCTION FIN PRIMARY RADIATOR

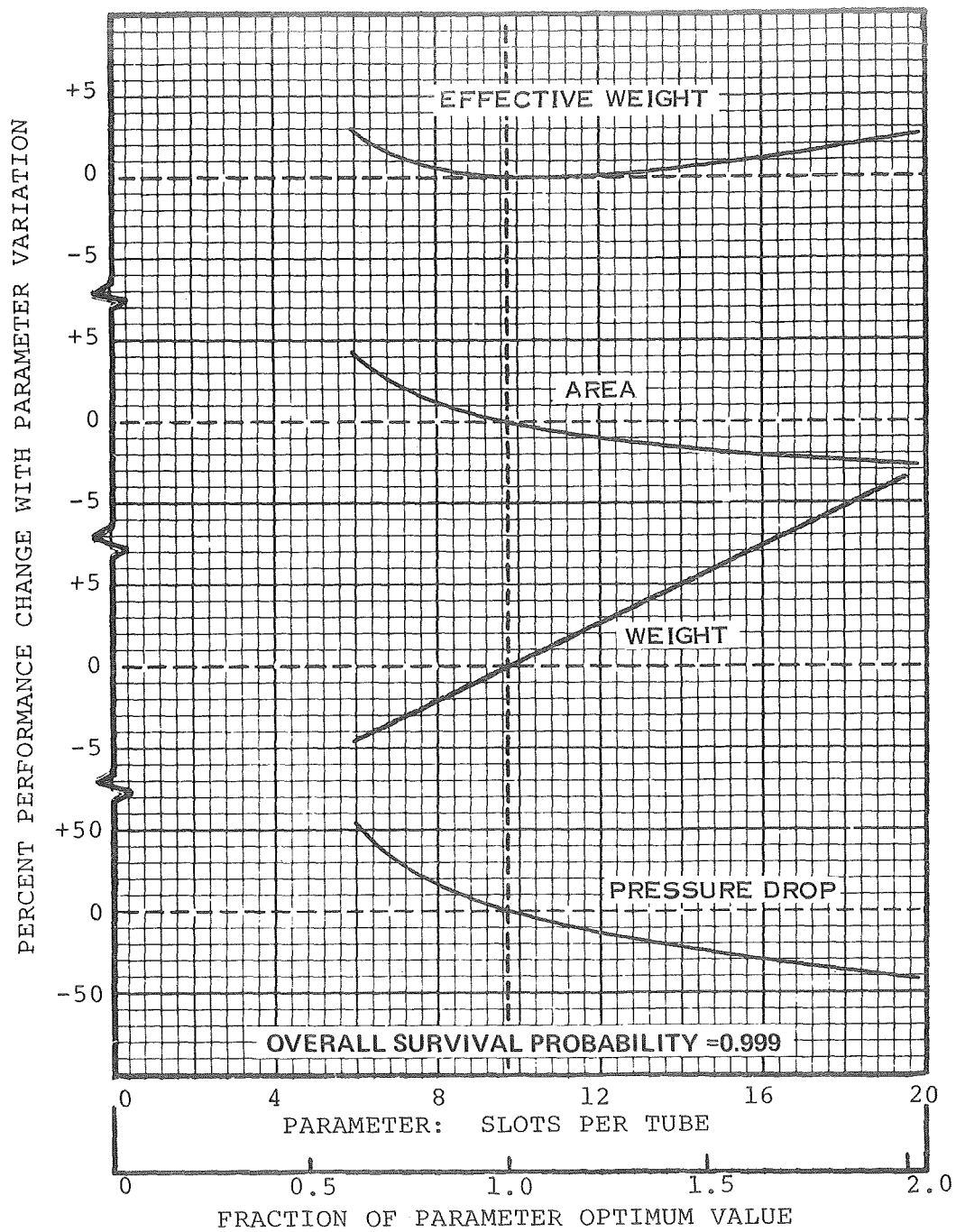


Figure 5-33. Effect of Number of Slots Per Tube for Conduction Fin Primary Radiator

function of payload weight. For a payload of approximately 6000 pounds, the load factors for the Atlas-Centaur launch vehicle are: (Ref. 6).

	<u>Axial Load Factor</u>	<u>Lateral Load Factor</u>
Maximum axial acceleration condition	6.2	0.3
Maximum lateral acceleration condition	2.3	1.56

The assumed spacecraft weight of 6000 pounds is based on an allowance of 1000 pounds for the radiator and 5000 pounds of equipment mounted above and supported by the radiator.

For design purposes, the launch loads are most conveniently expressed in terms of equivalent axial load.

$$P_{eq} = P_{ax} + \frac{2M}{R} \quad (5-14)$$

where:  $P_{eq}$  = equivalent axial load

$P_{ax}$  = axial load

$M$  = bending moment

$R$  = radius of radiator

Because the bending moment is a function of radiator length, the equivalent axial load is plotted for both launch load conditions as a function of radiator area in Figure 5-34. Radiator area is related to radiator length by assuming a diameter of 110 inches. For radiator areas greater than 200 square feet, the maximum lateral acceleration condition is more critical.

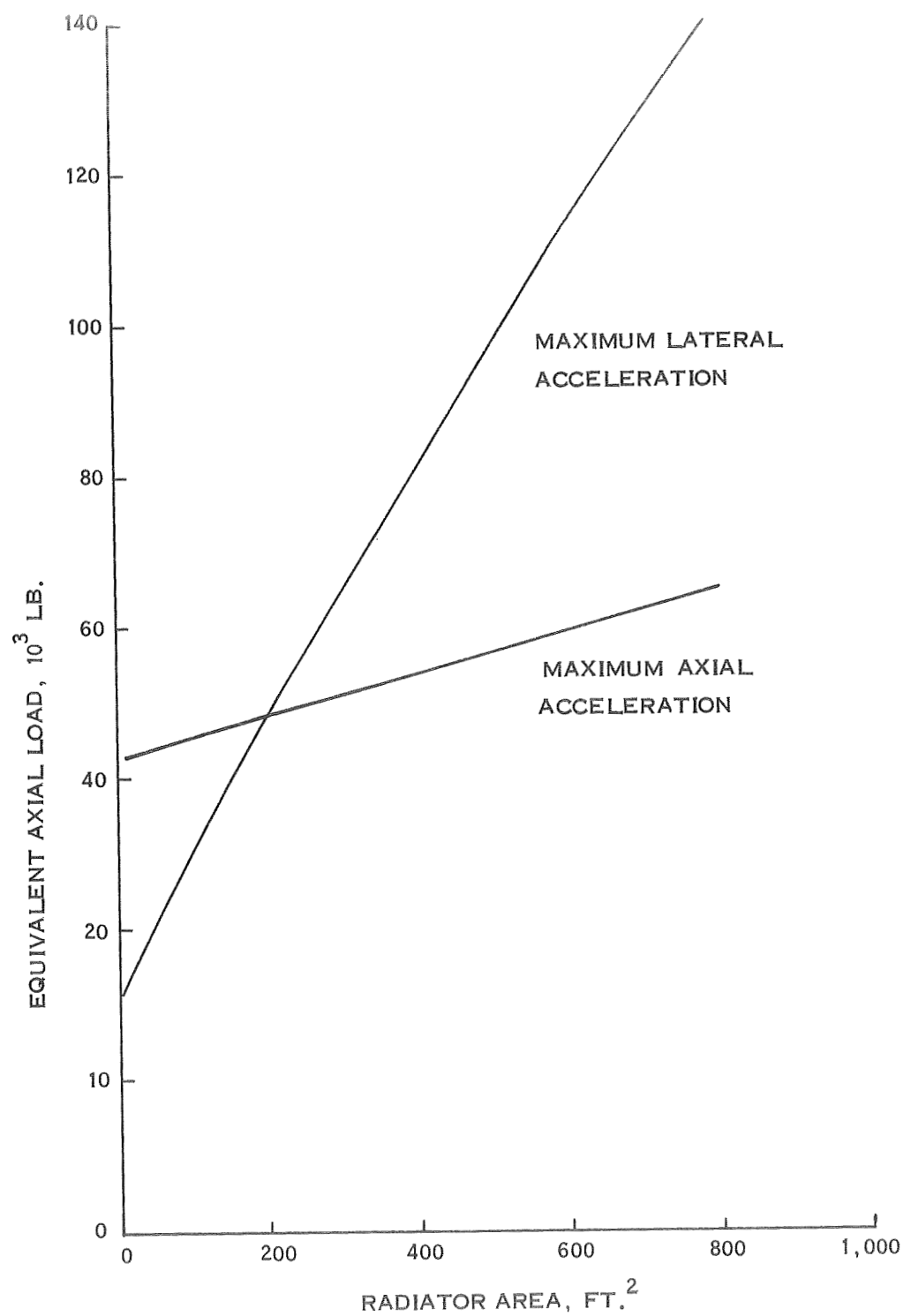


Figure 5-34. Launch Loads on Radiator



The loads shown in Figure 5-34 are ultimate loads, including a Factor of Safety of 1.25. The radiator areas and corresponding design loads used in the structural analysis are:

	<u>Area (ft<sup>2</sup>)</u>	<u>Shear Load (lb)</u>	<u>Equivalent Axial Load (lb)</u>
Conduction fin radiator	475	10,900	94,000
Vapor chamber fin radiator	508	10,900	99,000

The material used for structural elements of the radiators is assumed to be 6061-T6 with the following properties (Ref. 31):

Ultimate tensile	$\sigma_{tu} = 42,000$ psi
Ultimate yield	$\sigma_{ty} = 35,000$ psi
Modulus of Elasticity	$E = 9.9 \times 10^6$ psi

The radiator temperature during launch is assumed to be 200°F. At this temperature, the reduction factors on yield strength and elastic modulus are 0.92 and 0.98, respectively.

### 5.3.2 CONDUCTION FIN RADIATOR

The conduction fin radiator as a structural element can be regarded as a stiffened shell in axial compression, with the tubes acting as longitudinal stiffeners. The radiator was analyzed using the CRASS computer code. This code, which was written specifically for the structural analysis of radiators, considers local and panel instability modes as well as general instability. These failure modes are defined in Figure 5-35. Although buckling of the skin between stiffeners is permitted in many aerospace structures, it is not permitted in the analysis presented here because the radiator may have a relatively brittle coating on its surface for high emittance.

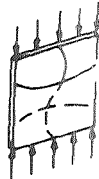
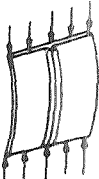
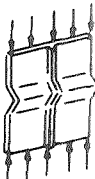

MODE	DEFINITION	
Local Instability	Buckling of the skin between the boundaries formed by the longitudinal and circumferential stiffeners	
Panel Instability	Buckling of the longitudinal stiffeners by bowing into one or more longitudinal halfwaves between circumferential stiffeners	
Crippling	The final ultimate compressive failure of a longitudinal stiffener which has a sufficient support to prevent panel instability	
General Instability	The simultaneous buckling of skin, longitudinal and circumferential stiffeners; the mode may be asymmetric (diamond shaped buckles) or axisymmetric (convolutions)	

Figure 5-35. Failure Modes

As part of the analysis performed by the CRASS computer program, the spacing of circumferential stiffening rings is determined to maintain a positive Margin of Safety in panel instability, and the rings are sized according to the Shanley criteria (Ref. 32). The radiator, including the added stiffening rings, is then analyzed for general instability using relations derived by Becker and Gerard (Ref. 33). The stresses and Margin of Safety for a radiator with the cross section shown in Figure 5-36 are summarized:

Ultimate design stress:	2929 psi
Local instability stress:	10,100 psi
Panel instability stress:	2955 psi
General instability stress:	13,200 psi
Margin of Safety:	1. %
Minimum spacing of stiffening rings:	37 in.

From the previous analysis, it is determined that a total of three stiffening rings, weighing 8.7 pounds, are required in addition to the attachment rings at the top and bottom of the radiator, and the ring joining the primary and secondary radiators. No additional longitudinal stiffening is required.

An analysis of the conduction fin secondary radiator revealed that no stiffening rings were required for this comparatively short section.

### 5.3.3 VAPOR CHAMBER FIN RADIATOR

The structural capability of the vapor chamber fin radiator lies primarily in the six coolant ducts which act as longerons. The vapor chamber fins have negligible stiffness in the axial direction, but contribute to the overall shear stiffness of the radiator. Buckling of the vapor chamber fins must be prevented, not only to avoid damage to the coating, but also to prevent rupture of the vapor chamber tubes.

The coolant ducts shown in Figure 5-37 have a cross sectional area of 0.686 in.<sup>2</sup> and a moment of inertia of 0.0747 in.<sup>4</sup>. Using data presented in Figure 5-35 the axial stress in each duct (longeron) is

$$\sigma_x = \frac{99,000}{6 \times 0.686} = 24,000 \text{ psi}$$

To prevent buckling of the ducts as an Euler column (Ref. 34) lateral support must be provided at spacing no greater than:

$$L = \left( \frac{C \pi^2 EI}{P} \right)^{1/2} \quad (5-15)$$

where: L = column length

C = fixity factor, assumed 2

E = elastic modulus

I = moment of inertia

P = axial load

From this relation the maximum spacing allowed is 30 inches. As will be shown, the stiffening rings required to prevent buckling of the vapor chamber fins are more closely spaced than those of the conduction fin radiator.

The analysis of shear loads in vapor chamber fins can account for the bending stiffness contributed by the vapor chamber tubes in the lateral direction by considering an equivalent flat plate thickness. For the cross section shown in Figure 5-38a, the area is 0.0557 in.<sup>2</sup> and the moment of inertia is 0.00069 in.<sup>4</sup>. In the lateral direction (parallel to the vapor chamber tubes), the equivalent thickness is 0.181 inch, while in the axial direction the equivalent thickness can be taken conservatively as that of the fins alone, 0.021 inch. The combined equivalent thickness is:

$$t_e = \sqrt{0.181 \times 0.021} = 0.0617 \text{ in.}$$

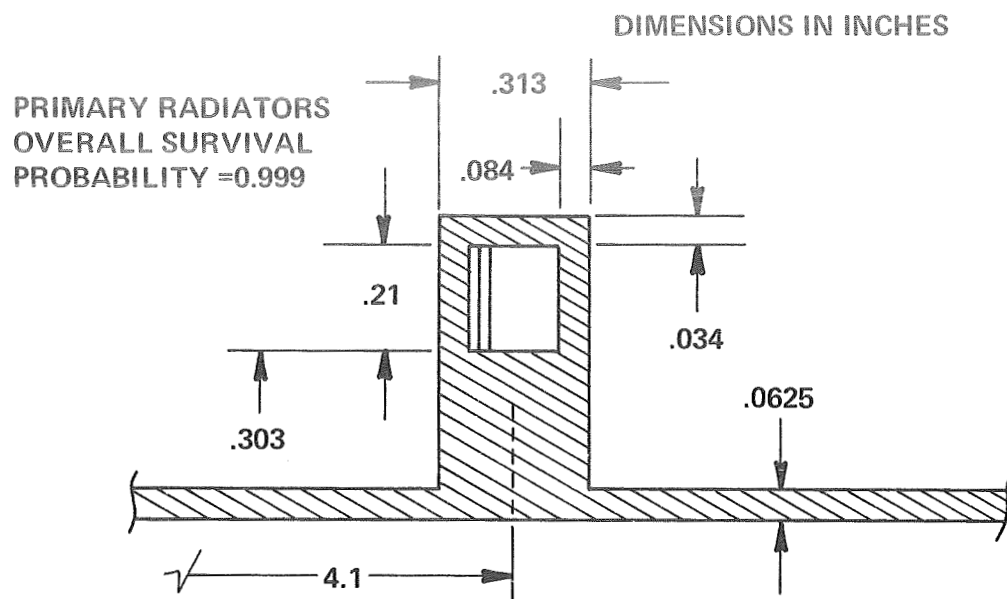


Figure 5-36. Cross Section Through Conduction Fin Radiator Duct

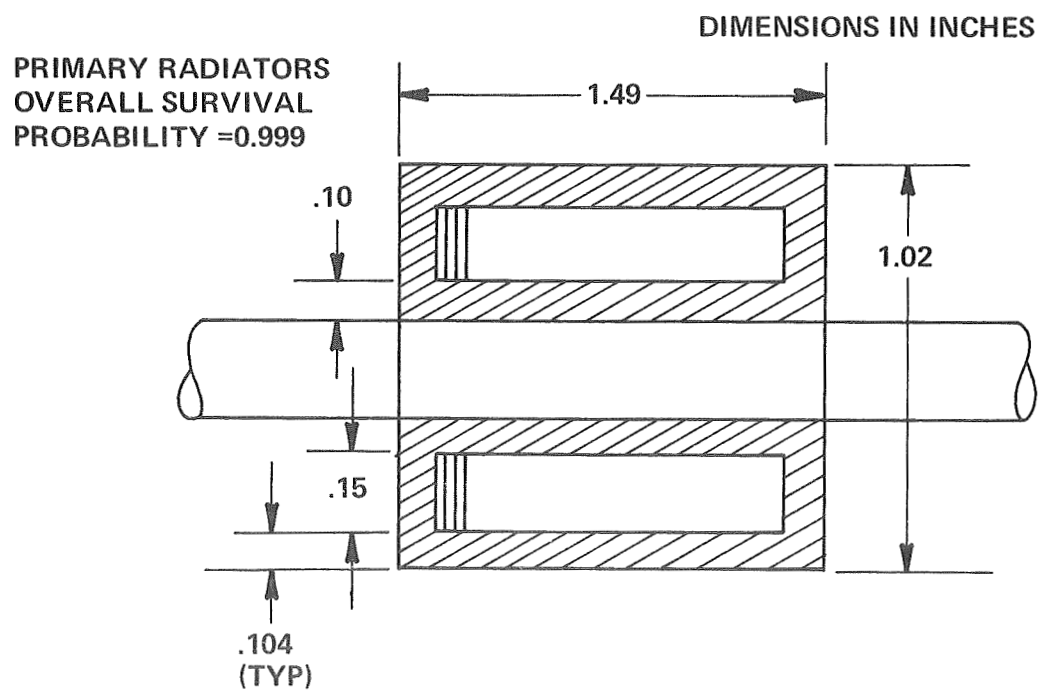


Figure 5-37. Cross Section Through Coolant Duct of Vapor Chamber Radiator

The critical shear buckling stress (Ref. 34) is:

$$\sigma_{CR} = \frac{k \pi^2 E}{12 (1-\mu^2)} \left( \frac{t_e}{b} \right)^2 \quad (5-16)$$

where:  $k$  = buckling coefficient (9 for simply supported edges)

$E$  = elastic modulus

$\mu$  = Poisson's ratio

$b$  = radiator panel matrix width (see Figure 5-38b) effective in resisting shear loads

Equation 5-16 can be reduced to the following:

$$\sigma_{CR} = \left( \frac{557}{b} \right)^2$$

Assuming that the shear load is carried entirely by the two panels parallel to the direction of the shear load, the shear stress is:

$$\sigma_s = \frac{P}{2 a t_{eff}}$$

where:  $P$  = shear load

$a$  = full panel width, 57.5 inches (based upon 110-inch hexagonal panel envelope)

$t_{eff}$  = effective panel thickness

The "effective" thickness used in this relation is not the "equivalent" thickness based on bending stiffnesses, but simply a measure of the average cross sectional area.

PRIMARY RADIATOR  
OVERALL SURVIVAL  
PROBABILITY = 0.999

DIMENSIONS IN INCHES

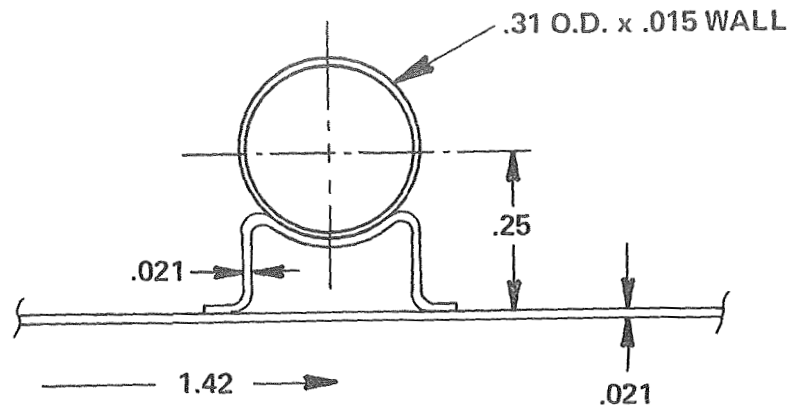


Figure 5-38a. Cross Section Through Vapor Chamber Tube and Fin

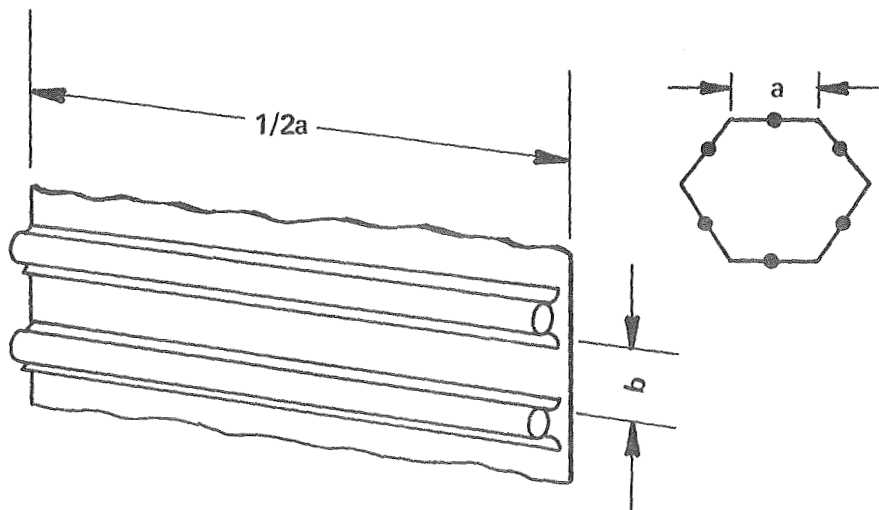


Figure 5-38b. Radiator Panel Matrix

$$t_{\text{eff}} = \frac{0.0557}{1.4} = 0.0398 \text{ in.}^2$$

$$\sigma_s = \frac{10\ 900}{(2)(57.5)(0.0398)} = 2380 \text{ lbs/in.}^2$$

Using an unsupported panel matrix width of 1.06 inches, which is the distance between vapor chambers, the critical shear stress can be calculated from Equation 5-16:

$$\sigma_{\text{CR}} = \left( \frac{557}{1.06} \right)^2 = 278,000 \text{ psi}$$

Therefore, the induced shear stress is far below the critical.

In order to achieve a moderate margin of safety stiffening rings were added every 10.7 inches rather than the maximum allowable of 30 inches.

As a further check, the critical buckling stress of the fins between the tubes was calculated. Using Equation 5-16 and a k of 1.0 the critical buckling stress is:

$$\sigma_{\text{CR}} = 31,900 \text{ (i.e., not critical)}$$

The following stresses and margin of safety are present with this design:

Axial stress in longeron:	24,000 psi
Shear stress in vapor chamber fins:	2,380 psi
Shear buckling stress between rings:	2,700 psi
Shear buckling stress between tubes:	31,900 psi
Margin of Safety:	1.3%
Column buckling stress of longeron:	40,200 psi



A total of 19 stiffening rings in the primary and secondary vapor chamber weighing 89 pounds, are required in addition to the attachment rings at the top and bottom of the fin radiator, radiator and the ring joining the primary and secondary sections.

The preceding analysis indicates that the conduction fin radiator is more suitable than the vapor chamber radiator as a load bearing structure. However, in either case, the weight of additional stiffening material required to enable the radiator to serve as the primary spacecraft structure is less than the weight that would be required for a separate structure.

The stresses in the radiator during launch are generally governed by buckling, well below the ultimate strength properties of 6061-T6. It may be concluded, therefore, that the selection of alloy and temper is not critical. The implication to manufacturing considerations is that it may permit the use of 6061 in the as-welded condition where heat treatment after welding is difficult.

The results described were obtained for radiators with survival probabilities of 0.999. These structural relationships applied to the 0.99 survivability cases indicated that the structural requirement is nearly proportional to radiator area. The conduction for radiator tube spacing can be decreased to improve fin efficiency, the additional weight to be added nearly equated by the increased structural capability of the tubes and the reduction in meteoroid protective armor.

#### 5.4 FABRICATION AND ASSEMBLY

##### 5.4.1 VAPOR CHAMBER FIN RADIATOR

The vapor chamber fin radiator layout and design details are shown in Figures 5-39 and 5-40. A concept for fabrication and assembly is given in steps 1 through 8 below.

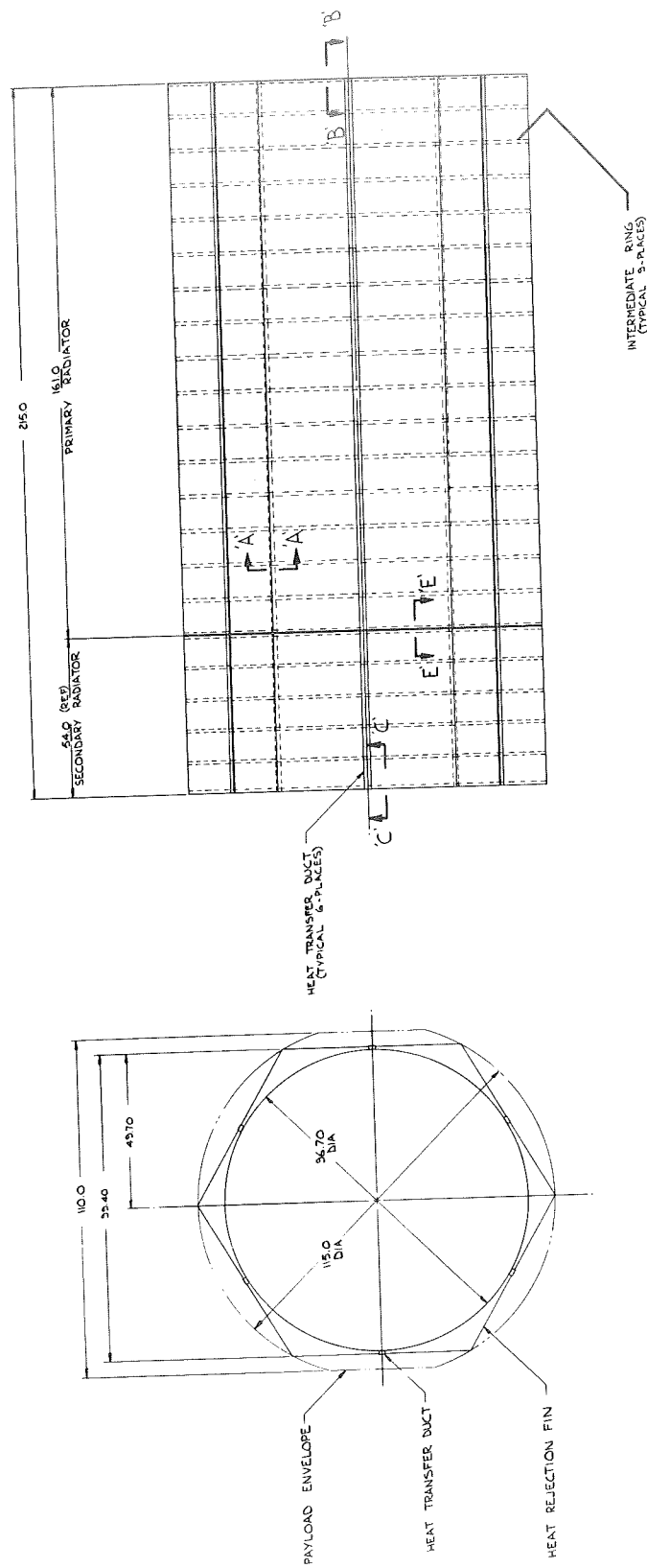


Figure 5-39. Vapor Chamber Radiator Design Layout

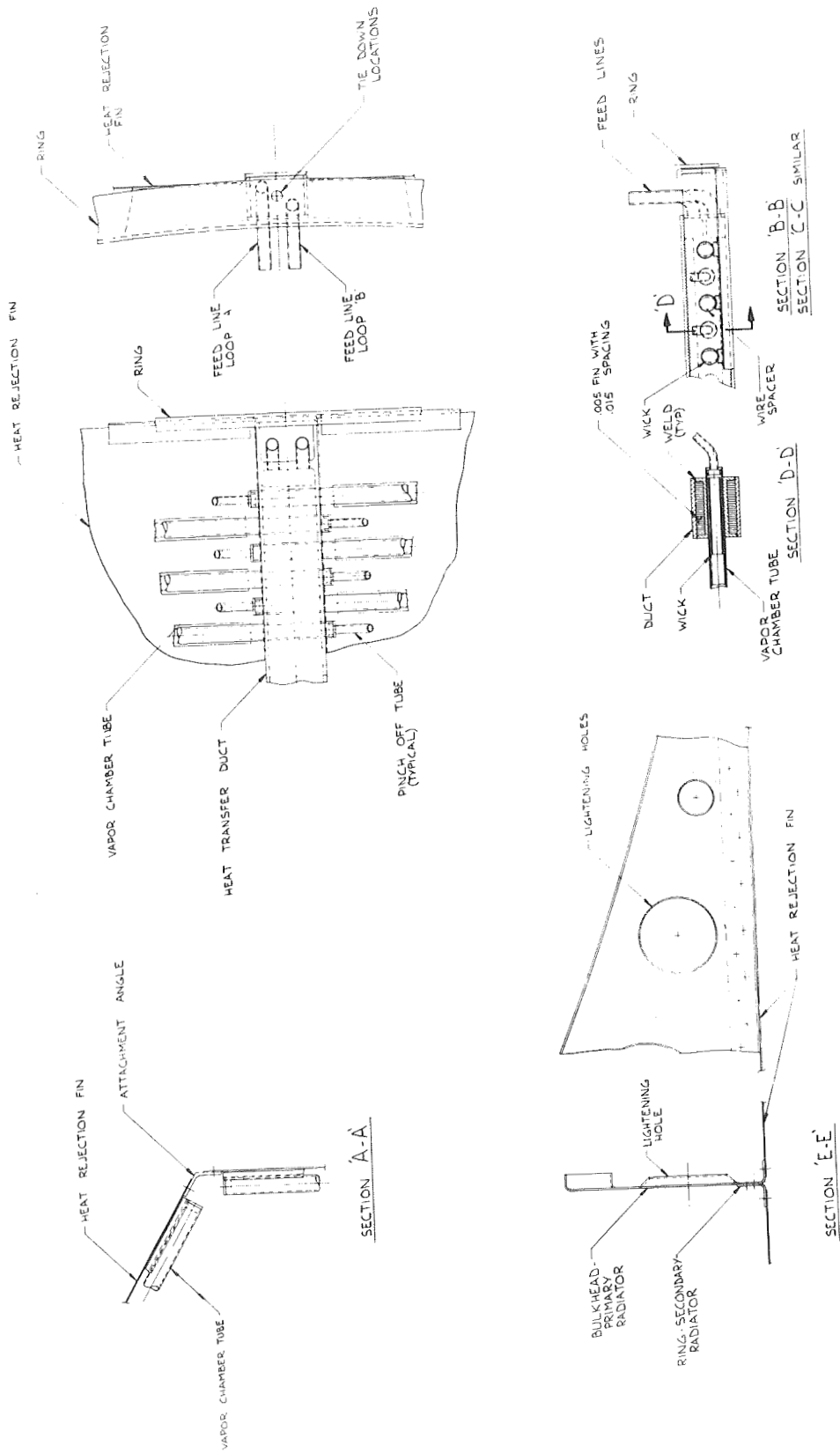


Figure 5-40. Vapor Chamber Fin Radiator Design Details

#### 5.4.1.1 STEP 1 Primary Coolant Duct (Figure 5-41)

The duct carrying the primary coolant (DC-200) is machined from aluminum bar.

#### 5.4.1.2 STEP 2 Internal Fins (Figure 5-42)

The internal fins are shown as they would be fabricated by chem milling. Internal fins would not necessarily be continuous for the length of the duct. Alternate concepts would be to form corrugation from sheet material, or to machine slots in duct. If the fins are made as a separate assembly, they must be joined to the duct for good thermal conductance. Soldering or brazing could be used for this joint.

#### 5.4.1.3 STEP 3 Assembly of Coolant Duct (Figure 5-43)

Assembly of the coolant duct is completed by welding in tubing connections for the feed lines and welding cover plates and end plates to the duct.

#### 5.4.1.4 STEP 4 Vapor Chamber Tubes (Figure 5-44)

The vapor chamber wicks are installed in the tubes with wire retainers. A plug is welded in one end and a pinch-off tube in the other. At this point, the vapor chamber may be checked for leaks and performance, but final charging with fluid must be done at a later stage in the assembly sequence.

#### 5.4.1.5 STEP 5 Fin Assembly (Figure 5-45)

Supports for the vapor chambers are welded to the fins.

#### 5.4.1.6 STEP 6 Panel Assembly (Figure 5-46)

The coolant ducts, vapor chamber tubes, and fin assemblies are joined in a panel assembly by brazing. The vapor chamber tubes will be brazed into holes in the coolant ducts, and to tube supports on the fin assembly. Edges of the fin assembly will be brazed to the coolant ducts.

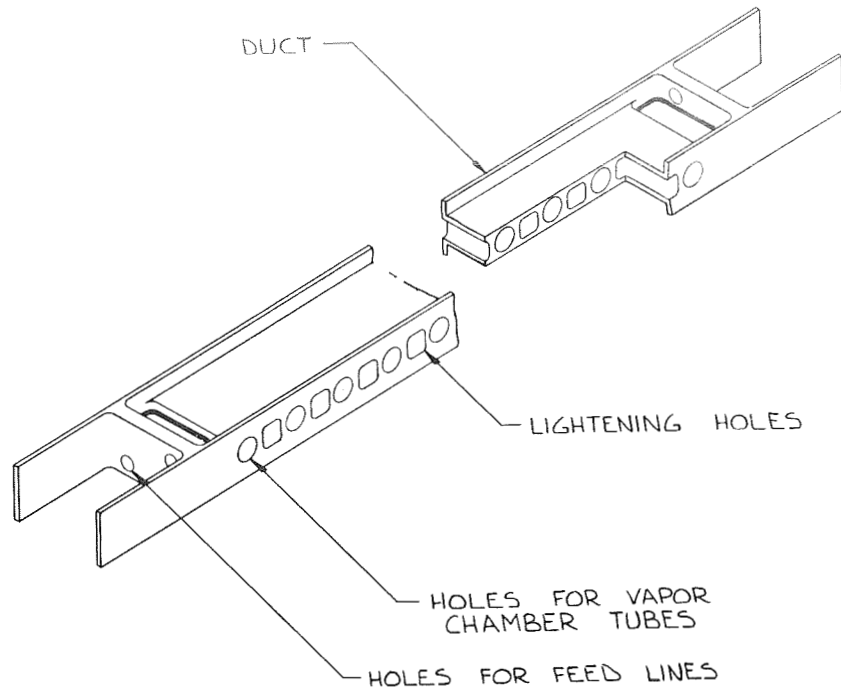


Figure 5-41. Vapor Chamber Fin Radiator Assembly Sequence Step 1

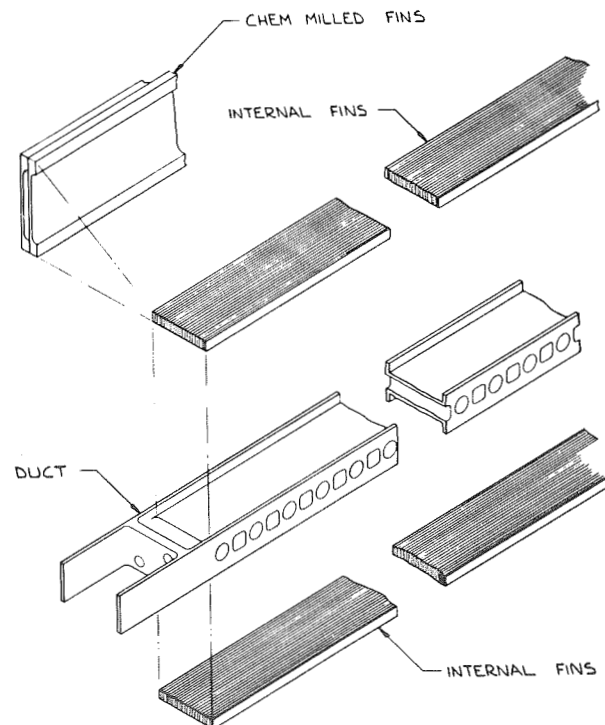


Figure 5- 42. Vapor Chamber Fin Radiator Assembly Sequence Step 2

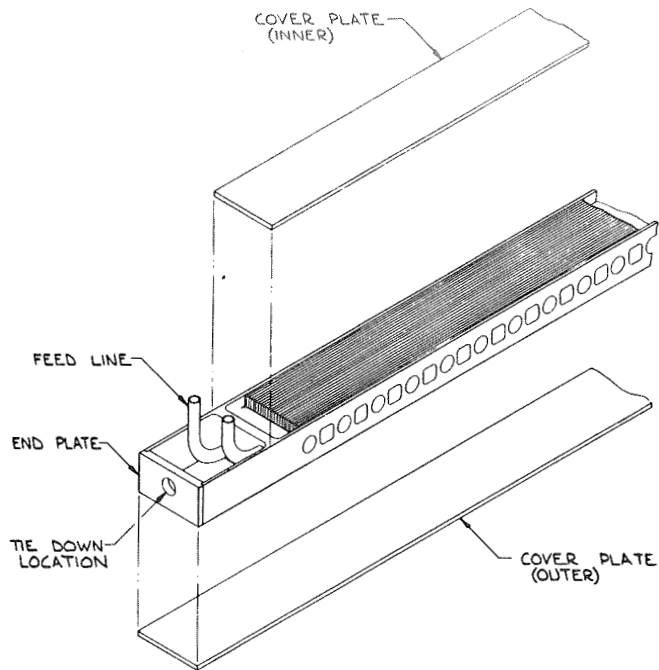


Figure 5-43. Vapor Chamber Fin Radiator Assembly Sequence Step 3

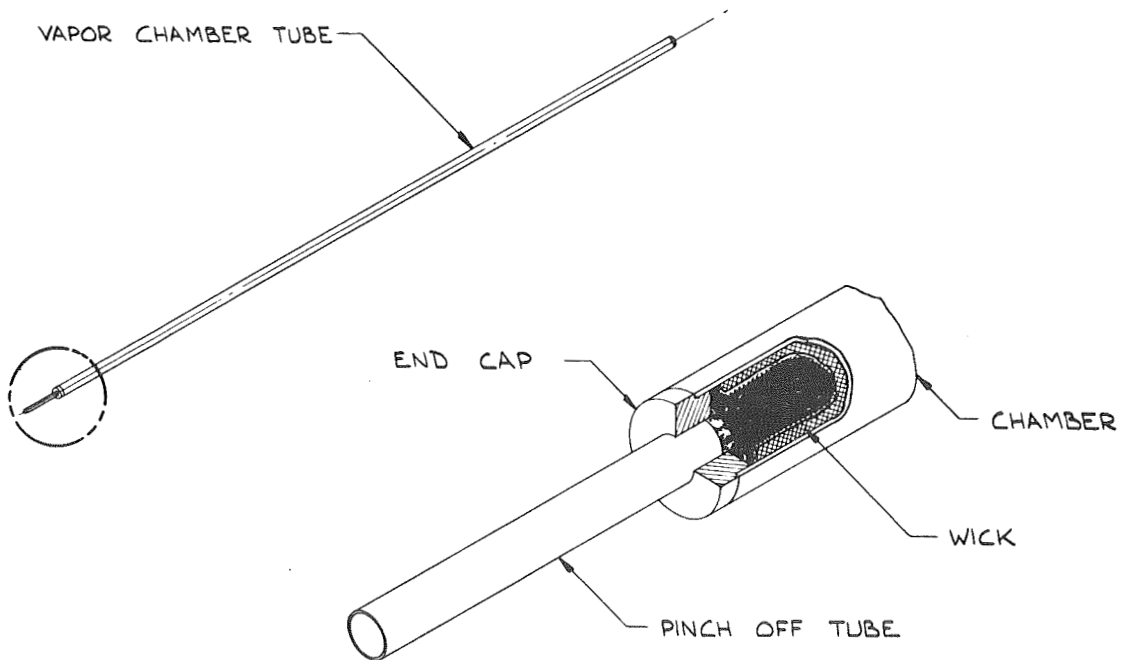


Figure 5-44. Vapor Chamber Fin Radiator Assembly Sequence Step 4

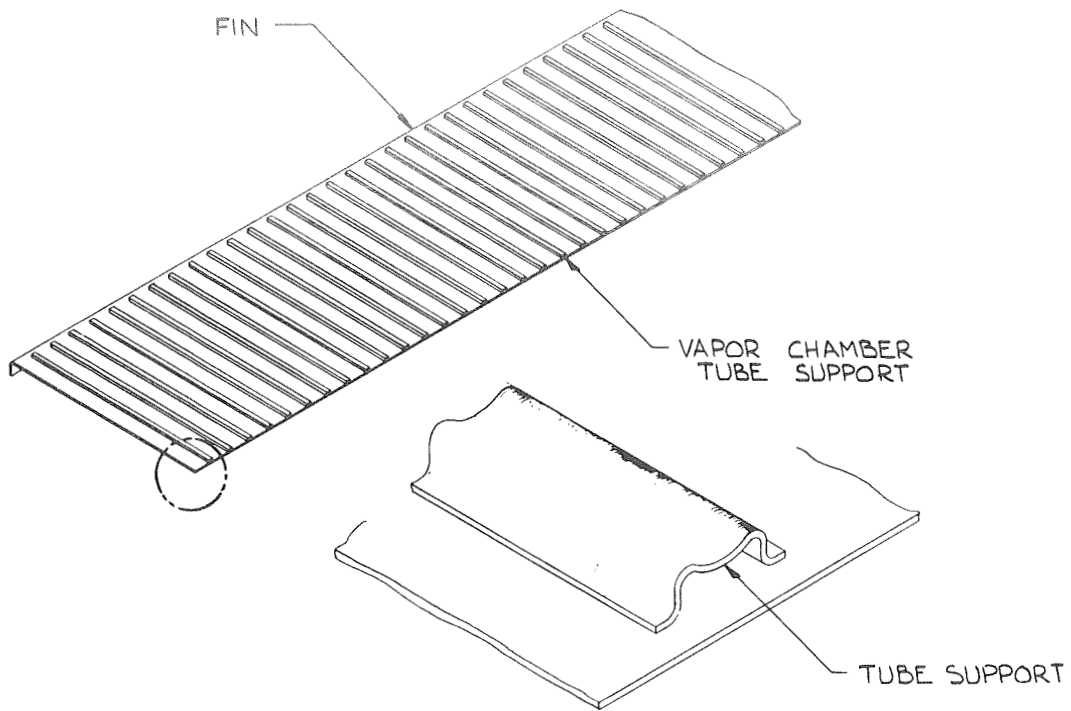


Figure 5-45. Vapor Chamber Fin Radiator Assembly Sequence Step 5

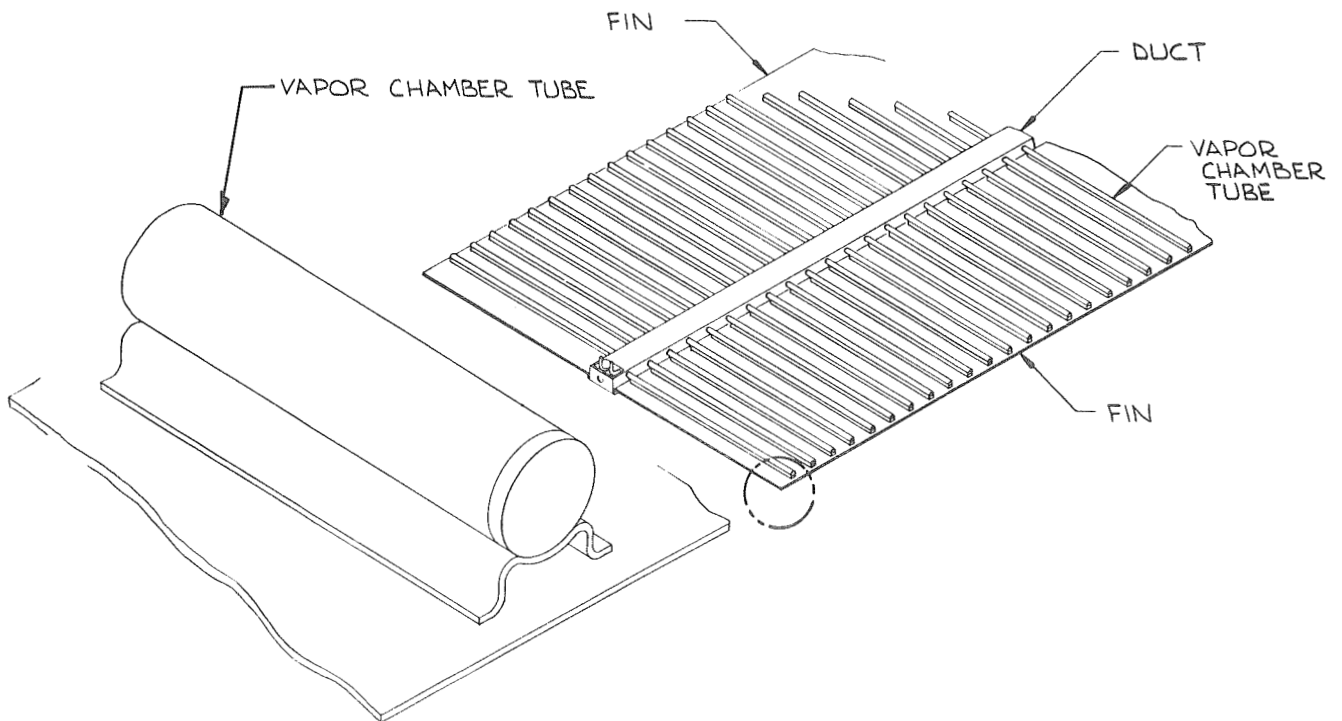


Figure 5-46. Vapor Chamber Fin Radiator Assembly Sequence Step 6

#### 5.4.1.7 STEP 7 Frame Assembly (Figure 5-47)

The attachment rings, intermediate stiffening rings, and corner splice angles are assembled as a riveted frame.

#### 5.4.1.8 STEP 8 Final Assembly (Figure 5-48)

Final assembly of the radiator consists of riveting the individual panels to the frame assembly. Structural attachment between the primary and secondary radiators is completed by bolting the end plates of the coolant ducts together.

### 5.4.2 CONDUCTION FIN RADIATOR

The conduction fin radiator layout and design details are shown in Figures 5-49 and 5-50. A concept for fabrication and assembly is given in steps 1 through 6 below.

#### 5.4.2.1 STEP 1 Parts Fabrication for Coolant Duct (Figure 5-51)

Each coolant duct is made up of four elements: a machined channel, internal fins, a cover plate, and bushings for inlet and outlet connections. The internal fins are shown as they would be fabricated by chem milling. Alternate concepts would be to form corrugated fins from sheet material, or to machine slots in the channel.

#### 5.4.2.2 STEP 2 Assembly of Coolant Ducts (Figure 5-52)

The internal fins are soldered into the channel for good thermal conduction. A suitable solder for this joint would be a 95% zinc, 5% aluminum composition. An alternate would be to use aluminum brazing. The assembly of the ducts can now be completed by welding the bushings to the cover plate, and the cover plate to the channel. Remelting of the solder during welding would be tolerable provided the ducts remain level and significant flow of the solder does not occur.

#### 5.4.2.3 STEP 3 Assembly of Panel Headers (Figure 5-53)

The panel headers are formed tubes with bushings for pigtail connections to the tubes. All joints are welded, including the plug in the dead end.



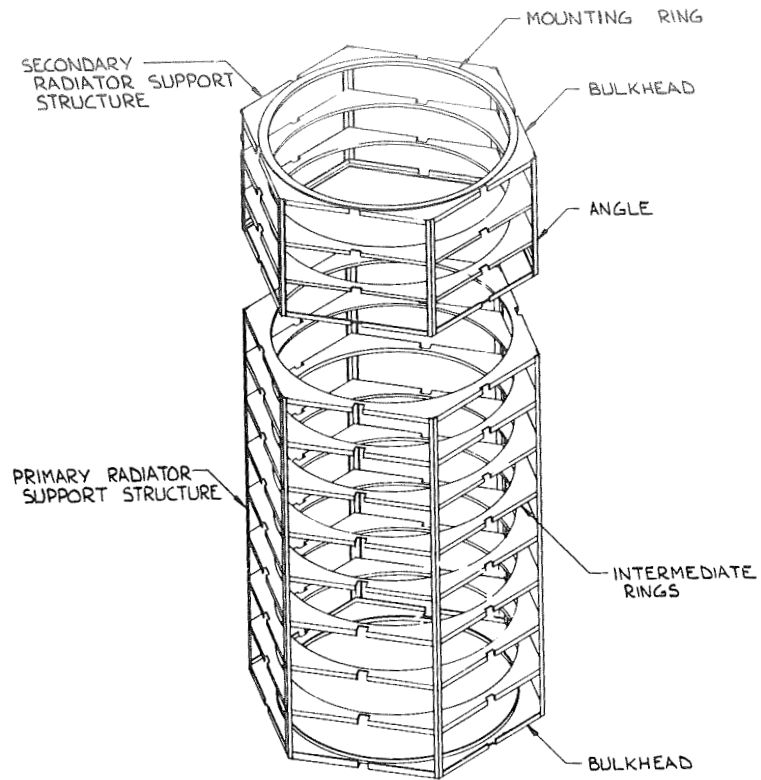


Figure 5-47. Vapor Chamber Fin Radiator Assembly Sequence Step 7

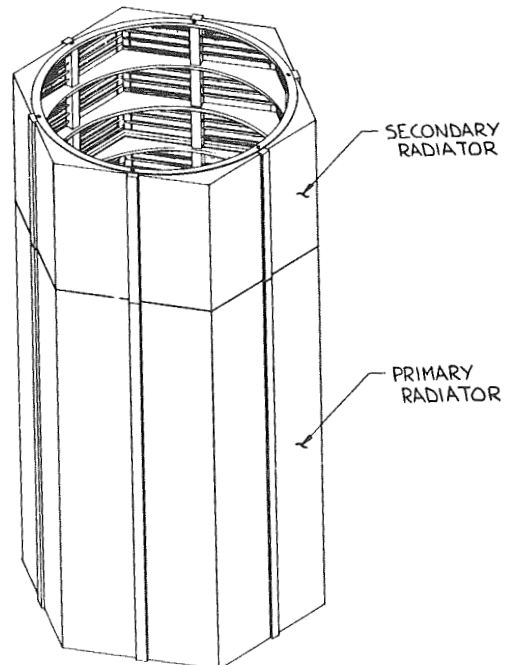


Figure 5-48. Vapor Chamber Fin Radiator Assembly Sequence Step 8

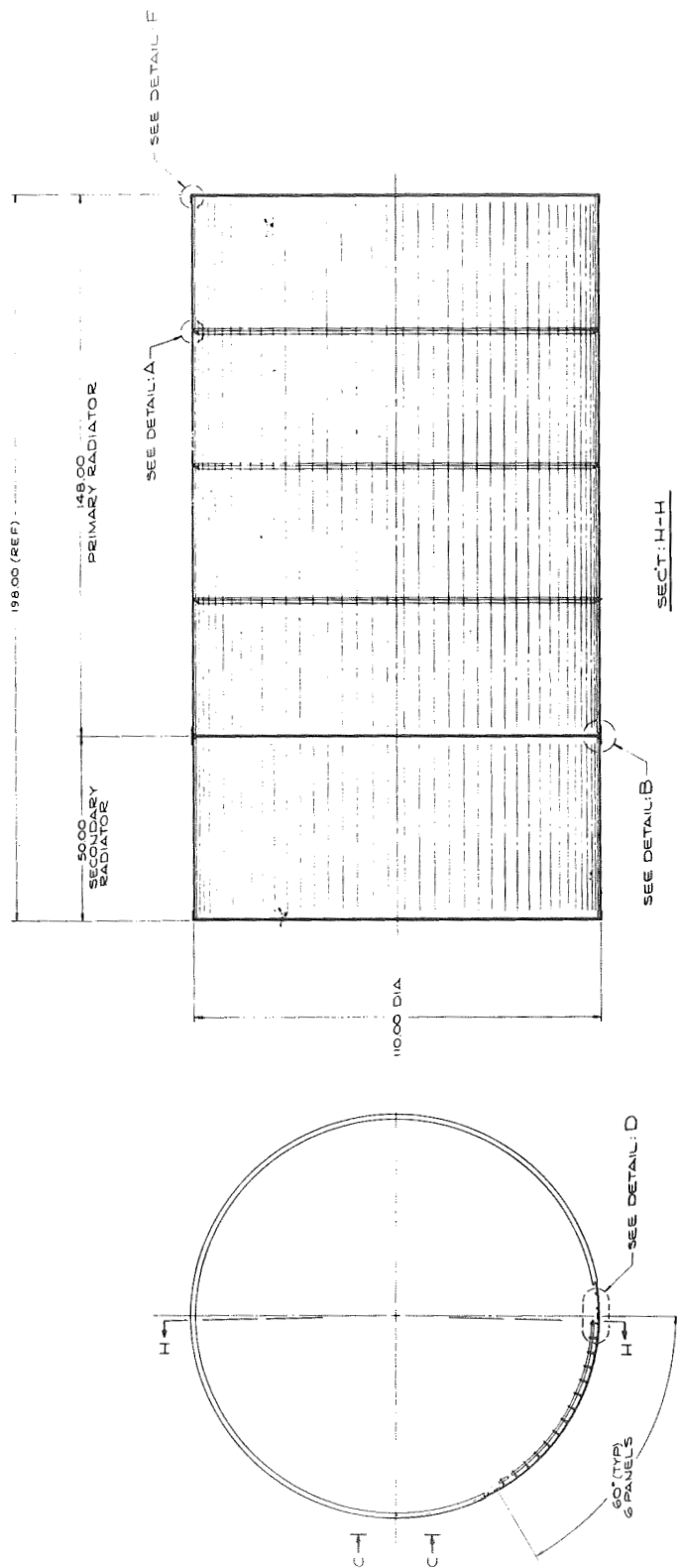


Figure 5-49. Conduction Fin Radiation Design Layout

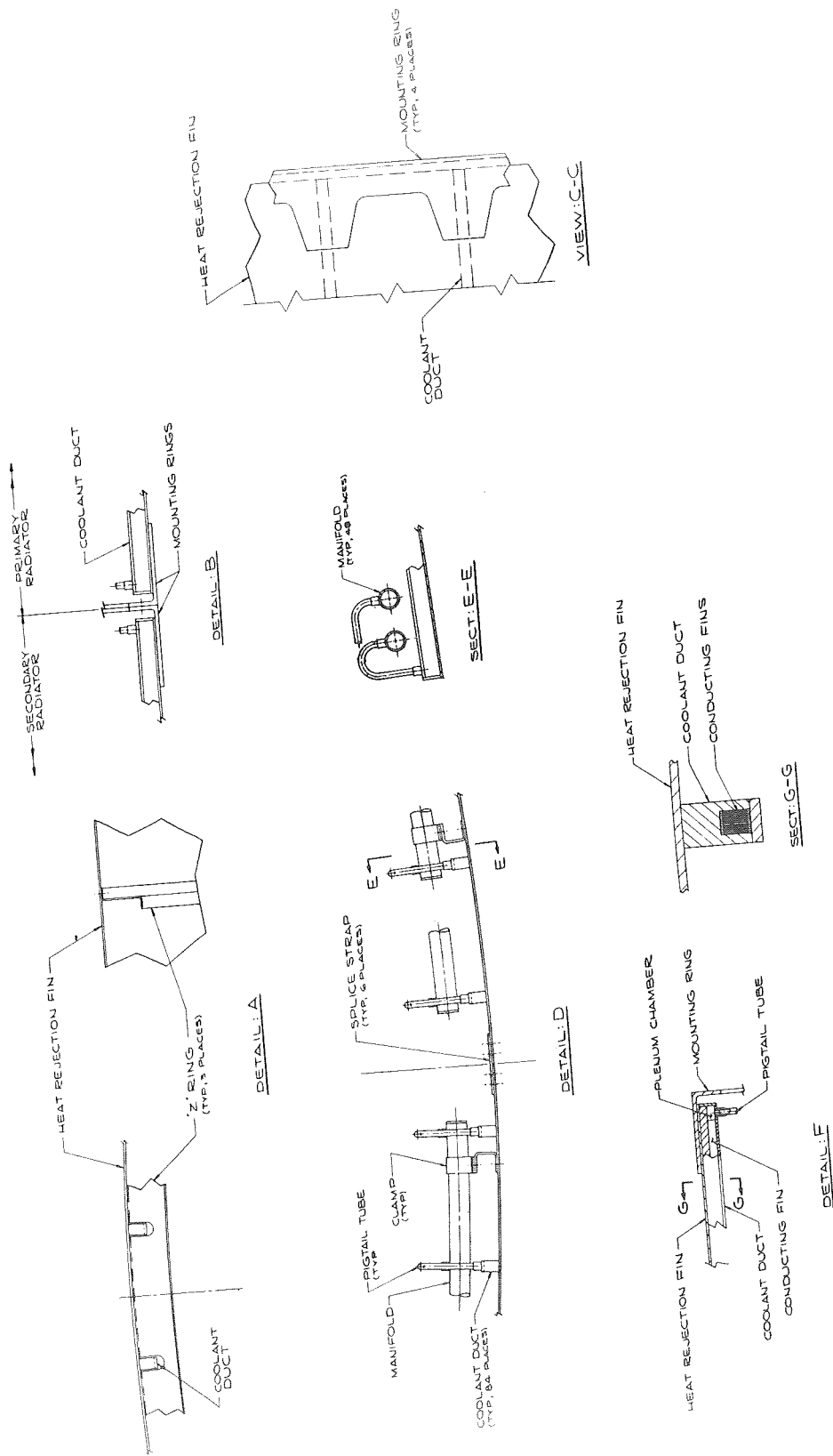


Figure 5-50. Conduction Fin Radiator Design Details

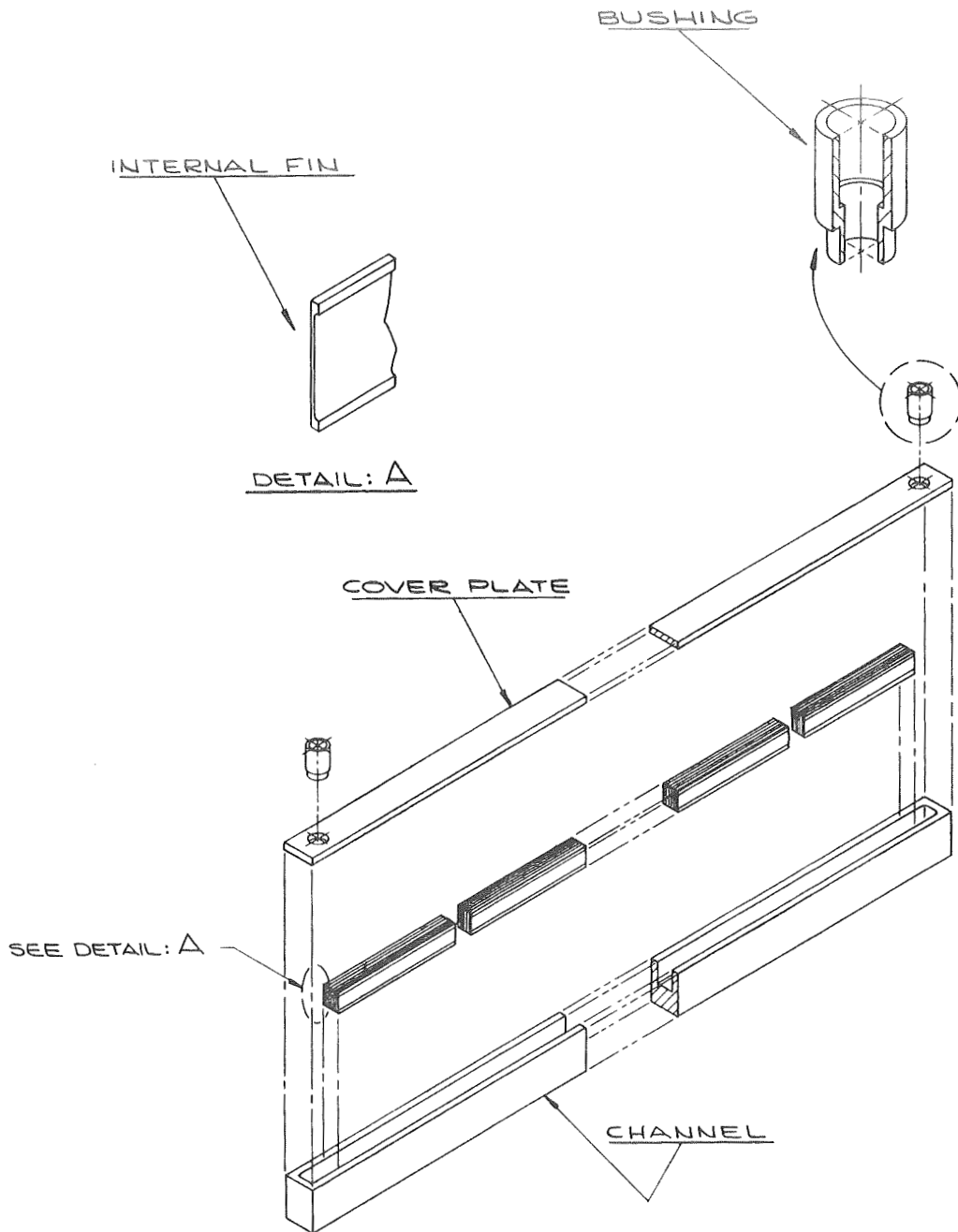


Figure 5-51. Conduction Fin Radiator Assembly Sequence Step 1

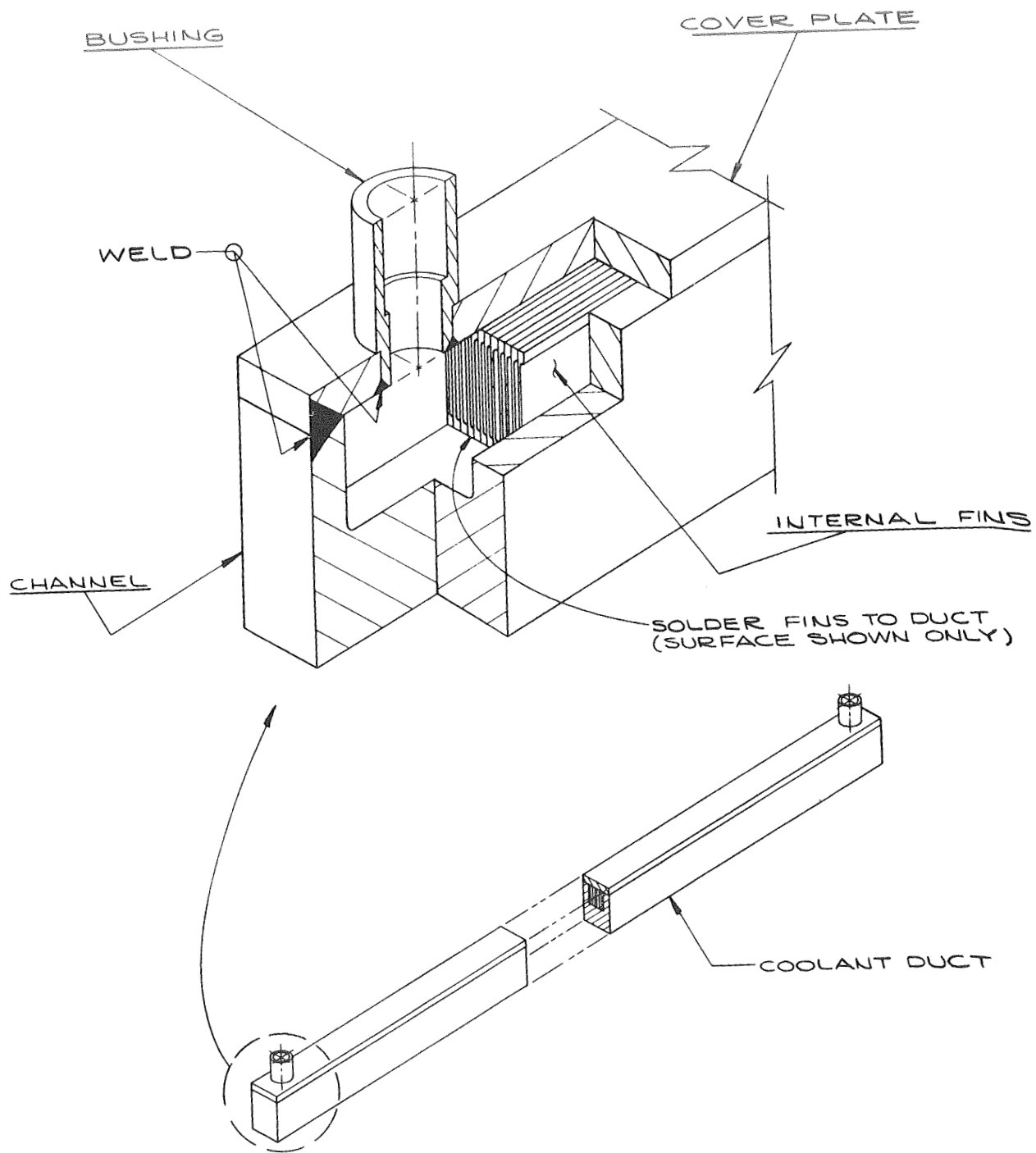


Figure 5-52. Conduction Fin Radiator Assembly Sequence Step 2

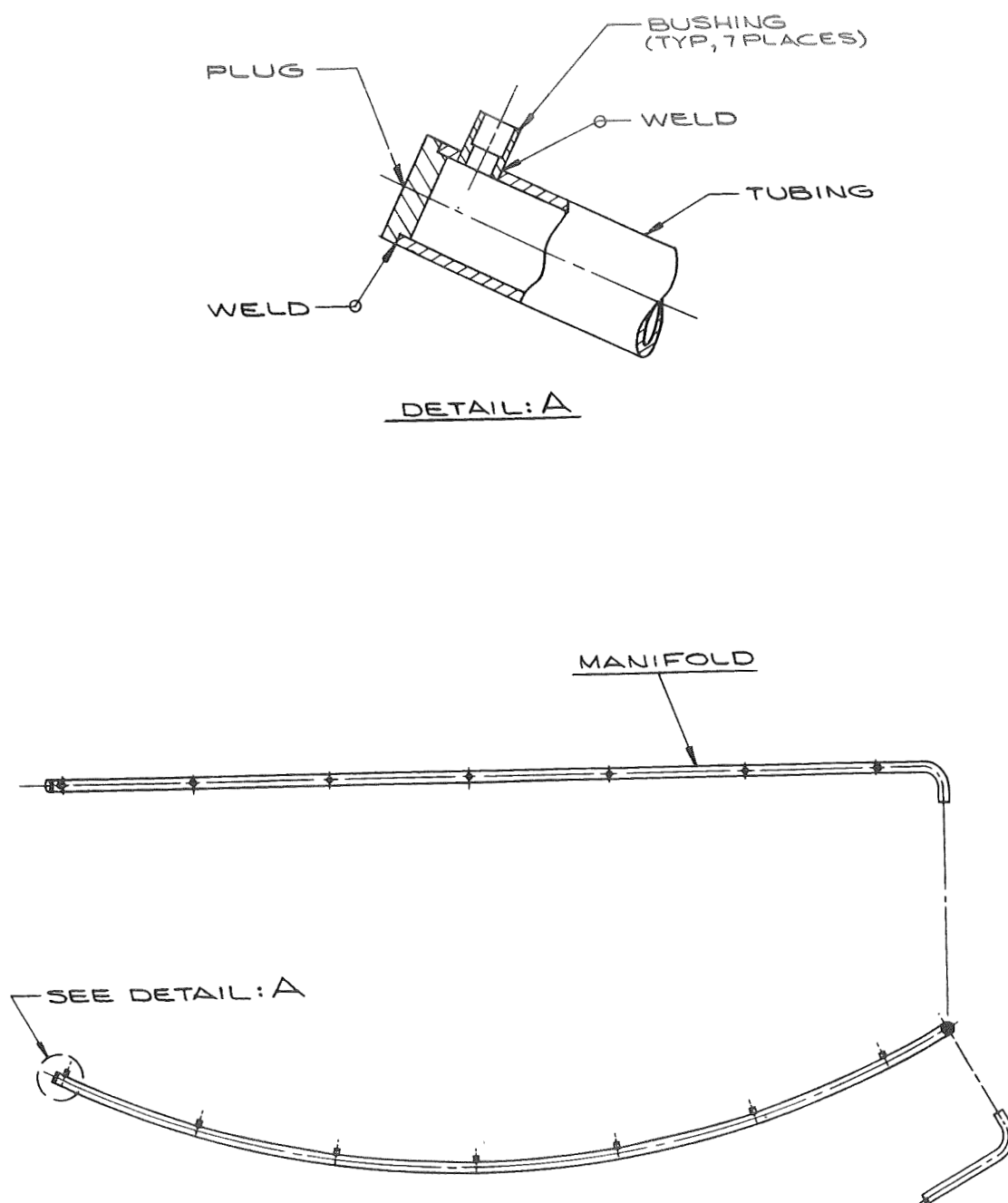


Figure 5-53. Conduction Fin Radiator Assembly Sequence Step 3

#### 5.4.2.4 STEP 4 Attachment of Fins (Figure 5-54)

The tubes are welded to the fins. Detail A shows the weld joint that would be used if the fin were made from a single sheet. The alternate joint shown allows a simpler weld, but requires more jiggling because the fins are made up of a series of strips. The Z rings for structural stiffening are riveted to the fins and cut out to clear the tubes.

#### 5.4.2.5 STEP 5 Pigtail Connections (Figure 5-55)

The tubes are connected to the inlet and outlet headers with short "pigtail" sections of tubing. The pigtails are welded to the bushings in the headers and tubes with a portable tube welder having an orbiting head. Alternate joining techniques are brazing, soldering or adhesive bonding. The headers for each panel are supported by clamps and brackets rivetted to the fins. There are inlet and outlet headers for each of the two redundant loops.

#### 5.4.2.6 STEP 6 Final Assembly (Figure 5-56)

Final assembly of the radiator consists of riveting the individual panels to attachment rings and riveting longitudinal splices between panels. The "Z" ring sections on each panel would also be spliced by riveting.

### 5.5 WEIGHT COMPARISON

The weight summary presented in Table 5-6 compares a vapor chamber fin radiator with a conduction fin radiator. The significant ground rules for the comparison are listed in Table 5-7.

The area penalty of  $3 \text{ lb/ft}^2$  was included as a means of incorporating the effect on the system weight of the presence of additional radiator area. In reality this penalty is made up of added shroud, structure, fittings, piping insulation, etc.

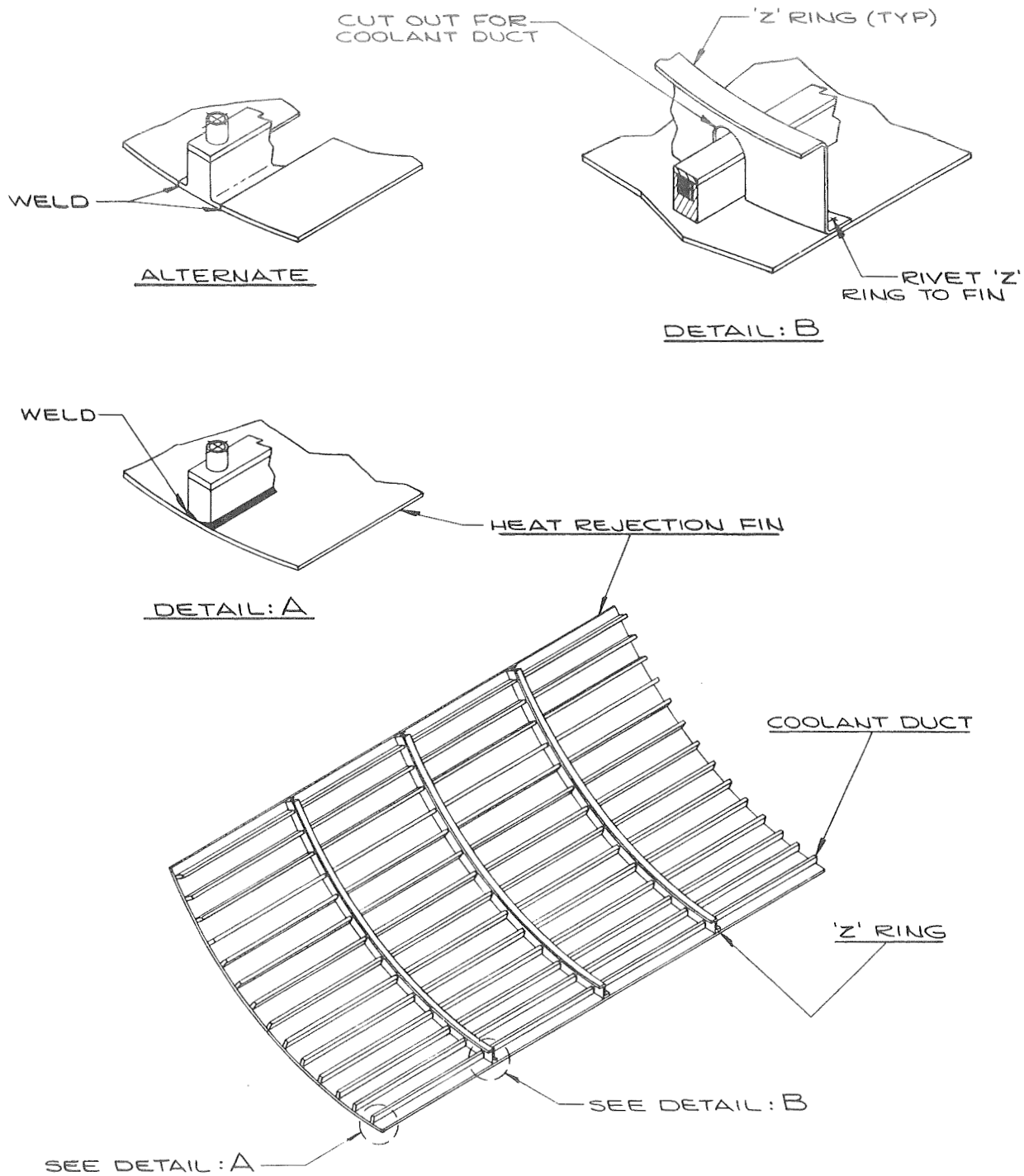
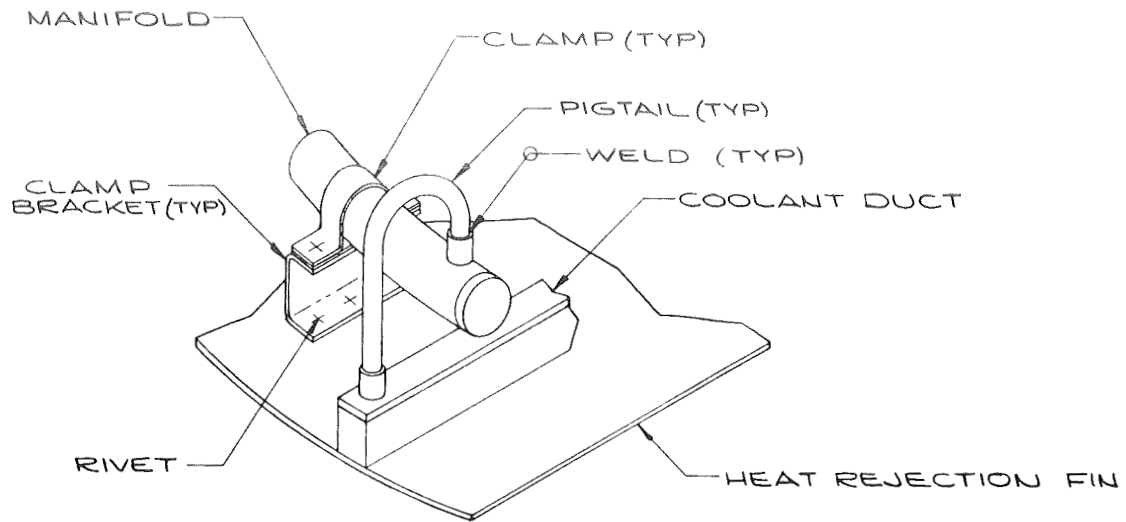


Figure 5-54. Conduction Fin Radiator Assembly Sequence Step 4





DETAIL: A

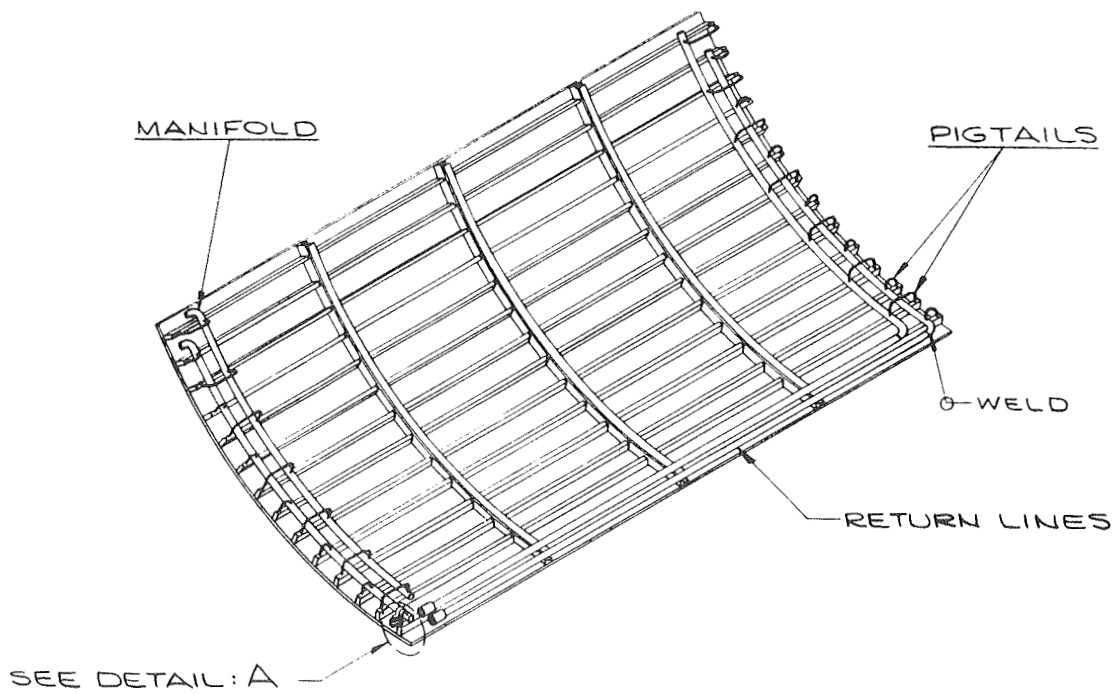


Figure 5-55. Conduction Fin Radiator Assembly Sequence Step 5

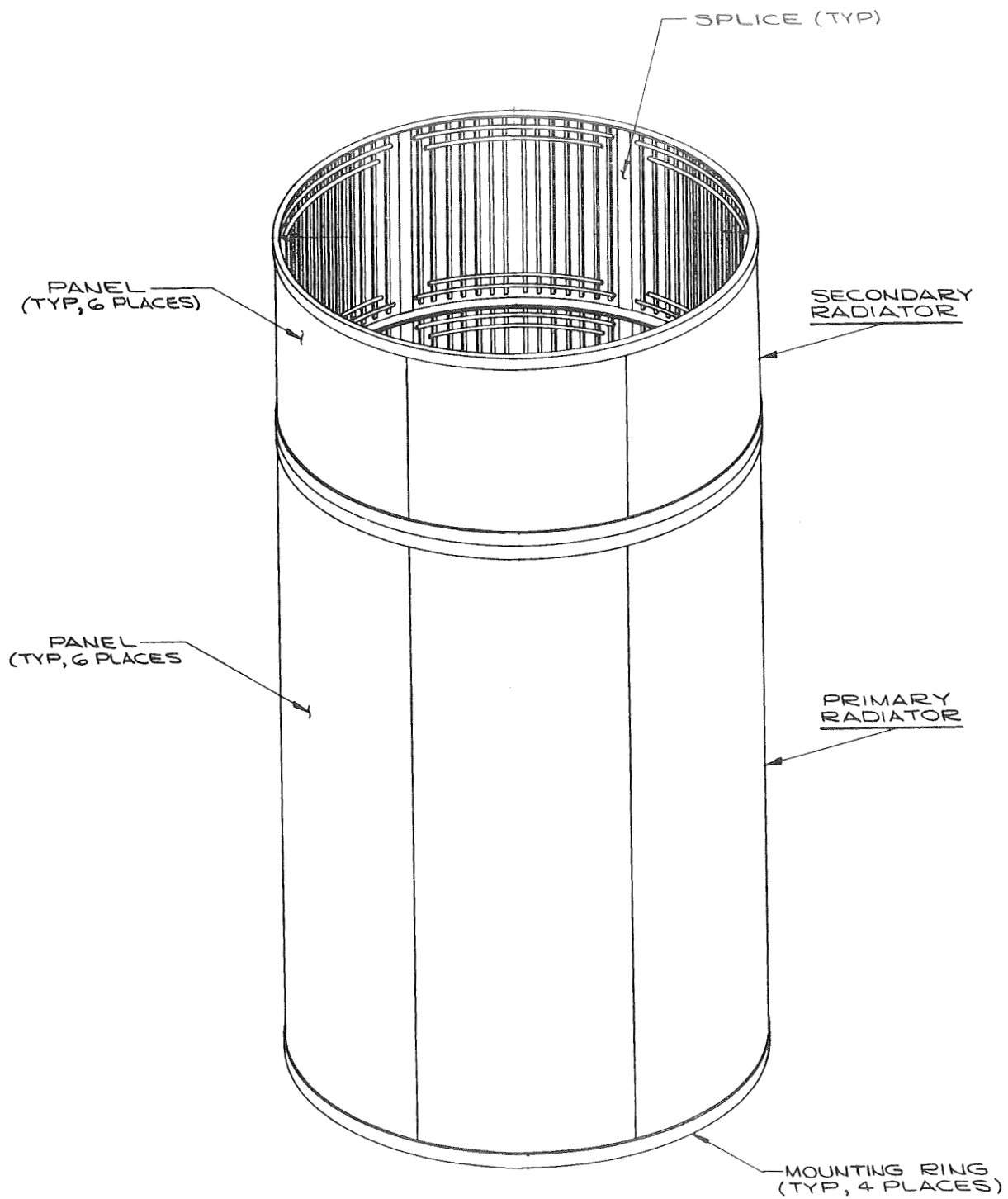


Figure 5-56. Conduction Fin Radiator Assembly Sequence Step 6

TABLE 5-6. RADIATOR WEIGHT SUMMARY (LB)

Survival Probability	Vapor Chamber Fin Radiator*		Conduction Fin Radiator*	
	0.999	0.99	0.999	0.99
Primary Radiator				
DC-200 ducts	89		190	
Internal fins	10.5		---	
Duct bumpers	9.3		---	
DC-200 coolant	8.5		8	
Headers	---		6.1	
Fins	113		311	
Vapor chamber tubes	61		---	
Wicks and coolant	28		---	
Vapor chamber supports	44		---	
Panel splice joints	15.7		14.9	
Interface rings	11.8		20.8	
Stiffening rings	65.8		8.7	
	456.6	455.0	559.5	441.0
Secondary Radiator				
Basic radiator	109		145	
Interface rings	12.8		10.4	
Stiffening rings	23.3		---	
Panel splice joints	5.3		5.0	
	150.4	145.0	160.4	136.0
Total Weight (lb)	607.0	600.0	719.9	577.0
Area, primary	379	377	355	344
secondary	127	127	122	122
Total Area (ft <sup>2</sup> )	506	504	477	466

\*See Table 5-7 for radiator ground rules. (The 0.999 cases were considered to be the baseline radiator design.)

TABLE 5-7. GROUND RULES FOR RADIATOR WEIGHT COMPARISON

Primary heat rejected	12.39 kW <sub>t</sub>
Secondary heat rejected	2.19 kW <sub>t</sub>
Inlet temperature, primary	288° F
Inlet temperature, secondary	118° F
Sink temperature	-10° F
Emissivity	0.85
Meteoroid survival probability (one of two DC-200 loops surviving)	0.999* 0.99
Survival time	5 years
Area penalty	3 lb/ft <sup>2</sup>
Shroud envelope	110 in. dia.
Launch loads:	Correspond to Atlas-Centaur trajectory with 5000 pound mass mounted on top of radiator (6000 pound mass includes radiator)

\*Combined probability for both primary and  
secondary radiators, divided as follows:

Primary:	0.9992	0.992
Secondary:	0.9998	0.998

## SECTION 6

### VAPOR CHAMBER TEST PROGRAM

#### 6.1 GENERAL DISCUSSION

The prime objective of the radiator design study was to identify a promising Brayton cycle vapor chamber radiator. To achieve this objective, it was necessary to design and evaluate representative vapor chamber/fluid configurations for inclusion in the preliminary radiator designs. Working fluid selection and materials compatibility testing was performed as described in Section 4. The Radiator Design is described in Section 5. This section is prepared for the purpose of describing the vapor chamber (heat pipe) test program.

Before a detailed discussion of the test program, a brief discussion of typical vapor chamber operation and significant test parameters is presented.

Consideration of the physical phenomena occurring within a vapor chamber reveals that three internal temperature drops are induced by the energy transfer process: the evaporative temperature drop at the heat input section, the axial temperature drop in the vapor, and the condensing temperature drop. For the fluids and the temperature levels of interest, the static pressure loss in the vapor is small so that the axial vapor temperature drop is negligible. Therefore, only two temperature drops were measured and of these the evaporative  $\Delta T$  was expected to be significantly larger.

Data for pool boiling heat fluxes versus the boiling  $\Delta T$  have been obtained for many fluids including water and various organic liquids. These investigations have shown the dependence of the boiling temperature drop on both the heat flux and absolute temperature level. Rohsenow (Ref. 35) has presented this data for water and Cichelli and Bonilla (Ref. 36) were able to correlate these relationships for many organics with an

empirical expression. In all cases, the  $\Delta T$  showed a logarithmic relationship to the heat flux. It is also true that the boiling  $\Delta T$  was sensitive to the fluid temperature level due to the variation in the equilibrium vapor pressure and density with temperature. Increasing the temperature level results in a decrease in the boiling  $\Delta T$  for the same heat flux; this phenomena is especially magnified at small values of reduced pressure.

The condensing temperature drop arises from the temperature loss across the vapor-liquid interface and from conduction through the condensate film on the walls of the pipe. For the fluids under consideration, the relatively poor thermal conductivities make the latter effect the more significant of the two. The difficulty in analytically predicting the value of the condensing temperature drop becomes one of estimating the liquid film thickness. For the situation in which the condenser walls are lined with a wick the condensate film thickness can be assumed to be equal to that of the wick thickness. In the case of the cruciform wick, the average condensate film thickness in a one-g environment becomes extremely difficult to predict. The low heat fluxes in the condenser section can be expected to yield small  $\Delta T$ 's, as compared to the boiling  $\Delta T$ .

## 6.2 TEST PROGRAM OBJECTIVES

The objectives of this test program were to:

1. Produce single vapor chambers capable of operation in the temperature range of 20 to 350°F using several selected working fluids for various portions of this total range
2. Demonstrate the operation of the vapor chamber for the conditions and geometry defined previously
3. Test these vapor chambers to evaluate internal fluid dynamic and heat transfer performance compatible with performance requirements of the radiator design and predicted analyses by achieving objective 2 above.

Although the main objective of the test was the demonstration of the operation of the vapor chamber for the conditions and geometry defined earlier in the program, a

substantial effort was made to obtain experimental data which would reasonably support the performance predicted by the phenomena described in Section 6.1.

The testing of the single vapor chambers was specifically directed toward determining the following operating characteristics:

1. The evaporative temperature drop  $\Delta T$
2. The condensing temperature drop  $\Delta T_c$
3. Limiting nucleate boiling heat fluxes
4. Vapor temperatures
5. Fluid pumping capabilities

The fluids used in the test program were selected from the results of the "Thermal Testing of Candidate Vapor Chamber Working Fluids" discussed in Section 4.

Ammonia, water, benzene and n-pentane were tested with the cruciform wick design and benzene was again tested with the "C" wick design.

### 6.3 VAPOR CHAMBER TEST CONFIGURATIONS

#### 6.3.1 DESIGN CONSIDERATIONS

The design of the test vapor chambers reflected the knowledge gained in previous parts of this study and was also influenced by the practicalities imposed by instrumentation requirements. The length of the test vapor chamber was determined by the interaction of the radiator with the launch vehicle. A change in radiator design could have resulted in shorter or longer chambers; however, the design chosen was shown to be optimum from thermal and structural considerations. Cylindrical vapor chamber geometry, as opposed to a rectangular cross section, was chosen because of the inherent internal pressure strength advantages of this design.

The vapor chamber diameter has been shown to exert a sizable effect on the radiator weight and area. Decreasing the vapor chamber diameter results in a reduction of vulnerable area to meteoroid penetration with the attendant loss in armor weight. However, insufficient vapor flow area can cause significant frictional pressure drops in the condensing vapor with a reduction in the effective radiating temperature. The parametric analyses described in Section 5.2 showed a vapor chamber inside diameter of 0.300 inch to be optimum from the standpoint of system weight. For the test vapor chamber, this diameter was increased to 0.500 inch in order to facilitate instrumentation procedures.

The design of the test vapor chambers was influenced by a number of additional factors. A low vapor velocity is desirable to avoid refluxing condensate entrainment in the vapor flow. Low vapor velocities also permit simpler, lighter-weight reflux capillary structures (wicks). A criterion used is the Weber number which is based on liquid phase surface tension,  $\sigma$ , reflux capillary characteristic dimension,  $d$ , vapor velocity,  $V$ , and vapor density,  $\rho_v$ . The expression obtained is

$$N_{We} = \frac{d \rho_v V^2}{\sigma g_c} \quad (6-1)$$

If this parameter is less than one, the vapor flow dynamic entrainment forces in the reflux flow are less than the surface tension forces.

Liquid refluxing must occur in sufficient quantities to continue vaporization of the condensate at the evaporator (heat input) end of the vapor chamber. Insufficient refluxing will cause thermal runaway and eventual burnout of the heated wick. Design factors aiding the refluxing process and likewise the heat pipe operation can be inferred by an analysis of the fluid pumping equations. These relations have been presented in Section 4.



### 6.3.2 VAPOR CHAMBER DESIGN

Vapor chambers of two different design configurations were selected for the test program. Both designs were based on the same tube diameter and length dimensions as shown in Figure 6-1. The differences were in the wick design. Vapor chamber Design No. 1 employed a cruciform refluxing wick (Figure 6-1) and chamber Design No. 2 a "C" wick (Figure 6-2). Tube material in all cases was 6061 aluminum except for the chamber where water was employed as the working fluid. A copper tube was used in this case. Tube end closures were 3003 aluminum with the exception of the water heat pipe, which used 304 stainless steel. Wicks were fabricated from aluminum with stainless steel wire cloth for the water chamber.

The designs selected do not necessarily represent the optimum chamber/wick configuration insofar as wick design, chamber size, material choices or performance are concerned. They are, however, selections of proven capability, and considered representative of the types of chambers that would be used for space radiators operating in the low temperature regime.

#### 6.3.2.1 Cruciform Wick Design

The cruciform wick design incorporates a five-layer 130 x 130 mesh aluminum cruciform refluxing wick and a three-layer cylindrical evaporative wick fitting tightly between the heated portion of the tube wall and the four legs of the refluxing wick (Figure 6-1).

The advantages of this design are:

1. It leaves a high percentage of the wall area available for direct condensing heat transfer through the thin film of liquid formed on the wall.
2. It exploits the axially short multiple layered ring evaporative wick which has proven to have very good vaporizing performance.

The effective spacing between the layers of refluxing wick is approximately 10 mils.

#### 6.3.2.2 "C" Wick Design

The "C" wick design is a conventional 150 x 150 mesh stainless steel cylindrical wick of 20 layers fitting against the tube wall along the entire tube length. An axial gap occurs in this wick along the entire length over approximately 3/16 in. of the tube periphery as shown in Figure 6-2. This gap is intended to facilitate access of the vapor to a portion of the cooled wall and eliminate the necessity for transferring all the rejected heat through the twenty layers of wick. With minimum inventory the film of condensate covering the wall area of this gap is, at the gap center, quite thin. The average effective interlayer spacing of the "C" wick is approximately 0.003 inch. The "C" wick design requires no reflux flow transition between refluxing and evaporative sections because the wick is common throughout the length of the tube. Better refluxing characteristics can be expected.

### 6.4 TEST PROGRAM

#### 6.4.1 TEST SET-UP

The test loop as configured for each vapor chamber test is shown schematically in Figure 6-3. An actual photograph of the test set-up in operation is shown in Figure 6-4.

The vapor chamber is mounted within a heat exchanger through which is flowed Coolanol 15 heat transfer fluid. A second heat exchanger is included in the loop which is used for removing heat from the Coolanol. The second heat exchanger is connected to a shop air line and also to a liquid nitrogen dewar, so that either air or cold nitrogen can be used as a coolant. All flow tubing with the exception of the portion of the loop between inlet  $T_{CI}$  and outlet  $T_{CO}$  thermocouples is wrapped with heating cable and is lagged with insulation. As much as 50 watts of power can be applied to the evaporator section of the vapor chamber by a copper heater block with embedded cartridge heaters. The heater is designed to split into two halves that are clamped around the evaporator section.

[illegible]

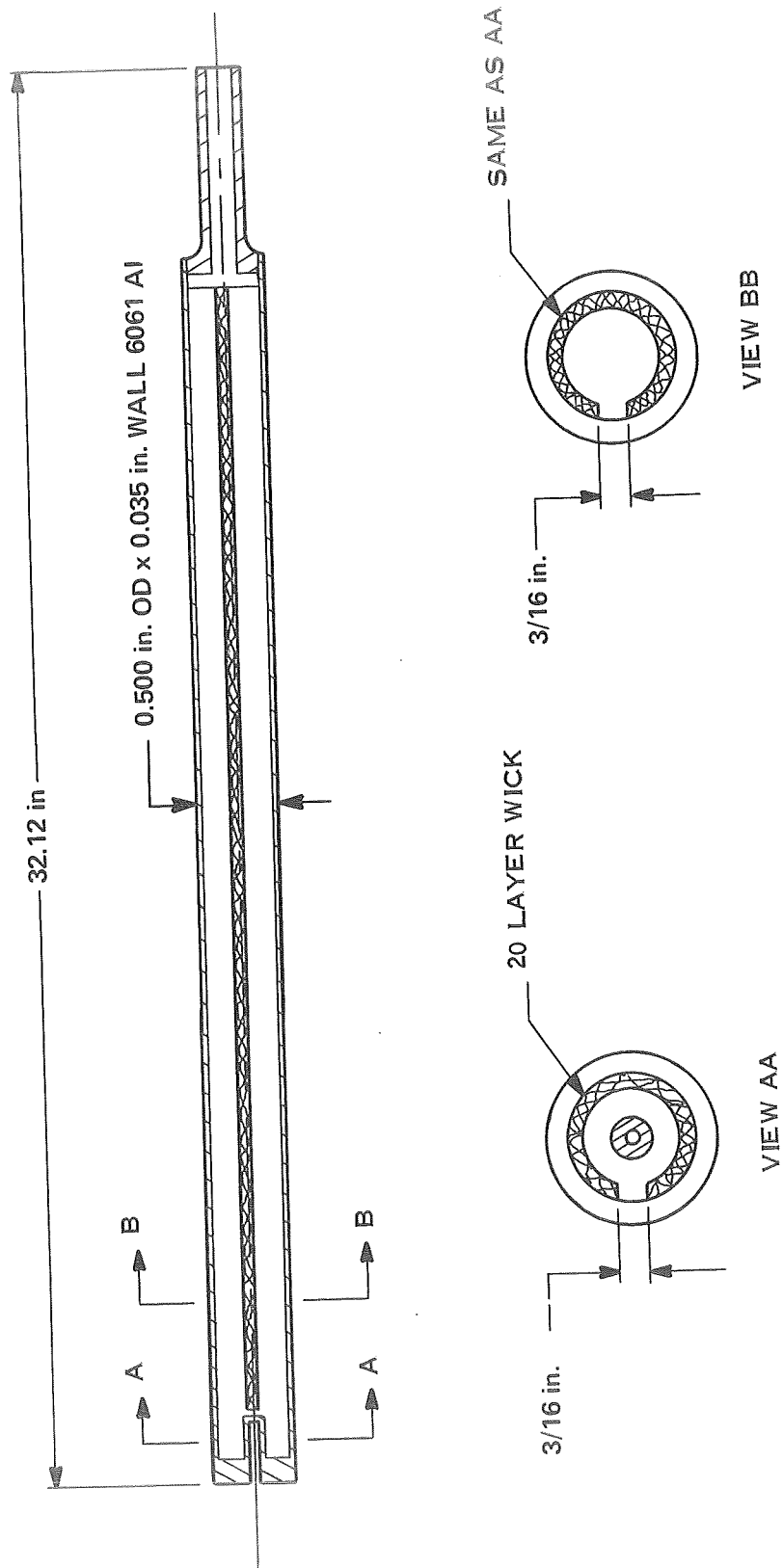


Figure 6-2. "C" Wick Design Vapor Chamber

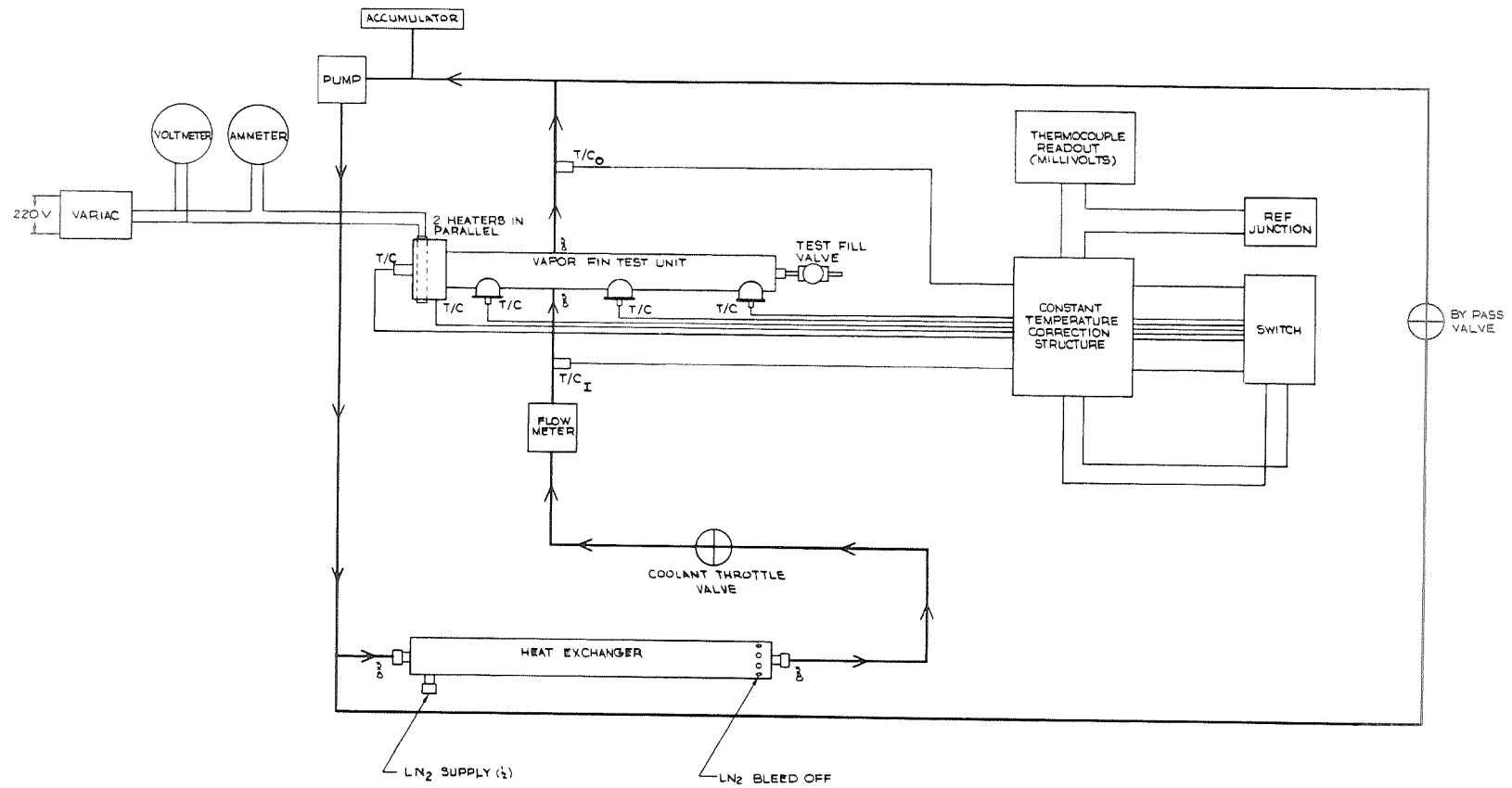


Figure 6-3. Flow Schematic Vapor Chamber Test Unit Brayton Cycle Radiator

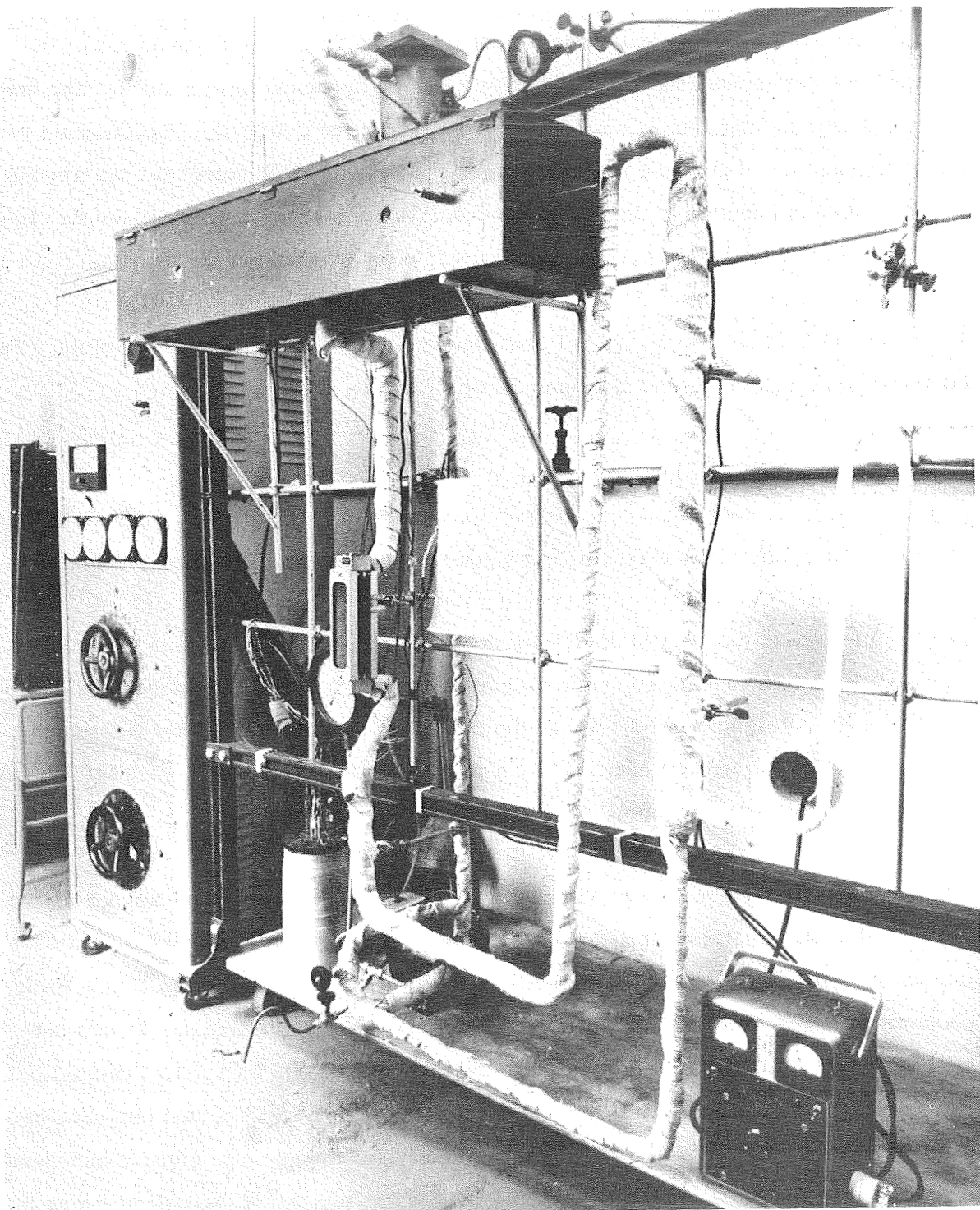


Figure 6-4. View of Test Loop

Figure 6-5 shows the test vapor chamber installed in the heat exchanger with the heater clamped at the evaporation end. The disassembled heat exchanger unit is shown in Figure 6-6 together with the vapor chamber sealing glands and heater block. The heat exchanger and sealing glands serves as a manifold for the Coolanol. The Coolanol is forced through the series of holes into the inner chamber which completely surrounds the heat rejection section of the vapor chamber. After passing over the chamber, the Coolanol exits through another series of holes into the exit side of the loop.

The complete heat exchanger, heater and vapor chamber assembly were carefully insulated and contained inside the steel box shown in Figure 6-4.

#### 6.4.2 INSTRUMENTATION

The test loop instrumentation consisted of a rotameter type flowmeter, various thermocouples, a wattmeter for measuring input power, and data recording equipment.

The flowmeter was inserted in the Coolanol line to measure coolant flow. Flow immersed sheath type thermocouples were inserted in the vapor chamber test unit inlet and outlet flow streams. Flow through the flowmeter was measured as a function of temperature and percent reading. The percent reading directly related to heat transfer capability of the coolant for a specified flow and inlet temperature.

A sheath-type thermocouple was clamped in a notch between the vapor chamber and one of the heater block halves. It measured the temperature of the heater/vapor chamber interface. Three thermocouples were attached to the vapor chamber itself with leads projecting through the two access flanges shown in Figure 6-5 (Part No. 11 was not used and the thermocouple was attached to the tube wall at this location). This latter thermocouple was used to measure the chamber vapor temperature, and was used in place of a thermocouple in the well shown in the evaporator end tube closure in Figure 6-5. The thermocouple location was changed as it was found that the well wall was in better thermal contact with the heater block than with the vapor so the vapor temperature

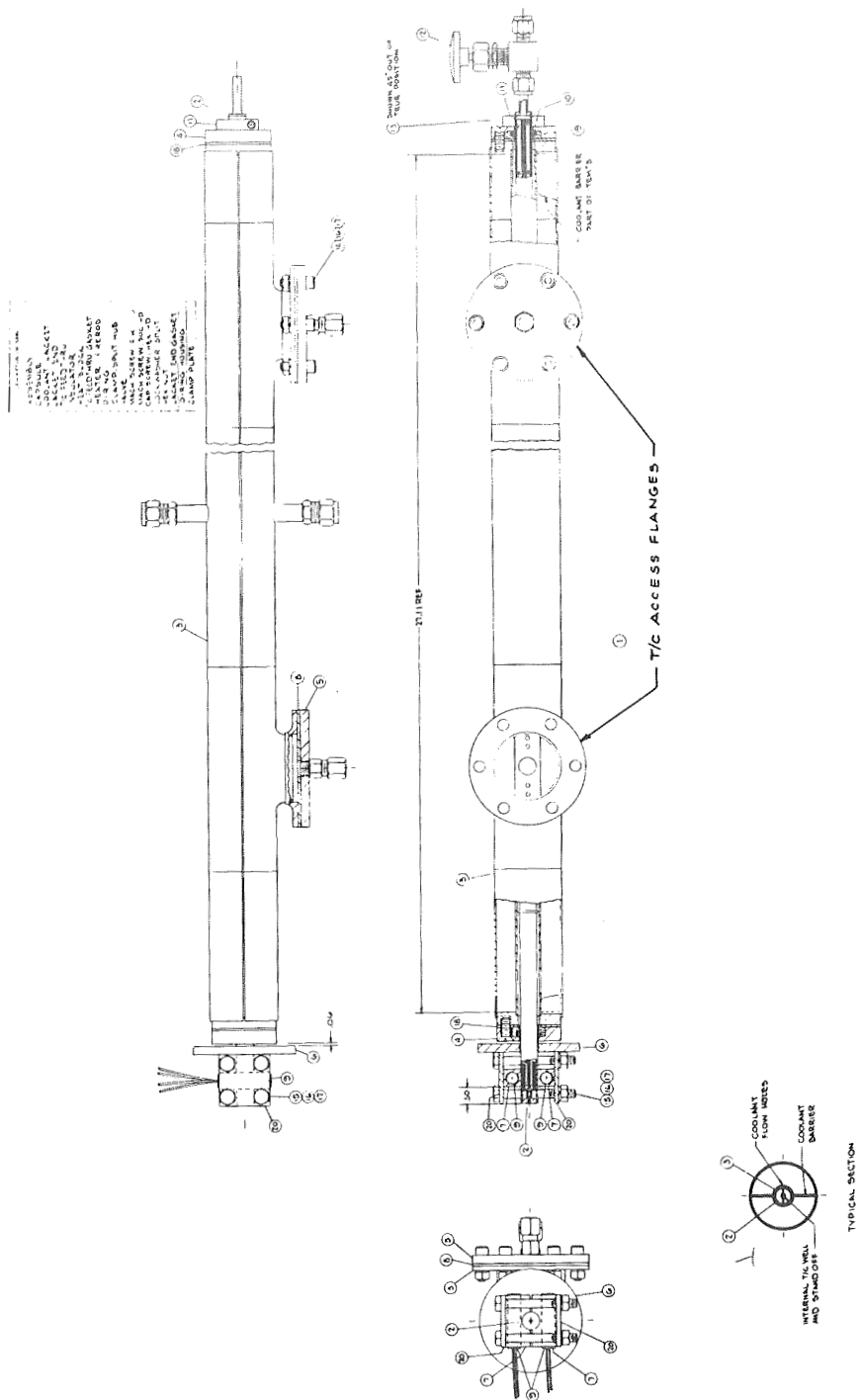


Figure 6-5. Heat Exchanger Assembly  
Vapor Chamber Test Unit Brayton  
Cycle Radiator



Figure 6-6. Disassembled Heat Exchanger and Heat Pipe

was obtained from the insulated portion of the chamber wall beyond the end of the heat exchanger.

The two thermocouples opposite the access flanges (Figure 6-5) measured the vapor chamber cooled wall temperature. All thermocouples were chromel-alumel type and were carefully calibrated over the operating range. This was accomplished by use of an oil bath and a mercury thermometer accurate to  $0.5^{\circ}\text{F}$ . Attachment of the vapor temperature and cooled wall temperature thermocouples to the chamber wall was accomplished by use of epoxy because no reliable procedure for spot-welding chromel-alumel thermocouple wire to aluminum was found.

#### 6.4.3 TEST PROCEDURE

Performance tests were made with each working fluid (ammonia, water, benzene, n-pentane) utilizing the cruciform wick design in a horizontal and tilted position. Only benzene was tested with the "C" wick. Fluid inventory of the vapor chambers tested was as follows:

Cruciform Wick Design		"C" Wick Design	
Ammonia	25 cc	Benzene	35 cc
Water	28 cc		
Benzene	35 cc		
n-Pentane	35 cc		

Heat input power to the cruciform wick vapor chambers was applied at three levels: 12.5 watts, 25 watts and 50 watts. These settings correspond to an input heat flux of 9200, 18,400 and 36,800 Btu/hr-ft<sup>2</sup>, respectively.

Heat losses could occur in several locations, such as the heat lost from:

1. The heater directly to the insulation, steel case and ambient air
2. The vapor chamber to the heat exchanger shell

3. From the Coolanol fluid through the flow tubing before arriving at the thermocouple junctions.

A determination of heat loss was made by measuring inlet to outlet  $\Delta T$  at a stable operating point where the Coolanol temperature was maintained essentially constant with no heat input from the heater to the vapor chamber. A series of tests at input power levels of 0, 12.5, 25 and 50 watts were made at a nearly constant average Coolanol temperature. For these various power levels at these conditions the losses remained substantially constant. Output power computation including losses, measuring the product of Coolanol flow rate, inlet to outlet  $\Delta T$ , density and specific heat, was usually within one watt of the input power. A conclusion to be made is that losses direct from the heater block to the ambient air were apparently very small compared to the losses from the heat exchanger shell.

Vapor chamber performance tests in the horizontal position were completed before tilting. The sequence in the horizontal position included initial testing at a power level of 12.5 watts operating at a selected low vapor temperature by adjustment of the Coolanol inlet temperature. After stabilization and taking of measurements, the inlet temperature was adjusted to increase the vapor temperature in several steps over the range specified for testing and within the limits of the test hardware. The test program was designed to evaluate performance of ammonia vapor chambers with vapor temperatures as high as 150<sup>o</sup>F. The vapor temperature range for the other fluids was limited from 150 to 300<sup>o</sup>F. Increases in power level were made after the range of vapor temperatures were achieved for the previous power level setting.

Stabilization of Coolanol inlet and outlet temperatures required at least an hour for each setting because of the low flow rate and the large quantity of heat stored in the heat exchanger as compared to the heat input rate. Vapor chamber heat transfer  $\Delta T$ 's (heater block temperature minus vapor temperature, and vapor temperature minus cooled wall temperature) stabilized much more rapidly than did Coolanol temperatures.

The only change in procedure for the benzene "C" wick configuration involved the limitation of input power levels due to heat transfer burnout of the heated wick at approximately  $18,000 \text{ Btu/hr-ft}^2$  with the fixed size heater block. Accordingly, input power levels of 12.5, 18.75 and 25 watts were used for this vapor chamber test.

Following testing in the horizontal (level) position the vapor chambers were tilted (evaporator end high) by one diameter ( $1/2$  inch), Figure 6-7. The primary purpose of these tests was to evaluate the pumping (refluxing) capability in an environment that more closely approximates zero g.

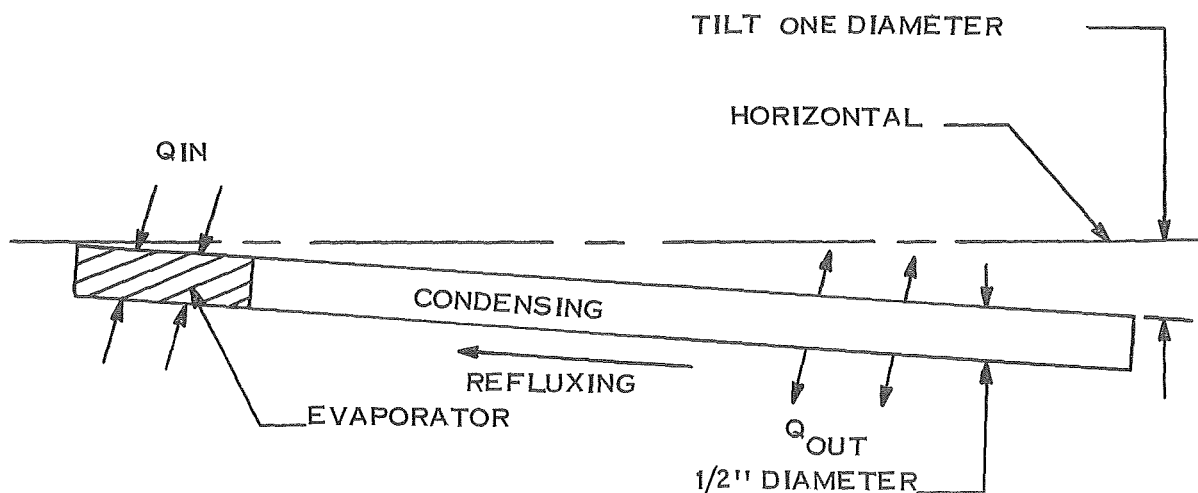


Figure 6-7. Vapor Chamber Tilted Position

For test purposes, it was assumed that good refluxing of the fluid in the chamber at normal operating power levels when tilted one diameter is reasonable evidence of potential zero g operability. The procedures used in the tilted tests usually involved the application of heater power at 25 or 50 watts for a duration sufficient to monitor and determine the heater block and vapor temperature. In cases which burnout of the evaporator wick occurred (the heater block temperature rose with no change in the vapor temperature), lower power levels were used and/or the chamber tilt was lessened

until performance became normal. These tests were followed by a determination of minimum fluid inventory levels. Vapor was incrementally bled off from the tube until heater block temperature increased uncontrollably. Inventory was then determined by weighing.

## 6.5 TEST RESULTS

### 6.5.1 TEST DATA

The successful transfer of energy from the heater block to the Coolanol demonstrated the feasibility of the low temperature vapor chamber Brayton cycle radiator concept. In particular, ammonia and water were shown to possess excellent capillary pumping capabilities. Although n-pentane and benzene exhibited marginal pumping capabilities, it seems reasonable to conclude from the analytical predictions (refer to Section 4) that these fluids could provide acceptable refluxing capability. This might be achieved by different wick geometries and/or materials. A partial substantiation of this idea was provided by the test of the "C" wick with benzene. Better anti-gravity refluxing than the cruciform design was demonstrated during the test.

Tables 6-1, 6-2 and 6-3 present the total reduced data taken during the test period. The evaporative and condensing heat flux values given are based on the input power and the tube inside wall area of the evaporative and condensing sections of the vapor chamber. This practice was followed after verifying that there were minimum losses of heat from the heater block as there was a close check (within 1.5 watts in all cases) between input power and output power, where output power was a product of Coolanol flow characteristics. The condensing  $\Delta T$  is based on the average differences between the vapor temperature and the temperature of the cooled tube wall as measured by the two tube wall thermocouples. The evaporative  $\Delta T$  is based on the difference between the temperature of the thermocouple wedged between the heater block and the tube, and the thermocouple on the insulated tube wall outside the cooled section of the vapor chamber.

TABLE 6-1. STANDARD INVENTORY LEVEL POSITION DATA  
CRUCIFORM WICK HEAT PIPES

	Vapor Temp. °F	Power (Watts)	Evaporative Heat Flux Btu/hr/ft <sup>2</sup>	Conductive Heat Flux Btu/hr/ft <sup>2</sup>	T <sub>wall</sub> -T <sub>vapor</sub> Evaporative $\Delta T_v$ (°F)	T <sub>vapor</sub> -T <sub>wall</sub> Condensing $\Delta T_c$ (°F)	Over- all $\Delta T_t$	Inventory (cc)
WATER	157.5	12.5	9200	174	10.1	0.3	10.4	28 ↓
	163	25.0	18,400	348	13.9	0.6	14.5	
	174	50.0	36,800	696	22.0	1.2	23.2	
	200.5	12.5	9200	174	9.7	0.3	10.0	
	204.3	25.0	18,400	348	12.2	0.6	12.8	
	214.3	50.0	36,800	696	20.4	1.2	21.6	
	230.7	12.5	9200	174	9.3	0.3	9.6	
	238.6	25.0	18,400	348	11.9	0.7	12.6	
	246.0	50.0	36,800	696	19.8	1.2	21.0	
	274.2	12.5	9200	174	9.2	0.3	9.5	
	280.7	25.0	18,400	348	12.3	0.6	12.9	
	295.0	50.0	36,800	696	20.5	1.3	21.8	
AMMONIA	53.5	12.5	9200	174	8.4	0.5	8.9	25 ↓
	58.2	25.0	18,400	348	10.2	1.1	11.3	
	68.4	50.0	36,800	696	15.7	2.5	18.2	
	97.2	12.5	9200	174	7.8	0.6	8.4	
	103.3	25.0	18,400	348	9.1	1.2	10.3	
	93.5	50.0	36,800	696	15.5	2.5	18.0	
	132.0	12.5	9200	174	7.5	0.5	8.0	
	140.1	25.0	18,400	348	8.5	1.2	9.7	
	144.6	50.0	36,800	696	13.5	2.4	15.9	
BENZENE	155.8	12.5	9200	174	14.0	1.5	15.5	35 ↓
	164.4	25.0	18,400	348	20.1	2.9	23.0	
	178.3	50.0	36,800	696	27.2	5.6	32.8	
	230.7	12.5	9200	174	13.8	1.4	15.2	
	237.6	25.0	18,400	348	19.4	2.9	22.3	
	251.0	50.0	36,800	696	23.1	5.6	29.7	
	227.0	12.5	9200	174	14.9	1.4	15.5	
	215.5	25.0	18,400	348	19.3	2.8	22.1	
	232.8	50.0	36,800	696	24.0	5.7	29.7	
	272.9	12.5	9200	174	14.0	1.4	15.4	
	282.1	25.0	18,400	348	19.0	2.9	21.9	
	286.7	50.0	36,800	696	24.0	5.7	29.7	
n- PENTANE	144.0	12.5	9200	174	9.0	1.4	10.4	35 ↓
	150.3	25.0	18,400	348	13.1	2.7	15.8	
	165.2	50.0	36,800	696	19.0	5.5	24.5	
	189.1	12.5	9200	174	9.4	1.4	10.8	
	198.4	25.0	18,400	348	12.1	2.9	15.0	
	210.5	50.0	36,800	696	17.1	5.7	22.8	
	233.2	12.5	9200	174	8.8	1.4	10.2	
	240.6	25.0	18,400	348	12.1	2.7	14.8	
	255.2	50.0	36,800	696	17.6	5.5	23.1	
	269.6	12.5	9200	174	9.0	1.4	10.4	
	278.5	25.0	18,400	348	12.1	2.8	14.9	
	293.0	50.0	36,800	696	21.0	5.5	26.5	

TABLE 6-2. TILTED, REDUCED INVENTORY OPERATING POINTS CRUCIFORM WICK

	*Inventory Level (cc)	Amount of Tilt (Inches)	Power (Watts)	Vapor Temp. (°F)	$\Delta T_v$ $T_{wall} - T_{vapor}$ Evaporative T (°F)	$\Delta T_c$ $T_{vapor} - T_{wall}$ Condensing T (°F)	Over-all $\Delta T_t$	REMARKS
WATER	14.1 14.1	1/2 1/2	25 50	245 251.9	16.0 27.3	0.5 1.3	16.5 28.6	50 watts input power was applied, and measured data indicated no change in overall performance from level operation. The results demonstrated capability for operation in zero g.
AMMONIA	15	1/2	25	113	11.5	1.0	12.5	25 watts input power was applied, and measured data indicated no change in overall performance from level operation. Results give evidence of good operability with minimum inventory in zero g. Minimum inventory 10.2cc
BENZENE	22	1/4	50	250	28	5.5	33.5	Thermal runaway at 25 & 50 watts in $\frac{1}{2}^\circ$ tilt. 50 watt $\frac{1}{4}^\circ$ tilt operation successful. Zero g operability inclusive. Minimum operating inventory was 20.1 cc
n-PENTANE	23	1/4	27	249	15.0	2.6	17.6	Thermal runaway at 25 & 50 watts in $\frac{1}{2}^\circ$ tilt. 30 watts at $\frac{1}{2}^\circ$ tilt appeared to be limit. Zero g operability inclusive minimum operating inventory was 20.6 cc

\*Wick Saturation Level - 15 cc

TABLE 6-3. BENZENE "C" WICK CONFIGURATION HEAT PIPE PERFORMANCE  
(TILTED 1/2 INCH, 30 cc INVENTORY)

Vapor Temp. (°F)	Power (Watts)	Evaporative Heat Flux (Btu/hr-ft <sup>2</sup> )	Conductive Heat Flux (Btu/hr-ft <sup>2</sup> )	$\Delta T_v$ (°F)	$\Delta T_c$ (°F)	Over-all $\Delta T_t$	REMARKS
148.8	12.5	9200	1000	22.5	4.2	26.7	<p>Operation at 25 watts was only possible with vapor temperature of nearly 300°F</p> <p>Limiting factor appeared to be thermal burnout of evaporative wick as tilt did not effect the limiting value.</p> <p>Minimum inventory was 30 cc and is approximately saturation level</p> <p>"C" wick demonstrated good anti-gravity refluxing performance at 25 watts.</p>
151.8	18.75	13,800	1500	84.9	6.7	91.6	
297.9	12.5	9200	1000	18.4	4.1	22.5	
300.5	18.75	13,800	1500	31.3	6.5	37.8	
299.3	25	18,400	2000	102.5	8.0	110.5	



The evaporative temperature drops recorded at the vapor chamber input section were lower than those predicted by the Cichelli and Bonilla correlation. These unexpected results could not be explained by the boiling mechanisms described in the literature for pool boiling. Although it is possible that the presence of the wick is improving the evaporative heat transfer, no plausible mechanism has been advanced to support this explanation. In addition to the deviation from the expected results, the test data did not show the sensitivity of the  $\Delta T$  with the absolute temperature level. A comparison of the experimental data with the correlation of Cichelli and Bonilla for organic fluids and with Rhosenow's data for water is shown in Figures 6-8 through 6-11.

The fact that the evaporator  $\Delta T$ 's were very small indicates that nucleate boiling was present to some degree. Conduction through the evaporator liquid with evaporative mass transfer would have imposed  $\Delta T$ 's an order of magnitude greater than that experienced due to poor fluid thermal conductivities. However, a substantial portion of the evaporator apparently did not experience nucleate boiling as "burn out" did not occur even in the tilted operating position. This implies the existence of capillary forces which would not be present if the only mass transfer mechanism were boiling. Therefore, the mass transfer phenomena occurring in the evaporator was judged to be a combination of nucleate boiling and evaporation.

The data obtained for the condensing temperature drop is shown in Figure 6-12 for the cruciform wick. As previously stated, this temperature drop is caused primarily by conduction through the condensate film.

Using the Fourier conduction equation, which is accurate as long as the film thickness is small, the condensate film thickness is equal to:

$$X_{\text{FILM}} = \frac{k \Delta T}{(q/A)} \quad (6-12)$$

where  $k$  is the effective thermal conductivity of capillary structure and  $q/A$  is the heat flux.

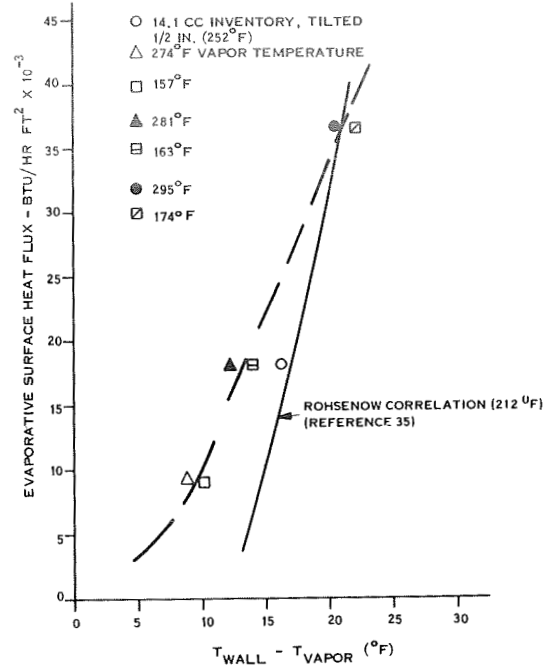


Figure 6-8. Water Heat Pipe (Cruciform Wick Configuration)  
Thermal Flux Versus Evaporative  $\Delta T$

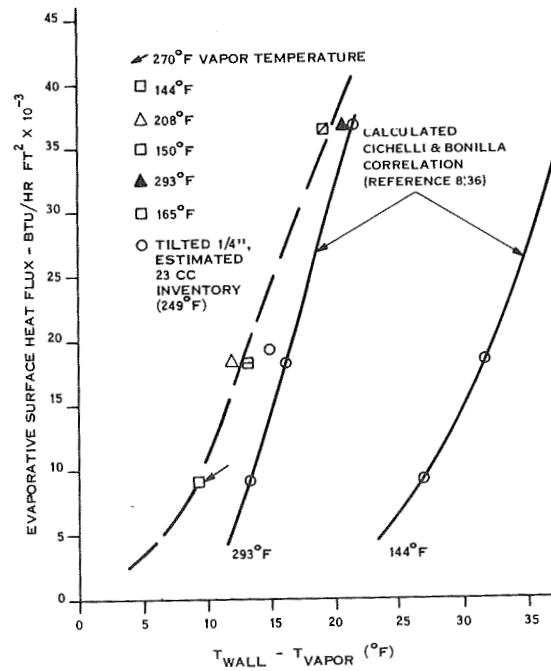
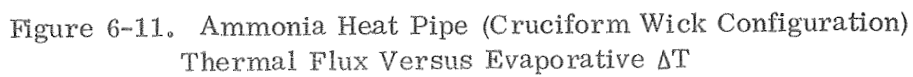
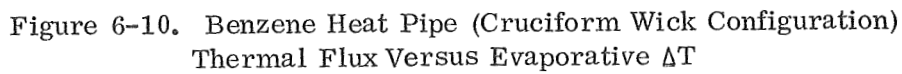


Figure 6-9. n-Pentane Heat Pipe (Cruciform Wick Configuration)  
Thermal Flux Versus Evaporative  $\Delta T$



The results obtained are shown in Table 6-4 below.

TABLE 6-4. CONDENSATE FILM THICKNESS

<div style="display: flex; align-items: center; justify-content: center;"> <div style="transform: rotate(-45deg); transform-origin: center;">Fluid</div> <div style="text-align: center;">           Condensing Flux, Btu/hr-ft<sup>2</sup> </div> </div>		Film Thickness, in.		
		700	500	200
H <sub>2</sub> O		0.00802	0.00786	0.00819
NH <sub>3</sub>		0.00943	0.00986	0.00793
C <sub>6</sub> H <sub>6</sub>		0.00783	0.00788	0.00817
n-C <sub>5</sub> H <sub>12</sub>		0.00660	0.00655	0.00672

Figure 6-13 shows the overall  $\Delta T$  versus the evaporative heat flux for the benzene "C" wick configuration.

#### 6.5.2 TEST ACCURACY

The source of the discrepancies observed between the test data and the data found in the literature cannot be determined precisely. The most likely explanation for the disparities would appear to be in the readings of the thermocouples at the heat input section and in the vapor space. The two thermocouples attached to the condenser wall showed good agreement. The reasonable and consistent data obtained for the condensing  $\Delta T$  infers that the vapor temperature measurement is fairly accurate; errors of several degrees in this measurement still could not explain the evaporative  $\Delta T$  discrepancies without contradicting the results for the condensing  $\Delta T$ 's. Poor thermocouple contact at the heat input section would explain the difference between the test data and the data cited in the literature. Insulation heat losses may also be a contributor.

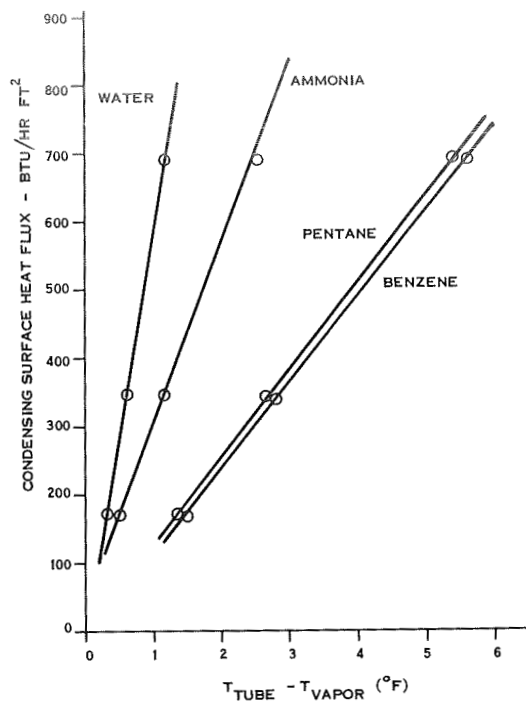


Figure 6-12. Test Data (Cruciform Wick Configuration)  
Condensing Heat Flux Versus Condensing  $\Delta T$

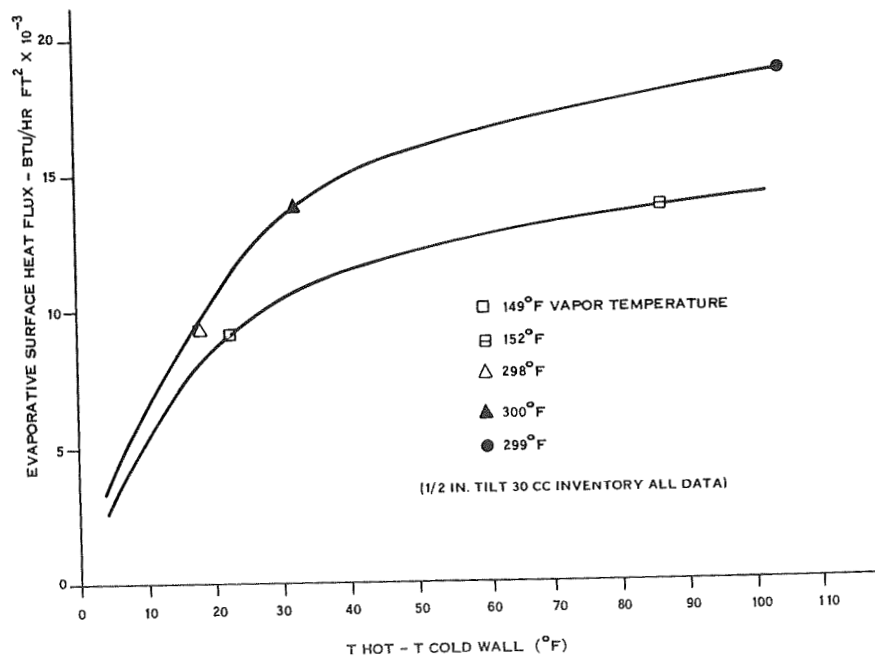


Figure 6-13. Benzene Heat Pipe ('C' Wick Configuration)  
Thermal Flux Versus Overall  $\Delta T$

## 6.6 TEST CONCLUSIONS

The following conclusions presented are primarily based upon an evaluation of the objectives as defined in Subsection 6.2.

1. All working fluids tested exhibited satisfactory performance in the level position with the cruciform wick vapor chamber as identified in Figure 6-1.
2. The "C" wick vapor chamber, Figure 6-2, operated satisfactorily. Its heat transfer performance is not expected to be as good as the cruciform wick in the level position due to the somewhat higher condensing  $\Delta T$ 's through the liquid/wick layer on the tube wall.
3. The "C" wick vapor chamber exhibited better refluxing capability than the cruciform wick in the tilted position.
4. The cruciform wick vapor chamber exhibited questionable zero g performance with n-pentane and benzene working fluids. This observation indicates that the cruciform wick presents a higher flow resistance path than the "C" wick design. Since n-pentane and benzene possess only marginal pumping capability, these fluids were affected significantly by the cruciform design. An implication of this result is the possibility that the space between the smooth pipe wall and first wick layer (not present in the cruciform design) provides a low resistance return flow path.
5. Ammonia and water exhibited the lowest overall  $\Delta T$  and are expected to offer the best heat transfer performance. The comparatively high thermal conductivities of water and ammonia are responsible for this result. n-Pentane's test performance was good except for inconclusive zero "g" operability.
6. Better instrumentation, in particular vapor temperature, is required to accurately determine  $\Delta T_C$  and  $\Delta T_V$ . Insulation heat losses are difficult to accurately measure.
7. Temperatures obtained at the evaporator were probably somewhat inaccurate due to somewhat poor thermal contact.
8. Ammonia is a good working fluid for operating temperatures up to 150°F and showed good compatibility with aluminum.
9. Configurations considered for the flight or test systems should not be limited to the cruciform or "C" wick designs. The "C" wick design could be incorporated with a different evaporator configuration.

## SECTION 7

### VAPOR CHAMBER RADIATOR EVALUATION AND CONCLUSIONS

#### 7.1 GENERAL

The purpose of this program was to identify a promising Brayton Cycle Vapor Chamber Radiator capable of operating in a zero gravity environment. The design derived from the study was then to be evaluated with a comparable conduction fin radiator to determine whether significant performance advantages could be obtained.

Detailed results of the evaluation of fluids, materials, radiator design and performance are contained in Sections 4, 5 and 6. This section contains a summary of the evaluations and conclusions to be made.

#### 7.2 EVALUATION CRITERIA SUMMARY

Selecting the operating working fluids for the range of temperatures from 20<sup>o</sup> to 350<sup>o</sup>F involved a number of evaluation criteria. The key parameters of interest are:

1. Fluid Performance
  - a. Evaporative  $\Delta T$
  - b. Condensing  $\Delta T$
  - c. Zero g and one g refluxing capability
  - d. Moderate Vapor Pressures
  - e. Thermal stability and operation over prescribed temperature ranges and heat fluxes of primary and secondary radiators.
2. Compatibility with aluminum

The radiator design comparison evaluation criteria is comprised primarily of the following:

1. Radiator weight and area
  - a. Thermal efficiency
  - b. Meteoroid survival probability
  - c. Structural capability
  - d. System pumping power penalty
2. Fabrication
  - a. Complexity
  - b. Degree of difficulty
  - c. State-of-art

### 7.3 EVALUATION SUMMARY

The evaluation of the candidate working fluids for compatibility with aluminum resulted in the following selections:

#### GOOD COMPATIBILITY

Ammonia  
Benzene  
Propane  
n-Butane  
n-Pentane  
n-Heptane  
n-Nonane  
Freon 11, 113  
Toluene

#### INCOMPATIBILITY

Water  
Alcohols  
Pyridine (CP-32)  
CP-34

Material compatibility was considered an essential requirement and thus fluids judged incompatible with aluminum were eliminated from final consideration.



An evaluation of fluid thermal performance characteristics independent of material incompatibility provided the following fluid selection (Table 7-1).

TABLE 7-1. FLUID SELECTION

High Temperature Operation (100 to 350°F)			
Choice	Fluid	Overall Performance Parameter	Comments
First	Water	Very good at higher temperature	Incompatible with A1
Second	n-Butane	Good over desired temperature range	Inadequate refluxing
Third	n-Pentane	Fair to good (somewhat better than benzene)	Marginal refluxing
Fourth	Benzene	Fair to good	Satisfactory refluxing
Low Temperature Operation (20 to 150°F)			
Choice	Fluid	Overall Performance Parameter	Comments
First	Ammonia	Very good by a substantial margin	
Second	Water	Fair (Good Refluxing)	Incompatible with A1
Third	Freons	Fair	

The final selections made, considering all the criteria, indicated that a use of n-pentane is most desirable for the high temperature regions of the primary radiator. Ammonia was clearly the choice for low temperature sections of both the primary and secondary radiators. Although water exhibited excellent performance over a wide range of operating temperatures, it could not be considered due to its known incompatibility with aluminum.

The evaluation of the vapor chamber radiator using the chosen working fluids against the comparable conduction fin radiator provided a number of interesting comparisons. A design point comparison of the two radiators is shown in Tables 7-2 and 7-3. The

two radiators were designed with equivalent materials and overall thermal performance. Therefore the characteristics which afforded a direct comparison were the effect on radiator weight and area when parameters such as survival probability and thermal efficiencies (evaporative  $\Delta T$  and condensing  $\Delta T$ ) were varied.

The vapor chamber radiator was noticeably sensitive to two parameters:

1. Evaporative  $\Delta T$
2. Condensing  $\Delta T$

The vapor chamber radiator is 12% lighter than the equivalent conduction fin radiator with a survival probability of 0.999, but proved to be 14% heavier at a probability of 0.99. The apparent crossover point is at 0.998. The insensitivity of the vapor chamber radiator to the changes in meteoroid survival requirements is due to the redundancy afforded by the large number of chambers and the fact that the primary fluid is concentrated in a few ducts. The conduction fin radiator, however, presents a significantly larger amount of vulnerable duct area since the fluid is constrained to flow in many small tubes.

The values selected for the evaporative and condensing  $\Delta T$ 's as discussed in Section 5.2.1 were derived using the Cichelli and Bonilla correlation. The results obtained during the test program indicated a reasonable correlation; however, values could be expected to vary considerably depending on the design of the system. If the evaporative  $\Delta T$  were to increase by 100% which may be a reasonable assumption, a 17% increase in weight and an 18% increase in area could be expected of the vapor chamber radiator. A similar effect is caused by the change in condensing  $\Delta T$  when the film thickness is increased by 100%; the weight is increased 9% while the area increases by 4%.

Most other parameters varied had little effect on the overall weight or area of the radiator.

TABLE 7-2. DESIGN POINT SUMMARY COMPARISON  
(Overall Survival Probability = 0.999)

Design Point Summary of Vapor Chamber Fin Radiator Characteristics			Design Point Summary of Conduction Fin Radiator Characteristics		
	Primary Radiator	Secondary Radiator		Primary Radiator	Secondary Radiator
Requirements			Requirements		
Thermal Heat Rejection, kWt	12.39	2.19	Thermal Heat Rejection, kWt	12.39	2.19
Primary Fluid Temperature Inlet-Outlet, °F	288-64	118-64	Primary Fluid Temperature Inlet-Outlet, °F	288-64	118-64
Background Temperature, °F	-10	-10	Background Temperature, °F	-10	-10
Survival Probability at 5 Years	0.9992	0.9998	Survival Probability at 5 Years	0.9992	0.9998
Design Description			Design Description		
High Temperature Fluid	n-Pentane	None	Radiator Outside Diameter, Ft.	9	9
Low Temperature Fluid	Ammonia	Ammonia	Radiator Length, Ft.	12.4	4.21
Radiator Outside Diameter, Ft.	9	9	Number of Fluid Ducts	42	36
Radiator Length, Ft.	14.0	4.7	Duct Spacing, In.	8.06	9.40
Vapor Chamber Length, In.	26.2	26.2	Fluid Passages Per Duct	10	11
Vapor Chamber I.D., In.	0.280	0.280	Fluid Passage Width, In.	0.010	0.0115
Number of Vapor Chambers	1537	432	Duct Conduction Fin Thickness, In.	0.005	0.0055
Average Vapor Chamber Spacing, In.	1.31	1.57			
Primary Fluid Passage Width, In.	0.013	0.0125			
Primary Duct Conduction Fin Thickness, In.	0.005	0.005			
Performance Data			Performance Data		
Physical Radiator Area, Ft <sup>2</sup>	379	127	Physical Radiator Area, Ft <sup>2</sup>	355	122
Primary Fluid Pressure Drop, PSI	8.88	3.8	Fluid Pressure Drop, PSI	13.7	5.8
Temperature Drops, °F			Temperature Drop, °F		
High Temperature Section	43	-			
Low Temperature Section	15	13			
Weight Tabulation			Weight Tabulation		
Primary Fluid Ducts	117.3	35.2	Fluid Ducts	198.0	42.0
Vapor Chambers	133.0	39.9	Conduction Fins	311.0	98.0
Conduction Fins	113.0	33.9	Headers	6.1	5.0
Panel Splice Joints	15.7	5.3	Panel Splice Joints	14.9	5.0
Interface Rings	11.8	12.8	Interface Rings	20.8	10.4
Stiffening Rings	65.8	23.3	Stiffening Rings	8.7	-
Total, Lb	456.6	150.4	Total, Lb	559.5	160.4

**TABLE 7-3. DESIGN POINT SUMMARY COMPARISON**  
(Overall Survival Probability = 0.99)

Design Point Summary of Vapor Chamber Fin Radiator Characteristics			Design Point Summary of Conduction Fin Radiator Characteristics		
	Primary Radiator	Secondary Radiator		Primary Radiator	Secondary Radiator
Requirements			Requirements		
Thermal Heat Rejection, kWt	12.39	2.19	Thermal Heat Rejection, kWt	12.39	2.19
Primary Fluid Temperature Inlet-Outlet, °F	288-64	118-64	Primary Fluid Temperature Inlet-Outlet, °F	288-64	118-64
Background Temperature, °F	-10	-10	Background Temperature, °F	-10	-10
Survival Probability at 5 Years	0.992	0.998	Survival Probability at 5 Years	0.992	0.998
Design Description			Design Description		
High Temperature Fluid	n-Pentane	None	Radiator Outside Diameter, Ft.	9	9
Low Temperature Fluid	Ammonia	Ammonia	Radiator Length, Ft.	12.0	4.21
Radiator Outside Diameter, Ft.	9	9	Number of Fluid Ducts	60	36
Radiator Length, Ft.	13.9	4.7	Duct Spacing, In.	5.2	8.8
Vapor Chamber Length, In.	26.2	26.2	Fluid Passages Per Duct	10	11
Vapor Chamber I.D., In.	0.280	0.280	Fluid Passage Width, In.	0.010	0.0105
Number of Vapor Chambers	1512	437	Duct Conduction Fin Thickness, In.	0.005	0.006
Average Vapor Chamber Spacing, In.	1.32	1.54			
Primary Fluid Passage Width, In.	0.0137	0.0135			
Primary Duct Conduction Fin Thickness, In.	0.005	0.005			
Performance Data			Performance Data		
Physical Radiator Area, Ft <sup>2</sup>	377	127	Physical Radiator Area, Ft <sup>2</sup>	344	122
Primary Fluid Pressure Drop, PSI	8.88	3.8	Fluid Pressure Drop, PSI	10.8	7.3
Temperature Drops, °F			Temperature Drop, °F		
High Temperature Section	43	-			
Low Temperature Section	15	13			
Weight Tabulation			Weight Tabulation		
Primary Fluid Ducts	116.0	315	Fluid Ducts	164	24
Vapor Chambers	133.	39.9	Conduction Fins	227	91
Conduction Fins	112.7	32.2	Headers	7.6	5
Panel Splice Joints	15.7	5.3	Panel Splice Joints		
Interface Rings	11.8	12.8	Interface Rings	42	16
Stiffening Rings	65.8	23.3	Stiffening Rings		
Total, Lb	455	145	Total, Lb	441	136.0

A structural analysis performed (Section 5.3) indicated the conduction fin radiator to be a better structural member than the vapor chamber radiator. However, the margin of difference was small and in either case the weight of additional structural members required to support a 6000-pound payload radiator was less than the weight required for a separate structure.

An evaluation of fabrication processes required for each radiator indicates no major advantages exist for either radiator. However, considering that each radiator requires the fabrication of finned ducts, the additional complexity of fabricating the vapor chambers gives the advantage to the conduction fin.

The requirement for the fabrication of finned ducts for each radiator is due to the use of DC-200 organic working fluid at low flow rates. The finned duct provides the necessary large heat transfer area required to reduce surface film temperature drops and increase overall radiator efficiency. The use of a higher performance primary fluid would possibly eliminate the need for extensive duct fins and substantially reduce the design and fabrication complexity of both radiators, in particular the conduction fin design.

#### 7.4 CONCLUSIONS

Several overall conclusions result from the study:

1. The Vapor Chamber Radiator offers no significant advantages over a more conventional conduction fin design for the Brayton cycle application.
2. Both radiators seem to be about equal in weight and area at a survival probability of 0.998. At higher probabilities, the vapor chamber radiator seems to be lighter and smaller, while at lower probabilities the conduction fin radiator is lighter and smaller. However, the differences in weight and area are less than 20 percent over the range of probabilities from 0.990 to 0.999.
3. Both radiator designs represent significant fabrication difficulties. The conduction fin radiator duct design is complicated by the poor heat transfer and flow properties of DC-200. The vapor chamber radiator has the same requirement in addition to a large number of heat pipes (vapor chambers).

4. Vapor chamber fluids compatible with aluminum are available in the Brayton cycle temperature range.
5. Of the fluids tested, ammonia is the best working fluid for vapor chambers operating at temperatures below 150°F. At operating temperatures above 150°F, water is the best working fluid on the basis of performance calculations. However, since water is incompatible with aluminum, n-pentane was selected for this temperature range.
6. Structural problems were not significant for the 6000-pound load considered.
7. The vapor chamber radiator is relatively insensitive to meteoroid survival probability; whereas, the conduction fin radiator is very sensitive.
8. A start-up investigation of these radiators was not performed.
9. The specific weight for both radiator types ranges between 1.0 and 1.5 lb/ft<sup>2</sup>.

## SECTION 8

### REFERENCES

1. Lieblein, S., "Meteoroid Armor and Bumper Criteria for Space Radiators," NASA Lewis Memorandum, October 7, 1966.
2. Leoffler, I. J., N. Clough, and S. Lieblein, "Recent Developments in Space Power System Meteoroid Protection," AIAA Paper No. 64-759, September 1964.
3. "A Study of Jupiter Fly-By Missions," General Dynamics Report FZM-4625, May 17, 1966.
4. Volkoff, J. J., "Protection Requirements for the Resistance of Meteoroid Penetration Damage of Interplanetary Spacecraft Systems," JPL Technical Report 32-410, July 1, 1964
5. Nestor Clough and James H. Diedrich, "Results of Hypervelocity Impact into Radiator Materials" NASA TM X-52142, National Aeronautics and Space Conf. (1965)
6. Centaur Payload User's Manual, NASA CR 72109, August 1966.
7. Brayton Cycle Subsystems and Components Environmental Specification, No. P1224-1, January 31, 1967.
8. McAdams, W. H., Heat Transmission, Third Edition, McGraw Hill Book Co., 1954.
9. Pomeroy, G. W., Determination of the Effects of Radiation Fields on Dielectric Materials, ONR Symposium Report No. ACR-2, December, 1954, pp. 133-138.
10. MacLennan, McMillan, and Greenblatt, The Corrosion of Aluminum and Aluminum Alloys in High Temperature Water, First International Congress on Metallic Corrosion, London, 10-15 April, 1961.
11. Draley and Ruther, "Corrosion," Vol. 12, 1956, p. 481.
12. Properties and Selection of Metals, Metals Handbook, American Society for Metals, Novelty, Ohio, 8th ed., 1961.
13. Vhlig, H. H., Corrosion and Corrosion Control, John Wiley and Sons, Inc., New York, 1963.

14. Vhlig, H. H., Corrosion Handbook, John Wiley and Sons, Inc., New York, 1948.
15. Mellan, L., Corrosion Resistant Materials Handbook, Noyes Department Corporation, Park Ridge, New Jersey, 1966.
16. Werkstoffe u. Korrosion, Vol. 10, 91-105, 1959.
17. Geiringer, P. L., Handbook of Heat Transfer Media, Reinhold Publishing Company, New York, 1962.
18. Fieser, L. F. and Fieser, M., Organic Chemistry, D. C. Heath and Company, Boston, Mass., 1944.
19. Matheson Gas Data Book, The Matheson Company, Inc.
20. Brochure No. X-1B, Freon Products Department, E. I. duPont de Nemours and Company, Inc., Wilmington, Delaware.
21. Madsen, J., King, P. P., and Johnston, R. P., et al., Experimental Evaluation of Expanded Pyrolytic Graphite for use in Space Radiators, Douglas Aircraft Company, Technical Report AFAPL-TR-67-54, May 1967.
22. Diamond, P. M. and Hopson, G. D., "Heat Rejection in Space," General Dynamics, Fort Worth, Texas, July 1961. (Text material for UCLA Short Course in Space Power Systems.)
23. T. P. Cotter, Theory of Heat Pipes, LA-3246-MS (1965).
24. Freon MF Solvent, E. I. duPont de Nemours and Co., Inc., Report X-120.
25. Freon TF Solvent, E. I. duPont de Nemours and Co., Inc., Technical Bulletin FST-1 (1965).
26. J. E. Deverall and J. E. Kemme, "Satellite Heat Pipe," LA-3278-MS (1965).
27. "CP-34 Thermodynamic Fluid Candidate," Monsanto Company Report (November 1966).  
"CP-32," Monsanto Company Report (August 1967).
28. E. H. Dix, Jr., R. H. Brown, and W. W. Binger, "The Resistance of Aluminum Alloys to Corrosion," Metals Handbook, Vol. 1., American Society for Metals, Novelty, Ohio (1961).
29. Foust, A., Wenzel, L., Clump, C., Maus, L., and Andersen, L., "Principles of Unit Operations," John Wiley and Sons Inc., 1960.



30. Seider, E.N., late, C.E., "Heat Transfer and Pressure Drop of Liquids in Tubes," Ind. Eng. Chem., Vol. 28 (1936).
31. Metallic Materials and Elements for Aerospace Vehicle Structures, MIL-HDBK-5A, February 8, 1966.
32. Shanley, F.R., "Weight-Strength Analysis of Aircraft Structures," Dover Publication, 1952.
33. Becker, H. and Gerard, G., "Elastic Stability of Orthotropic Shells," Journal of the Aerospace Sciences, May 1962.
34. Olsen, G., "Elements of Mechanics of Materials," Prentice Hall, Inc., 1958.
35. Rohsenow, W.M., "A Method of Correlating Heat Transfer Data for Surface Boiling Liquids," Trans. ASME, Vol. 74, pp. 969-975, 1955.
36. Cichelli, M.T. and Bonilla, C.F., "Heat Transfer to Liquids Boiling Under Pressure," Trans. Am. Inst. Chem. Engineers, Vol. 41, pp. 755-787, 1945.

## TABULATED VALUES OF FLUID PROPERTIES

## TABULATED VALUES OF FLUID PROPERTIES\*

FLUID: Propane  $C_3H_8$   
 MELTING POINT: - 305.9 °F  
 BOILING POINT: - 43.8 °F  
 CRITICAL PRESSURE  $P_C$ : 618 psia  
 CRITICAL TEMPERATURE: 206.2 °F  
 LIQUID THERMAL CONDUCTIVITY\*: 0.07 Btu/hr-ft-°F

TEMPERATURE °F	HEAT OF VAPORIZATION BTU/LB	LIQUID DENSITY LB/FT <sup>3</sup>	VAPOR DENSITY LB/FT <sup>3</sup>	VAPOR PRESSURE PSIA	LIQUID VISCOSITY CENTIPOISE	VAPOR VISCOSITY CENTIPOISE	LIQUID SURFACE TENSION DYNE / CM
20	166.3	33.67	0.526	55.5	0.138	0.0072	13.0
40	160.3	32.73	0.730	78.0	0.121	0.0075	10.8
60	152.6	31.75	0.990	107.1	0.106	0.0079	8.8
100	135.6	29.58	1.69	187.0	0.083	0.0084	4.9
140	112.5	27.00	2.78	305.0	0.064	0.0090	2.1

\*data sources listed at end of Appendix B  
 \*estimated

## TABULATED VALUES OF FLUID PROPERTIES

FLUID:	n-Butane C <sub>4</sub> H <sub>10</sub>					
MELTING POINT:	- 216.9 °F					
BOILING POINT:	31.1 °F					
CRITICAL PRESSURE P <sub>C</sub> :	552 psia					
CRITICAL TEMPERATURE:	305.6 °F					
LIQUID THERMAL CONDUCTIVITY: *	0.07 Btu/hr-ft-°F					
TEMPERATURE °F	HEAT OF VAPORIZATION BTU/LB	LIQUID DENSITY LB/FT <sup>3</sup>	VAPOR DENSITY LB/FT <sup>3</sup>	VAPOR PRESSURE PSIA	LIQUID VISCOSITY CENTIPOISE	
50	161.6	36.82	0.246	21.6	0.188	
100	150.5	34.84	0.552	52.2	0.143	
150	134.5	32.70	1.115	108.0	0.108	
200	115.2	30.58	2.08	197.0	0.082	
250	--	--	--	331.0	0.062	

\*estimated

# TABULATED VALUES OF FLUID PROPERTIES

FLUID: n-Pentane  $C_5H_{12}$   
 MELTING POINT: - 201.5 °F  
 BOILING POINT: 96.9 °F  
 CRITICAL PRESSURE  $P_C$ : 489.5 psia  
 CRITICAL TEMPERATURE: 385.9 °F  
 LIQUID THERMAL CONDUCTIVITY: 0.07 Btu/Hr-Ft-°F

TEMPERATURE °F	HEAT OF VAPORIZATION BTU/LB	LIQUID DENSITY LB/FT <sup>3</sup>	VAPOR DENSITY LB/FT <sup>3</sup>	VAPOR PRESSURE PSIA	LIQUID VISCOSITY CENTIPOISE	VAPOR VISCOSITY CENTIPOISE	LIQUID SURFACE TENSION DYNE/CM
50	162.4	39.7	0.07	5.5	0.25	0.0055	17.1
150	142.8	36.1	0.44	35.8	0.16	0.007	11.5
200	130.5	34.1	0.87	75.5	0.13	0.0078	8.8
250	115.4	31.7	1.6	147	0.12	0.009	6.7
300	97	28.9	2.9	253	0.10	0.010	4.8

## TABULATED VALUES OF FLUID PROPERTIES

FLUID: n-Heptane  $C_7H_{16}$   
 MELTING POINT: - 131 °F  
 BOILING POINT: 209.1 °F  
 CRITICAL PRESSURE  $P_C$ : 396 psia  
 CRITICAL TEMPERATURE: 512.6 °F  
 LIQUID THERMAL CONDUCTIVITY: 0.08 Btu/Hr-ft-°F

TEMPERATURE °F	HEAT OF VAPORIZATION BTU/LB	LIQUID DENSITY LB/FT <sup>3</sup>	VAPOR DENSITY LB/FT <sup>3</sup>	VAPOR PRESSURE PSIA	LIQUID VISCOSITY CENTIPOISE	VAPOR VISCOSITY CENTIPOISE	LIQUID SURFACE TENSION DYNE/CM
50	160	43.2	0.016	0.398	0.47		21.3
150	146.9	40.2	0.098	5.0	0.27		15.8
200	139.3	38.6	0.187	12.6	0.22		13.3
250	130.8	36.9	0.387	27.4	0.18	0.007	10.9
300	120.0	35.0	0.737	50.5	0.16	0.008	8.5

# TABULATED VALUES OF FLUID PROPERTIES

FLUID: n-Nonane  $C_9H_{20}$   
 MELTING POINT: - 64.6 °F  
 BOILING POINT: 302.4 °F  
 CRITICAL PRESSURE  $P_C$ : 362 psia  
 CRITICAL TEMPERATURE: 565 °F  
 LIQUID THERMAL CONDUCTIVITY: .06 Btu/hr-ft-°F

TEMPERATURE °F	HEAT OF VAPORIZATION BTU/LB	LIQUID DENSITY LB/FT <sup>3</sup>	VAPOR DENSITY LB/FT <sup>3</sup>	VAPOR PRESSURE PSIA	LIQUID VISCOSITY CENTIPOISE	VAPOR VISCOSITY CENTIPOISE	LIQUID SURFACE TENSION DYNE /CM
50	158.5	45.3	0.0007	0.03	0.83		23.9
150	147.4	42.6	0.0146	0.75	0.42		18.6
200	141.1	41.1	0.043	2.38	0.33	0.006	16.3
250	134.5	39.7	0.105	6.2	0.26		13.9
300	127.3	38.1	0.221		0.21	0.007	11.7

## TABULATED VALUES OF FLUID PROPERTIES

FLUID: Benzene  $C_6H_6$   
 MELTING POINT: - 42 °F  
 BOILING POINT: 176 °F  
 CRITICAL PRESSURE  $P_C$ : 714 psia  
 CRITICAL TEMPERATURE: 553 °F  
 LIQUID THERMAL CONDUCTIVITY: 0.08 Btu/hr-ft-°F

TEMPERATURE °F	HEAT OF VAPORIZATION BTU/LB	LIQUID DENSITY LB/FT <sup>3</sup>	VAPOR DENSITY LB/FT <sup>3</sup>	VAPOR PRESSURE PSIA	LIQUID VISCOSITY CENTIPOISE	VAPOR VISCOSITY CENTIPOISE	LIQUID SURFACE TENSION DYNE / CM
50	190	55.5	0.022	0.9	0.76	0.0075	30.2
150	174	51.8	0.108	9.2	0.37	0.009	23.3
200	165	49.9	0.237	21.7	0.28		19.6
250	156	47.9	0.487	42.8	0.23	0.01	16.4
300	145	45.7	0.874	72.0	0.20	0.011	13.1

TABULATED VALUES OF FLUID PROPERTIES

FLUID: Toluene  $C_6H_5CH_3$   
 MELTING POINT: - 139 °F  
 BOILING POINT: 231 °F  
 CRITICAL PRESSURE  $P_C$ : 590 psia  
 CRITICAL TEMPERATURE: 609 °F  
 LIQUID THERMAL CONDUCTIVITY: 0.07 Btu/hr-ft-°F

TEMPERATURE °F	HEAT OF VAPORIZATION BTU/LB	LIQUID DENSITY LB/FT <sup>3</sup>	VAPOR DENSITY LB/FT <sup>3</sup>	VAPOR PRESSURE PSIA	LIQUID VISCOSITY CENTIPOISE	VAPOR VISCOSITY CENTIPOISE	LIQUID SURFACE TENSION DYNE/CM
50	181	54.7	0.004	0.24	0.67	0.007	29.7
150	168	51.5	0.047	3.3	0.36	0.0084	23.4
200	161	49.9	0.114	8.7	0.28	0.0085	20.3
250	153	48.3	0.238	19.6	0.23	0.009	17.3
300	145	46.7	0.435	38.1	0.19	0.01	14.2



## TABULATED VALUES OF FLUID PROPERTIES

FLUID: 0-Xylene  $C_6H_4(CH_3)_2$

MELTING POINT:

- 13.3 °F

BOILING POINT:

291.9 °F

CRITICAL PRESSURE  $P_C$ :

530 psia

CRITICAL TEMPERATURE:

678 °F

LIQUID THERMAL CONDUCTIVITY: 0.06 Btu/hr-ft-°F

TEMPERATURE °F	HEAT OF VAPORIZATION BTU/LB	LIQUID DENSITY LB/FT <sup>3</sup>	VAPOR DENSITY LB/FT <sup>3</sup>	VAPOR PRESSURE PSIA	LIQUID VISCOSITY CENTIPOISE	VAPOR VISCOSITY CENTIPOISE	LIQUID SURFACE TENSION DYNE / CM
50	179.1	55.5	0.0009	0.049	0.94		33.1
150	167.7	52.5	0.016	1.01	0.47		25.2
200	161.6	51.0	0.045	3.03	0.36		22.2
250	155.1	49.5	0.106	7.6	0.29		19.1
300	148.0	47.9	0.216	16.5	0.24	0.009	16.1

TABULATED VALUES OF FLUID PROPERTIES

FLUID: Freon 11  $\text{CCl}_3\text{F}$   
 MELTING POINT:  $-168^\circ\text{F}$   
 BOILING POINT:  $74.9^\circ\text{F}$   
 CRITICAL PRESSURE  $P_c$ : 639 psia  
 CRITICAL TEMPERATURE:  $388^\circ\text{F}$   
 LIQUID THERMAL CONDUCTIVITY:  $0.058 \text{ Btu/hr-ft-}^\circ\text{F}$

TEMPERATURE $^\circ\text{F}$	HEAT OF VAPORIZATION BTU/LB	LIQUID DENSITY LB/FT <sup>3</sup>	VAPOR DENSITY LB/FT <sup>3</sup>	VAPOR PRESSURE PSIA	LIQUID VISCOSITY CENTIPOISE	VAPOR VISCOSITY CENTIPOISE	LIQUID SURFACE TENSION DYNE/CM
20	82.2	96.7	0.118	4.35	0.59	0.0099	22.5
40	80.5	95.1	0.18	7.0	0.52	0.010	21.1
60	78.9	93.5	0.28	10.5	0.46	0.0106	19.6
120	73.3	88.6	0.78	32.5	0.35	0.011	15.4
150	70.4	85.8	1.21	52.4	0.31	0.012	13.2

## TABULATED VALUES OF FLUID PROPERTIES

FLUID: Freon 113  $\text{CCl}_2\text{F} - \text{CClF}_2$

MELTING POINT:

- 31 °F

BOILING POINT:

117.6 °F

CRITICAL PRESSURE  $P_C$ :

495 psia

CRITICAL TEMPERATURE:

417 °F

LIQUID THERMAL CONDUCTIVITY: 0.04 Btu/hr-ft-°F

TEMPERATURE °F	HEAT OF VAPORIZATION BTU/LB	LIQUID DENSITY LB/FT <sup>3</sup>	VAPOR DENSITY LB/FT <sup>3</sup>	VAPOR PRESSURE PSIA	LIQUID VISCOSITY CENTIPOISE	VAPOR VISCOSITY CENTIPOISE	LIQUID SURFACE TENSION DYNE/CM
20	69.7	102	0.056	1.5	1.04	0.0095	22.9
40	68	100	0.10	2.6	0.88	0.0098	21.5
60	67	99	0.14	4.8	0.75	0.010	20.2
120	62	93	0.48	15.5	0.49	0.0105	16.3
150	60.4	91	0.78	25.9	0.41	0.011	14.3

TABULATED VALUES OF FLUID PROPERTIES

FLUID: Methyl Alcohol, Methanol  $\text{CH}_3\text{OH}$   
 MELTING POINT:  $-144^\circ\text{F}$   
 BOILING POINT:  $+148.4^\circ\text{F}$   
 CRITICAL PRESSURE  $P_c$ : 1155 psia  
 CRITICAL TEMPERATURE:  $464^\circ\text{F}$   
 LIQUID THERMAL CONDUCTIVITY: 0.12 Btu/hr-ft- $^\circ\text{F}$

TEMPERATURE $^\circ\text{F}$	HEAT OF VAPORIZATION BTU/LB	LIQUID DENSITY LB/FT <sup>3</sup>	VAPOR DENSITY LB/FT <sup>3</sup>	VAPOR PRESSURE PSIA	LIQUID VISCOSITY CENTIPOISE	VAPOR VISCOSITY CENTIPOISE	LIQUID SURFACE TENSION DYNE/CM
50	507	49.9	0.006	1.05	0.69	0.009	23.6
150	472	46.7	0.074	15.1	0.33	0.011	18.8
200	443	45.0	0.20	40.3	0.24		16.3
250	407	43.0	0.45	94.7	0.18		13.8
300	364	40.6	0.96	189	0.14	0.0145	11.1

## TABULATED VALUES OF FLUID PROPERTIES

FLUID: Ethyl Alcohol, Ethanol  $\text{CH}_3\text{CH}_2\text{OH}$   
 MELTING POINT: - 174 °F  
 BOILING POINT: 173 °F  
 CRITICAL PRESSURE  $P_c$ : 927 psia  
 CRITICAL TEMPERATURE: 469 °F  
 LIQUID THERMAL CONDUCTIVITY: 0.11 Btu/hr-ft-°F

TEMPERATURE °F	HEAT OF VAPORIZATION BTU/LB	LIQUID DENSITY LB/FT <sup>3</sup>	VAPOR DENSITY LB/FT <sup>3</sup>	VAPOR PRESSURE PSIA	LIQUID VISCOSITY CENTIPOISE	VAPOR VISCOSITY CENTIPOISE	LIQUID SURFACE TENSION DYNE/CM
50	389	49.8	0.003	0.44	1.45	0.009	23.6
150	370	46.7	0.06	8.5	0.55	0.01	18.6
200	355	45.1	0.175	24.6	0.36	0.011	16.1
250	327	43.2	0.421	63.9	0.24		13.5
300	291	40.6	0.910	137	0.17	0.012	10.8

TABULATED VALUES OF FLUID PROPERTIES

FLUID: Isopropyl Alcohol, Isopropanol  $\text{CH}_3\text{-CH-OH-CH}_3$   
 MELTING POINT: - 127.8 °F  
 BOILING POINT: 180.3 °F  
 CRITICAL PRESSURE  $P_C$ : 779 psia  
 CRITICAL TEMPERATURE: 462.5 °F  
 LIQUID THERMAL CONDUCTIVITY: 0.09 Btu/hr-ft-°F

TEMPERATURE °F	HEAT OF VAPORIZATION BTU/LB	LIQUID DENSITY LB/FT <sup>3</sup>	VAPOR DENSITY LB/FT <sup>3</sup>	VAPOR PRESSURE PSIA	LIQUID VISCOSITY CENTIPOISE	VAPOR VISCOSITY CENTIPOISE	LIQUID SURFACE TENSION DYNE/CM
50	331	49.5	0.0036	0.329	32.6		25.7
150	298	46.7	0.066	7.17	7.04		22.1
200	279	45.3	0.190	22.3	4.0	0.01	20.2
250	257	43.9	0.39	49.5	2.18	0.011	18.1
300	232	42.5	0.67	90	1.5		16.1

## TABULATED VALUES OF FLUID PROPERTIES

FLUID: Pyridine N:CHCH:CHCH:CH  
 MELTING POINT: - 43.6 °F  
 BOILING POINT: 241 °F  
 CRITICAL PRESSURE  $P_C$ : 817 psia  
 CRITICAL TEMPERATURE: 657 °F  
 LIQUID THERMAL CONDUCTIVITY: 0.09 Btu/Hr-ft-°F

TEMPERATURE °F	HEAT OF VAPORIZATION BTU/LB	LIQUID DENSITY LB/FT <sup>3</sup>	VAPOR DENSITY LB/FT <sup>3</sup>	VAPOR PRESSURE PSIA	LIQUID VISCOSITY CENTIPOISE	VAPOR VISCOSITY CENTIPOISE	LIQUID SURFACE TENSION DYNE / CM
50	222	59.1	0.0025	0.176	0.975		39.8
150	208	55.8	0.0327	2.7	0.702		35.5
200	200	54.1	0.0837	7.4	0.533		31.3
250	191	52.3	0.1843	17.3	0.429	0.009	27.2
300	182	50.4	0.361	35.6	0.390	0.010	25.0

# TABULATED VALUES OF FLUID PROPERTIES

FLUID: Ammonia NH<sub>3</sub>  
 MELTING POINT: -107.9 °F  
 BOILING POINT: - 28 °F  
 CRITICAL PRESSURE P<sub>C</sub>: 1636 psia  
 CRITICAL TEMPERATURE: 271.2 °F  
 LIQUID THERMAL CONDUCTIVITY: 0.22 Btu/hr-ft-°F

TEMPERATURE °F	HEAT OF VAPORIZATION BTU/LB	LIQUID DENSITY LB/FT <sup>3</sup>	VAPOR DENSITY LB/FT <sup>3</sup>	VAPOR PRESSURE PSIA	LIQUID VISCOSITY CENTIPOISE	VAPOR VISCOSITY CENTIPOISE	LIQUID SURFACE TENSION DYNE /CM
20	553	40.4	0.17	48.2	0.161	0.009	26
40	535	39.5	0.28	73.3	0.140	0.009	24
60	520	38.5	0.36	107.6	0.12	0.0096	22
120	452	35.2	0.96	286.4		0.01	17
150	435	34		425			12



## TABULATED VALUES OF FLUID PROPERTIES

FLUID: Water H<sub>2</sub>O  
 MELTING POINT: 32 °F  
 BOILING POINT: 212 °F  
 CRITICAL PRESSURE P<sub>C</sub>: 3211 psia  
 CRITICAL TEMPERATURE: 705.6 °F  
 LIQUID THERMAL CONDUCTIVITY: 0.39 Btu/Hr-ft-°F

TEMPERATURE °F	HEAT OF VAPORIZATION BTU/LB	LIQUID DENSITY LB/FT <sup>3</sup>	VAPOR DENSITY LB/FT <sup>3</sup>	VAPOR PRESSURE PSIA	LIQUID VISCOSITY CENTIPOISE	VAPOR VISCOSITY CENTIPOISE	LIQUID SURFACE TENSION DYNE/CM
50	1064	62.7	0.0006	0.18	1.3		74.2
150	1007	61.5	0.01	3.7	0.43		65.2
200	978	60.4	0.03	11.5	0.31	0.012	60.1
250	945	59.1	0.07	29.8	0.23	0.013	54.6
300	910	57.6	0.15	67	0.19	0.014	48.6

#### DATA SOURCES

1. Lange, N. A., Handbook of Chemistry (1956).
2. Hodgman, C. D., Handbook of Chemistry and Physics, 44th Ed. (1962).
3. Timmermans, J., Physics - Chemical Constants of Pure Organic Compounds, (1950).
4. Perry, R. H., Chemical Engineers Handbook, (1963).
5. Weast, R. C., Handbook of Chemistry and Physics, 45th Ed., (1964).
6. Maxwell, J. B., Data Book of Hydrocarbons (1950).
7. Rossini, F. D., Selected Values of Physical and Thermodynamic Properties of Hydrocarbons and Related Compounds, (1953).

APPENDIX B

BRAYTON CYCLE SPACE POWER SYSTEM

ATMOSPHERIC ENVIRONMENTAL SPECIFICATION

(SPECIFICATION NO. P1224-2, JANUARY 31, 1967)

1.0. SCOPE

- 1.1. This specification lists the anticipated atmospheric environmental conditions to which the Brayton Cycle Space Power System and components shall be designed to withstand without malfunction or performance degradation.

This specification does not cover development and/or acceptance tests.

Structural load environments (shock, vibration, acceleration, etc.) are covered in NASA Specification P1224-1.

1.2. Environments

Environmental conditions specified are applicable to each of the components and the complete space power system through manufacture, storage, transportation, pre-launch lift-off, and boost.

2.0. Environmental Conditions

2.1. Storage and Transportation

The Brayton Cycle Space Power System and components shall be shipped and stored in suitable containers designed to eliminate or mitigate the effects of environmental conditions as described herein.

2.1.1. Rain, Humidity, Sand, Dust and Salt Spray

The system and the components packaging and storage conditions shall provide protection from rain, humidity, sand, dust and salt spray.

2.1.2. Normal Storage

The system and the components in their containers shall be capable of storage for a period of two years without deterioration.

2.1.3. Temperature

During storage and transportation, the system and components will be protected by the container from the ambient temperature environment and the changes in this thermal environment.

#### 2.1.4. Pressure

During the storage and transportation phase, the items (if the container is not pressurized) will be subjected to pressures from sea level to a maximum altitude of 50,000 feet. The maximum change in pressure to which the items will be subjected is a reduction or increase in pressure of 1.25 psi per minute. This will occur in either a climb to 50,000 feet or a descent from 50,000 feet.

#### 2.1.5. Fungus

The system and components shall be adequately protected from fungi and bacteria growth as experienced at the Atlantic Missile Range. (Reference NASA TM X-53023, Section XL)

The components shall be designed and fabricated to withstand or resist fungus growth as specified in MIL-STD-810 A (USAF), Method 508.1.

### 3.0 Handling and Vehicle Integration

During handling and vehicle integration, it can be anticipated that the components and complete system may be exposed to atmospheric and weather environments for maximum periods of six weeks. The natural environmental extremes for the Atlantic Missile Range are specified in NASA TM X-53023.

#### 3.1. Rain, Humidity, Sand, Dust, Salt Spray, and Fungus

##### 3.1.1. Rain:

The following table gives the expected extreme rainfall rates at ground level based on a return period of 10 years for the Atlantic Missile Range, Pacific Missile Range and West Coast transportation.

	1 Minute	1 Hour	24 Hours
Total Amount (mm.)	7.6	63	305
(in.)	0.3	2.5	12
Rate (mm./hr.)	460	64	13
(in./hr.)	18	2.5	0.5
Average Drop Diameter (mm.)	3.8	2.6	2.0
Average Rate of Fall (m/sec.)	8.5	7.3	6.4
Peak Wind Speed (m/sec.)	20	20	20

### 3.1.2. Humidity

The system and components shall be designed and fabricated to withstand simulated humidity cycle of 24 hours with a steady-state wind of less than 5 m/sec. (9.7 knots) as follows:

- a. Six (6) hours of 37.2°C (99°F) air temperature at 50 percent relative humidity and vapor concentration of 26.9 g/m<sup>3</sup> (11.7 gr/ft<sup>3</sup>);
- b. Six (6) hours of decreasing air temperature to 24.4°C (76°F) with relative humidity increasing to 100 percent (saturation);
- c. Eight (8) hours of decreasing air temperature to 21.1°C (70°F), with a release of 3.9 grams of water as fluid per cubic meter of air (1.7 gr/ft<sup>3</sup>), humidity remaining at 100 percent;
- d. Four (4) hours of increasing air temperature to 37.2°C (99°F) and a decrease to 41 percent relative humidity.

The preceding schedule of temperature and humidity simulates the conditions encountered at the Atlantic Missile Range.

### 3.1.3. Sand and Dust

The system and components shall be designed and fabricated to withstand the tests specified in MIL-STD-810A (USAF), Method 510.1 with the exception that the test will be conducted at a temperature of 90° ± 20°F instead of 160°F.

### 3.1.4. Fungus

The system and components shall be adequately protected from fungi and bacteria growth as experienced at the Atlantic Missile Range. (Reference NASA TM X-53023, Section XI.)

The components shall be designed and fabricated to withstand or resist fungus growth as specified in MIL-STD 810 A (USAF), Method 508.1.

### 3.1.5. Salt Spray

The components and system shall be capable of withstanding salt spray as experienced at the coastal regions of the continental United States for periods up to six (6) weeks. The components shall be capable to withstand the environment specified in MIL-STD-810A (USAF), Method 509.1.

3.2. Temperature

The system and components shall withstand the surface air temperature extremes, sky radiation temperature and solar radiation as specified for the Atlantic Missile Range in NASA TM X-53023, Section II, Temperature.

3.3. Wind

The system and components shall withstand the surface wind speed envelope (99 percentile) for the Atlantic Missile Range as specified in NASA TM X-53023, Table 5.4B.

3.4. Shock and Vibration

The techniques used in handling the system and components shall be such that the shock and vibration imposed will not exceed that experienced during transportation and launch.



POSTMASTER: If Undeliverable (Section 158  
Postal Manual) Do Not Return

*"The aeronautical and space activities of the United States shall be conducted so as to contribute . . . to the expansion of human knowledge of phenomena in the atmosphere and space. The Administration shall provide for the widest practicable and appropriate dissemination of information concerning its activities and the results thereof."*

— NATIONAL AERONAUTICS AND SPACE ACT OF 1958

## NASA SCIENTIFIC AND TECHNICAL PUBLICATIONS

**TECHNICAL REPORTS:** Scientific and technical information considered important, complete, and a lasting contribution to existing knowledge.

**TECHNICAL NOTES:** Information less broad in scope but nevertheless of importance as a contribution to existing knowledge.

**TECHNICAL MEMORANDUMS:** Information receiving limited distribution because of preliminary data, security classification, or other reasons.

**CONTRACTOR REPORTS:** Scientific and technical information generated under a NASA contract or grant and considered an important contribution to existing knowledge.

**TECHNICAL TRANSLATIONS:** Information published in a foreign language considered to merit NASA distribution in English.

**SPECIAL PUBLICATIONS:** Information derived from or of value to NASA activities. Publications include conference proceedings, monographs, data compilations, handbooks, sourcebooks, and special bibliographies.

**TECHNOLOGY UTILIZATION PUBLICATIONS:** Information on technology used by NASA that may be of particular interest in commercial and other non-aerospace applications. Publications include Tech Briefs, Technology Utilization Reports and Technology Surveys.

*Details on the availability of these publications may be obtained from:*

SCIENTIFIC AND TECHNICAL INFORMATION OFFICE

NATIONAL AERONAUTICS AND SPACE ADMINISTRATION

Washington, D.C. 20546